İZMİR
KÂTİP ÇELEBİ
ÜNİVERSİTESİ
2010
GRADUATE SCHOOL OF NATURAL
AND APPLIED SCIENCES

Evaluation of Some Neurological Disorders by the Analysis of EEG Signals

Submitted to the Graduate School of Natural and Applied Sciences
in partial fulfillment of the requirements for the degree of

Doctor of Philosophy

in Department of Biomedical Technologies

by
Özlem Karabiber Cura

ORCID 0000-0001-8650-1137

July, 2021

This is to certify that we have read the thesis **Evaluation of Some Neurological Disorders By The Analysis of EEG Signals** submitted by **Özlem Karabiber Cura**, and it has been judged to be successful, in scope and in quality, at the defense exam and accepted by our jury as a DOCTORAL THESIS.

APPROVED BY:

Advisor: **Prof. Dr. Aydın Akan**
                        Izmir University of Economics

Committee Members:

                        Prof. Dr. Olcay Akay
                        Dokuz Eylul University

                        Assist. Prof. Dr. Sibel Kocaaslan Atlı
                        Izmir Katip Celebi University

                        Prof.Dr. Mustafa Altınkaya
                        Izmir Institute of Technology

                        Doç.Dr. Yalçın İşler
                        Izmir Katip Celebi University

Date of Defense: July 29, 2021

Declaration of Authorship

I, **Özlem Karabiber Cura**, declare that this thesis titled **Evaluation of Some Neurological Disorders by the Analysis of EEG Signals** and the work presented in it are my own. I confirm that:

- This work was done wholly or mainly while in candidature for the Doctoral degree at this university.

- Where any part of this thesis has previously been submitted for a degree or any other qualification at this university or any other institution, this has been clearly stated.

- Where I have consulted the published work of others, this is always clearly attributed.

- Where I have quoted from the work of others, the source is always given. This thesis is entirely my own work, with the exception of such quotations.

- I have acknowledged all major sources of assistance.

- Where the thesis is based on work done by myself jointly with others, I have made clear exactly what was done by others and what I have contributed myself.

Date: 29.07.2021

Evaluation of Some Neurological Disorders by the Analysis of EEG Signals

Abstract

Epilepsy and Alzheimer's dementia are highly prevalent among all neurological disorders. In the evaluation of epilepsy, three different approaches are presented to distinguish seizure and seizure-free EEG segments. In the first method, multichannel EEG signals collected from epilepsy patients are decomposed into Intrinsic Mode Functions (IMFs) using Empirical Mode Decomposition (EMD), Ensemble EMD (EEMD) methods, and then essential IMFs are selected. Finally, time- and spectral-domain, and nonlinear features are extracted from selected IMFs and coefficients of discrete wavelet transform (DWT). Dynamic mode decomposition (DMD) is a new matrix decomposition method proposed as an iterative solution to problems in fluid flow analysis. We present single-channel, and multi-channel EEG -based DMD approaches for the analysis of epileptic EEG signals. As a third method, we use the Synchrosqueezing Transform (SST) representations of seizure and pre-seizure EEG data. For Alzheimer's dementia (AD), various signal decomposition methods such as EMD, EEMD, and DWT and Time-Frequency (TF) representation-based approaches such as Short Time Fourier Transform (STFT) and SST are presented to classify EEG segments of control subjects and AD patients. Time-domain and spectral-domain features are calculated using selected 7 IMFs and 5 detail and approximation coefficients of DWT. TF density functions obtained utilizing the SST and STFT approaches are used to calculate 18 different TF features to achieve distinctive information between EEG segments of control subjects and AD patients. Various classification techniques namely Support Vector Machine (SVM), k-Nearest Neighbor (kNN), Naive Bayes (NB), Logistic Regression (LR), Boosted Trees (BT), Subspace kNN (S-kNN), and Random Forest (RF) are utilized to distinguish different groups. Simulation results demonstrate that the proposed approaches achieve outstanding validation accuracy rates.

Keywords: Epileptic EEG Classification, Alzheimer's dementia EEG classification, Empirical Mode Decomposition, Dynamic Mode Decomposition, Synchrosqueezing Transform, Machine Learning.

EEG Sinyallerinin Analizi ile Bazı Nörolojik Bozuklukların Değerlendirilmesi

Öz

Epilepsi ve Alzheimer demans, tüm nörolojik bozukluklar arasında oldukça yaygındır. Epilepsi değerlendirmesinde nöbet ve nöbetsiz EEG segmentlerini ayırt etmek için üç farklı yaklaşım sunulmaktadır. İlk yöntemde, epilepsi hastalarından toplanan çok kanallı EEG sinyalleri, Görgül Kip Ayrıştırma (GKA), Grup GKA (GGKA) yöntemleri kullanılarak IMF'lere ayrıştırılır ve ardından gerekli IMF'ler seçilir. Son olarak, seçilen IMF'lerden ve ayrık dalgacık dönüşümü (ADD) katsayılarından zaman ve spektral alan ve doğrusal olmayan özellikler çıkarılır. Dinamik kip ayrıştırma (DKA), akışkan akış analizindeki sorunlara yinelemeli bir çözüm olarak önerilen yeni bir matris ayrıştırma yöntemidir. Epileptik EEG sinyallerinin analizi için tek kanallı ve çok kanallı EEG tabanlı DKA yaklaşımları sunuyoruz. Üçüncü bir yöntem olarak, nöbet ve nöbet öncesi EEG verilerinin Senkronize Sıkma Dönüşümü (SSD) temsillerini kullanıyoruz. Alzheimer demansı (AD) için, kontrol deneklerinin ve AD hastalarının EEG segmentlerini sınıflandırmak için GKA, GGKA ve ADD gibi çeşitli sinyal ayrıştırma yöntemleri ve Kısa Süreli Fourier Dönüşümü (KSFD) ve SSD gibi Zaman Frekans (ZF) temsiline dayalı yaklaşımlar sunulmaktadır. Zaman alanı ve spektral alan özellikleri, seçilen 7 IMF ve ADD'nin 5 detay ve yaklaşıklık katsayıları kullanılarak hesaplanır. SSD ve KSFD yaklaşımları kullanılarak elde edilen ZF yoğunluğu fonksiyonları, kontrol deneklerinin ve AD hastalarının EEG segmentleri arasında ayırt edici bilgiler elde etmek için 18 farklı ZF özniteliğini hesaplamak için kullanılmıştır. Destek Vektör Makinesi (DVM), k-En Yakın Komşu (kEYK), Naive Bayes (NB), Lojistik Regresyon (LR), Yükseltilmiş Ağaçlar (YA), Altuzay kEYK (A-kEYK) ve Rastgele Orman (RO) olmak üzere çeşitli sınıflandırıcı teknikleri farklı grupları ayırt etmek için kullanılmıştır. Simülasyon sonuçları, önerilen yaklaşımların olağanüstü doğrulama oranlarına ulaştığını göstermektedir.

Anahtar Kelimeler: Epileptik EEG Sınıflandırması, Alzheimer demans EEG sınıflandırması, Görgül Kip Ayrıştırma, Dinamik Kip Ayrışımı, Senkronize Sıkma Dönüşümü, Makine Öğrenmesi.

To my family…

Foreword

Table of Contents

List of Figures

List of Tables

List of Abbreviations

AC   Approximation Coefficient

ACC   accuracy

AD   Alzheimer's dementia

BT   Boosted Trees

CNN   convolutional neural network

CNS   Central Nervous System

CS   control subjects

CV   cross-validation

DALYs   Disability-Adjusted Life years

DC   Detail Coefficients

DMD   Dynamic mode decomposition

DMD-HOS   Higher-order DMD spectral moments

DWT   Discrete Wavelet Transform

EEG   Electroencephalogram

EEMD   Ensemble Empirical Mode Decomposition

EMD   Empirical Mode Decomposition

FD   fractal dimension

FDR   False Discovery Rate

FPR   False positive Rate

F1-S   F-score

FT   Fourier Transform

GLCM   Gray Level Co-occurrence Matrix

HE	The value of Hurst Exponent
HFD	Higuchi Fractal Dimension
HOJ-TF	Higher Order Joint Time-Frequency
HOS	higher order spectra
IF	instantaneous frequency
IMFs	Intrinsic Mode Functions
KLD	Kullback Leibler Distance
kNN	k-Nearest Neighbor
LOOCV	leave-one-out cross-validation
LR	Logistic Regression
MC-DMD	multi-channel DMD approach
MMT	Mini-mental test score
MSE	mean squared error
NB	Naive Bayes
PET	Positron Emission Tomography
PCD	patient-correlated detection
PID	patient-independent detection
PRE	precision
PSD	Power Spectral Density
RM	reassignment methods
RF	Random Forest
QEEG	Quantitative Electroencephalography
SC-DMD	single-channel DMD approach
SEN	sensitivity
S-kNN	Subspace kNN
SPE	selectivity
SST	Synchrosqueezing Transform

STFT	Short Time Fourier Transform
SVD	singular value decomposition
SVM	Support Vector Machine
TF	Time-Frequency
TFR	Time-Frequency Representations
WHO	World Health Organization

List of Symbols

E	energy
μ	mean value
S	Skewness value
K	Kurtosis value
δ	delta
θ	theta
α	alpha
β	beta
γ	gamma
μV	micro volt
$S(\omega_k)$	Power Spectral Density
$X(\omega_k)$	Discrete Fourier Transform of the signal
S_T	total power
M_j	higher order spectral moments
H	spectral entropy
f_m	oscillation frequency of mth DMD mode
P_m	the power value of DMD mode
P_δ	Delta Band Power of DMD spectra
P_θ	Theta Band Power of DMD spectra
P_α	Alpha Band Power of DMD spectra
P_β	Beta Band Power of DMD spectra
P_γ	Gamma Band Power of DMD spectra

P_T	Total Power of DMD spectra
$< t^i \, \omega^j >$	Higher-order joint TF moments
$S(t, \omega)$	density obtained by the magnitude square of the SST and STFT
$G(n, m)$	GLCM matrix
G_C	Contrast features calculated from the GLCM matrix
G_{Corr}	Correlation features calculated from the GLCM matrix
G_E	Energy features calculated from the GLCM matrix
G_H	Homogeneity features calculated from the GLCM matrix

1. Introduction

Neurological disorders may spring from any disorder in the brain or the central and autonomic nervous systems. Changes in any metabolite involved in regulating brain functions can cause fatal damage to the central nervous system due to its complex structure [1]. According to the World Health Organization (WHO), neurological disorders are the diseases with the highest rate of disability worldwide, and they are the second disease category with the highest mortality rate (16.8% of all deaths) [2, 3]. The burden of neurological disorders in all disability causing disorders is compared in Figure 1.1 with the burden of other selected common diseases as a percentage of total disability-adjusted life years (DALYs). Here, one DALY represents a loss that is equivalent to one year of total health loss [2]. The primary neurological diseases affecting people are Alzheimer's disease, and other dementias, Parkinson's disease, Epilepsy, multiple sclerosis, migraine, stroke, poliomyelitis, tetanus, meningitis, and Japanese encephalitis [3, 4].
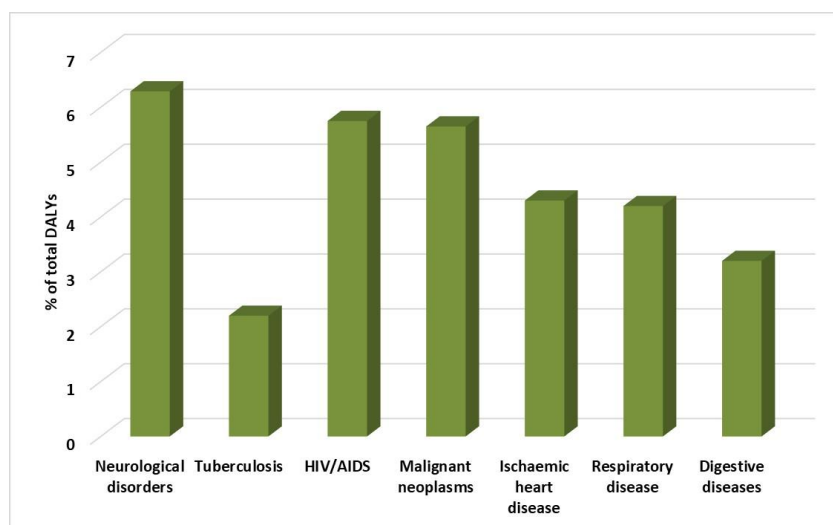
Figure 1.1: Percentage of total DALYs for neurological disorders and selected common diseases.

1

Stroke is responsible for 47.3% of the total DALYs and 67.3% of total deaths due to neurological disorders. Among the neurological disorders, while Alzheimer's disease and other dementias are the fourth-largest contributors (9.5%) (Shown in Figure 1.2a) of DALYs, they are the second largest contributor (20.3%) (Shown in Figure 1.2b) of deaths [2, 3]. Epilepsy accounts for 5% (shown in Figure 1.2a) of total DALYs, but it is one of the most commonly reported neurological diseases in primary care [2, 3, and 5].
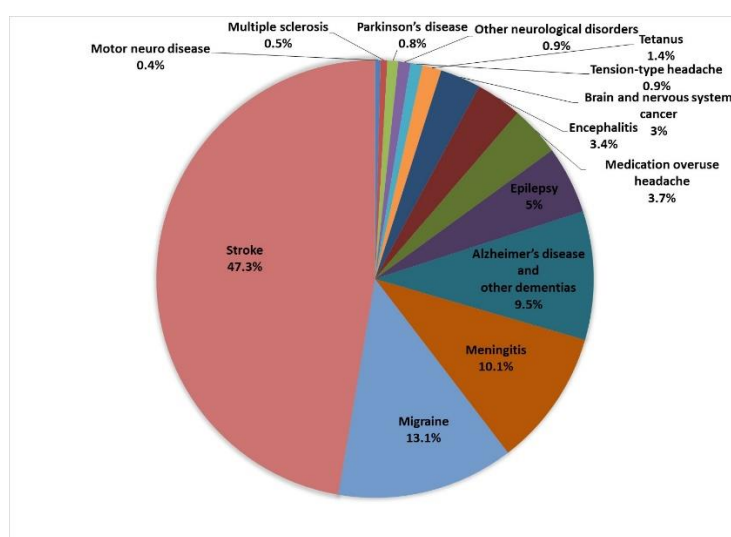
(a)
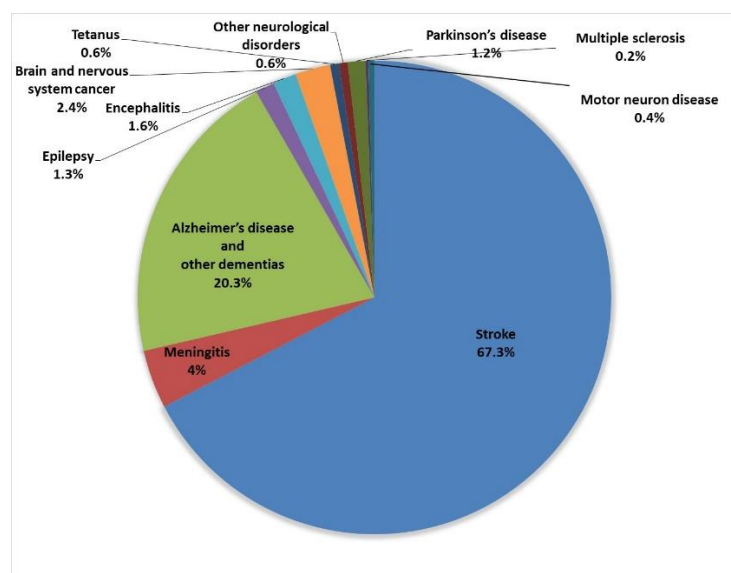
(b)

Figure 1.2: (a) DALYs and (b) death rates for particular neurological disorders as a percentage of total neurological disorders [3].

Search results of the most prevalent 5 neurological disorders on Science Direct and PubMed are plotted in Figure 1.3 for the last 20 years. It is obviously seen on each database search results that dementia and epilepsy are the most studied diseases after stroke. For this reason, it is aimed to evaluate the data of dementia and epilepsy patients within the scope of the thesis, as it is thought to contribute to the literature and provide more opportunities for comparative analysis. Different signal and image processing techniques such as Electroencephalogram (EEG), Magnetic resonance imaging (MRI), Magnetoencephalography (MEG), Functional Magnetic Resonance Imaging (fMRI), single photon emission computed tomography (SPECT), Positron Emission Tomography (PET), Diffusion Tensor Imaging (DTI), and quantitative electroencephalography (QEEG) have been used for detecting abnormalities in brain functions [6]. However, non-invasive, widely available, and relatively cost effective EEG method is the most commonly used method for examining brain functions [6–9].
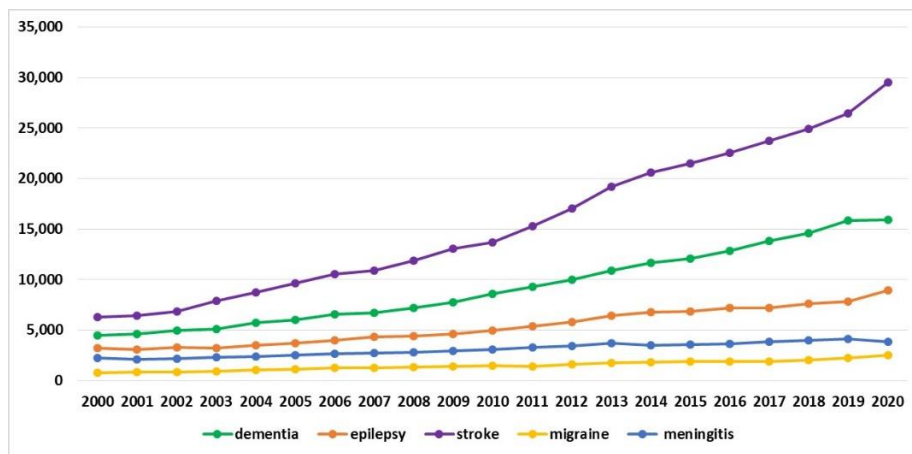
(a)
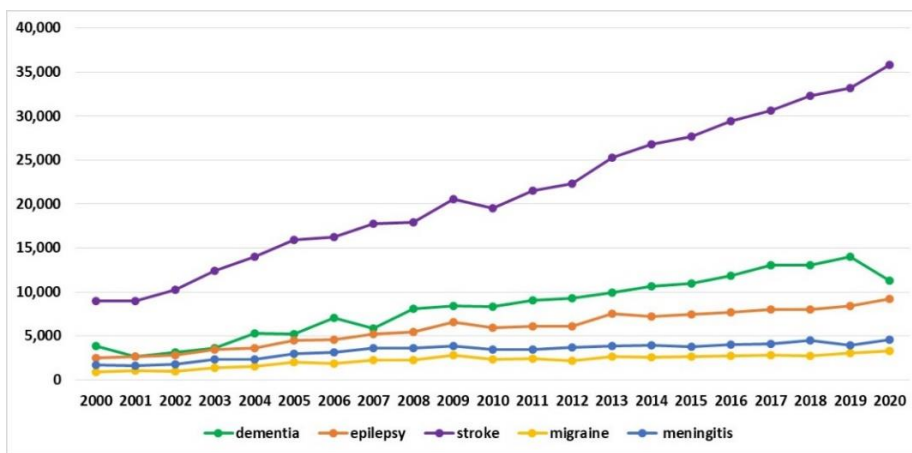
(b)

Figure 1.3: Search results of the 5 neurological disorders on (a) PubMed and (b) Science Direct.

1.1 Objectives of the Thesis

The main purpose of the presented thesis is to achieve high EEG classification successes with advanced signal processing methods for two neurological disorders, epilepsy, and Alzheimer's dementia, which are highly prevalent among all neurological disorders and are frequently studied in the literature. Three different advanced signal analysis methods are utilized for the classification of EEG signals. The EEG segments were investigated using (i) EMD and its derivative EEMD methods, (ii) DMD method, and finally, (iii) SST and traditional STFT methods to achieve high classification performances. The main objectives of the thesis are listed below;

1. Distinguishing of EEG signals by classifying the features extracted from selected IMFs of EMD, or EEMD was performed. Simulations are performed to evaluate the effectiveness of selecting IMFs based on some metrics as opposed to using the first several IMFs for the classification.
2. We investigated whether the recently proposed DMD can be used for the representation and classification of single-channel EEG signals.
3. We aimed to define different features using the DMD spectrum.
4. We propose high-resolution SST method-based feature extraction and classification model for EEG signals.

1.2 Contribution of the Thesis to Literature

Different uses and features from the literature have been proposed for the advanced signal processing methods, and high classification performances have been obtained for EEG signals of both disease types. The innovative contributions of this thesis can be highlighted as follows;

(a) For the EMD and derivative EEMD based approaches;
1. We propose a hybrid IMF selection method considering different approaches such as energy, correlation, power spectral distance, and statistical significance test.

2. We demonstrate the advantages of using selected IMFs by the proposed approaches of either EMD or EEMD as opposed to randomly selecting the first several IMFs.

3. We investigate the performance improvement by using ensemble EMD in the classification of epileptic seizures as compared to traditional EMD, the EEG signal itself, and DWT-based approaches.

(b) For the DMD based approach;

1. We propose a single channel-based DMD algorithm for the analysis of EEG signals. In the literature, multi-channel EEG data are used for the DMD analysis. Here we show that the proposed DMD algorithm can successfully be applied to data recorded from a single channel.

2. The DMD Spectrum provides similar results to Power Spectral Density estimates. However, while different EEG segments are analyzed simultaneously using the DMD algorithm by creating a high dimensional EEG data matrix, these EEG segments must be analyzed separately using the Fourier transform or similar approaches. In contrast to traditional spectral analysis where the frequency content is calculated at uniform frequency samples, the DMD spectrum is calculated only at the mode frequencies of the signal. This is why the DMD spectrum might have more than one power or no power values at some frequencies.

3. We define novel features from the DMD spectrum in this study: higher-order DMD moments, and DMD sub-band powers, and use them in the classification of EEG signals. Thus, we show that a single channel DMD-based approach provides a computationally efficient method for the classification of EEG signals.

(c) For the SST based approach;

1. The magnitude of SST is used for feature extraction. Higher-order joint TF moments, traditional TF features, and Gray Level Co-occurrence Matrix (GLCM) based features are extracted.

2. For the first time, TF moment, various traditional TF features, and GLCM based features are implemented to EEG signals of both epilepsy and Alzheimer's dementia disorders.

3. It has been observed that the SST method, which offers high TF resolution, allows successful classification of EEG signals in various neurological disorders.

2. Background Information and Literature Review

This section contains information about the brain, the main source of neurological diseases, the EEG recording method, frequently used in the clinic and used in our study, epidemiology, clinical course, and literature review of epilepsy and Alzheimers' Dementia.

2.1 The Main Structures and Functions of the Brain

The brain is the highly developed part of the Central Nervous System (CNS). An adult human brain weighs about 1.5 kg and consists of an average of 84 billion neurons and trillions of glial. It receives sensory information from the spinal cord and related nerve, processes this information, and controls the activities of trunks and limbs. It accounts for only 2% of the total body mass but is responsible for 20% of the total energy consumption, as it is responsible for the control of most physiological processes [10–12]. The location of the brain in the nervous system, the three main divisions of the brain, each performing different functions, and the subdivisions of these main parts are summarized in Figure 2.1 [10–13].

The brain is divided into three important parts including the forebrain, midbrain, and hindbrain. The hindbrain is the division of the brain that helps regulate autonomic functions, direct sensory information, regulate movement, and maintain balance. The midbrain is the smallest division of the brain that helps to regulate movement and process auditory and visual information. The forebrain is the division of the brain that processes sensory information, helps reasoning and problem solving, and regulates autonomic, endocrine, and motor functions. The forebrain contains the cerebral cortex, which represents about 75% of the brain's mass and covers most of the other brain structures. The cerebral cortex includes functions such as processing sensory

6

information, controlling motor functions, and executing higher-level functions like thinking and problem solving and have four important lobes (Shown in Figure 2.2) [10–13].
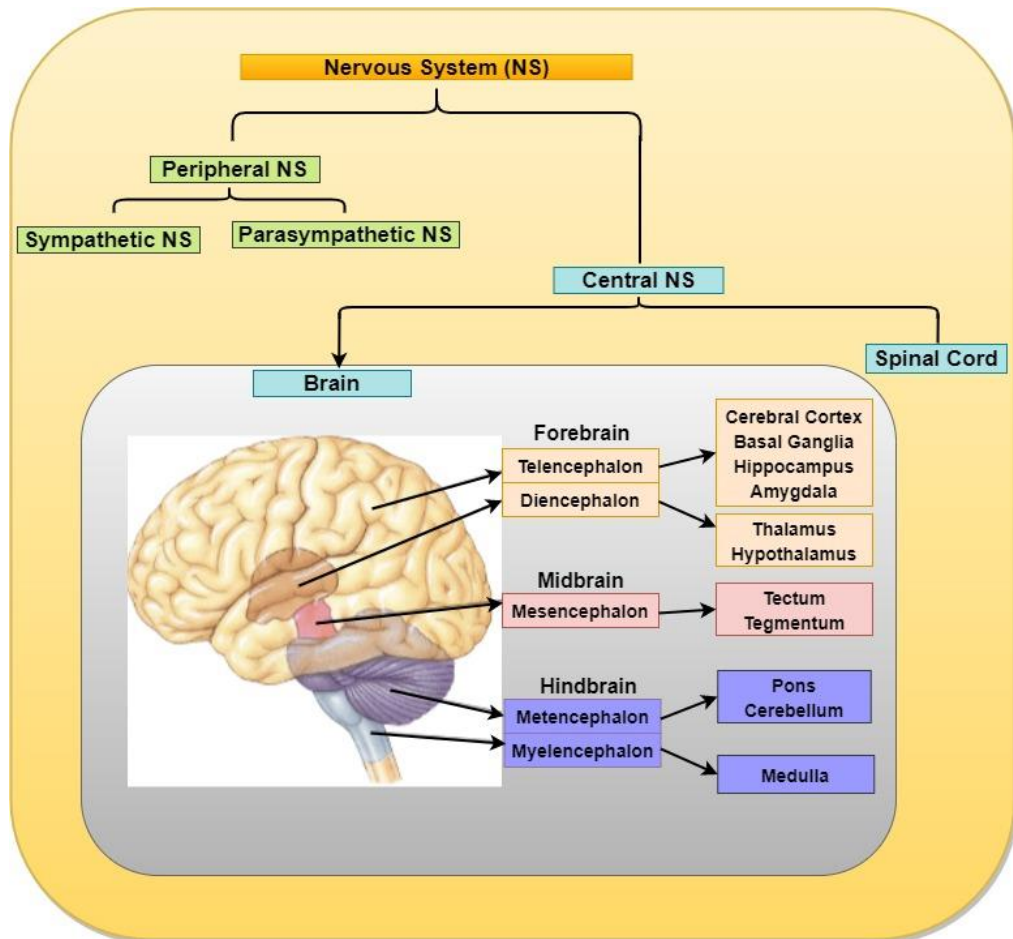
Figure 2.1: Schematic representation of parts of the nervous system.

- **Frontal Lobe:** Responsible for important functions such as motor control of voluntary movements, consideration, judgment, and memory.
- **Parietal lobe:** Responsible for all kinds of sensory functions such as receiving and processing sensory information.
- **Temporal lobe:** Responsible for functions related to hearing sense, balance, and memory.
- **Occipital lobe:** Responsible for functions related to the sense of vision
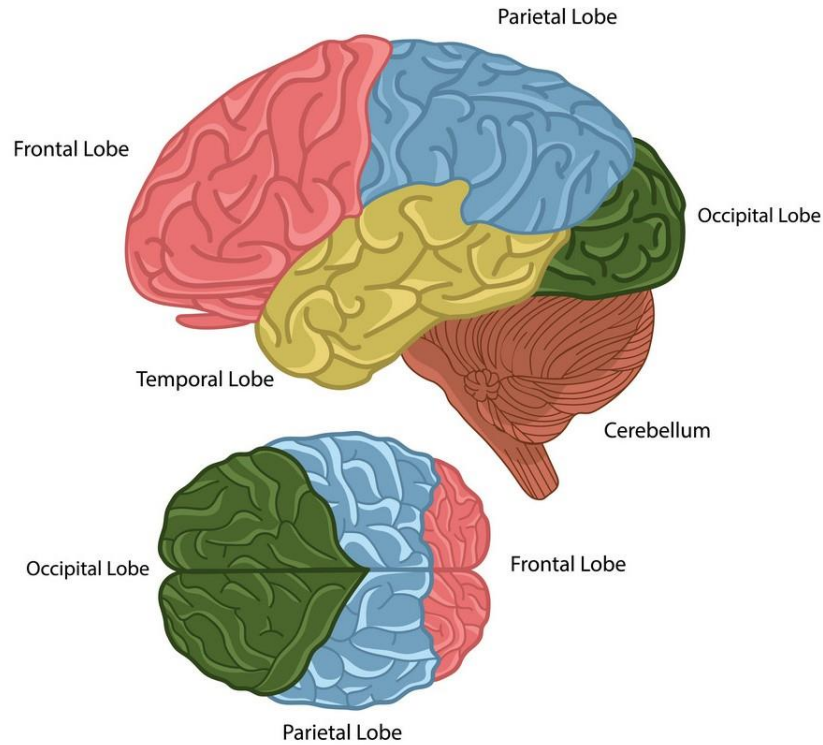
Figure 2.2: The four lobes of the brain.

2.2 EEG

The measurement of the electrical activity resulting from the communication activity of neurons in the brain with electrodes placed on the scalp is called the EEG and the first person to record the electrical field of the human brain was German psychiatrist Hans Berger [14]. The EEG signal has been a valuable clinical tool used to evaluate a variety of neurophysiological conditions. For EEG recordings, electrodes are placed on the surface of the scalp according to the internationally recognized 10-20 electrode placement system as illustrated in Figure 2.3 [14, 15].

The amplitude of a standard EEG signal varies between 0-200µV, while its frequency varies between 0.5-50Hz, and includes different frequency subbands such as delta (δ), theta (θ), alpha (α), beta (β), and gamma (γ). EEG subbands, frequency ranges of corresponding subbands, their characteristics waveforms, and general personal state are summarized in Table 2.1.
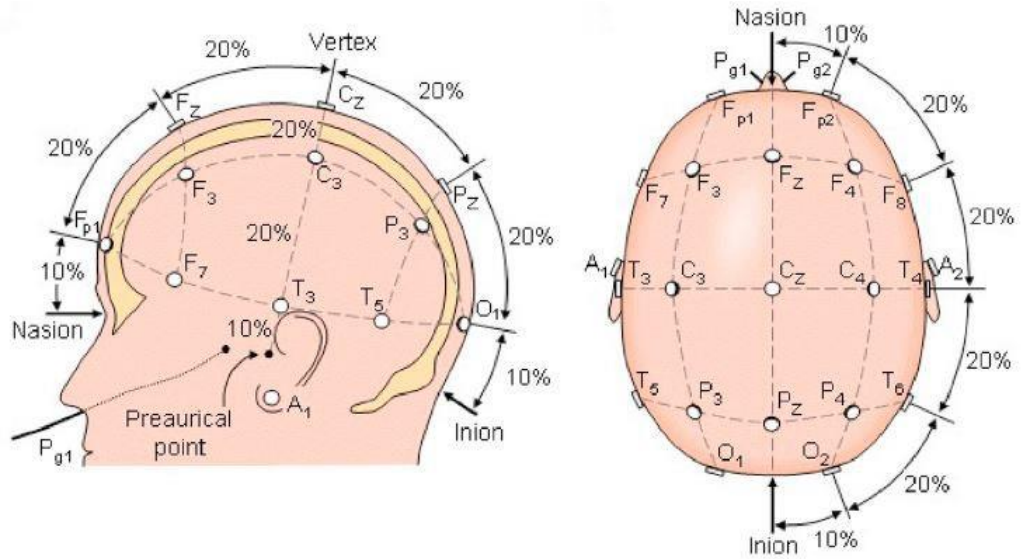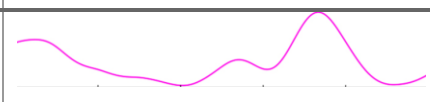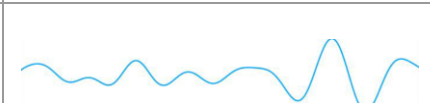
Figure 2.3: Internationally recognized 10-20 electrode placement system [14].

Table 2.1: Description of EEG Subbands [14].

Wave Type	Frequency Range (Hz)	Region of the Brain	Person State	Example Waveform
Delta (δ)	0.5-4	prefrontal orbitofrontal	deep sleep babies	
Theta (θ)	4-8	temporal parietal	Children, sleeping adults REM sleep	
Alpha (α)	8-13	occipital frontal parietal	Awake Eye closed resting state	
Beta (β)	13-30	parietal frontal	mental activations Stress / Anxiety	
Gamma (γ)	> 30	Frontocentral	Whole-brain activity	

2.3 Epilepsy and Literature Review

Epilepsy is a neurological disease caused by the excessive and instant electrical discharge of the neurons. This disease affects millions of people worldwide, regardless of gender, age or social status. In the most general sense, epilepsy is a neurological disease that meets one or more of the following conditions; (1) at least two uncaused, non-stimulated (or reflex) seizures that occur more than 24 hours interval, (2) possibility of having an additional seizure similar to the overall risk of relapse (at least 60%) after an uncaused (or reflex) seizure and two uncaused seizures within the next ten years, (3) an epilepsy syndrome diagnosis [16, 17]. According to data from the WHO in 2005, there existed at least 50 million people with epilepsy. Until the 19th century, it was believed that epilepsy was caused by vascular problems [2].

2.3.1 Epidemiology and Clinical Course of Epilepsy

According to WHO, while the overall incidence of epilepsy varies from 0.27% to 5% worldwide, the proportion of patients with active epilepsy varies from 0.4% to 0.8%, which is lower in industrialized countries than in developing countries. The incidence of epilepsy in the second and third decade of life tends to be higher, and moreover, the incidence of epilepsy is higher in men than in women [2].

Due to the large number of seizure types and epilepsy, a single etiology and consequence cannot be determined. The simplest classification according to the types of seizures and epilepsy and the factors causing the disease is given in Figure 2.4. The initial stage of seizure classification is establishing whether the first sign of any seizure is generalized or focal. Seizures are called focal onset seizures if they have focal onset, and are called generalized onset seizures if they have a generalized onset. If the onsets of the seizures are unclear or cannot be detected for any reason, they are classified as unknown onset seizures. Another classification is conducted according to the type of epilepsy. Here, persons with generalized epilepsies can have various seizure types, with the inclusion of absence, myoclonic, atonic, tonic, and tonic-clonic seizures, and generalized spike-wave activity is observed on their EEGs. In another epilepsy type, Focal epilepsy, people may have unifocal disorders as well as multifocal disorders, and these disorders may even cover an entire hemisphere. If the person has both

generalized and focal seizures, the epilepsy type is classified as a combination of generalized and focal epilepsy. Additionally, epilepsy is classified as unknown epilepsy in cases where the patient is diagnosed with epilepsy by experts but the type of epilepsy cannot be detected because of various reasons. Although there is no classical epilepsy syndrome classification, the most common epilepsy syndromes are Childhood absence epilepsy, West syndrome, Dravet syndrome. In addition to correctly classifying the type of epilepsy and seizure, it is important to know the cause of the disease for correct treatment. While, epilepsy may have many causes such as structural, genetic, infectious, metabolic, and immune-related causes, it may also be due to an unknown cause. On the other hand, epilepsy can be seen as a single disease in the person, as well as in most cases, one or more diseases such as learning, behavioral and psychological problems may accompany epilepsy (comorbilities) [16, 17].
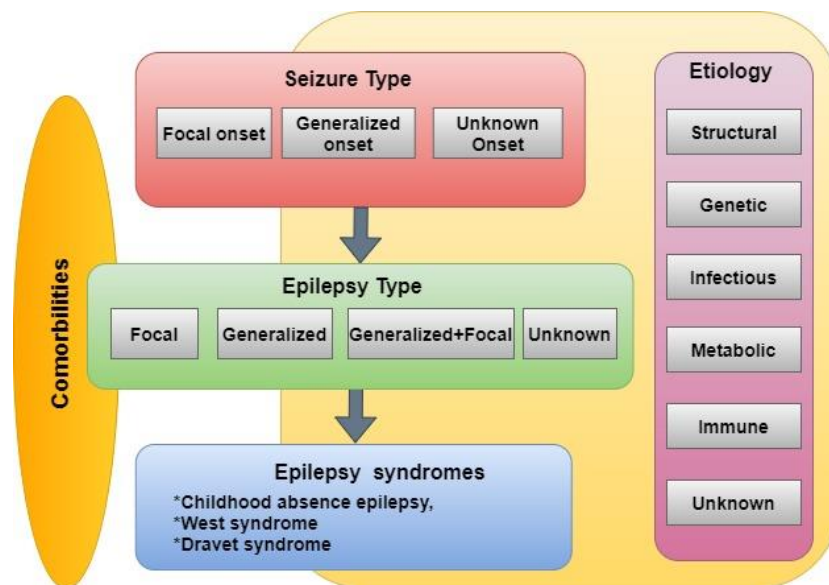
Figure 2.4: The simplest block diagram of the seizure and epilepsy classification [16, 17].

2.3.2 Literature Review

Detection of epileptic seizures is performed by neurologists by a visual examination of longterm EEG signals. However, this method is very time consuming and generally yields incorrect results. On the other hand, epileptic seizures are initiated in different brain lobes of different individuals, so it is not possible to determine a standard focus

center for the studies. Therefore long-term EEG recordings are needed to detect epileptic seizures and determine focus center [18–21]. Since visual examination of long-term EEG data makes it difficult to diagnose the disease, automatic seizure detection has become a very popular research area and various signal processing methods have been applied to solve this problem [18, 21, and 22].

Epileptic seizure detection and classification studies have been reported frequently in the literature using various signal processing and classification methods. Variety of features such as temporal, spectral, statistical and nonlinear features are exploited to improve the detection and classification performance.

Several methods have been presented for the detection and classification of seizure and seizurefree EEG segments by using time and frequency domain features such as energy [23], exponential energy [24], matrix determinant [18], spectral power of Hjorth's mobility components [25], crosscorrelation, power spectral density [26], subband spectral powers [27], average value, maximum value, and minimum value [21]. Weighted multiscale Renyi permutation entropy (WMRPE), Weighted Permutation Entropy (WPE), fuzzy entropy (FuzzyEn), a sigmoid entropy, approximate entropy (ApEn) based methods have also been frequently applied to this problem [28–30]. Additionally, non-linear parameters such as fractal dimension, scaling exponent obtained with detrended fluctuation analysis (DFA), Hurst's exponent have been utilized in many studies and successful results have been obtained for the detection and classification of seizure and seizure free epileptic EEG signals [31, 32].

One of the most employed methods for the analysis is the Fourier Transform (FT) which generates spectral features. However, FT assumes that the signal to be analysed is stationary which is not the case; like most of the real-world signals, EEG signals are non-stationary. Another drawback of the FT is that it does not contain any time information [33]. Thus other methods have been developed based on time-frequency representations such as Short-Time Fourier Transform (STFT) which analyzes the local characteristics of a signal by using a window. However, since STFT utilizes only one filter, time and frequency resolutions of the resulting TF representation cannot be increased simultaneously. Wavelet Transform (WT) introduces a multiresolution analysis utilizing several filters with different bandwidths to overcome this problem [34]. In WT, a window containing all the signal to extract low frequencies is used

which produces good time resolution, then it is translated and scaled to extract higher frequency information which produces good frequency resolution [35]. Unfortunately, despite these advantages, WT fails to provide simultaneously improved time and frequency resolutions. In order to overcome these problems, Empirical Mode Decomposition (EMD) algorithm was developed to analyze non-stationary and non-linear signals [36]. EMD is a data-driven approach which decomposes the signal into a finite number of oscillations called Intrinsic Mode Functions (IMFs) that are not predefined basis functions, but satisfying the following criteria: (i) Number of extrema and number of zero-crossings must be equal or differ at most by one. (ii) At any point, the mean of the envelope defined by local maxima and the envelope defined by the local minima is zero. The advantages of EMD are that scales are adaptive, separation of oscillation is data-driven and multi-resolution analysis is local, unlike WT which analyze the signal globally and based on pre-determined scales of filters [15].

Signal decompositions such as WT, STFT, EMD and derivatives, variational mode decomposition (VMD), singular value decomposition (SVD), synchrosqueezing transform (SST), and their variants have been successfully applied in classification and prediction problems [15, 35, 37–47].

Bajaj and Pachori used the EMD method, and calculated amplitude- and frequency-modulation bandwidths using Hilbert Transform (HT) of the IMFs. They differentiated seizure and nonseizure EEG signals using Support Vector Machine (SVM) classifier with Morlet kernel function and concluded that the proposed method can be used for the detection of epilepsy and for the analysis of non-stationary signals [15]. In 2017, Alickovic et al. investigated the performances of EMD, Discrete WT (DWT) and Wavelet Packed Decomposition (WPD) for epileptic seizure classification. Wu et al. introduced the complete ensemble empirical mode decomposition (CEEMD) method and Extreme Gradient Boosting (XGBoost) based seizure detection approach, and promising classification performance was achieved for seizure detection [40]. In 2019, Kumar et al. presented a VMD and semantic feature-based epileptic seizure detection approach [41]. In another work [48], the STFT and several other Time-Frequency (TF) distributions were employed to obtain the energy distribution of epileptic EEG signals. In a different approach [32], the analytic time-frequency flexible wavelet transform (ATFFWT) and fractal dimension (FD) were used to detect epileptic seizures

automatically. The direction of the energy of the signal in the TF field was used as a feature in another study to classify seizure and non-seizure EEG segments. The Wigner–Ville distribution (WVD) was utilized to obtain TF distribution [23]. In another seizure detection study [49], EEG signals were mapped into two-dimensional space, and texture images were obtained to distinguish seizure and seizure-free events. Using the GLCM, various texture features were obtained. In another study [50], TF images of EEG signals were obtained using continuous WT (CWT), and features are extracted from Gaussian Mixture Model (GMM) and GLCM. In a recent seizure detection study [51], CWT, DWT, higherorder spectra (HOS), GLCM, run-length matrix, fractal features, and local binary pattern based features are presented with outstanding performance. A new TF representation method called SST, is recently proposed by using reassignment of the TF coefficients into the instantaneous frequency trajectory to approximate the ideal TF distribution. Using STFT or CWT as initial TFR, SST provides a highly localized TF representations for multi-component non-stationary signals that is not usually possible with other TF analysis methods [52–57]. In a recent study, the STFT (Fourier) based synchrosqueezed transform (FSST) was applied to the classification of seizure and seizure-free EEG signals using Bonn University data set. In this approach, the magnitudes of FSST were calculated and used to obtain 5 non-overlapping frequency sub-bands for each EEG signal. GLCM features of the five subbands were calculated and classified [57].

In [58], authors proposed a method for the detection of epileptic seizures using Dynamic mode decomposition (DMD). They calculated DMD powers by using augmentation and applied thresholding for feature reduction. The clustering of the DMD powers by frequency along with normalization was performed. Curve lengths of time-domain EEG signals were calculated as features. RUSBoost approach was adopted for classification. It was concluded that DMD is capable of differentiating seizure and non-seizure EEG signals. Using multi-resolution dynamic mode decomposition (MRDMD), seizure detection approach was conducted in another study [59]. The power of DMD modes and temporal features of EEG signals were used as features. Two different feature sets were obtained by combining temporal features with either DMD mode powers, or MRDMD mode powers to compare the performances of DMD and MRDMD methods.

After a brief investigation, it may be observed that successful classification results have been obtained by using classification algorithms such as SVM [21, 28–30, 32], Artificial Neural Networks (ANN) [14, 60, and 61], K-Nearest Neighbor (kNN) algorithm [62], Extreme Learning Machine (ELM) [22, 31], Multilayer Perceptron Neural Network (MLPNN) [63], etc. In addition to above machine learning based classification studies, deep learning (DL) approaches have been successfully utilized for seizure detection and classification in recent studies [64–67].

2.4 Dementia and Literature Review

Dementia is one of the most common neurological disorders in which the person suffers from the defection of cognitive functions that can affect daily life and activities, resulting from physical changes in the brain. These cognitive dysfunctions consist of multiple dysfunctions, including memory, learning capacity, language, orientation, comprehension, thinking, calculation, and reasoning.

2.4.1 Epidemiology and Clinical Course of Dementia

According to WHO, 24.3 million people suffer from dementia at the present time, and it is considered that the number of dementia patients will be 81.1 million by 2040. Approximately 2% of all dementia cases are seen before the age of 65, but the disease usually begins at an older age [2, 68, and 73]. There are many risk factors that increase or decrease an individual's likelihood of developing dementia. The incidence of dementia doubles every 5 years between the ages of 65 to 85. Therefore, age is one of the biggest risk factors for dementia. Gender is an important risk factor for dementia, and the incidence of different types of dementia in men and women varies [2, 68]. In addition, the likelihood of developing disease is closely related to genetic factors, and depression is another risk factor for dementia. There are vascular risk factors such as blood pressure and diabetes, as well as stroke and heart diseases are important disorders that cause dementia. Excessive smoking and alcohol use are also some of the factors that increase the likelihood of dementia, which is linked to lifestyle [68, 69].

Main causes of dementia

Alzheimer's disease

- The most common type of dementia
- There is an unusual deposition of amyloid plaques in the brain
- Common symptoms;
  - memory loss
  - word-finding difficulties
  - language difficulties
  - anxiety
  - lack of motivation
  - change of mood and personality

Vascular dementia

- The second most common type of dementia
- The interruption of the brain's oxygenated blood supply for any reason (stroke) may cause it.
- Common symptoms;
  - memory and language difficulties
  - slowing of cognitive processes
  - walking problems
  - depression
  - anxiety
  - apathy

Dementia with Lewy bodies

- The third most common type of dementia
- It is characterized by the formation of small aggregations of a protein called alpha-synuclein in cells in various parts of the brain.
- Common symptoms;
  - memory loss
  - alertness difficulty
  - planning difficulty
  - trembling in limbs
  - walking problem
  - reduced facial expression
  - visual hallucinations
  - recurrent falls
  - fluctuations of conscious awareness levels
  - uncomfortable sleep and nightmare

Frontotemporal dementia

- The uncommon type of dementia
- It is caused by cell damage in frontal or temporal regions of the brain
- Common symptoms;
  - behavioral and personality changes
  - speech and language problems
  - change of eating habits
  - problems of movement

Mixed dementia

- There are more than one type of dementia, usually Alzheimer's and vascular dementias.
- It is common in older ages, especially over the age of 80.

Parkinson's Disease Dementia

- It is a type of dementia seen in people with Parkinson's disease.
- Its symptoms are very similar to those of Dementia with Lewy bodies

Less Common couses of Dementia

- Huntington's disease
- Corticobasal degeneration
- Creutzfeldt-Jacob disease
- Multiple sclerosis
- Normal-pressure hydrocephalus
- Human immunodeficiency virus-related dementia

Figure 2.5: The most common causes of dementia [68–72].

Figure 2.6: Sypmtoms of dementia in different stages [2, 70, and 71].

Dementia is a clinical syndrome that consists of a combination of symptoms and other characteristics that coexist and form a recognized model, so it is not a disease by itself. There are several causes of this syndrome, some of which are more common than others. This syndrome can occur differently in everyone, and symptoms related to the disease can be grouped into three stages named early, middle, and late stage [2]. In Figure 2.5 and Figure 2.6, the most common causes of dementia and stages of dementia are summarized, respectively [2, 68–72].

Within the scope of this thesis, the EEG data of early-stage Alzheimer's Dementia (AD) were studied. AD is the most common type of Dementia, accounting for approximately 50-75% of all Dementia after the age of 65, and it is the most common cause of death compared to other dementia syndromes [68, 70–72]. While the risk of developing AD is 20% for women and 10% for men around the age of 45, the risk of developing AD increases for both gender groups after the age of 65 [71]. The protein fragment beta-amyloid accumulation outside of neurons and the accumulation of an abnormal form of tau protein within neurons is two of the most known brain changes associated with AD [68, 70, and 71]. Additionally, symptoms associated with AD are summarized in Figure 2.5.

2.4.2 Literature Review

The diagnosis of Alzheimer's disease and the follow-up of the response to treatment can be conducted by many medical methods. MRI, Computer Tomography (CT), and recording of the electrical activity of the brain with Electroencephalography are performed together with the general neurological and physical examination. In recent years, due to its low cost and being a non-invasive diagnosis method, EEG has started to attract great scientific attention and various researchers have focused on analyzing the EEG records of AD patients in order to follow changes such as complexity, synchronization, and regularity of EEG activity. EEG recording method has been a frequently used method not only for the detection of the disease but also for the follow-up of the treatment and the determination of the response of the patients to the treatment [74, 75]. In the literature, there are many studies that have been carried out using the EEG recording method, which is frequently used during the diagnosis of AD and follow-up of the treatment, and remarkable results have been reported.

Automatic EEG classification studies for dementia patients have been conducted using EEG sub-bands (δ, θ, α, β, and γ) and relative sub-bands powers were computed as features [74, 76–78]. In these studies, it was reported that δ and θ relative band powers of AD patients increased and α, β, and and γ relative band powers decreased. Tzimourta et al. [74] proposed the automated Alzheimer's Disease detection study in which several statistical and spectral features were calculated using EEG signals of AD patients and healthy controls (14 AD patients, 10 healthy subjects). Considering the different EEG segment lengths (ranging from 5 to 12 s) and different brain regions, features were calculated for both the entire time domain EEG segment and their 5 subbands. It was stated that the best performance for 5 different brain regions and for all classification problems evaluated was obtained using the Random Forest classifier with 12 s segment long (ACC: 88.79% to 96.78%, the highest performance was achieved in the CN/moderate AD classification problem.). Cassani et al. [79] used three different automated artifact removal (AAR) algorithms before the EEG feature extraction process to achieve higher AD detection performance. EEG signals of 20 mild AD patients, 15 moderate AD patients, and 24 healthy control subjects were evaluated. Various features such as spectral power, magnitude square coherence, phase coherence/synchrony, and EEG amplitude modulation rate-of-change were calculated

18

to create the feature set. In the result of the study, a maximum of 89% AD detection performance is indicated. In another AD detection study, EEG amplitude modulation rate-of-change is calculated as features for each EEG sub-bands. EEG signals of 11 healthy subjects, 11 mild AD, and 10 moderate AD patients were investigated for this research. It is reported that compared with the benchmark parameters, this study yields a higher accuracy gain [80]. Another AD detection approach was introduced in which three different feature sets named spectral, wavelet, and complexity-based feature sets were utilized by Kulkarni et al [81]. In this study, EEG recordings of 50 AD patients and 50 healthy subjects were evaluated. To construct the spectral-based feature set, relative EEG sub-band powers were calculated for each EEG sub-band; similarly to achieve the wavelet-based feature set, mean and variance values were calculated for each wavelet coefficient obtained using 5 decomposition levels. Additionally, to achieve the complexity-based feature set, Spectral entropy, Spectral centroid, Spectral roll-off, and Zero crossing rate were computed for each EEG segment. The highest classification accuracy of 96% with SVM classifier was obtained using the complexity-based feature set.

Many studies have also been conducted to measure brain complexity using EEG signals. Various entropy values such as Approximate Entropy [74, 77, and 82], Permutation Entropy [78, 82], Sample Entropy [76, 78], Tsallis Entropy [76], Spectral Entropy [83], multiscale entropy [84], and Multivariate Multiscale Weighted Permutation Entropy [85]; and various nonlinear features such as correlation dimension [86], Higuchi Fractal Dimension [83, 87, and 88], Lyapunov Exponent [86], and the Lempel – Ziv Complexity [89, 90] value were often calculated in literature. In all of these studies, it was emphasized that there was a decrease in brain complexity in AD patients compared to the control group, and promising results have been provided. Two different non-linear methods such as Lempel–Ziv (LZ) complexity which is the non-parametric metric of the one-dimensional signal's complexity and computation of the central tendency metric (CTM) that summarizes the degree of variability in the signal, were used in another AD detection research (EEG recordings of 11 AD patients and 11 healthy subjects were used) [89]. In the consequence of the study, it was reported that 90.9% sensitivity and 72.7% specificity values were obtained. In study [90], the calculation of the distance-based Lempel–Ziv complexity (dLZC) metric, which could be used to analyze non-linear signals, was

performed to achieve distinctive information between EEG signals of healthy subjects and AD patients. In this study, EEG signals of 11 healthy subjects and 11 AD patients were analyzed and it is reported that lower dLZC values for AD patients were achieved than that of healthy subjects in the most electrode pairs. The maximum distinguish accuracies of 77.27% and 78.25% were obtained for subject-based and epoch-based classification methods, respectively. On the other hand, various synchronization parameters such as Random event synchronization, Granger causality, State-Space based synchronization, and amplitude and phase correlation were also calculated for the analysis of brain synchronization of AD patients [91].

In addition to calculating various features from EEG signals or EEG sub-bands, different decomposition methods have also been used for the analysis of AD patients' EEG data. Various signal decomposition approaches including DWT, and EMD, and different classifiers were utilized to distinguish EEG signals of healthy, mild AD, and moderate AD subjects [92]. For this purpose, EEG signals of 35 healthy, 31 mild AD, and 20 moderate AD subjects were investigated. Different wavelet families were used for the DWT method and for each of them, number of decomposition level was chosen as 6. For the EMD method, the first 5 obtained IMFs were evaluated. Lots of features such as skewness, kurtosis, Shannon entropy, sure entropy, and Hjorth parameters were calculated for each case. Both K-fold cross-validation and leave-one-subject-out (LOSO) cross-validation methods were utilized and Daubechies type 4 (db4) wavelet of DWT yielded the highest classification performance (97.64%) using the kNN classifier for k-fold cross-validation. In study [93], spectral features and DWT features were calculated using EEG signals to distinguish healthy and Alzheimer's subjects. EEG signals of 50 healthy and 50 Alzheimer's subjects were recorded and evaluated. Relative band powers were calculated as spectral features. Using Daubechies wavelet and 5 decomposition levels, DWT coefficients were obtained, and the mean and variance of each DWT coefficient were calculated as DWT features. In the result of the study, it is mentioned that by using the combination of two feature sets, 94% classification accuracy was obtained. In another study [94], various analyses were conducted by means of the combined use of ANN, GA, and DWT to determine the degree of cognitive impairment and promising results have been obtained.

3. Materials and Methods

In this section, advanced signal processing methods utilized for signal analysis, and classification algorithms used for classification stages of proposed approaches are introduced.

3.1 Advanced Signal Decomposition Methods

In this thesis, three different advanced signal analysis methods are utilized for the classification of EEG signals. The pre-seizure and seizure EEG segments are investigated using (i) EMD and its derivative EEMD methods, (ii) DMD method, and finally, (iii) SST and traditional STFT methods to achieve high classification performances.

3.1.1 Empirical Mode Decomposition and its Variant

We applied the EMD and Ensemble EMD methods for the analysis of EEG signals in our study. In the following, we present a brief introduction to these decomposition methods.

3.1.1.1 Empirical Mode Decomposition

Empirical Mode Decomposition which produces a collection of IMFs with zero-mean oscillations, is used as an adaptive time-frequency signal analysis method. In non-linear and non-stationary processes, it is applied as a feature extraction and noise reduction method in signal processing applications. It is the most important rule of the EMD method that the sum of these obtained IMFs give the original signal. It is essential for the IMF to satisfy two conditions: (1) the number of zero crossing and extrema should be equal or should differ at most by one, (2) the mean value of the

upper and lower envelopes should be zero. The process of the EMD algorithm is to extract IMF, also called Sifting, can be performed as shown in **Algorithm 1** [14, 95].

Algorithm 1: EMD

1. Local minima Lm_i, $i = 1, 2, ...$ and Local maxima Lx_j, $j = 1, 2, ...$ are found using input signal $x[n]$.

2. Calculate $Ue[n]$ and $Le[n]$ which upper and lower envelopes respectively, using cubic interpolation.
3. Mean of envelopes value is found.

$$Me[n] = (Ue[n] - Le[n])/2$$

4. Compute $d_1[n] = x[n] - Me[n]$. If $d_1[n]$ satisfies the condition of IMF,

   $d_1[n] = IMF_1[n]$. Else go to step 1 and repeat every processes using $d_1[n]$ instead of $x[n]$.

5. After obtaining $IMF_1[n]$ calculate the residue $R_1[n] = x[n] - IMF_1[n]$. If this residue has more than a zero-crossing, return step 1 and calculate again new IMF.

   This process will continue until last residue $R_L[n]$, which has no zero crossing is obtained and all necessary conditions are satisfied.

   We can reconstruct the original signal $x[n]$ using the following formulation:

$$x[n] = \left(\sum_{l=1}^{L} IMF_l[n] \right) + R_L[n]$$

   Here, L is the number of $IMFs$ and $R_L[n]$ is the residue.

3.1.1.2 Ensemble Empirical Mode Decomposition

Although the standard EMD algorithm provides successful results in signal processing applications as a time-frequency analysis method, it suffer from a problem called "mode mixing". The problem of mode mixing can be described as the occurrence of very different oscillations in one mode, or very similar oscillations in different modes. The Ensemble EMD method has been developed to overcome this problem. In the EEMD method, Gaussian white noise is added to the signal to be analyzed and the signal is decomposed into the IMF using the EMD method. Due to the statistical properties of Gaussian white noise, the continuity of the signal is obtained in different

frequency regions, so that the problem of mode mixing is reduced. The process of the EEMD algorithm is demonstrated in **Algorithm 2** [96].

Algorithm 2: EEMD

---

1. Gaussian white noise with different mean and variance is added to the analyzed signal.

$$x_i[n] = x[n] + g_i[n] \quad i = 1, 2, \dots, K.$$

   Here, K is the number of ensemble, $x[n]$ is the original signal, and $g_i[n]$ is the Gaussian noise added at ith i^{th} iteration.

2. From the noise added signal $x_i[n]$, the Intrinsic Mode Functions $(IMFs)$ $IMF_j^{\ i}[n], j = 1, 2, \dots, J^i$ of the ith iteration are obtained by the EMD algorithm. Here J^i is the number of $IMFs$ at i^{th} iteration.

3. After K iteration, the means $\overline{IMF_j[n]}$ are obtained.

$$\overline{IMF_j[n]} = \frac{1}{K} \sum_{i=1}^{K} IMF_j^{\ i}[n]$$

3.1.2   Dynamic Mode Decomposition

Most of the real-world signals are observed from non-linear and dynamic systems, and the behavior of these processes may not be revealed by using traditional time or frequency domain methods. In DMD, measurements that are collected over a certain time interval are used for generalizing and expressing the process with a function, and also being able to predict the behavior of the system at a future point in time. Basic idea is to linearize the system with the Least-Squares Approximation (LSA), and obtain the eigenvalues and eigenvectors of the system to construct the dynamic modes which represent the observed signal. The algorithm constructs an original matrix whose columns are time snapshots, and time shifted versions of it. Afterwards, DMD obtains the best matrix that can linearly transform the current state of the system to the next state which can be calculated with least squares regression [97]. In recent studies, DMD algorithm has been used to analyze neural recordings and successful results have been obtained [58, 97–100].

EEG signals recorded from a single channel are represented by $T-$samples long data vectors. In DMD algorithm, $N \times M -$ data matrices are processed. In order to obtain $N \times M$ size data matrix from EEG channels, M samples long EEG data recorded from N different channels are previously used [58]. Here N represents the number of used EEG segments and M represents the time samples called "snapshot".

In order to extract sufficient number of modes and to precisely capture the dynamics of neurological activity, the number of measurements (N) must be at least twice the number of time points M, called snapshots [101]. As such, an augmented data matrix X_{Aug} of size ($K \times L$) is obtained by applying a data augmentation process to the data matrix X. The augmentation process is based on the principle of creating the Hankel matrix specified in [98, 102]. In our experiments, we use $K = 200$ and $L = 100$ for the dimensions of the augmented matrix.

Using the augmented EEG data matrix, two $K \times (L-1)$ new EEG data matrices X_{aug} and X'_{aug} given in Equation (3.1) can be constructed. Here, X'_{aug} is the Δt shifted version of X_{aug} in time.

$$X_{aug} = \begin{bmatrix} \vdots & \vdots & \cdots & \vdots \\ x_1 & x_2 & \cdots & x_{L-1} \\ \vdots & \vdots & \cdots & \vdots \end{bmatrix} \quad X'_{aug} = \begin{bmatrix} \vdots & \vdots & \cdots & \vdots \\ x_2 & x_3 & \cdots & x_L \\ \vdots & \vdots & \cdots & \vdots \end{bmatrix} \qquad (3.1)$$

$$X'_{aug} = A \times X_{aug} \qquad (3.2)$$

DMD works with the A matrix given in Equation (3.2), which best maps the original X_{aug} matrix and its time-shifted version $X'_{aug.}$ To determine a high-dimensional linear regression-based relation between data matrix pair X_{aug} and X'_{aug}, this transition matrix A should be estimated. Using the eigen-decomposition of A, dynamic mode decomposition of the data matrix pair X_{aug} and X'_{aug} is estimated. One possible approach to obtain the transition matrix A is to compute the pseudo-inverse of X_{aug}. However, as in the case of high-dimensional data such as neural recordings, this will cause computational confusion. By using the DMD algorithm, introduced in **Algorithm 3**, low-rank approximation $\tilde{A}$ of A, and its eigen-decomposition may be calculated [58, 97, 98, and 102].

Algorithm 3: **DMD** [58, 97, and 98]

---

1. Calculate the Singular Value Decomposition of augmented EEG data matrix $X_{aug} = U\sum V^*$ explained in Section 3.1.2, and rewrite Equation (3.2);

$$X'_{aug} = AU\sum V^*$$

2. Define $\tilde{A}$;

$$A = X'_{aug}X^+_{aug} = X'_{aug}V\sum^{-1}U^*$$
$$\tilde{A} = U^*AU$$

$$\tilde{A} = U^*X'_{aug}V\sum^{-1}U^*U$$

$$\tilde{A} = U^*X'_{aug}V\sum^{-1}$$

   Here, U is the matrix of Left singular vectors, $\sum^{-1}$ is the inverse of the singular values, V is the matrix of Right singular vectors, and $\tilde{A}$ denotes the approximate value of the transition matrix A.

3. Calculate the eigendecomposition of $\tilde{A}$;

$$\tilde{A}W = W\Omega$$

   Here, W is the matrix of eigenvectors, Ω is the diagonal matrix of eigenvalues λ_m which are the eigenvalues of DMD modes.

4. Calculate the DMD modes of augmented EEG data matrix X_{aug}.

$$\Phi = X'_{aug}V\sum^{-1}W$$

   Each column of Φ contains the DMD mode Φ_m extracted from the augmented EEG data matrix matching to eigenvalues λ_m.

3.1.3   Synchrosqueezing Transform

In this study, STFT based SST are utilized to obtain the joint TFR of EEG segments. STFT is a traditional method which relies on short-time processing of non-stationary signals to capture the time-varying frequency content. STFT uses a sliding window to divide the signal into short-time and usually overlapping segments. Fourier transforms of the short-time segments are calculated and process is repeated until the whole signal is covered by windowing. Parameters used in windowing such as window type, length,

and amount of overlapping affect the resolution of the resulting STFT [48, 103]. Magnitude square of the STFT is referred to as the "Spectrogram" and widely used to estimate how the energy of a signal is distributed over joint TF plane.

$$X(t, \omega) = \int_{-\infty}^{\infty} x(\tau)\omega(\tau - t)e^{-j\omega\tau}d\tau \tag{3.3}$$

where $x(t)$ is the analyzed signal, $\omega(t)$ is the window function, and $X(t, \omega)$ is the STFT.

STFT of a given signal $x(t)$ and a selected window function $\omega(t)$ may also be formulated using their Fourier transforms $X(\omega)$ and $W(\omega)$ by,

$$X(t, \omega) = \frac{1}{2\pi}\int_{-\infty}^{\infty} X(\varphi)W(\omega - \varphi)e^{j\varphi\tau}d\varphi \tag{3.4}$$

Spectrogram of the signal is defined by,

$$S_{SP}(t, \omega) = |X(t, \omega)|^2 \tag{3.5}$$

Synchrosqueezing Transform that belongs to the family of TF reassignment methods (RM) initially developed to analyze the audio signals [52, 53, 104, and 105]. RM and SST were developed to enhance the localization properties of TFRs. Using the reassignment or squeezing process, the TF coefficients of conventional TF analysis approaches approximate the instantaneous frequency (IF) trajectory close to the ideal TFR. SST and RM map the TF coefficients "$X(t, \omega)$" calculated by another TF analysis method according to below procedure;

$$RM: (t, \omega) \rightarrow \big(\tau_0(t, \omega), \omega_0(t, \omega)\big)$$
$$SST: (t, \omega) \rightarrow (t, \omega_0(t, \omega)) \tag{3.6}$$

Here, $\omega_0(t, \omega)$ is the approximation of the instantaneous frequency and $\tau_0(t, \omega)$ is the approximation of the group delay [54].

While high resolution in both time and frequency may be achieved with the RM method by reassigning the spectrogram into the IF trajectory, signal reconstruction is not possible. On the other hand, by squeezing the TF coefficients into the IF trajectory, resolution only in the frequency direction can be obtained with SST. Additionally, signal reconstruction may be achieved using SST, but TF resolution is lower than RM [54, 106]. SST method can be used to obtain TF representation of signals in complex systems based on continuous wavelet transform or Short-Time Fourier Transform. In our proposed study, the STFT based SST is utilized to analyze EEG segments. The energy concentration of $x(t)$ in the joint TF plane is improved by the squeezing procedure in the SST method. The IF information required in SST is obtained from the derivative of the STFT. Using the estimated IF information, the STFT coefficients that have the same frequency are collected where they should appear [54, 57, and 106]. The steps of SST are given in **Algorithm 4.**

Algorithm 4: **SST**

---

1. Let $x(u)$ be the EEG segment to be analyzed and $\omega(u - t)$ is the shifted window function. SST process starts by taking the STFT. Using the Fourier Transforms of analyzed signal $(X(\varphi))$ and window function $(W(\omega - \varphi))$, STFT $X(t, \omega)$ is obtained.

$$X(t, \omega) = \frac{1}{2\pi} \int_{-\infty}^{\infty} X(\varphi) W(\omega - \varphi) e^{j\varphi\tau} d\varphi$$

2. In order to obtain the IF $\omega_0(t, \omega)$ from STFT, the derivative of $X(t, \omega)$ is calculated with respect to time.

$$\omega_0(t, \omega) = -j \frac{1}{X(t, \omega)} \frac{\partial X(t, \omega)}{\partial t}$$

3. By using instantaneous frequency $\omega_0(t, \omega)$, STFT coefficients that have the same frequency are collected where they should appear. The SST $T(t, \eta)$ is formulated by using synchrosqueezing operator $\int_{-\infty}^{\infty} \delta(\eta - \omega_0(t, \omega)) d\omega$.

$$T(t, \eta) = \int_{-\infty}^{\infty} X(t, \omega) \delta(\eta - \omega_0(t, \omega)) d\omega.$$

3.2   Classification and Performance Evaluation

3.2.1 Classification

In the proposed thesis, features extracted utilizing the three different approaches are classified using six different classifiers such as Decision Tree (DT), Logistic Regression (LR), Naïve Bayes (NB), kNN, SVM, Random Forest (RF), Boosted Trees (BT), and Subspace kNN (S-kNN) to distinguish related EEG segments. In the following, we present the fundamentals of these classification methods.

3.2.1.1   Support Vector Machine

SVM, a supervised machine learning algorithm, is a successful algorithm that is frequently used in both classification and regression studies. In this algorithm, the elements of the dataset containing n features are placed as elements of the coordinate system in an n-dimensional space. Then, the classification is performed by finding the hyperplane that separates the classes best. There are many possible hyperplanes that can separate the two classes. What is important here is to choose the hyperplane from which the highest classification performance may be achieved.

Let (x_k, y_k) be given as a separable sample example. Here k indicates the size of the feature set and $y \in \{-1, 1\}$ indicates the class label. Hence, separating hyperplane can be formulated via $f(x) = \overline{\omega}\vec{x} + c$ here $\vec{\omega}$ indicates the hyperplane parameters and c indicates the offset. The hyperplanes that can separate the two classes from each other with minimum error provide $y_k[(\overline{\omega}\vec{x}_k) + c] - 1 \geq 0, \ k = 1, 2, \ldots, n$ condition. The main purpose here is to achieve the maximum margin. Here the margin is the distance between the support vectors (shown in Figure 3.1) belonging to two different class. Finally, the data falling on different sides of the hyperplane is assigned as an element of the different class [28, 29, 62, and 95]. The basic representation of the SVM algorithm for 2 classes problem is given Figure 3.1a.
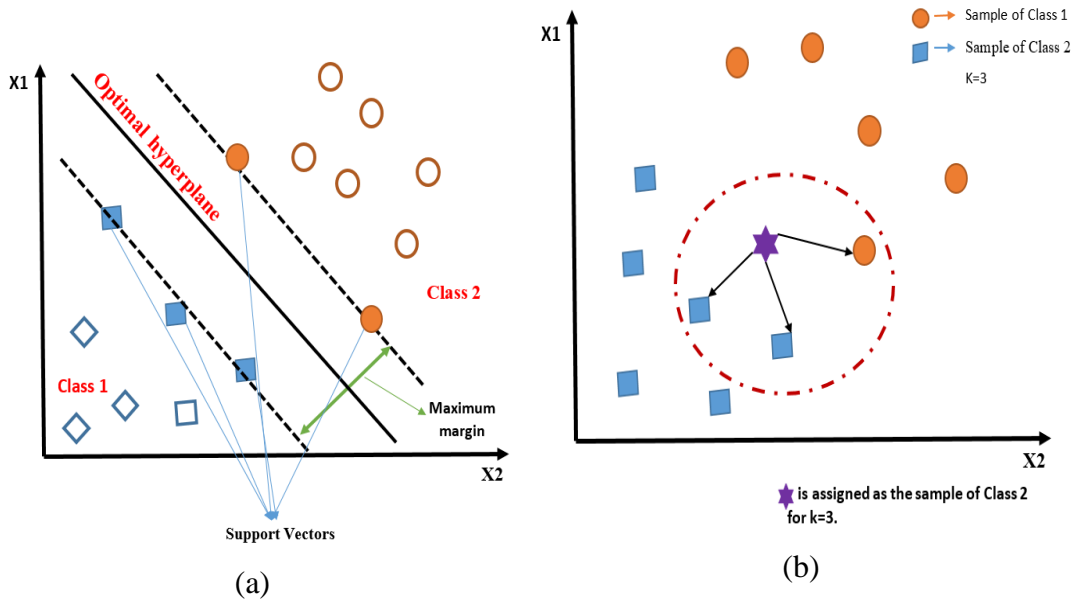
Figure 3.1: Basic representation of the (a) SVM algorithm, (b) kNN algorithm

3.2.1.2   k-Nearest Neighbor

It is one of the learning-based pattern recognition methods. The dataset is divided into two parts as training and test then the learning process is performed according to the data in the training set. First, the distance between the sample to be classified and all the data in the training set is calculated. Then, the k nearest neighbors that have minimum distance is determined. Finally, the most common class among these k nearest neighbors is selected as the class of the new sample. Various distance measurement methods such as Euclidean, Manhattan, Minkowski, and Hamming can be used for distance calculation [49, 62]. In our study, the most commonly used Euclidean distance calculation method is used (shown in Equation (3.7)) and k value is chosen as 5. The basic representation of the kNN algorithm for 2 class problem is given in Figure 3.1b.

$$ED = \sqrt{\sum_{m=1}^{n} (x_m - y_m)^2} \qquad (3.7)$$

29

3.2.1.3   Naive Bayes

It is one of the probabilistic classifiers based on Bayes theorem in which classification is performed according to probability basics. The classification process is performed by calculating the membership probability of a sample to all classes in the dataset.

Let $X = \{x_1, x_2, \dots, x_n\}$ be given. Here, n is the number of features, X indicates the sample in the feature set. In addition, $\{M_1, M_2, \dots, M_m\}$ represents classes, here m is the number of classes. The probability that each X data in the data set is a member of the M_i class is calculated as given in Equation (3.8):

$$P(M_i/X) = \frac{P(X/M_i)P(M_i)}{P(X)}$$

$$\text{if;} \quad P(M_i/X) > P(M_j/X), \quad 1 \le j \le m, \ j \ne i$$

(3.8)

Then the X data is assigned to the class in which class membership is highest. Here, X data is assigned to the M_i class. Where $P(M_i)$ indicates the class prior probabilities, $P(X)$ indicates the prior probability of sample X, $P(X/M_i)$ indicates the probability of X conditioned on Mi and $P(M_i/X)$ indicates the probability of M_i conditioned on X [48, 49]. A basic graphical representation for the NB algorithm is given in Figure 3.2a.

(a)   (b)
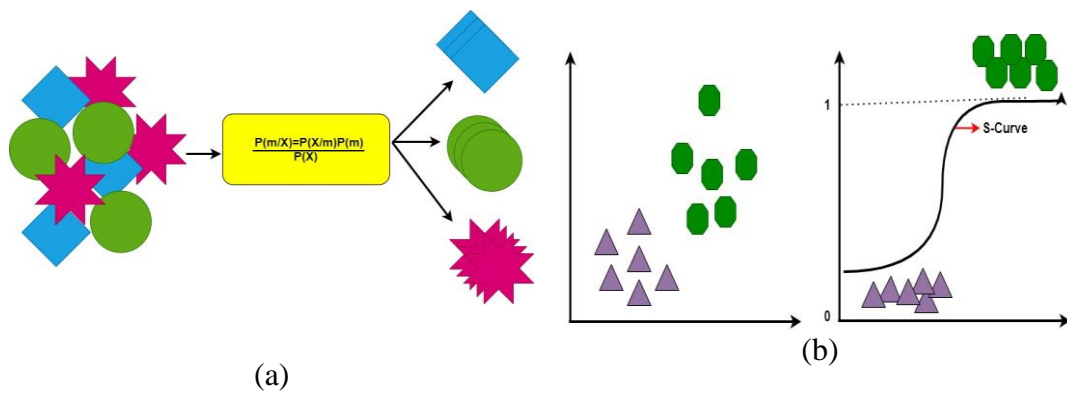
Figure 3.2: Basic representation of the (a) NB, and (b) LR algorithm

3.2.1.4 Logistic Regression

LR is a frequently used statistical classification technique in which the probability (P1), of dichotomous outcome event limited to two values such as yes/no, on/off, or 1/0, is related to a set of independent variables as given in Equation (3.9).

$$Logit(P_1) = \ln\frac{P_1}{1 - P_1} = \beta_0 + \beta_1 X_1 + \cdots + \beta_n X_n \qquad (3.9)$$

Here, β_0 is the intercept and $\{\beta_1 X_1 + \cdots + \beta_n X_n\}$ are the coefficients associated with the independent variable $\{X_1 + X_2 + \cdots + X_n\}$. Generally, in the Logistic regression method, the maximum likelihood estimation (MLE) method is used to calculate the coefficients $\{\beta_1 X_1 + \cdots + \beta_n X_n\}$. The probability of existing of an event as a function of the independent variables is nonlinear as extracted from Equation (3.10) [48].

$$P_1(X) = \frac{P_1}{1 + e^{-Logit(P_1(X))}} \qquad (3.10)$$

Here, $P_1 \in \{0, 1\}$ indicates the probability value.

If the result of Equation (3.10) is $-\infty$, the probability is 0 ($P_1 = 0$), and if the result of this equation is ∞, our probability is 1. A basic graphical representation for the LR algorithm is given in Figure 3.2b.

3.2.1.5 Decision Tree

DT algorithm is a machine learning method that can separate the data into several sub-groups and can be used for classification as well as regression. The name of the algorithm comes from the tree-like structures as branches or nodes that are used. In this algorithm, training is performed by learning a set of decision rules. When a decision is made a leaf node is created whereas when the decision is not certain a decision node which is another branch, is created. In this thesis, coarse tree algorithm is used for the classification process [48].

31

3.2.1.6 Random Forest

The random forest classifier is an ensemble classifier that is composed of many individual decision trees. Trees randomly selected from among many possible trees are called random trees, and these random trees are a decision tree that takes into account "k" features randomly selected at each node. By randomly selecting N samples, with replacement, from the data set, a training set is created for each tree. Here, each sample has "K" features. Then, without replacement, a subset "$k = \sqrt{K}$" of the features "K" of the training set are randomly chosen to split the nodes of the decision tree. The best splitting feature in the "k" subset is used to split each node in a tree. This process continues until all selected samples have been sorted. Thus, an output is obtained for each decision tree. The class that is common among the outputs of all the used decision trees is select by the random forest algorithm [38, 41, and 45]. For our experiment, 30 is selected as the number of the decision tree.

3.2.1.7 Subspace kNN

S-kNN is one of the ensemble learning classifiers in which subsets of a specific number of features are randomly selected and categorized in the feature set. For n-dimensional feature set $\{X_1,\ X_2, \dots, X_n\}$, m-dimensional random subspaces $\{X_1,\ X_2, \dots, X_m\}$, $m < n$ are selected, and k nearest neighbors of each test sample are calculated for each subset using Euclidean distance. The class labels of those k neighbors $\{c^1{}_l,\ c^2{}_{l,}, \dots, c^k{}_{l,}\}$ are collected in a list. Finally, the most common class in that list is selected as the class of the test sample [107]. In our experiments, subspace dimension and number of learners are selected as 8 and 30, respectively.

3.2.1.8 Boosted Tree

Boosting is one of the frequently used powerful ensembles learning approaches for classification and regression. In this approach, initially, a 'weak' hypothesis $\{T_1,\ T_2, \dots, T_D\}$ of D decision trees with K nodes is created for training data $\{X_1,\ X_2, \dots, X_N\}$ with weight$s$ $\{\omega^t{}_1,\ \omega^t{}_{2,}, \dots, c^t{}_{N,}\}$, where t is the number of trials. The learning process starts by using the initial ω^t for the decision tree of K nodes. The weights of training data are updated using the weight of decision trees' each node

$d(t, k)$. This process continues until $t = D$. Two parameters such as the number of learner trees and the number of nodes per tree are important for the success of boosted decision trees [108]. In the proposed boosted tree classification experiment, the number of learners is equaled to 30 and the maximum number of the nodes is selected as 20.

3.2.2 Statistical Analysis and Performance Evaluation Metrics

In this thesis, accuracy (ACC), sensitivity (SEN), selectivity (SPE), precision (PRE), false positive rate (FPR), and false discovery rate (FDR) expressed as the performance criteria and F-score (F1-S) values that is the combination of previous parameters are used for performance evaluation. K-fold cross-validation (CV) method has been used to establish the performances of the classifiers.

$$ACC = \frac{TP + TN}{TP + FN + FP + TN} * 100\%$$

$$SEN = \frac{TP}{TP + FN} * 100\%$$

$$SPE = \frac{TN}{FP + TN} * 100\%$$

$$PRE = \frac{TP}{TP + FP} * 100\% \qquad (3.11)$$

$$FPR = \frac{FP}{FP + TN} * 100\%$$

$$FDR = \frac{FP}{FP + TP} * 100\%$$

$$F - Score = 2 * \frac{PRE * SEN}{PRE + SEN} * 100\%$$

Here, true-positive (TP) is the sample number of $class - 1$ classified in the same class, and true-negative (TN) is the sample number of $class - 0$ classified in $class - 0$. While false-positive (FP) is the number of samples not in $class - 1$ but classified

in $class - 1$, false-negative (FN) indicates the number of samples in $class - 1$ but classified in $class - 0$ [28, 29, and 48]. In order to obtain a consistent classification accuracy, $K -$fold cross-validation is employed in our experiments. In the $K -$fold cross-validation process, the feature set is divided into K equal size subsets. The method is repeated K times, and each time $(K - 1)/K$ of the sub-sets are utilized for training, and the remaining $1/K$ is used for testing. Then the average accuracy for K trials is computed as classification accuracy [32, 38, and 48]. Visual demonstration of K-fold Cross-Validation is illustrated in Figure 3.3.
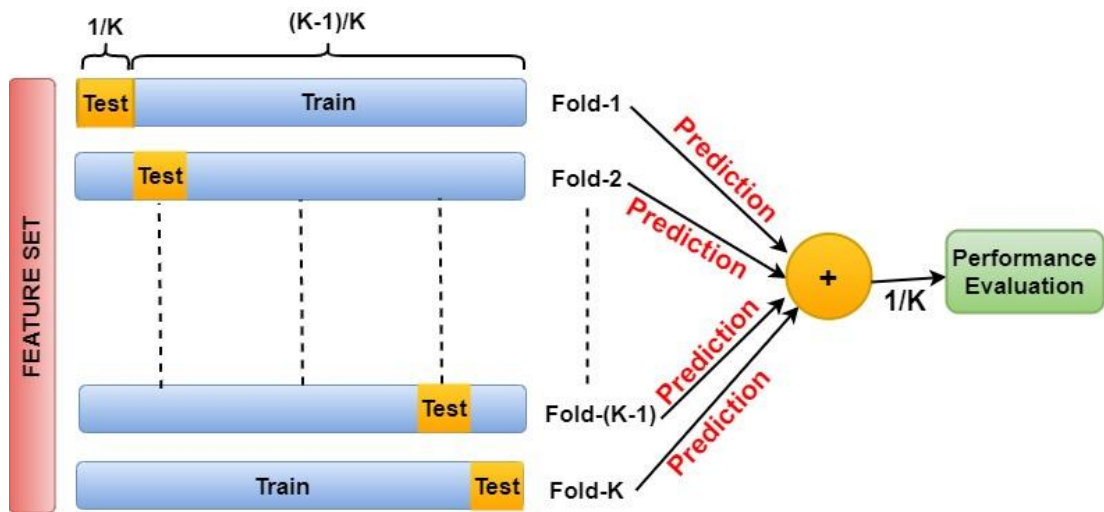
Figure 3.3: Visual demonstration of K-fold Cross Validation.

4. Classification of Epileptic EEG Signals Using Advanced Signal Decomposition Methods

In this study, three different approaches are presented to distinguish seizure and seizure-free EEG segments. In the first method, various temporal, spectral, and non-linear features are extracted from the IMFs obtained using EMD and EEMD approaches. In the second method we present, epileptic EEG segments are analyzed using a simple matrix decomposition method, namely the DMD approach. Finally, in the third approach the SST method with high TF resolution is utilized to extract features and achieve high classification performance in distinguishing seizure and seizure-free EEG segments. The results of these three approaches are compared in line with the classification performances of various machine learning algorithms used in our study.

4.1 Experimental Data sets

In this thesis, two different Epileptic EEG data sets are evaluated. The first one is our own IKCU data set that was collected from patients under treatment at Izmir Katip Celebi University Medical School Hospital. The other one is CBH-MIT data set that is publicly available epileptic EEG data collected at Children's Hospital Boston.

4.1.1 Epileptic EEG data set-1 (IKCU Epilepsy data set)

Epileptic EEG data of 16 epilepsy patients recorded using surface electrodes in Izmir Katip Celebi University, School of Medicine, and Neurology Department were used in this study. EEG data were recorded using the Neurofax EEG device, from 18 different channels and at a sampling frequency of 100 Hz. Surface EEG data were

recorded from, Fp1-F7, F7-T1, T1-T3, T3-T5, T5- O1, Fp1-F3, F3-C3, C3-P3, P3-O1, Fp2-F8, F8-T2, T2-T4, T4-T6, T6-O2, Fp2-F4 F4-C4, C4-P4, P4-O2, electrode positions, according to the International 10-20 electrode placement system. In order to use this EEG data within the scope of our study, Izmir Katip Celebi University Non-Invasive Clinical Research Ethics Committee was applied and Ethical Approval dated 08.08.2019 and numbered 296 was obtained. As discussed in [109], EEG signals recorded from the temporal and frontal lobe-weighted 10 channels (Fp1-F7, F7-T1, T1-T3, T3-T5, Fp1-F3, Fp2-F8, F8-T2, T2-T4, T4-T6, Fp2-F4) are used in the study.

One-minute pre-seizure and seizure epochs were marked by neurologist in the Epileptic EEG signals recorded from selected channels. A total of 2 EEG epochs, one pre-seizure, and one seizure EEG epoch were used for each patient for our study. Thus, a total of 32 EEG epochs (containing 10 channels, for one minute) were analyzed. Summary of the EEG dataset used in the proposed study is presented in Table 4.1.

Table 4. 1: Summary of the IKCU EEG dataset used proposed study (F: Female, M: Male, LTemp: Left Temporal, RTemp: Right Temporal, RFron.-Temp: Right Fronto-Temporal)

Subject	Gender	Epileptic Focus Area	Age/Duration
Patient 1	F	LTemp	
Patient 2	F	LTemp	
Patient 3	F	LTemp	
Patient 4	F	LTemp	
Patient 5	F	LTemp	
Patient 6	M	LTemp	
Patient 7	M	LTemp	
Patient 8	M	RFron.-Temp	Age: 37.3±7
Patient 9	M	RFron.-Temp	Duration: 1 min.
Patient 10	M	LTemp	
Patient 11	M	LTemp	
Patient 12	M	LTemp	
Patient 13	M	LTemp	
Patient 14	M	LTemp	
Patient 15	M	LTemp	
Patient 16	M	LTemp	

4.1.2   Epileptic EEG data set-2 (CHB-MIT data set)

In order to demonstrate the success of the proposed approach on a second data set, the multichannel (23 or 18 channels) epileptic EEG data collected at Children's Hospital Boston, CHB MIT [110] are used for seizure detection. This data set contains epileptic EEG data recorded from 24 pediatric patients with 256 Hz sampling frequency. In the proposed experiments, the temporal and frontal lobe-weighted 10 EEG channels (FP1-F7, F7-T7, T7-P7, FP1-F3, T7- FT9, FP2-F8, F8-T8, T8-P8, FP2-F4, FT10-T8) of 23 patients (chb01-chb23) are used in order to make the experiment parallel to the IKCU data set.

1s duration, non-overlapping EEG segments from the seizure EEG signals, and 10-minute inter- seizure EEG signals that are maximum 1-2 hours prior to the onset of the seizure are obtained for each patient.

4.2   Results and Discussions of EMD and its Derivative

IKCU EEG Data set including pre-seizure and seizure EEG signals was analyzed using EMD, and EEMD methods and various classifiers. In the proposed method, we had 10 channel and two epoch EEG signal for each patient (total number of patients is 16). Hence the size of the pre-seizure and seizure EEG dataset is 16x10. Maximum numbers of obtained IMFs after applying the EMD and EEMD are 16 and 15 respectively. Therefore, since it would be time-consuming and meaningless to obtain features from all IMFs, IMF selection process is carried out for EMD and EEMD methods in order to identify the IMF that best represents the original signal, before the feature extraction.

4.2.1   Selection of Intrinsic Mode Functions

In this study we propose a hybrid IMF selection method by using energy based, correlation based, PSD-distance based, and t-test based approaches. Pre-seizures and seizures Epileptic EEG data of 16 patients recorded from 10 channels (IKCU EEG data set) were decomposed into the IMFs using both EMD and EEMD approaches

(example signals are shown in Figure 4.1), then the proposed IMF selection procedure described below is executed.

4.2.1.1 Energy Based Selection Method

The energies of each IMFs are calculated as shown in Equation (4.1). Since the higher-energy IMF is considered to be the best representative of the original signal, the IMFs were ranked from the high-energy IMF to the low-energy IMF [111].

$$E_{IMF_i} = \sum_{n=0}^{N-1} |IMF_i[n]|^2, \quad i = 1, 2, \ldots, L. \tag{4.1}$$

Here, IMF_i is the ith IMF and E_{IMF_i} is the energy of this IMF.
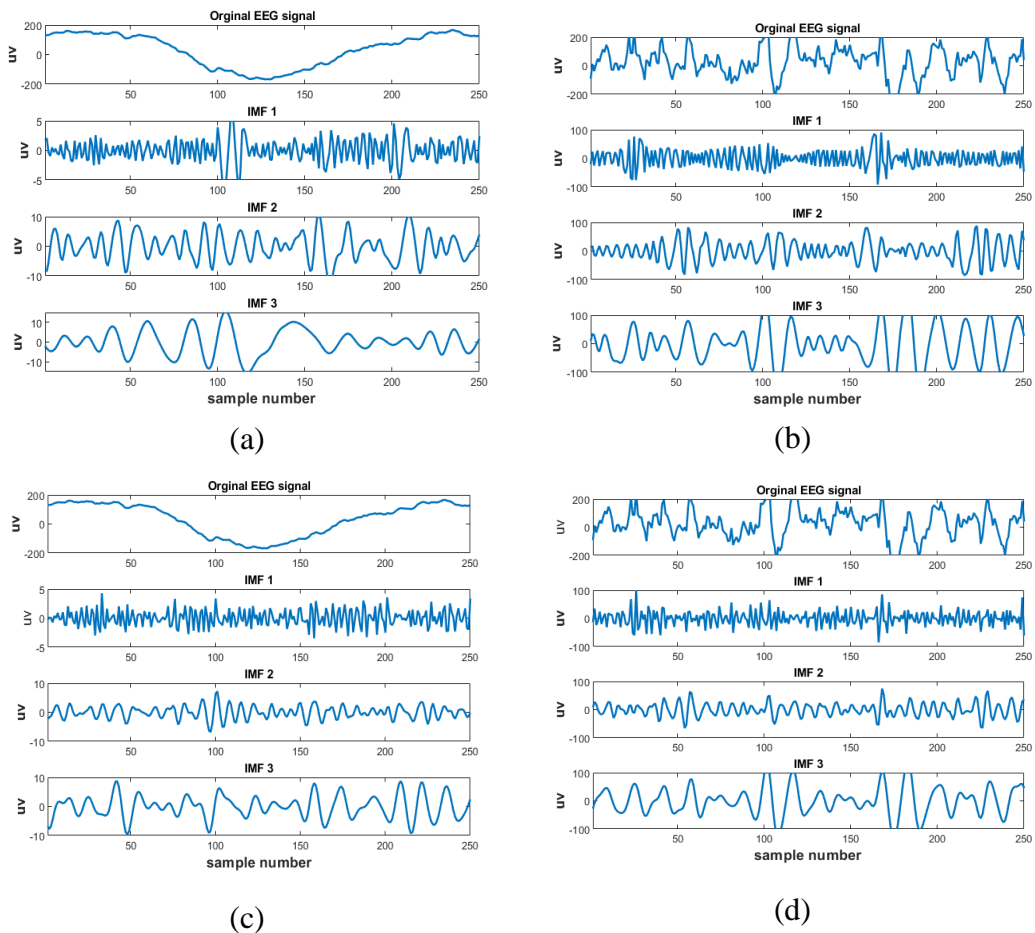
Figure 4.1: (a) Surface pre-seizure EEG signal and its first three IMFs obtained using EMD, (b) Surface seizure EEG signal and its first three IMFs obtained using EMD, (c) Surface pre-seizure EEG signal and its first three IMFs obtained using EEMD, (d) Surface seizure EEG signal and its first three IMFs obtained using EEMD

4.2.1.2   The Correlation Based Selection Method

The correlation coefficient of each IMFs are calculated as shown in Equation (4.2). Since the IMF with high correlation coefficient is considered to be a good representative IMF of the original signal, the IMFs are ranked from the high correlation coefficient IMF to the low correlation coefficient IMF [112].

$$\rho_{x,IMF_i} = \frac{C_{x,IMF_i}}{\sigma_x \sigma_{IMF_i}} \tag{4.2}$$

Here, C_{x,IMF_i} is the crosscovariance of the original signal and i^{th} IMF, σ_x, and σ_{IMF_i} are the standard deviations of the original signal and IMF_i respectively, ρ denotes the correlation coefficient.

4.2.1.3   The PSD-distance Based Selection Method

Another IMF selection method, based on power spectral densities (PSD) was also utilized by using the power spectral densities of the original signal and IMFs. The distances between the estimated PSDs are calculated using the Kullback Leibler Distance (KLD) method as shown in Equation (4.3). If the distance between the PSDs of original signal and an IMF is minimum, that IMF is considered to be the best representative IMF of the original signal. Hence, the IMFs are ranked from the low PSD distance IMF to the high PSD distance IMF [113, 114].

$$dis_{KLD}(x, IMF_i) = \sum_{n=0}^{N-1} log \frac{PSD_x(\omega_k)}{PSD_{IMF_i}(\omega_k)}, \quad \omega_k = \frac{2\pi}{N}k. \tag{4.3}$$

In Equation (4.3), PSD_x is the power spectrum of the original signal, PSD_{IMF_i} is the power spectrum of the ith IMF, $dis_{KLD}(x, IMF_i)$ shows the KLD between the power spectrum of the ith IMF and the power spectrum of the original signal.

4.2.1.4　T-test Based Selection Method

We also use the t-test statistical significance measure for the selection of best IMFs [14]. As such we calculate the p score for every IMF by applying the t-test in MATLAB. Since the p-value obtained here shows the statistical significance of signals, the IMFs are ranked from the high p-value IMF to the low p-value IMF. As a result of the above four selection approaches, we obtain a ranking matrix of the IMFs. An example of this matrix for a single EEG channel of a patient is shown in Table 4.2.

Table 4.2: Example of IMF Ranking Matrix for EEMD method

Component	Order of IMF											
	1st	2nd	3rd	4th	5th	6th	7th	8th	9th	10th	11th	12th
Energy	7	6	8	5	9	10	4	1	3	2	11	12
Corr. Coef.	7	6	8	9	5	4	10	3	11	12	1	2
PSD dis.	1	2	3	4	5	6	7	8	9	10	11	12
P value	3	2	1	7	4	9	5	6	10	8	11	12

Here;
- 7th IMF has the highest Energy while 12th IMF has the lowest Energy.
- 7th IMF has the highest Correlation Coefficient while 2nd IMF has the lowest Correlation Coefficient.
- 1st IMF has the lowest PSD distance while 12th IMF has the highest PSD distance.
- 3rd IMF has the highest p value while 12th IMF has the lowest p value.
- Each row shows the ranking of the obtained IMFs according to those features.
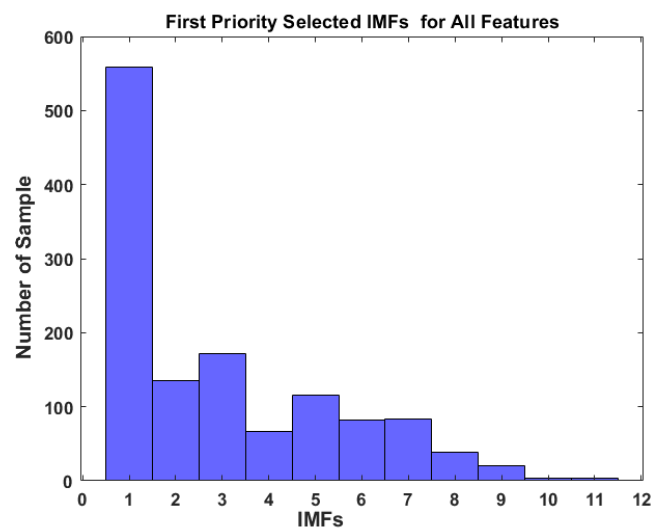
Figure 4.2: Histogram of first priority selected IMFs for EEMD method

These procedures were applied to the pre-seizure and seizure EEG data of 10 different channels of each patient separately. As a result of these procedures, 40 metrics for 10 channels are calculated for each patient. All ranking matrices were combined and a 1280x16 dimensional ranking matrix for all pre-seizure and seizure EEG data was obtained. To determine the first priority selected IMFs for all signals, the histogram of the 1st column of the ranking matrix was calculated. The resulting histogram is shown in Figure 4.2. When the histogram shown in Figure 4.2 is evaluated, It is seen that in the 558 of the 1280 features calculated, the IMF-1 is the first priority selected IMF. Also, it is seen that in the 135 of the total features calculated, IMF-2 is the first priority selected IMF. Last, it is seen that 172 of the 1280 features calculated, IMF-3 is the first priority selected IMF. As a result of these processes, it is decided to use these three IMFs (IMF-1, IMF-2, and IMF-3) in our study.

4.2.2   Feature Extraction

4 time domain, 5 spectral, and 2 non-linear features are calculated for each pre-seizure and seizure EEG segment using the selected IMFs. For comparison, the same features are calculated from the EEG segment itself, without using the EMD or EEMD method. DWT has widely been used for the analysis of non-stationary signals [38]. In our study, we use the DWT based approach for feature extraction and classification of epileptic EEG segments to investigate the advantages of proposed EMD and EEMD based approaches. DWT decomposes a given signal x[n] into detail and approximation coefficients by using a set of mother wavelet function [38, 87]. In our study, Daubechies4 (db4) mother wavelet and 3 level subband decomposition are used.

4.2.2.1   Time Domain Feature Set

After the IMF selection process is carried out, the time domain feature dataset was created, using directly the EEG signals, using the first three of the IMFs obtained by EMD and EEMD methods, and using the subbands of DWT. Energy, Mean value, Skewness, and Kurtosis values are calculated for 3 IMFs, DWT subbands, and EEG signals in the time domain [24, 38].

$$E = \sum_{n=0}^{N-1} |X[n]|^2$$

$$\mu = \frac{1}{N} \sum_{n=0}^{N-1} X[n]$$

(4.4)

$$S = \frac{\frac{1}{N} \sum_{n=0}^{N-1} (X[n] - \mu)^3}{\left(\sqrt{\frac{1}{N} \sum_{n=0}^{N-1} (X[n] - \mu)^2} \right)^3}$$

$$K = \frac{\frac{1}{N} \sum_{n=0}^{N-1} (X[n] - \mu)^4}{\left(\frac{1}{N} \sum_{n=0}^{N-1} (X[n] - \mu)^2 \right)^2}$$

In the above equations, $X[n]$ indicates the EEG signal or IMFs, N is the size of the signal or IMFs. E denotes the energy, μ is the mean value; S indicates the Skewness, K is the Kurtosis value.

In the EMD and EEMD based approaches a total of 320x12 size, and DWT based approach a total of 320x16 size feature sets are obtained. Applying the same procedure to the EEG signal itself, a total of 320x4 size feature set for pre-seizure and seizure EEG data is obtained.

4.2.2.2 Spectral Domain Feature Set

To generate this feature dataset, the spectrum of the signal or IMF calculated by the periodogram method was used. Total power, Spectral Entropy, 1st, 2nd, and 3rd moments are calculated using the spectrum of signals [26, 62].

$$S(\omega_k) = \frac{1}{N} |X(\omega_k)|^2$$

$$S_T = \sum_{k=0}^{N-1} S(\omega_k)$$

(4.5)

$$M_j = \sum_{k=0}^{N-1} (\omega_k)^j S(\omega_k), \quad j = 1, 2, 3.$$

42

$$H = - \sum_{k=0}^{N-1} P(\omega_k) \log_2 P(\omega_k)$$

Here, in Equations (4.5), $S(\omega_k)$ denotes the Power Spectral Density of the signal estimated by periodogram method, $X(\omega_k)$ is the Discrete Fourier Transform of the signal $x[n]$ [26], and S_T is the total power. In addition, N indicates the size of the corresponding signal and $\omega_k = \frac{2\pi}{N} k$. M_j indicateS the higher order spectral moments of the corresponding signal. H denotes the spectral entropy of the signal, and $P(\omega_k) = \frac{S(\omega_k)}{S_T}$ indicates the normalized power spectral distribution [62].

In the EMD and EEMD based approaches a total of 320x15 size, and DWT based approach a total of 320x20 size feature sets are obtained. Applying the same procedure to the EEG signal itself, a total of 320x5 size feature set for pre-seizure and seizure EEG data is obtained.

4.2.2.3   Non-Linear Feature Set

Non-linear features such as the Hurst Exponent and Higuchi Fractal Dimension are computed to obtain this feature data set. These nonlinear features are used to analyze the complexity and self-similarity of brain recordings and other biological signals. Calculation of Hurst Exponent and Higuchi Fractal Dimension are given in Equations (4.6), and (4.7); respectively.

$$X[n] = \{X[1], X[2], \dots, X[N]\}$$

$$X_A[n] = \sum_{i=1}^{n} X[i] - \mu, \quad n = 1, \dots, N.$$

$$R[m] = \max(\{X_A[1], X_A[2], \dots, X_A[m]\}) \\ - \min(\{X_A[1], X_A[2], \dots, X_A[m]\}) \tag{4.6}$$

$$S[m] = \sqrt{\frac{1}{m} \sum_{k=1}^{m} (X[k] - \overline{X}_m)^2}, \quad m = 1, \dots, N.$$

43

$$LN = \ln\frac{R(k)}{S(k)} \quad k = 1, \dots, N$$

where, $X[n]$ given in Equation (4.6) shows the EEG signal or the IMFs to be analyzed and μ indicates the mean value of this signal. $X_A[n]$ indicates the accumulated deviation value of $X[n]$. $R[m]$ is the range series and $S[m]$ denotes the standard deviation of the time series $X[n]$, and $\overline{X}_m$ is the mean value from $X[1]$ to $X[m]$. LN shows the logarithmic value. The Hurst exponent is calculated as the slope of the line where LN is plotted with respect to $\ln(k)$.

The value of Hurst Exponent (HE) ranges from 0 to 1. If there is no correlation in the time series, $HE = 0.5$; if time series has long range anti-correlations, $0 < HE < 0.5$ and if there is long-range correlations in the time series, $0.5 < HE < 1$ [31].

Higuchi FD (HFD) is used to calculate the FD directly from time-series signals. The most important parameter that must be determined for the calculation of Higuchi Fractal Dimension is k_{max}. The HFD values calculated in a given k_{max} range are plotted against this range in order to determine the optimal value for the k_{max} parameter. The k value that the obtained curve reaches the saturation point is determined as k_{max} [32, 88].

$$X[n] = \{X[1], X[2], \dots, X[N]\}$$

$$X_k{}^m = \{X[m], X[m + k], X[m + 2k] \dots, X[m + int(.) * k]\},$$
$$m = 1, 2, \dots, k.$$

$$L[m, k] = \frac{\left\{\left(\sum_{i=1}^{int(.)}|X[m + ik] - X[m + (i - 1)k]|\right)\frac{N - 1}{int(.)}\right\}}{k} \quad (4.7)$$

$$L[k] = \frac{1}{k}\sum_{m=1}^{k} L[m, k], \quad m = 1, 2, \dots, k.$$

In Equation (4.7), $X[n]$ indicates the one dimensional time series EEG signal or the IMFs and $X_k{}^m$ indicates the new time series. Here, k and m are integers and the $int(.)$ operation indicates the integer part of the $(N - M)/k$ value, N is the length of the original signal. The $L[m, k]$ calculated in Equation (4.7) indicates the size of the

new time series signals. The $L[k]$ calculated by using the average of the $L[m,k]$ values indicates the length of the curve for the k new time interval. HFD is calculated as the slope of the line where $L[k]$ is plotted with respect to $\ln[1/k], k = 1, 2, ..., k_{max}$.

In our study, HFD values calculated against different k_{max} values are plotted and a graph was obtained (shown in Figure 4.3). It is observed that this graph reached saturation point when $k_{max} = 30$. Therefore, the k_{max} value is set to 30.
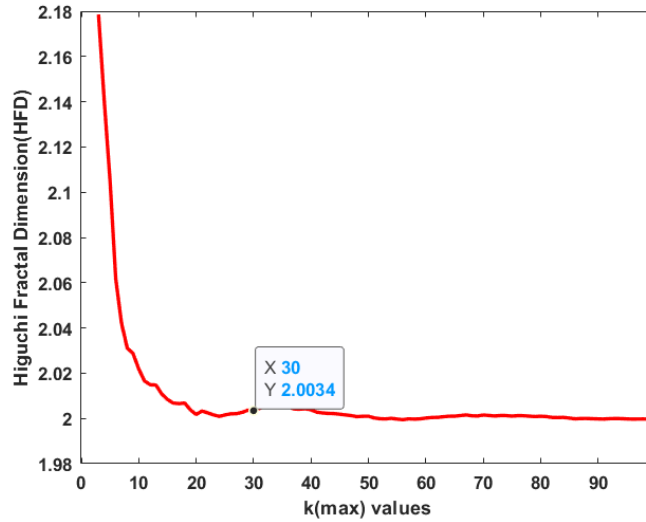
Figure 4.3: HFD values calculated against different k_max values

In the EMD and EEMD based approaches a total of 320x6 size, and DWT based approach a total of 320x8 size feature sets are obtained. Applying the same procedure to the EEG signal itself, a total of 320x2 size feature set for pre-seizure and seizure EEG data is obtained.

4.2.3 Experimental Results and Discussion

EEG signals including pre-seizure and seizure segments obtained from 10-channel EEG recordings of 16 epilepsy patients who are under treatment at Izmir Katip Celebi University School of Medicine, Department of Neurology, were analyzed using EMD, and EEMD approaches and various classifiers. The hybrid IMF selection process including energy, correlation, power spectral distance, and statistical significance measures was carried out for EMD and EEMD approaches in order to identify the

IMFs that best represent the original signal as described in Section 4.2.1. After the IMF selection process, time-domain (Energy, Mean value, Skewness, and Kurtosis) and spectral-domain (Total power, Spectral Entropy, 1st, 2nd, and 3rd moments), and non linear (Hurst Exponent and Higuchi Fractal Dimension) feature-sets were created using the selected three IMFs (IMF1, IMF3, IMF2) obtained by EMD, and EEMD approaches, and the EEG signal itself. In addition, we also performed simulations to compare the performance of our proposed approach with that of DWT. Since three selected IMFs of EMD and EEMD approaches are used for feature extraction and classification, three level decomposition is used for DWT utilizing Daubechies4 (db4) mother wavelet function [38]. Finally, SVM, kNN, NB, and LR classifiers are used for the classification, and the results are evaluated.

Performance evaluation results of our proposed approach are given in Tables 4.3-4.6. In these tables IMF1, IMF2, or IMF3; show that the features for classifications are calculated by using the corresponding IMF; IMF 1-3 denotes that the features are extracted using all three IMFs. On the other hand IMF1- IMF2 shows that the features are extracted from IMF1 and IMF2. Additionally, AC+DC1-3 show that the features are extracted from Approximation Coefficient (AC) and 3 Detail Coefficients (DC) of DWT. Furthermore, the boldface numbers in table cells indicate the best performance in accuracy for each approach and classifier (in Tables 4.3-4.6).

Table 4.3 summarizes the performance evaluation of time-domain features used for classification. Using the time domain features calculated from the IMF1-IMF3 (the most favorable two IMFs) of EMD, we obtain 97.18% classification accuracy and 97.14% F1-S using the Logistic Regression classifier. While the Logistic Regression algorithm yields the highest accuracy (98.13%) and F1-S (98.13%) values by using the time domain features calculated from IMF1-IMF3 of EEMD, the SVM algorithm performs the worst (ACC: 62.44%, F1-Skor:60.80%) for the same features calculated from IMF2. When the same features calculated from the subbands obtained using DWT, we achieved 94.25% accuracy and 94.31% F1-S for the kNN classifier. To reveal the effect of decomposition, we analyzed the EEG signal itself and repeated the above feature extractions and classification. Using the time-domain features and kNN classifier, we obtain 89.75% accuracy and 89.96% F1-S, where the SVM performed

very poorly (ACC: 53.94% and F1-S: 45.26%). Results of all classification using time-domain features are provided in Table 4.3.

Table 4.3: Performance results (%) for pre-seizure and seizure EEG signal classification using the time-domain feature-set.

Method	Component	SVM		kNN		NB		LR	
		ACC	F1-S	ACC	F1-S	ACC	F1-S	ACC	F1-S
EMD	IMF1	55.81	43.64	94.56	94.45	91.56	91.24	94.69	94.94
	IMF2	77.75	79.54	93.50	93.40	91.44	91.06	94.38	94.19
	IMF3	86.19	87.75	93.88	93.75	93.38	93.24	94.69	94.60
	IMF1-IMF2	94.63	94.72	96	95.94	92.25	92.02	93.44	93.42
	IMF1-IMF3	96.12	96.14	95.25	95.19	94.94	94.86	**97.18**	**97.14**
	IMF2-IMF3	78.63	73.11	94.69	94.60	93	92.84	94.38	94.30
	IMF1-3	74.44	69.07	95.75	95.71	94.19	94.08	96.88	96.88
	IMF1-4	78.88	75.24	95.63	95.54	93.50	93.39	91.56	91.03
EEMD	IMF1	91.38	91.28	95.19	95.20	92.69	92.52	95.31	95.27
	IMF2	62.44	60.80	90.94	90.63	90.63	90.14	92.81	92.60
	IMF3	71.44	69.75	94.44	94.34	93.63	93.55	94.38	94.27
	IMF1-IMF2	96.06	96.04	95.06	95.06	91.75	91.56	95.31	95.30
	IMF1-IMF3	95.50	95.22	96.31	96.28	93.56	93.50	**98.13**	**98.13**
	IMF2-IMF3	92.75	92.33	94.50	94.39	92.38	92.24	94.38	94.30
	IMF1-3	73.44	64.36	96.63	96.61	93.81	93.73	90.94	90.61
	IMF1-4	73.13	68	96.50	96.43	92.81	92.71	90.63	90.51
DWT	AC+DC1-3	71.38	60.51	**94.25**	**94.31**	93.50	93.39	92.09	92.06
EEG	all EEG	53.94	45.26	**89.75**	**89.96**	78.94	75.38	87.81	87.21

We give the performance metrics for spectral features used in classification for different IMF combinations in Table 4.4. We observe that NB provides 96.88% accuracy and 96.77% F1-S using spectral features calculated from IMF1-IMF3 of EMD. However, higher classification performance is obtained by the same features calculated from IMF2-IMF3 of EEMD with Logistic Regression. While 95% accuracy and 94.87% F1-S were obtained from the spectral feature of DWT using Naive Bayes classifier; 93.31% accuracy and 93.37% F1-S are achieved using the same feature obtained from EEG signals itself.

Table 4.4: Performance results (%) for pre-seizure and seizure EEG signal classification using the spectral feature-set.

Method	Component	SVM		kNN		NB		LR	
		ACC	F1-S	ACC	F1-S	ACC	F1-S	ACC	F1-S
EMD	IMF1	94.12	94	94.38	94.35	94.56	94.28	85	82.73
	IMF2	94.06	93.81	92.94	92.77	93.75	93.42	94.06	93.97
	IMF3	93.63	93.60	94.75	94.59	95.81	95.66	77.19	80
	IMF1- IMF2	94.69	94.53	93.25	93.15	94.94	94.70	83.13	84.75
	IMF1- IMF3	85.50	86.56	95.44	95.35	**96.88**	**96.77**	94.69	94.50
	IMF2- IMF3	93.34	93.77	94.81	94.66	96.13	95.99	83.44	82.03
	IMF1-3	93	93.31	94.88	94.80	96.19	96.06	82.50	82.93
	IMF1-4	93.81	94.03	94.66	94.59	95.75	95.62	84.38	83.77
EEMD	IMF1	96.06	96.02	95.06	95.05	94.44	94.26	96.25	96.25
	IMF2	92.13	91.90	91.94	91.88	93	92.56	92.50	92.31
	IMF3	94.56	94.48	94.25	94.20	95.56	95.39	96.88	96.86
	IMF1- IMF2	94.38	94.26	94.94	94.88	94.81	94.61	81.88	81.29
	IMF1- IMF3	74.31	73.80	95.31	95.26	96.75	96.6	79.69	78.83
	IMF2- IMF3	94.94	94.83	93.75	93.74	95.69	95.52	**96.88**	**96.89**
	IMF1-3	95.12	94.84	96.69	96.66	96.06	95.93	88.13	88.34
	IMF1-4	91.25	90.64	96.31	96.29	96.81	96.68	90.31	89.42
DWT	AC+DC1-3	81.25	77.56	93.31	93.24	**95**	**94.87**	88.75	88.82
EEG	all EEG	72.06	67.29	**93.31**	**93.37**	77.37	71.59	89.06	88.14

Table 4.5: Performance results (%) for pre-seizure and seizure EEG signal classification using the non-linear feature-set.

Method	Component	SVM		kNN		NB		LR	
		ACC	F1-S	ACC	F1-S	ACC	F1-S	ACC	F1-S
EMD	IMF1	80.50	79.17	83.13	82.82	82.69	82.05	83.13	82.80
	IMF2	81.38	80.11	83.31	83.15	86.19	86.79	85.63	85.80
	IMF3	84.75	85.05	81.81	81.52	86.06	86.46	86.25	86.34
	IMF1- IMF2	84.19	83.23	87.31	87.27	88.94	89.18	87.81	87.93
	IMF1- IMF3	88.87	87.85	89.31	89.32	90.75	91.02	89.69	89.72
	IMF2- IMF3	88.19	88.21	86.88	86.93	92	92.32	87.5	87.5
	IMF1-3	90.37	90.15	90.44	90.39	91.81	92.17	90.94	90.97
	IMF1-4	**95**	**95.01**	93.94	93.86	92.38	92.61	94.38	94.41
EEMD	IMF1	55.88	42.68	59.63	59.05	63.75	56.97	55.63	50
	IMF2	69.73	61.66	79.38	79.47	82.88	84.07	81.25	81.82
	IMF3	70.31	67.75	73.88	73.58	79.88	79.80	77.81	78.15
	IMF1- IMF2	70.06	62.49	77.87	77.63	84.50	84.99	87.50	87.58
	IMF1- IMF3	70.19	66.94	74.19	74.08	80.25	79.65	81.88	81.65
	IMF2- IMF3	77.31	75.39	78.38	78.20	84.50	85.10	83.44	83.28
	IMF1-3	76.69	74.32	78.63	77.69	85.56	85.77	89.06	88.89
	IMF1-4	**92.94**	**92.90**	91.50	91.35	90.69	90.74	91.25	91.19
DWT	AC+DC1-3	64.63	58.12	68.88	67.53	84.50	84.22	**87.50**	**87.42**
EEG	all EEG	58.19	64.84	67.31	65.83	**69.38**	**68.95**	62.81	65.51

Classification result using nonlinear features are given in Table 4.5. The results suggest that the nonlinear features extracted from IMF1-4 of EMD provided classification

performance with 95% accuracy and 95.01% F1-S using SVM. However, EEMD approach provided 92.94% accuracy and 92.90% F1-S using the same features with SVM. Using the features obtained from the EEG signal itself, accuracy and F1-S are obtained 69.38% and 68.95%, respectively with NB. On the other hand, 87.50% accuracy and 87.42% F1-S were obtained using the non-linear feature of the DWT approach by the Logistic Regression classifier.

Table 4.6: Performance results (%) for pre-seizure and seizure EEG signal classification using the combined feature-set.

Method	Component	SVM		kNN		NB		LR	
		ACC	F1-S	ACC	F1-S	ACC	F1-S	ACC	F1-S
EMD	IMF1	94.31	94.16	94.38	94.31	94.31	94.03	86.25	87.06
	IMF2	94.12	93.85	92.62	92.48	93.13	92.79	94.06	94.22
	IMF3	93.38	93.36	94.63	94.45	95.63	95.48	87.50	86.58
	IMF1- IMF2	**94.56**	**94.40**	93.81	93.70	94.56	94.33	92.5	92.31
	IMF1- IMF3	92.06	92.38	**95.63**	**95.53**	**96.88**	**96.77**	**96.25**	**96.23**
	IMF2- IMF3	94.50	94.35	94.81	94.66	95.88	95.74	89.69	89.39
	IMF1-3	90	90.99	94.88	94.81	96.19	96.07	93.75	93.59
	IMF1-4	87.38	85.90	94.63	94.59	96	95.89	92.81	92.55
EEMD	IMF1	**96.06**	**96.04**	94.44	94.43	93.75	93.60	**96.25**	**96.30**
	IMF2	92.44	92.19	91.81	91.69	93.50	93.12	87.19	86.38
	IMF3	94.50	94.42	94.06	94.02	95.44	95.27	92.19	91.80
	IMF1- IMF2	94.94	94.86	94.81	94.76	94.12	93.91	92.50	92.68
	IMF1- IMF3	81.69	80.29	95.94	95.90	**97**	**96.91**	84.38	84.66
	IMF2- IMF3	94.44	94.32	94.25	94.21	95.38	95.18	91.25	91.36
	IMF1-3	94.19	94.39	**97**	**96.97**	95.75	95.62	90.31	90.22
	IMF1-4	93.56	93.30	96.19	96.17	96.88	96.77	93.13	92.86
DWT	AC+DC1-3	80.81	76.83	93.44	93.38	**94.56**	**94.43**	90.94	90.97
EEG	all EEG	59.75	66.33	**93.25**	**93.35**	78.94	74.41	88.44	87.46

In order to determine the effect of IMF selection on the classification performance and to compare the approaches, the classification is performed with the combination of time, spectral, and nonlinear features. The classification results are shown in Table 4.6. In EMD approach, the SVM provided the maximum classification accuracy (94.56%) using combined features of IMF1-IMF2. However kNN (95.63%), Naive Bayes (96.88%), and Logistic Regression (96.25%) classifiers resulted the highest accuracies using combined features of IMF1- IMF3. On the other hand, in the EEMD approach SVM (96.06%) and Logistic Regression (96.25%) classifiers provided the highest classification accuracy for the combined features of IMF1. While kNN (97%) achieves

the best performance using combined features of IMF1-3, Naive Bayes (97%) yielded maximum classification accuracy using the combined feature of IMF1-IMF3. DWT approach provided maximum classification accuracy of 94.56% with Naive Bayes classifier for the combined features of subbands. Notice that by using the same features extracted from the EEG signal (the last row), kNN (93.25%) provides the best classification performance. We also observed that the classification performance of the combined feature-set created by using the EEG signal is worse than the EMD and EEMD approaches. Furthermore, the highest classification performance for all classifiers is achieved using features extracted by EEMD approach. Apart from the selected first 3 IMFs, the success of the classification was not improved when the features obtained using the 4th IMF were included in the classification process.

(a)

(b)

(c)
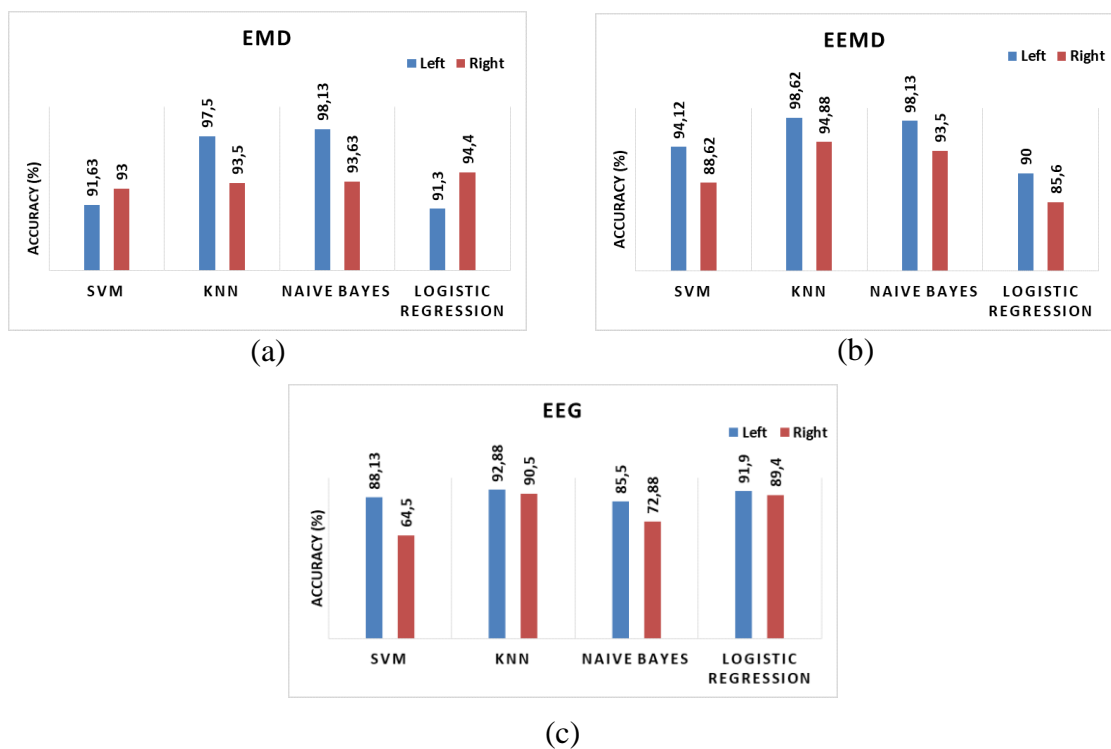
Figure 4.4: Hemisphere based mean classification accuracy for (a) EMD approach, (b) EEMD approach, and (c) EEG signals. Here, left and right Hemispheres were represented with blue and red, respectively.

In order to investigate the channel based performance of our approaches, the classification is performed for 10 channels separately using total features of IMF1-3.

The average mean classification accuracies for the channels in the left (Fp1-F7, F7-T1, T1-T3, T3-T5, Fp1-F3 channels) and right (Fp2-F8, F8-T2, T2-T4, T4-T6, Fp2-F4 channels) hemispheres are calculated. The classification accuracy of EEMD and EEG signal based approaches are higher in the left hemisphere for all four classifiers (shown in Figure 4.4b and 4.4c). These results are supported by the clinical information about epileptic focus areas of patients in our study shown in Table 4.1. However, in the EMD based approach, the classification accuracy is higher for the left hemisphere only for kNN and NB classifier (shown in Figure 4.4a).

In our proposed study, the main objective is to present a hybrid IMF selection method and explore the effect of selected IMFs extracted by EMD and EEMD, on the classification performance. Our approach investigates the advantage of using EEMD where noise added versions of the signal are decomposed to eliminate the well-known, mode-mixing problem of EMD. The problem of mode mixing can be described as the occurrence of very different oscillations in one mode, or very similar oscillations in different modes. EEMD method has been developed to overcome this shortcoming of EMD. As such, in our experiments we included EEMD as well as EMD to compare their classification performance.

We have applied the proposed IMF selection approach on the classification of EEG signals recorded from epilepsy patients who are under treatment at our collaborator hospital. We have used 10 channel EEG signals recorded from 16 patients, providing a total of 160 pre-seizure, and 160 seizure (320 total) EEG segments. In addition, 4 time-domain, 5 frequency domain, and 2 nonlinear features are extracted from each selected IMF of those EEG segments. The timedomain, spectral-domain, and non-linear features obtained from the selected three IMFs (IMF1, IMF3 and IMF2; in this order) were classified using SVM, kNN, Naive Bayes, and Logistic Regression classifiers, and the performances of EMD and EEMD approaches were compared. Then by using this selection approach, we explore the advantages of IMF selection in either EMD or EEMD approaches as opposed to using first several IMFs (IMF1-4). In order to reveal the advantages of using EMD or EEMD approaches, the same features were extracted from the EEG signal itself, and the subbands obtained by the DWT approach, and classification processes is repeated.

51

Performance of SVM classifier with time feature-set was found to be poor for both approaches. When nonlinear feature-set was used, the success of four classifiers was found to be low in both approaches. Using the spectral feature-set, we obtain higher accuracies for all classifiers except Logistic Regression. This suggests that epileptic seizures cause distinctive changes in the frequency domain. In addition, when IMF-based classification results were evaluated, we noticed that the success of classification performed only by the features obtained from the combination of selected IMFs was higher or similar to randomly selected first 4 IMFs (except nonlinear feature set). This shows that the IMF selection process helps improve the classification performance as selected IMFs carry the most useful information for the discrimination between the seizure and pre-seizure segments of EEG signals. The classification accuracy obtained using EMD or EEMD approaches using each feature-set is higher than that of the features obtained directly from EEG signals, and subbands of DWT, for all four classifiers. The computational complexity of EMD and its derivative, over classical approaches such as DWT, and Fast FT (FFT) is generally considered as a disadvantage. Contrary to common knowledge, if the number of sifting steps in the EMD algorithm is equal to 10, the computational complexity is given as $O(N \log N)$ which is same as the computational complexity of FFT, where O denotes the order of computation, and N shows the signal sample size. In addition to EMD, the number of ensembles is added to the computational complexity in the EEMD approach [115]. Therefore, in signal processing applications, EMD based approaches may be preferred considering the trade-off between the performance and computational cost.

Evaluating the channel based classification performances, the classification success of the features obtained by EEMD approach was found to be higher than other approaches for all 4 classifiers (shown in Figure 4.4). The innovative contributions of our study can be highlighted as follows;

- We propose a hybrid IMF selection method considering different approaches such us energy, correlation, power spectral distance, and statistical significance test.
- We demonstrate the advantages of using selected IMFs by the proposed approach of either EMD or EEMD approaches as opposed to randomly selecting first several IMFs.

- We investigate the performance improvement by using ensemble EMD in the classification of epileptic seizures as compared to traditional EMD, the EEG signal itself, and DWT based approaches.

4.3   Results and Discussions of DMD Methods

In this thesis, a DMD based epileptic seizure classification approach is proposed. Epileptic EEG data set (IKCU EEG data set) labeled as pre-seizure and seizure segments by physicians, is used. Dynamic modes are obtained by using the DMD algorithm for pre-seizure and seizure EEG segments and various features such as DMD subband powers, and higher-order DMD moments are calculated using these DMD modes. Finally, the extracted features are classified by using DT, LR, NB, kNN, SVM, and RF classifiers. All signal processing, feature extraction, and classification processes are performed using MATLABc 2019 software running on a personal computer with Intel (R) Core (TM) i7 processor and 8 GB of RAM. The steps of the proposed approach are represented as a block diagram given in Figure 4.5.
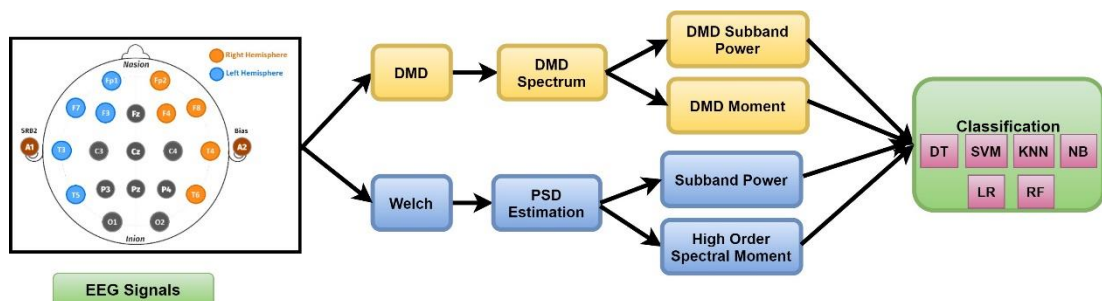
Figure 4.5: Block diagram of the proposed DMD based method
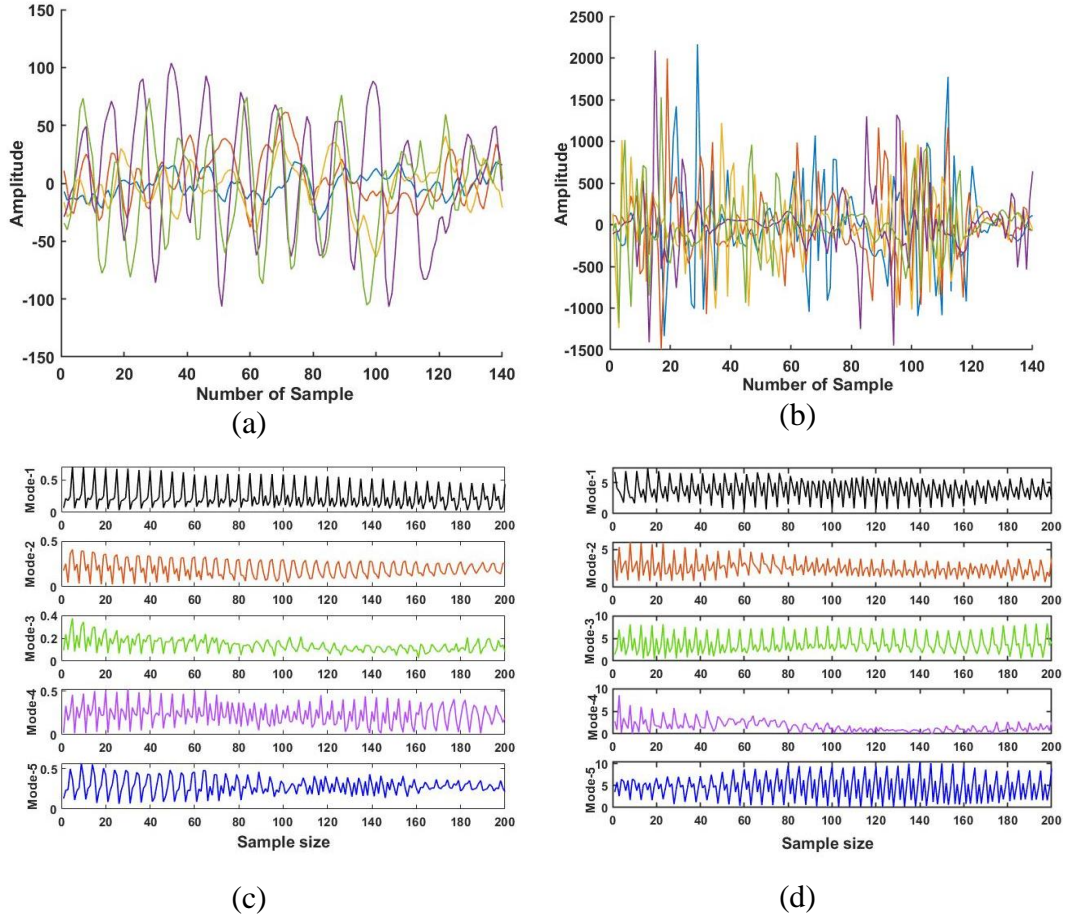
Figure 4.6: Example Single Channel EEG based DMD modes; (a) 5 Pre-Seizure EEG segments, (b) 5 Seizure EEG segments, First 5 DMD modes of; (c) Pre-Seizure EEG segments shown in (a), (d) Seizure EEG segments shown in (b).

In literature, previously, $K \times T -$ sized multi-channel EEG signals are evaluated using the DMD approach. Here, T is the sample size of a single EEG channel, and K is the number of channels. Using this data matrix, $K \times L -$ sized X data matrices in which L denotes the time samples named "snapshot" is obtained, and the DMD algorithm is applied to these obtained data matrices [58]. In our study, both the multi-channel DMD approach used in the literature is performed and the single-channel DMD approach is proposed, unlike the literature, and $K \times L -$ sized X data matrices are constructed using these two different approaches.

In the **single-channel DMD approach (SC-DMD),** the single-channel EEG signals with $T -$ samples long are divided into non-overlapping, L samples long EEG segments. The $(K \times L)$ EEG data matrices are constructed using K of these obtained

segments [100]. For our epileptic seizure classification experiment, $L = 140$ and $K = 5$ are chosen.

Additionally, in the **multi-channel DMD approach (MC-DMD),** $(K \times L)$ EEG data matrices with no overlap are generated using $L = 140$ samples of $K = 5$ different EEG channels. In our experiment, these data matrices are obtained using the $K = 5 -$ EEG channel in the left hemisphere (Fp1-F7, F7-T1, T1-T3, T3-T5, Fp1-F3) and the $K = 5 -$EEG channel in the right hemisphere (Fp2-F8, F8-T2, T2-T4, T4-T6, Fp2-F4). Also (10 $\times$ 120 EEG data matrices are constructed using the $K = 10 -$EEG channel with $L = 120$ sample long in both hemisphere. In Figure 4.6, we give the first 5 of the extracted DMD modes by the proposed single channel EEG based DMD approach for pre-seizure and seizure epileptic EEG segments.

In the next section, we apply the proposed DMD approaches to the detection of epileptic seizures in EEG signals.

4.3.1 The DMD Spectrum

The dynamic modes (achieved using Algorithm 3) are associated with complex eigenvalues λ$_m$, the real part of which shows the decay frequency of the dynamic modes and the imaginary part of which shows the oscillation frequencies of the dynamic modes shown in Equation (4.8) [97, 98, 100, and 102].

$$f_m = \left| imag(\frac{\omega_m}{2\pi}) \right| \tag{4.8}$$

Here, f_m is the oscillation frequency of mth DMD mode in Hz, $\omega_m = \frac{\log(\lambda_m)}{\Delta t}, \Delta t = 0.001s$ denotes the time difference between sequential snapshots, and $imag(.)$ is the imaginary part of a complex number. The sorted set of different mode frequencies f_m is defined as $F_{DMD} = \{f_m\}$.

The power of these modes P_m can be calculated using norm-square as given in Equation (4.9) and used to obtain the DMD Spectrum. However, before calculating the power of the modes, the scaling process specified in [98] is applied to the modes.

The frequencies of DMD modes do not spread uniformly as in the conventional Fourier spectrum [97], hence more than one mode may be present at one frequency, or there may not be any mode at some frequencies. Therefore, before the DMD Spectrum was obtained, the mode powers corresponding to the same frequency are combined together as shown in Equation (4.10), then a single power value is calculated for each frequency.

$$P_m = \|\Phi_m\|^2 \tag{4.9}$$

where $\| \, . \, \|^2$ indicates the Euclidian norm.

$$P_{DMD}(f_m) = \sum_{i=1}^{L_k} P_m{}^i(f_m), \quad \forall\{f_m\} \in F_{DMD} \tag{4.10}$$

Here, L_k is the number of modes at frequency f_m, $P_m{}^i(f_m)$ is the power value of ith DMD mode at the frequency f_m, and $P_{DMD}(f_m)$ denotes the sum of DMD powers at the frequency f_m. To obtain the DMD spectrum, $P_{DMD}(f_m)$ vector is plotted with respect to the oscillation frequency vector F_{DMD}.

Examples of the proposed Single-Channel EEG based, and Multi-Channel EEG based DMD spectra for pre-seizure and seizure epileptic EEG data are given in Figures 4.7 and 4.8. Single- Channel EEG based DMD spectra of pre-seizure and seizure epileptic EEG data matrices are given in Figs. 4.7-a, and 4.7-b respectively. Figs. 4.7-c and 4.7-d show the PSD estimates of corresponding EEG segments calculated using Welch method. Similarly, Multi-Channel EEG based DMD spectra of 5-channel pre-seizure and 5-channel seizure epileptic EEG data are given in Figs. 4.8-a and 4.8-b respectively. The Welch spectral estimates of corresponding channels individually are given in Figs. 4.8-c and 4.8-d. Notice that the similarity between DMD spectra and Welch PSD estimates are remarkable. However, while the DMD spectra are simultaneously calculated for 5 EEG segments, Welch estimates are calculated for each EEG segment individually. In Figs. 4.7-c, 4.7-d, 4.8-c, and 4.8-d, the black bold lines show the average of 5 spectral estimates.
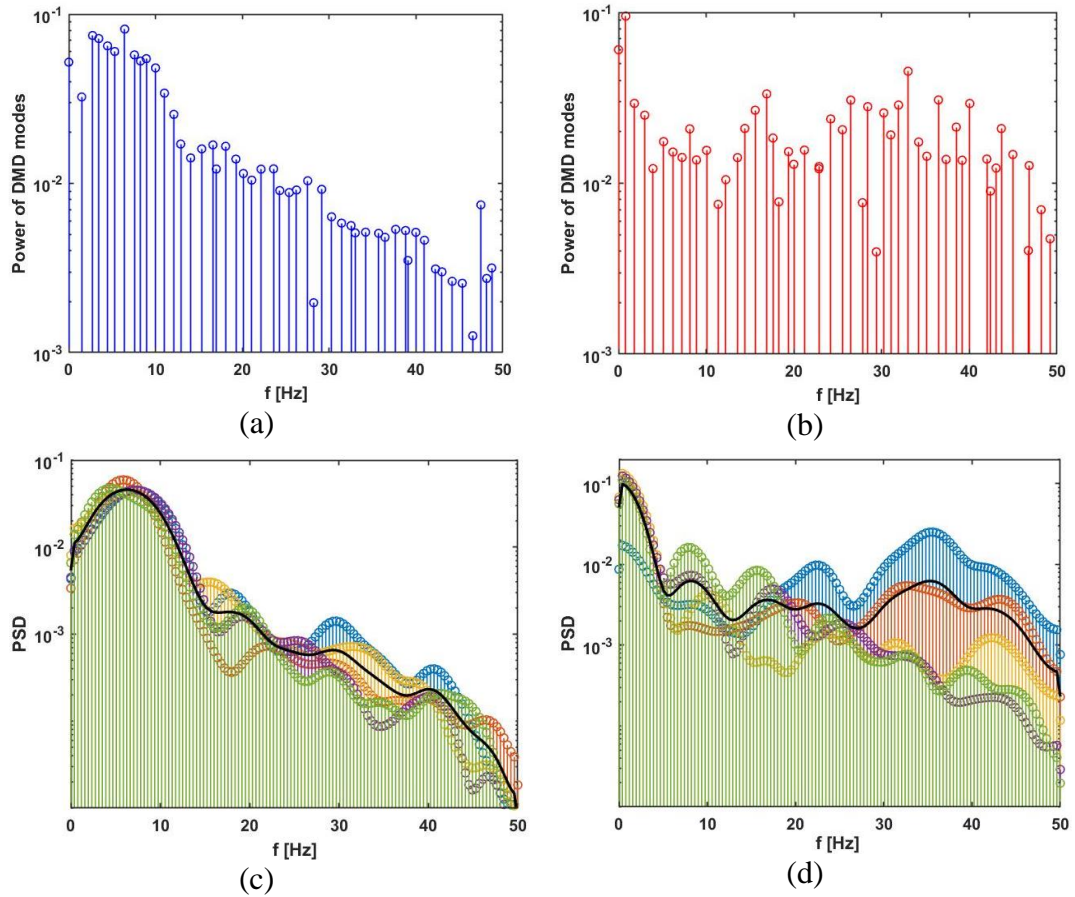
Figure 4.7: An example of Single Channel EEG based DMD representation. DMD Spectrum of (a) 5 Pre-Seizure EEG segments, (b) 5 Seizure EEG segments, PSD estimates of (c) 5 Pre-Seizure EEG segments together, (d) 5 Seizure EEG segments together. In (c) and (d) bold black lines show the average of 5 PSD estimates.
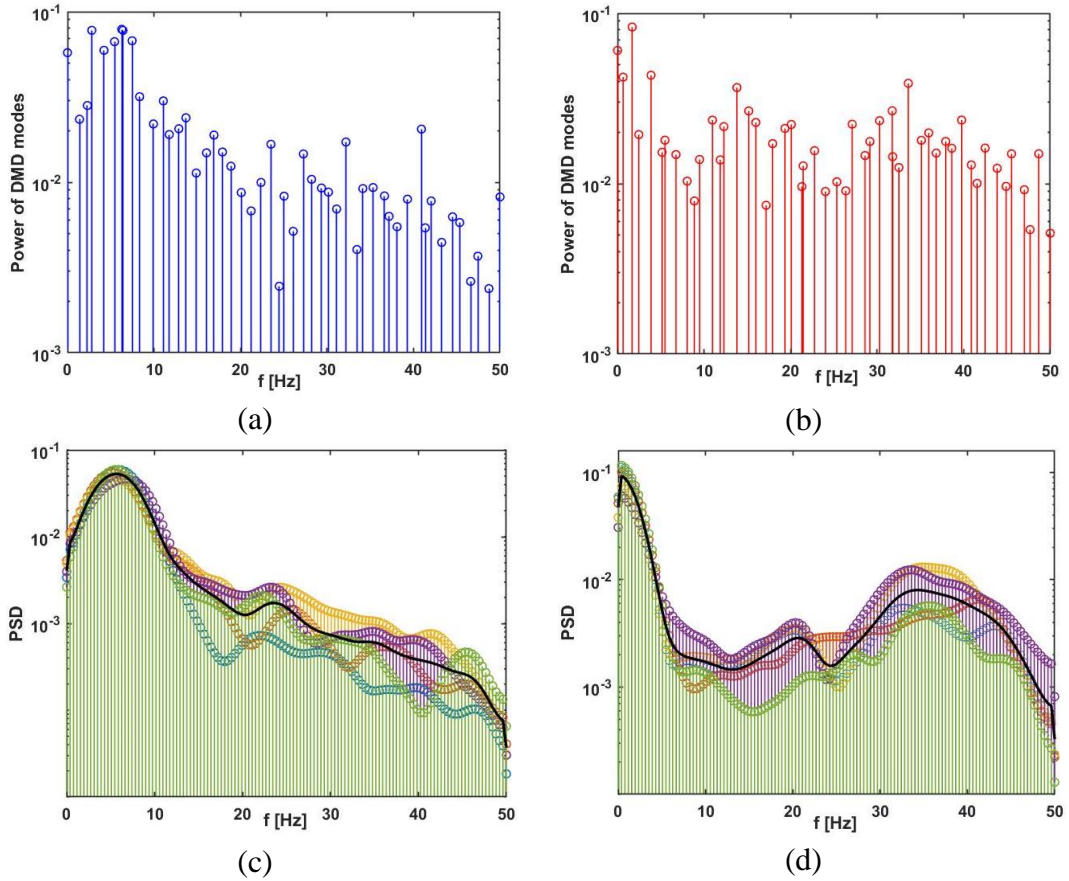
Figure 4.8: An example of Multi Channel EEG based DMD representation. DMD Spectrum of (a) 5-channel Pre-Seizure EEG segments, (b) 5-channel Seizure EEG segments, PSD estimates of (c) 5-channel Pre-Seizure EEG segments together, (d) 5-channel Seizure EEG segments together. In (c) and (d) bold black lines show the average of 5 PSD estimates.

4.3.2 DMD Features

In this study, we propose two sets of DMD features for the classification of epileptic EEG segments. First approach uses the EEG sub-band powers and total power calculated from the DMD spectrum. As a second approach, we introduce a new method called Higher-order DMD spectral moments (DMD-HOS).

4.3.2.1 DMD Sub-band Powers

In the first approach, we define EEG Sub-band Powers in the DMD domain; Delta (P_δ), Theta (P_θ), Alpha (P_α), Beta (P_β), and Gamma (P_γ) band powers, and the total DMD power (P_T) calculated from the DMD Spectrum.

EEG signals are composed of different oscillations which are known to be responsible for different cognitive functions. These are called Delta (δ), Theta (θ), Alpha (α), Beta (β), and Gamma (γ) waves. The frequency bands of these EEG sub-bands are; delta (0–4Hz), theta (4–8Hz), alpha (8–12 Hz), beta (12–30 Hz), and gamma waves (30–60Hz).

$$P_\delta = \sum_{f_m \in f_\delta} P_{DMD}(f_m); \quad P_\theta = \sum_{f_m \in f_\theta} P_{DMD}(f_m);$$

$$P_\alpha = \sum_{f_m \in f_\alpha} P_{DMD}(f_m); \quad P_\beta = \sum_{f_m \in f_\beta} P_{DMD}(f_m);$$

$$P_\gamma = \sum_{f_m \in f_\gamma} P_{DMD}(f_m); \quad P_T = \sum_{f_m} P_{DMD}(f_m); \tag{4.11}$$

where f_δ is a subset of extracted DMD mode frequencies $F_{DMD} = \{f_m\}$ corresponding to δ sub-band of EEG, f_θ is the subset of the DMD modes frequencies corresponding to θ sub-band of EEG, and so on.

EEG sub-band powers and total power calculated from traditional power spectrum are commonly used as frequency domain features of EEG signals in computer aided diagnosis algorithms in a variety of problems [22, 44, and 100]. In the proposed method, DMD sub-band powers and total power are calculated as indicated in Equation (4.11).

4.3.2.2 Higher-order DMD Spectral Moments

Similar to the higher-order frequency moments calculated using traditional PSD, we propose **Higher-order DMD Spectral Moments** as the second approach of feature

extraction [100]. The Higher-order DMD Spectral Moments $< f_m{}^j >$, $j = 1, 2, 3, ...$ are defined as;

$$M^j{}_{DMD} = \sum_{f_m \in F_{DMD}} (f_m)^j P_{DMD}(f_m), \qquad j = 1, 2, 3 ... \tag{4.12}$$

Here, f_m denotes the extracted mode frequencies in the set F_{DMD}, $P_{DMD}(f_m)$ is the value of the DMD spectrum at frequency f_m, and $M^j{}_{DMD}$ denotes the jth order DMD Spectral Moment. In our experiments, we calculated the first three DMD Spectral Moments, $j = 1, 2, 3$, and used for classification.

In order to investigate the advantages of using the DMD methods, the Sub-band Powers and Higher-order Spectral Moments are calculated using the classical PSD estimate as well. Power Spectrum of each pre-seizure and seizure EEG segment was estimated using the Welch method which is an improved version of the Periodogram. In this method, the data is divided into K segments which are overlapping. Then the windowed Periodograms of each segment are calculated and averaged to estimate the PSD. In our simulations, we use a Hamming window and 50% overlapping [22, 44, 116, and 117].

Pre-seizure and seizure EEG signals are divided into segments containing 140 samples (1.4 sec) to obtain the similar segment sizes used in the proposed DMD method. Afterward, the PSD of each EEG segment was estimated using the Welch method. Sub-band Powers (Delta (S_δ), Theta (S_θ), Alpha (S_α), Beta (S_β), and Gamma (S_γ)), total power (S_T), and Higher-order Spectral Moments $< \omega_k{}^j >$ are calculated as follows;

$$S_\delta = \sum_{f_k \in f_\delta} S(f_k); \quad S_\theta = \sum_{f_k \in f_\theta} S(f_k);$$

$$S_\alpha = \sum_{f_k \in f_\alpha} S(f_k); \quad S_\beta = \sum_{f_k \in f_\beta} S(f_k); \tag{4.13}$$

$$S_\gamma = \sum_{f_k \in f_\gamma} S(f_k); \quad S_T = \sum_{k=0}^{N-1} S(f_k);$$

$$M^j{}_{PSD} = \sum_{k=0}^{N-1} (f_k)^j S(f_k), j = 1, 2, 3, \dots \qquad (4.14)$$

Here, N denotes the length of the corresponding EEG signal, $f_k = \frac{F_s}{N}k$, $k = 0, 1, \dots, N-1$ are the uniform frequency samples, F_s is the sampling frequency, $S(f_k)$ is the Power Spectral Density estimate of the EEG signal at frequency f_k. Frequency subset f_δ contains frequency values corresponding to δ sub-band frequencies $(f_k \in [0-4] \text{ Hz})$ of the EEG, f_θ contains frequency samples corresponding to θ sub-band frequencies $(f_k \in [4-8] \text{ Hz})$ of the EEG, etc. Hence 5 subband power features for $\delta: [0-4]$ Hz, $\theta: [4-8]$ Hz, $\alpha: [8-13]$ Hz, $\beta: [13-22]$ Hz, and $\gamma: [22-50]$ Hz bands are obtained considering the sampling frequency of 100 Hz. $M^j{}_{PSD}$ indicates the jth-order Spectral Moment of the EEG segment.

4.3.3 Experimental Results and Discussions

In this study, we aim at distinguishing the pre-seizure and seizure EEG segments using the DMD spectral based approaches. Pre-seizure and seizure segments of 10-channel EEG recordings of 16 epilepsy patients are used for the proposed study. DMD approach utilized to obtain DMD Spectra of each EEG segment as described in previous section. The Sub-band Powers and total power of DMD Spectrum, and Higher-order DMD Spectral Moments are calculated as features using the DMD Spectra. The analysis is also performed by utilizing the PSD estimated using the Welch method to compare the performance of the proposed approach. Hence, traditional Sub-band Powers, total power, and Higher-order Spectral Moments are also calculated from the estimated PSD of EEG segments. Finally, various classifiers such as DT, SVM, kNN, NB, LR, and RF were used for the classification and the results of each of them were investigated.
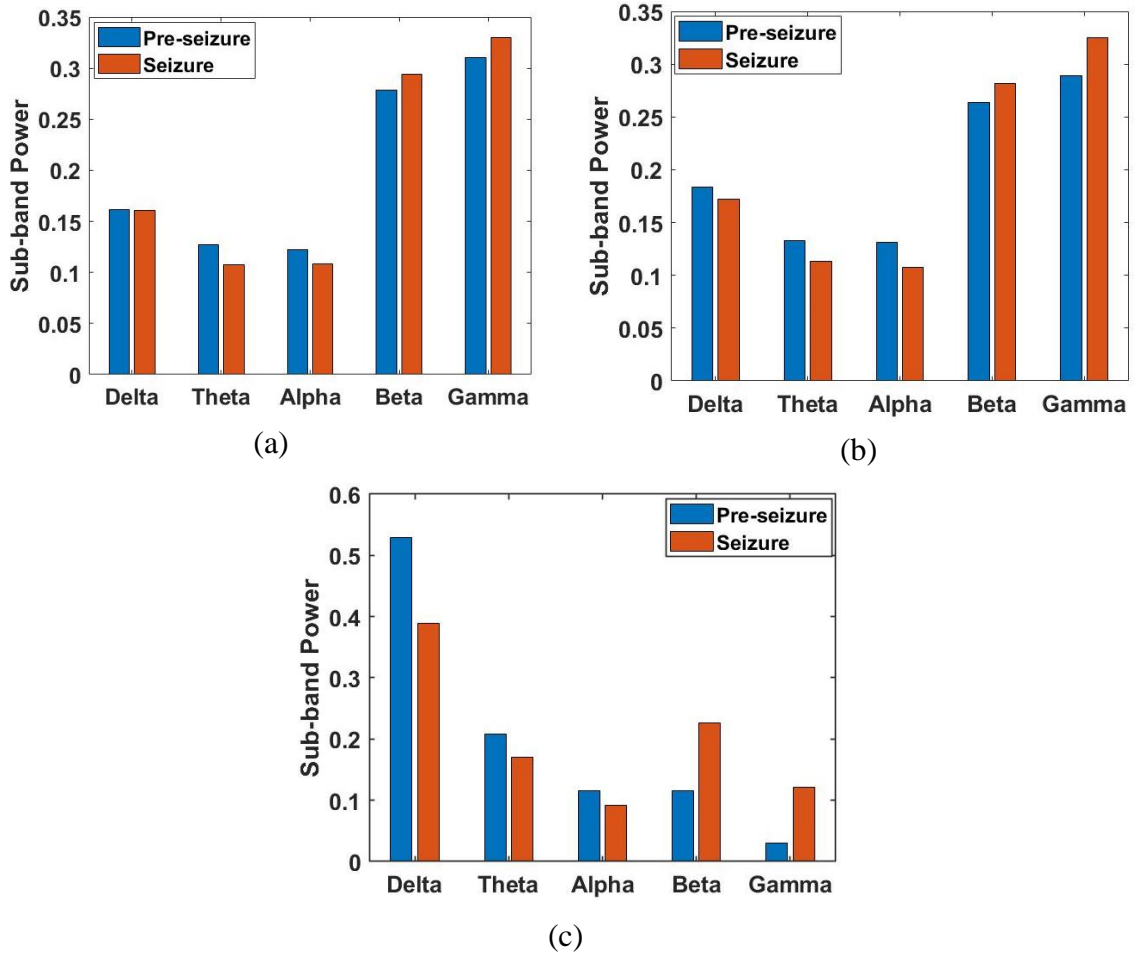
Figure 4.9: The mean Sub-band power values for pre-seizure and seizure EEG segments calculated using; (a) Single Channel DMD Spectrum, (b) Multi Channel DMD Spectrum, (c) Power spectral estimates.

Figure 4.9 shows the average values of sub-band powers calculated from the DMD Spectrum (Figgure 4.9-a,b) and the PSD estimate (Figgure 4.9-c) for pre-seizure and seizure epileptic EEG segments of 10 EEG channels of 16 epilepsy patients. While sub-bands (Delta (P_δ), Theta (P_θ), Alpha (P_α)), containing low-frequency information are dominant for the pre-seizure, the increase in high frequencies (Beta (P_β), and Gamma (P_γ)) for seizure data is noticed. In general, the power of higher frequencies bands of EEG signals such as beta and gamma increases before and during epileptic activity by the transfer of energy of lower frequencies bands to higher frequency bands [118, 119].

The averages over all channels and subjects of higher-order DMD spectral moments (Figure 4.10-a,b) and traditional higher-order spectral moments (Figure 4.10-c) for pre-seizure and seizure EEG segments are given in Figure 4.10 to compare the two methods. Similar to traditional spectral moments, the first 3 DMD spectral moments of both DMD approach contain distinctive information about pre-seizure and seizure EEG data.

(a)

(b)

(c)
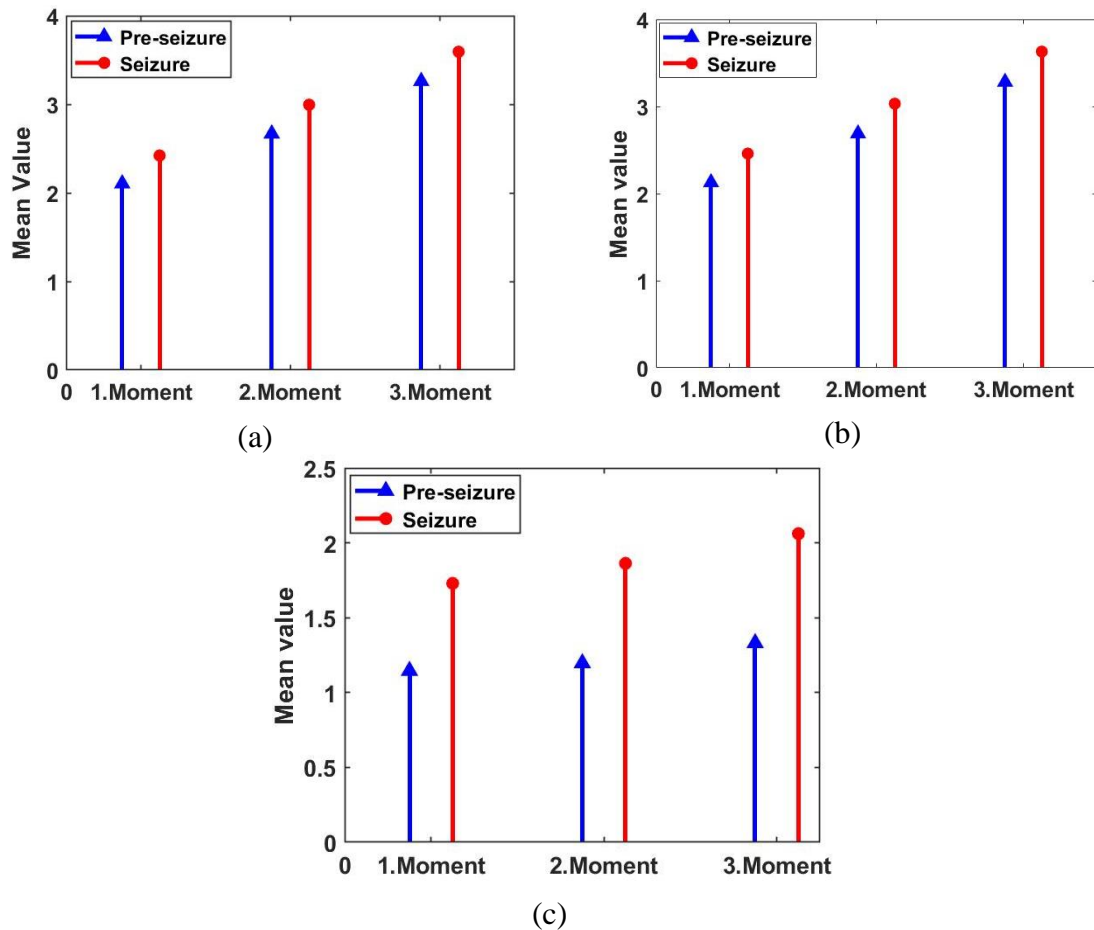
Figure 4.10: The mean moment values for pre-seizure and seizure EEG segments calculated using; (a) Single Channel DMD Spectrum, (b) Multi Channel DMD Spectrum, (c) Power spectral estimates.

Tables 4.7-4.9 demonstrate the performance evaluation results of proposed approaches. The boldface numbers in the tables show the highest classification result for that component. The performance evaluation of the proposed Single-channel based DMD approach is summarized in Table 4.7. Here, Fp1-F7, F7-T1, T1-T3, T3-T5, Fp1-F3, Fp2-F8, F8-T2, T2-T4, T4-T6, Fp2- F4 show that the classifications are performed using the feature sets obtained from the EEG segments of related channels. On the other hand, "Left Hems" and "Right Hems." indicate that the classifications are

performed using the feature sets created by combining the features obtained from the channels in the left hemisphere (Fp1-F7, F7-T1, T1-T3, T3-T5, Fp1-F3) and the right hemisphere (Fp2-F8, F8-T2, T2-T4, T4-T6, Fp2-F4) respectively. Additionally, "Two Hems." denotes that the classifications are performed using the feature sets generated by combining the features obtained from the channels in both hemispheres.

Table 4.7: Performance evaluation results (ACC %) of single-channel based DMD Approach

Component	Subband Power Based Feature Set						Moment Based Feature Set					
	DT	LR	NB	SVM	kNN	RF	DT	LR	NB	SVM	kNN	RF
FP1-F7	91.2	91.7	92.3	91.7	90.6	92.8	87.8	92.3	86.7	87.8	90.1	87.8
F7-T1	94.5	92.8	93.9	93.4	91.7	96	88.4	93.9	88.4	89.5	88.4	86.2
T1-T3	95	96.1	95.6	94.5	95.6	96.1	91.2	96.1	91.7	91.7	95	90.6
T3-T5	96.1	95.6	95	96.1	97.2	95	95.6	96.1	92.8	93.9	95.6	95.6
FP1-F3	91.2	92.8	91.7	91.7	91.2	89.5	90.1	92.3	88.4	89.5	87.8	87.8
FP2-F8	91.2	91.2	89.5	89	85.6	91.2	86.2	89.5	84.5	86.2	86.2	80.1
F8-T2	92.3	92.3	92.3	92.8	92.3	91.7	87.8	92.8	84.5	89.5	89.5	90.1
T2-T4	88.4	89.5	88.4	89.5	86.2	90.1	89.5	88.4	87.8	87.8	84	85.1
T4-T6	85.6	90.1	90.6	89.5	90.1	89.5	84	87.8	83.4	86.7	87.8	84.5
FP2-F4	85.6	88.4	85.1	86.2	88.4	85.6	81.2	84.5	80.1	83.4	84	82.3
Right Hems	89.1	90.2	89.5	90.2	90.6	90.9	86.1	89.1	83	87.1	88	86.7
Left Hems	92.9	94	93.5	93.8	94.3	93.3	91.7	93.3	90.2	92.7	91.9	92.3
Two Hems	91.3	91.7	91.3	91.6	91.7	91.7	88.5	91	87.3	90.4	90.5	89.9

Table 4.8: Performance evaluation results (ACC %) of PSD based approach

Component	Subband Power Based Feature Set						Moment Based Feature Set					
	DT	LR	NB	SVM	kNN	RF	DT	LR	NB	SVM	kNN	RF
FP1-F7	93.1	68.5	91.3	88.5	90.9	92.6	92.6	87.2	90.7	89.6	92.4	92.4
F7-T1	94.9	94.2	92	92	94.9	94.7	94.6	94.3	93	93	94	94.4
T1-T3	95.4	95.7	95.2	92	95.6	95.3	96.1	96.3	95.1	95.3	96.3	95.3
T3-T5	95.2	96.9	95	94.8	93.6	96.2	96	96.4	95.7	95.1	95.6	95.7
FP1-F3	89	88.7	88.8	88.8	89.6	91	91.3	88.8	89.9	88.9	88.2	91.2
FP2-F8	89.5	88.2	89	86	87.2	90.5	91.8	87.3	89	87.4	90.4	91.2
F8-T2	91.5	82.3	89.1	89.3	91	92.9	91	90.3	88.1	89.7	90	91.6
T2-T4	89.6	83.9	88.4	86.4	88.7	91.1	89	86.6	87.6	84.5	89.6	89.5
T4-T6	91.6	66.4	88.1	87	88	92.7	90.9	86.4	88.1	86.4	88.8	89.8
FP2-F4	88.4	81	84.1	80.7	83.8	88.6	86.1	81.9	83.5	78.5	85.2	85.4
Right Hems	89.3	85.8	86.8	86.1	87.1	90.8	89.2	85.2	86.8	85.3	88.1	89.2
Left Hems	91.9	92	91.2	91.9	92.2	93.3	92.9	92.1	92.5	92.6	91.7	91.9
Two Hems	90.5	88.7	88.4	89.2	89.6	91.8	90.2	88	89.3	88.5	89.4	90.2

The highest accuracy (97.2%, 96.1%) values are achieved using the both proposed DMD subband power, and higher-order DMD spectral moment features calculated in the T3-T5 channel (in the left hemisphere) with the kNN and LR classifier. However,

the lowest classification accuracy for both feature sets is obtained from the Fp2-F4 channel (in the right hemisphere). In addition, for the DMD sub-band power-based feature set calculated from the left hemisphere (Left Hems.), the kNN classifier achieved 94.3% accuracy, while 93.3% classification accuracy with the LR classifier is achieved for the DMD spectral moment-based feature set obtained from the same hemisphere (given in Table 4.7).

In order to investigate the advantages of the proposed DMD-based approaches, similar feature sets (Subband Powers and Higher-Order Spectral Moments) are calculated from the PSD estimated by the Welch periodogram method. Classification performance results are given in Table 4.8. Fp1-F7, F7-T1, T1-T3, T3-T5, Fp1-F3, Fp2-F8, F8-T2, T2- T4, T4-T6, Fp2-F4 shows the Channel-based classification results of the features obtained from the traditional PSD estimate of the EEG segments in respective channels. Right Hems, Left Hems, and Two Hems; denote the hemisphere-based classification result, where the features are combined separately for the Right hemisphere, Left Hemisphere and both hemispheres. The highest classification accuracies are achieved from the T3-T5 channel using LR classifier for both Subband Power-based features (96.9 %) and Moment based features (96.4 %), obtained from the Channel-based PSD approach. On the other hand, the highest classification accuracies (93.3%, 92.9%) are obtained with the RF and DT classifiers using the subband power based features and moment based features, calculated from "Left Hems" of the hemisphere based PSD approach.

Table 4.9: Performance evaluation (ACC %) of multi-channel based DMD approach

Component	Subband Power Based Feature Set						Moment Based Feature Set					
	DT	LR	NB	SVM	kNN	RF	DT	LR	NB	SVM	kNN	RF
Right Hems	89.9	89.9	89.8	90.4	89.9	90.7	84	89.3	81.5	88.2	86.5	87.1
Left Hems	93.9	92.6	92.5	93	94.1	93.9	90.9	93	87.5	92.5	92.5	92.9
Two Hems	94.3	94.9	93.5	95	94.6	94.1	91.3	94.6	88.7	92.8	92.2	92

Table 4.9 lists the performance evaluation results of the Multi-Chanel based DMD Approach. Here, while "Left Hems." shows that the EEG matrices utilized in the DMD algorithm are obtained from the left hemisphere channels, "Right Hems." indicates that the EEG matrices are obtained from the right hemisphere channels. In addition, "Two Hems." denotes that these EEG matrices are obtained using both hemisphere

channels. Using those EEG matrices, the DMD algorithm is performed, and Subband Power based and Moment based features are obtained from the DMD Spectrum. In the "Right Hems" of DMD, while RF provides 90.7% accuracy using Subband Power-based feature set, LR provides 89.3% accuracy using the Moment-based feature set. However, higher classification accuracies for Subband Power-based features and Moment based features of the "Left Hems." of DMD are obtained with kNN (94.1%) and RF (92.9%), respectively. On the other hand, using the features obtained from the "Two Hems" of DMD, (94.9% and 94.6%) accuracies are achieved with LR for the Subband Power-based and Moment based features respectively. Note here that, DMD spectral features extracted from the proposed single-channel EEG-based DMD approach provides the highest classification performance among all other combinations.

Classifier based changes of sensitivity and specificity values obtained from the "Two Hems" of both single- and multi-channel DMD and PSD approaches are given in Figure 4.11. Here, while the sensitivity value denotes the ratio of the correctly classified seizure data, the specificity value indicates the ratio of the correctly classified pre-seizure data. Higher SEN values are obtained using the Multi-channel DMD approach than the other two approaches for all feature sets and classifiers except the SEN value of the DT classifier obtained using the moment-based feature set of the PSD approach (shown in Figure 4.11a and 4.11c). In both subband power based and momentbased feature sets, the single-channel DMD approach provided higher SEN values than the PSD approach, except for DT and NB classifiers. Additionally, for the Multi-channel DMD approach, higher SPE values are obtained for all classifiers and feature sets than other two approaches, except the SPE value of the NB classifier obtained from the moment-based feature set of the PSD approach (shown in Figure 4.11b and 4.11d). Overall, the single-channel DMD approach provided higher SPE values than the PSD approach.
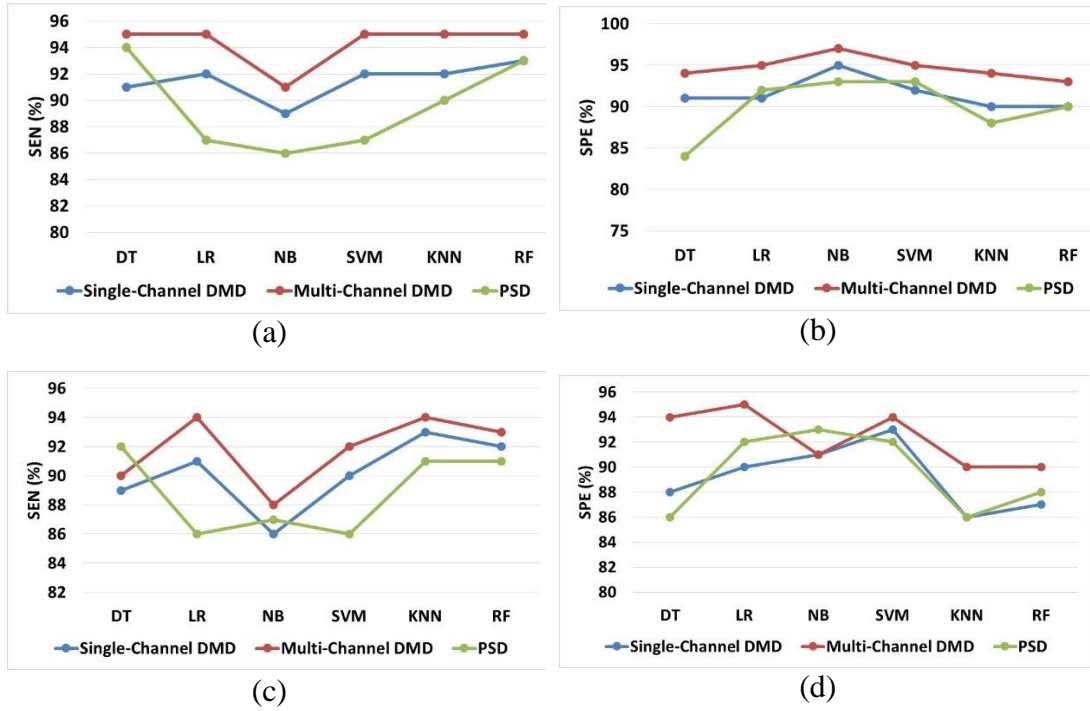
Figure 4.11: Classifier based change of; (a) sensitivity and (b) specificity values obtained from Subband-power based feature sets of approaches; (c) sensitivity and (d) specificity values obtained from Moment based feature sets of approaches.

In order to evaluate the performance of the proposed DMD approach on a publicly available epileptic EEG data set, single-channel and multi-channel DMD algorithms are also tested on CHB-MIT epilepsy data [110]. In our experiments, we used EEG data of 14 patients (chb01, chb02, chb03, chb04, chb05, chb07, chb09, chb10, chb17, chb18, chb19, chb20, chb22, chb23), which yielded successful epileptic seizure detection and prediction results in previous studies [29, 65, 120, and 121]. (i) Seizure segments (60 seizure event) of these patients, (ii) 5 minutes pre-seizure segments that end before the onset of those seizures, and (iii) 10 minute inter-seizure segments for each patient are used to perform (a) seizure prediction and (b) seizure detection experiments. By using the 10-channel CHB-MIT data set, moment-based and subband-based features are obtained with single-channel and multi-channel DMD approaches. In our CHB-MIT experiment, M = 308 samples long (1.2 sec.) EEG segments with no overlap, and N = 10 snapshots are chosen for single channel DMD approach, and the procedure is repeated for 10 channels. Additionally, $10 \times 308-$size EEG data matrices are generated using the whole $110-$channel EEG segments for the multi-channel DMD approach. In both single-channel, and multi-channel DMD

approaches, (520×256) – sized augmented EEG data matrices are obtained. The details of both single-channel and multi-channel DMD approaches are described previously. These augmented EEG data matrices are used to extract the DMD modes for seizure, pre-seizure, and inter-seizure EEG segments. Moment-based and subband-based features are calculated using these DMD modes. For (a) seizure detection experiment, features obtained from seizure, and inter-seizure EEG segments are combined to create seizure detection feature set. As for (b) seizure prediction experiment the features obtained from pre-seizure and inter-seizure EEG segments are combined to generate seizure prediction feature set for each patient. Finally, these feature sets are classified using DT, NB, kNN, SVM, and RF and their classification performances are evaluated using various statistical performance metrics such as SEN, SPE, and ACC.

Table 4.10: Average performance evaluation results (ACC %, SEN %, and SPE %) of 14 patients of CHB-MIT data set for seizure detection experiment.

Method	Metric	Subband Power Based Feature Set					Moment Based Feature Set				
		DT	NB	kNN	SVM	RF	DT	NB	kNN	SVM	RF
SC-DMD	ACC	96.2	95.6	96.3	96.1	**96.5**	93.8	91.4	94.9	**95.2**	94.7
	SEN	91.5	91.4	91.1	89.2	**92.5**	86.6	83.2	89.2	86.5	88.4
	SPE	97.6	97.3	98.2	**98.6**	97.8	95.9	94.9	96.9	**97.7**	96.9
MC-DMD	ACC	96.6	95.8	96.4	96.1	**96.7**	93.2	90.7	94.5	**94.5**	94.2
	SEN	92.8	92.9	91.5	88.6	**92.9**	84.4	81.9	**87.9**	84.8	87.5
	SPE	97.6	96.8	98.1	**98.5**	97.8	96.3	94.6	96.8	**98.2**	96.4

Performance evaluation results of the seizure detection experiment are summarized in Table 4.10. The RF classifier yields the highest accuracy and sensitivity values for the subband power based feature set of both single-channel and multi-channel DMD approaches (SC-DMD: 96.5 % ACC, 92.5% SEN; MC-DMD: 96.7% ACC, 92.9% SEN), while the maximum specificity values are achieved using SVM classifier for both approaches (SC-DMD: 98.6 % SPE; MC-DMD: 98.5% SPE). On the other hand, for the moment based feature set of single-channel DMD approach, the highest classification accuracy, and specificity values (95.2 % ACC, 97.7% SPE) are achieved using the SVM classifier, but the maximum sensitivity is obtained by the RF classifier. For the same feature set of the multi-channel DMD approach, the SVM classifier gives

the highest classification performance with 94.5 % ACC, and 98.2 % SPE values, while the maximum sensitivity value is achieved using the kNN classifier.

Table 4.11: Average performance evaluation results (ACC %, SEN %, and SPE %) of 14 patients of CHB-MIT data set for seizure prediction experiment.

Method	Metric	Subband Power Based Feature Set					Moment Based Feature Set				
		DT	NB	kNN	SVM	RF	DT	NB	kNN	SVM	RF
SC-DMD	ACC	84.7	83.1	85.1	82.2	**86.7**	76.5	74.1	81.2	80.9	**81.2**
	SEN	83.3	80.8	85.7	84.5	**86.1**	76.7	72.2	82.4	**83.7**	81.8
	SPE	86.3	86.9	84.1	80.1	**87.1**	75.7	76.8	78.7	78.3	**79.9**
MC-DMD	ACC	86.3	83.9	86.9	83.7	**88.5**	80.1	76.1	83.3	82.6	**83.5**
	SEN	87.9	82.6	89.5	89.2	**89.7**	86.4	80.5	87.2	**88.1**	86.6
	SPE	85.5	85.2	83.2	74.7	**86.1**	69.1	70.6	77.1	73.6	**77.8**

Table 4.11 shows the performance evaluation results of the seizure prediction problem. For the subband power-based feature sets of both single-channel and multi-channel DMD approaches, the highest accuracy, sensitivity, and specificity values are achieved using the RF classifier (SC-DMD: 86.7% ACC, 86.1% SEN, and 87.1% SPE; MC-DMD: 88.5 % ACC, 89.7% SEN, and 86.1% SPE). Moreover, for the moment based feature set of both DMD approaches, the highest accuracy and specificity values (SC-DMD: 81.2% ACC, 79.9% SPE; MC-DMD: 83.5 % ACC, 77.8% SPE) are obtained by the RF classifier, while the SVM classifier yields the maximum sensitivity values (SC-DMD: 83.7% SEN; MC-DMD: 88.1% SEN).

The classification performance of the Subband Power-based features is higher in the single channel based DMD approach than the multi-channel based DMD approach except "Two Hems." However, the classification accuracy of the Moment-based features is higher in the multi-channel based DMD approach than the single-channel based DMD approach except "Left Hems."(Shown in Table 4.7 and Table 4.9). In addition, the maximum classification performances of Subband Power-based features of DMD-based approaches are higher for each feature set and each condition than the maximum classification successes of the Subband Power-based features of PSD based approach.

Table 4.12: Classification performance comparison of various epileptic seizure detection and prediction studies.

Problem	Author	Data Set	Approaches	Performance Metrics
Seizure Detection	Alickovica et al. [38]	CHB-MIT*	EMD,DWT,WPD	100% ACC
		Freiburg	MD,DWT,WPD	100% ACC
	Moctezuma et al. [39]	CHB-MIT*	EMD	93% ACC
	Moctezuma et al. [122]	CHB-MIT*	EMD, DWT	93%–97% ACC
	Pachori et al. [42]	Bonn	EMD	100% ACC
	Wu et al. [40]	CHB-MIT*	CEEMD	95.8% ACC, 95.7% SEN, 95.9% SPE
		Bonn	CEEMD	99.5%–100% ACC
	Hassan et al. [43]	Bonn	CEEMDAN	97.6%–100% ACC, 97.7%–100% SEN, 97.4%–100% SPE
	Quintero et al. [46]	CHB-MIT*	DWT and GGD	92%–97% ACC, 97%–99% SEN, 79%–92% SPE
	Ibrahim et al. [47]	Bonn	WT	100% ACC
	Correa et al. [44]	Freiburg	WT	85.39% SEN, 83.17% SPE
	Bhattacharyya et al. [123]	CHB-MIT*	EWT	99.41% ACC, 97.91% SEN, 99.57% SPE
	Kumar et al. [41]	Bern-Barcelona	VMD	78.5% ACC, 95% SEN, 95% SPE
		Bonn	VMD	94.1% ACC, 95.33% SEN, 96.67% SPE
	Zhang et al. [45]	Bonn	GST and SVD	88.04%–99.12% ACC
	Ayodele et al. [65]	CHB-MIT*	CNN	71.45% SEN, 76% SPE
		TUSZ	CNN	78.35% SEN, 90% SPE
	Xiang et al. [29]	CHB-MIT*	Fuzzy Entropy	98.31% ACC, 98.27% SEN, 98.36% SPE
			Sample Entropy	97.16% ACC, 97.01% SEN, 97.34% SPE
		Bonn	Fuzzy Entropy	100% ACC, 100% SEN, 100% SPE
			Sample Entropy	88.5 % ACC, 90.36% SEN, 87.63% SPE
	Fu et al. [124]	Original	Sparse CSP	99.75% ACC
	Solaija et al. [58]	CHB-MIT*	MC-DMD	87% SEN, 99% SPE
		KU Leuven	MC-DMD	88% SEN, 99% SPE
	Bilal et al. [59]	CHB-MIT*	DMD	91% SEN, 99.2% SPE
			MRDMD	93.7% SEN, 99.2% SPE
		KU-Leuven	DMD	90.6% SEN, 99.3% SPE
			MRDMD	96.1% SEN, 99.1% SPE
	K.Cura et al. [125]	IKCU	EMD	97.14% ACC
			EEMD	98.13% ACC
			DWT	94.56% ACC
	Proposed Study	CHB-MIT*	SC-DMD	96.5% ACC, 92.5% SEN, 98.6% SPE
			MC-DMD	96.7% ACC, 92.9% SEN, 98.5% SPE
		IKCU	SC-DMD	97.2% ACC, 93% SEN, 95% SPE
			MC-DMD	94.9% ACC, 95% SEN, 97% SPE
Seizure Prediction	Alickovica et al. [38]	CHB-MIT	EMD,DWT,WPD	99.7% ACC
		Freiburg	EMD,DWT,WPD	99.5% ACC
	Alotaiby et al. [120]	CHB-MIT	CSP	89% SEN, 37% SPE
	Cui et al. [121]	CHB-MIT	Bag-of-Wave	88.24% SEN
	Proposed Study	CHB-MIT	SC-DMD	86.7% ACC, 86.1% SEN, 87.1% SPE
			MC-DMD	88.5% ACC, 89.75% SEN, 86.1% SPE

In order to demonstrate the performance of the DMD approach on a different dataset, the performances of the DMD approaches are evaluated using the publicly available CHB-MIT EEG dataset. Both seizure detection and seizure prediction problems are

considered and DMD based solutions are provided on this dataset. In the seizure detection and prediction experiments, the higher classification performances are achieved for subband power-based feature sets of both single-channel and multi-channel DMD approaches than that of the moment-based feature set (Shown in Tables 4.10-4.11). In case of seizure detection problem, no significant difference is observed between the performance of single-channel and multi-channel DMD approaches using both feature sets.

In Table 4.12, we summarize some of the previous epileptic "seizure detection" and "seizure prediction" studies, and compare their performances with that of the proposed study. In [38] seizure detection and prediction problems are considered where 1000 seizure, 1000 inter-seizure, and 1000 pre-seizure EEG segments (each 8s long) from CHB-MIT database were used. In seizure detection, the maximum 97.5% accuracy was achieved by the EMD approach, while the highest classification accuracy (100 %) was obtained using the DWT and WPD approaches. In seizure prediction problem, the maximum 99.7 % accuracy is achieved using the multiscale principal component analysis (MSPCA)+WPD+SVM approach. However, no information is provided about which patient's EEG data is used. The number of EEG segments is a factor that directly affects the success of the study. In our study, the number of evaluated EEG segments is higher than that of the study. In [123], EWT based, and in [122] EMD and DWT based seizure detection approaches were presented using different EEG channels of CHB-MIT data set. Higher ACC, SEN, and SPE values were reported than our proposed approach. However, in those studies channel selection process is conducted before the feature extraction which is not the case in our study. We consider all channels with high and low classification performance, which slightly decreases the overall seizure detection performance, but eliminates a channel selection step. In another study [39], EMD based seizure detection approach was presented. 5-channel EEG signals of 24 patients in the CHB-MIT data set were decomposed into IMFs using EMD methods. Then, utilizing the most relevant IMFs (IMF1 and IMF2), various features such as Teager and instantaneous energy, Higuchi and Petrosian fractal dimension, and detrended fluctuation analysis (DFA) were calculated, and an average classification accuracy of 93% was obtained. Although more EEG channels were evaluated, the classification accuracy is lower than that of our proposed DMD-based approach. In [40], seizure (2675 segments) and non-seizure (2675 segments) EEG

segments of randomly selected five patients in the CHB-MIT dataset, and five subsets of Bonn data sets were investigated. Using the CEEMD method, seizure and non seizure EEG segments decomposed into IMFs and one residue. Time-domain, frequency-domain, time-frequency domain, and entropy-based features were calculated using obtained IMFs, residue, and raw EEGs. 95.70% SEN, 95.89% SPE, and 95.79% ACC were achieved for the CHB-MIT data using XGBoost classifier. Our proposed DMD approach yields higher ACC, PRE values but lower SEN value, using the EEG segments of 14 patients rather than 5 patients. In [42], the EMD, and in [43] the derivative of CEEMD, called the CEEMDAN method are applied to epileptic EEG signals on the Bonn data set, resulting higher classification performances. EMD and its derivative approaches have more computational complexity than the proposed DMD approaches as detailed in the discussion section.

13 seizure, 26 non-seizure EEG signals from 1 to 5 minutes of 9 different subjects in the CHB-MIT data set were evaluated in [46]. Five spectral components of EEG signals, namely delta, theta, alpha, beta, and gamma, were decomposed using Dauchebies (Db4) wavelet filter bank. Dimension reduction based on a statistical model was conducted using the zero-mean generalized Gaussian distribution (GGD) method. Seizure and non-seizure EEG classification performances of each EEG component were evaluated using the linear discriminant analysis (LDA). 97%–99% SEN, 79%-92% SPE, and 92%–97% ACC were reported as the results of the study. Fewer patient data were evaluated compared to our proposed DMD-based study. Moreover, fewer epileptic EEG segments have been evaluated. Despite all this, the SEN value is higher, but the SPE and ACC values are lower than that of our proposed study.

In two seizure detection studies [44, 47] conducted using WT methods, publicly available Freiburg and Bonn data sets were used. While higher seizure detection performance was achieved on the Bonn data set [47] compared to our DMD-based study, the study conducted using the Freiburg data set [44] provided lower performance evaluation results than that of our proposed approach implemented on the CHB-MIT data set. Seizure detection performances reported in the literature using the CHB-MIT data set are generally lower than those obtained using the Bonn data set.

In 2018, Kumar et al. presented a VMD and semantic feature-based epileptic seizure detection approach. Two different public epileptic EEG data sets, known as the Bern-Barcelona data set and Bonn data set were utilized for the seizure detection study. Band-limited IMFs (BLIMFs) were extracted by VMD. By using high-frequency BLIMFs, semantic features (differential entropy and peak-magnitude of root mean square ratio) were extracted. Various classifiers such as ANN, SVM, K-NN, NB, and RF are employed to separate seizure and seizure-free EEG segments. The experimental results yielded superior recognition performance with an average of 78.5% ACC, 95% SEN, 95% SPE and 94.1% ACC, 95.33% SEN, 96.67% SPE values for the Bern-Barcelona and Bonn data sets respectively [41]. While our proposed DMD-based approach provided higher ACC and PRE values than the VMD-based approach, the SEN value was slightly lower.

In [45], a seizure detection study using generalized Stockwell transform (GST) and SVD was proposed. The time-frequency distributions of EEG segments in the Bonn data set were obtained using GST methods. Utilizing SVD matrix decomposition algorithm, GST matrices were decomposed into singular values and various features were extracted. Average classification accuracies between 88.04% and 99.12% were obtained using RF classifier. Compared to studies performed using the Bonn data set, this study achieved an average seizure detection performance. In addition, proposed DMD approach uses the SVD method in the matrix decomposition step, however the computational complexity of our approach is lower because no signal representation is required such as GST.

In [65], using the convolutional neural network (CNN), seizure detection experiment was conducted utilizing the CHB-MIT data set. The 71.45 % average seizure detection sensitivity was achieved by their approach. Sample entropy (SampEn) and fuzzy entropy (FuzzyEn) based seizure detection was presented in another study [29]. The EEG recordings of patients from the CHB-MIT data set (Patients 1-18) and Bonn data set were used for the seizure detection. In fuzzy entropy, the higher mean accuracy, sensitivity, and specificity (98.31 % ACC, 98.27%, and 98.36%) values were achieved than in the Sample entropy (97.16% ACC, 97.01%, and 97.34%) for CHB-MIT dataset. The Sparse common space pattern (SCSP) based automatic seizure detection approach was utilized in another study [124]. 22 channel-EEG signals of 10 patients

were collected with 256 Hz sampling frequency. The interictal, pre-ictal (10–50 min before the onset), and the ictal EEG segments of each patient were evaluated. Using three different search methods based on the eigenvalue decomposition, EEG feature sparsity was carried out. Fisher linear discriminant method was used for the classification resulting over 99.75 % classification accuracy.

Among these previous studies, there is one seizure detection study [58] conducted using the DMD approach that reports the performance by means of SEN and SPE. CHB-MIT data set was used to detect seizure event and 87% SEN, 99% SPE values were achieved. Compared to this study, higher SEN and SPE values were obtained in our seizure detection approach performed with the CHB-MIT dataset (96.7% ACC, 92.9% SEN, 98.5% SPE). Bilal et. al [59] presented an MRDMD based seizure detection approach. DMD powers and temporal features, of the CHB-MIT dataset, were used as features. The highest 93.7% SEN, and 99.2% SPE values were achieved in the results of that study. Again, compared to the performance of DMD-based seizure detection experiment on CHB-MIT dataset in our study, there is no significant performance improvement despite the additional computational expense of temporal features.

In another study [120], using the common spatial pattern (CSP) based feature extraction, the seizure prediction problem was considered. The maximum average 89 % SEN and 37 % SPE, and 68.71 minute prediction time were obtained using the CHB-MIT data set. In another epileptic seizure prediction study [121], bag-of-wave (BoWav) based feature extraction and ELM based classification approach was presented. The EEG recordings of patients from the CHB-MIT data set (Patients 1, 5, 7, 8, 9, 10, 14, 15, and 22) with a total of 62 seizure events were utilized and 88.24 % sensitivity was achieved. Compared with these two studies [120, 121], higher SEN and SPE values were achieved in our MC-DMD-based seizure prediction study performed with the CHB-MIT dataset.

On the other hand, in our previous study [125] conducted using the same IKCU data set, and applying EMD, EEMD and DWT methods, we achieved 97.14%, 98.13%, and 94.56% accuracy values respectively. However, as discussed in that study, EMD and EEMD approaches have the disadvantage of computational complexity over DWT method. The computational complexity of EMD is $O(N_s L N_x)$ where N_s is the number

of shifting iterations to extract each IMFs, L denotes the number of IMFs, N_x is the length of the signal, and $O(.)$ shows the order of computation. This complexity is multiplied by the number of ensembles N_e in EEMD [115, 125], making EMD and its variants computationally expensive iterative methods. The single channel-based DMD approach proposed by us, which clearly has the computational advantages, resulted in 96.7% classification accuracy. The computational complexity of the DMD algorithm is reported as $O(KNM)$ where K is the number of modes, N and M are the dimensions of the data matrix [126]. Thus, the above encouraging classification results together with the computational advantages, indicate that the proposed DMD method may be applied to the analysis of univariate signals such as single EEG channels and other non-stationary signals.

4.4   Results and Discussion of SST Methods

In this section, a novel time-frequency representation based approach is presented to distinguish pre-seizure (or inter-seizure) and seizure EEG segments. The proposed method involves obtaining joint TF representation of "pre-seizure (or inter-seizure)" and "seizure" EEG segments labeled by expert neurologists. The TF representations of EEG segments are obtained using SST and STFT for each EEG channel separately. SST-based machine learning and deep learning approaches are performed to epileptic EEG detection and prediction.

4.4.1   Machine Learning Based Approach

In the machine learning-based approach, two different methods are presented for feature extraction: (i) higher-order joint TF moments are calculated using the joint densities obtained by SST and STFT. (ii) The resulting TFRs from SST and STFT are processed as images, and GLCM are calculated from these TFR images. Four statistical GLCM features: contrast, correlation, energy, and homogeneity are calculated to obtain GLCM based feature sets. Finally, both single and ensemble machine learning algorithms such as SVM, kNN, NB, LR, BT, and S-kNN are used for the classification of generated feature sets. In proposed SST based seizure detection

approach, two different data sets are evaluated. The first one is our own IKCU data set that is collected from patients under treatment at Izmir Katip Celebi University Medical School Hospital. The other one is CBH-MIT data set that is publicly available epileptic EEG data collected at Children's Hospital Boston.
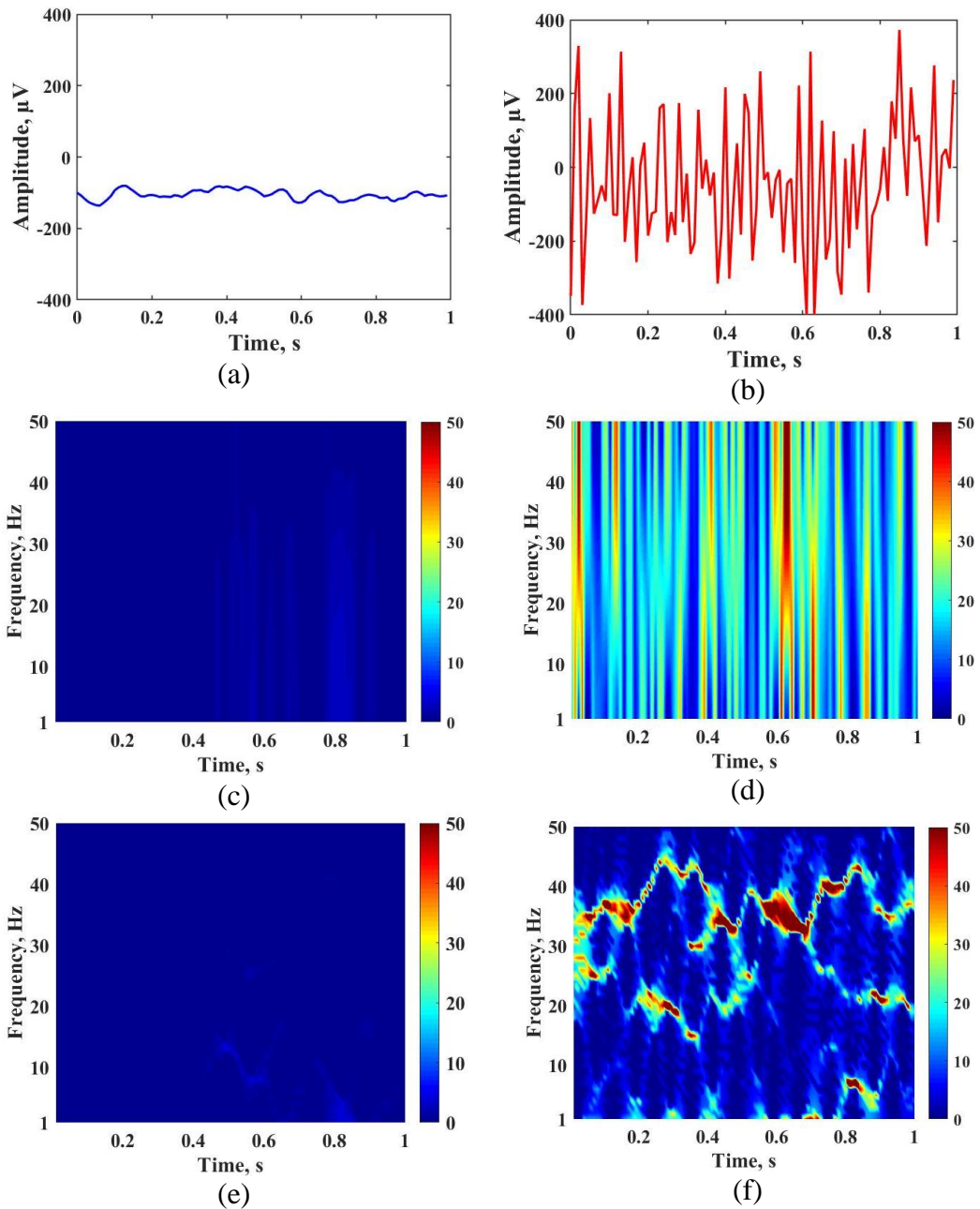
Figure 4.12: 1 s. long, (a) pre-seizure, (b) seizure EEG; magnitude STFT of (c) pre-seizure, (d) seizure EEG segment; magnitude SST of (e) pre-seizure, (f) seizure EEG segment.

TF representations of 1 s. duration pre-seizure and seizure EEG segments (in IKCU data set) obtained using STFT and SST methods are given as examples in Figure 4.12. It is observed from Figure 4.12c- 4.12f that the SST method is able to resolve the components of the EEG signals for both pre-seizure and seizure cases and represent them better in the TF plane than the STFT method. Note here that the resolution of the TF representation obtained by the STFT is based on the selection of the analysis window function. In our experiments, we utilized a window size that provides optimal time and frequency resolutions in the STFT analysis of epileptic EEG signals. Even in that case, reassigned SST method shows clear advantages in the representations of these signals.

4.4.1.1 Feature Extraction

In this study, we present two approaches to extract features from the TF representations of EEG signals; Higher Order Joint Time-Frequency (HOJ-TF)-moments, and GLCM based feature sets are generated from STFT and SST images. In the STFT calculations, a Hamming window is used with a 50% overlap.

- **HOJ-TF moment based features:** Higher-order joint TF moments $< t^i \, \omega^j >$; $i, j = 1, 2, ...$ are calculated using the joint TF density estimates obtained by SST and STFT methods.

$$< t^i \, \omega^j >= \iint t^i \, \omega^j \, S(t, \omega) \, dt d\omega, \qquad i, j = 1, ... \qquad (4.15)$$

where $S(t, \omega)$ is the density obtained by the magnitude square of the SST and STFT. The joint TF moments are log-normalized to reduce the dynamic range as [127],

$$\overline{< t^i \, \omega^j >} = \log \left(\frac{< t^i \, \omega^j >}{i! \, j!} \right), \qquad i, j = 1, ..., n \qquad (4.16)$$

In our experiments, log-normalized HOJ-TF moments are calculated for $n = 4$, hence 1×16 feature vector is obtained for each inter-seizure, pre-seizure, and seizure EEG segment.

- **GLCM based features:** GLCM is one of the texture descriptors and may be utilized in many pattern recognition applications. To obtain GLCM matrix $G(m, n)$ of the gray-level image $I(k, l)$, the joint probability distributions of two neighboring image pixel pairs with a specific angle "θ" and distance "d" are calculated [57, 128].

$$G(n, m) = \begin{pmatrix} 1, & \begin{matrix} if\ I(k, l) = n\ and \\ I(k + d\cos\theta, l + d\sin\theta) = m \end{matrix} \\ 0, & otherwise \end{pmatrix} \qquad (4.17)$$

Here, $n, m \in \{0, 1, ..., N_g - 1\}$ are intensity values of pixels, $I(k, l)$ is the intensity value of $(k, l)^{th}$ image pixel, and $K \times L$ is the size of the image with N_g gray levels.

In this study, we propose considering the magnitude of STFT and SST of each EEG segment as a gray-scale image, and calculating GLCM features. Examples of STFT and SST magnitudes are shown in Figure 4.12, for pre-seizure and seizure EEG segments of IKCU data set. Therefore, we calculate the GLCM matrices using $\theta = 0^o$ and distance $d = 1$ and extract efficient features [49, 57]. Second-order statistical features, namely, contrast, correlation, energy, and homogeneity given below are calculated from the GLCM matrices corresponding to each EEG segment [49, 128];

$$G_C = \sum_{n=0}^{N_g-1} \sum_{m=0}^{N_g-1} (n - m)^2 G^2(n, m)$$

$$G_{Corr} = \sum_{n=0}^{N_g-1} \sum_{m=0}^{N_g-1} (n - \mu)(m - \mu)G(n, m)/\sigma^2$$

$$G_E = \sqrt{\sum_{n=0}^{N_g-1} \sum_{m=0}^{N_g-1} G^2(n, m)} \qquad (4.18)$$

$$G_H = \sum_{n=0}^{N_g-1} \sum_{m=0}^{N_g-1} \frac{1}{1 + (n - m)^2} G(n, m)$$

where N_g denotes the number of gray levels, $G(n, m)$ is the $(n, m)^{th}$ entry of the GLCM matrix, μ is the mean value, and σ^2 is the variance of the GLCM matrix.

G_C, G_{Corr}, G_E, G_H are the Contrast, Correlation, Energy, and Homogeneity features calculated from the GLCM matrix.

Hence, 1×4 GLCM feature vector is obtained for each pre-seizure, seizure, and inter-seizure EEG segment.

4.4.1.2   Experimental Results and Discussions

In this section we present the results of epileptic EEG classification obtained by the proposed SST representation based approaches using various machine learning techniques. We compare the performance of the proposed method with that of the conventional TF method, i.e., STFT on the epileptic EEG data sets.

Statistical analysis of the proposed method is performed using the one-way analysis of variance (ANOVA) test at 95% confidence level ($\alpha = 0.05$) to determine the statistical significance of the difference between the extracted feature sets of two classes. The small p-value obtained as a result of ANOVA for all our experiments suggest that the difference between feature set of the groups is significant [29, 37]. In addition, the performances of the classifiers are investigated by means of different statistical metrics which are ACC, PRE, SEN, FPR, and F1-S.

In the first stage of proposed approach, SST and STFT based TFR approaches are proposed to obtain distinctive information between pre-seizure and seizure EEG segments of IKCU data set. 1s and 5s duration EEG segments are obtained from pre-seizure and seizure EEG signals, and time-frequency representations are obtained for each EEG segment using both SST and STFT approaches detailed in Section 3.1.3. First, the ANOVA test is applied to all feature sets obtained and the statistical significance level of the difference between groups is determined. The difference between the seizure and pre-seizure groups is found to be significant with p < 0.0001 for both HOJ-TF moment-based and GLCM-based feature sets obtained from both 1s and 5s segment duration of SST and STFT approaches. Then, various classifiers are utilized to classify both 1s, and 5s pre-seizure and seizure EEG segments duration, and different statistical performance metrics are calculated. The features obtained from the left hemisphere (Fp1-F7, F7-T1, T1-T3, T3-T5, and Fp1-F3) and right hemisphere

(Fp2-F8, F8-T2, T2-T4, T4-T6, Fp2-F4) EEG channels are evaluated separately in order to reveal the hemisphere effect in distinguishing between pre-seizure and seizure.

Table 4. 13: Performance Evaluation results of HOJ-TF-moment based feature sets for 1s (p < 0.0001) and 5s (p < 0.0001) EEG segments duration in the Left hemisphere.

		SST based HOJ-TF moment Feature Set						STFT based HOJ-TF moment Feature Set					
	Metric	LR	SVM	kNN	NB	BT	S-kNN	LR	SVM	kNN	NB	BT	S-kNN
1s	ACC	93	**93.1**	92.5	92.1	92.8	91.2	**92.6**	92.1	91.6	85.3	91.5	89.9
	PRE	94.8	95.4	93.9	96.7	94.7	93.2	94.2	94.5	93.8	94.4	94.3	92.4
	SEN	94.3	93.9	94.5	90.9	94.1	93.1	94.3	92.9	93.1	81.9	92.3	91.8
	F1-S	94.6	94.6	94.2	93.7	94.4	93.2	94.2	93.8	93.5	87.7	93.3	92.1
5s	ACC	94.6	**95.1**	94.2	94.4	94.1	93.3	**94.4**	93.7	93.6	89	93.3	92.7
	PRE	95.9	96.9	96.3	97.5	95.6	95.4	95.7	95.9	95.6	95.9	95.4	93.9
	SEN	95.7	95.5	94.7	93.8	95.2	94.3	95.7	94.3	94.5	86.7	94.2	94.7
	F1-S	95.8	96.2	95.5	95.6	95.4	94.8	95.7	95.1	95.1	91.1	94.8	94.4

Table 4.14: Performance Evaluation results of HOJ-TF-moment based feature sets for 1s (p < 0.0001) and 5s (p < 0.0001) EEG segments duration in the Right hemisphere

		SST based HOJ-TF moment Feature Set						STFT based HOJ-TF moment Feature Set					
	Metric	LR	SVM	kNN	NB	BT	S-kNN	LR	SVM	kNN	NB	BT	S-kNN
1s	ACC	88.4	88.4	**88.5**	83.6	88.4	86.2	**87.6**	87.2	86.6	79.1	85.9	84.1
	PRE	91.1	90.8	91.2	94.2	90.2	89.9	89.6	89.9	89.3	92.9	89.4	87.7
	SEN	91.1	91.3	90.9	79.4	92.1	88.6	91.2	90.2	89.8	72.9	88.5	87.4
	F1-S	91.1	91	91.1	86.2	91.1	89.3	90.4	90	89.5	81.7	88.9	87.6
5s	ACC	90.5	90.9	90.5	87.1	**91**	90.2	**89.8**	88.6	88.1	83.6	86.7	86.7
	PRE	92.5	93	94.4	94.9	93.1	93.1	91.4	91.7	92.5	95.2	91.2	90.1
	SEN	92.9	92.9	90.7	84.7	93.2	91.8	93.1	90.6	88.8	78.6	87.9	89.4
	F1-S	92.7	92.9	92.5	89.5	93.1	92.4	92.2	91.2	90.6	86.1	89.5	89.7

The performance evaluation results of the proposed SST approach, together with a comparison to STFT based method are given in Tables 4.13-4.16. The highest classification accuracy for 1s and 5s EEG segments are demonstrated with boldface numbers in the tables. The performance evaluation results of HOJ-TF-moment based feature sets obtained using SST and STFT approaches for both 1s and 5s seizure and pre-seizure EEG segments obtained from the left hemisphere and right hemisphere are summarized in Table 4.13 and Table 4.14, respectively. The highest classification

performance is achieved with 93.1% ACC, 95.4% PRE, 93.9% SEN, and 94.6% F1-S values using SVM classifier from SST approach of 1s EEG segments obtained from the left hemisphere. For the same EEG segment size and same hemisphere, the maximum classification performance is obtained for the STFT approach with 92.6% ACC, 94.2% PRE, 94.3% SEN, and 94.2% F1-S values using LR classifier. In addition, the classification successes are increased both SST (95.1% ACC) and STFT (94.4% ACC) approaches for 5s EEG segment duration. On the other hand, the classification performances are decreased in both SST and STFT approaches for the right hemisphere (shown in Table 4.14). While the highest classification performance is achieved with 88.5% ACC, 91.2% PRE, 90.9% SEN, and 91.1% F1-S values using kNN for SST approach of 1s EEG segment; 91% ACC, 93.1% PRE, 93.2% SEN, and 93.1% F1-S values are obtained using the BT classifier for the SST approach for 5s EEG segments. Whereas lower classification performances are obtained in STFT approach for both 1s (87.6% ACC), and 5s EEG segments (89.8% ACC) with the LR classifier.

Table 4.15: Performance Evaluation results of GLCM based feature sets for 1s (p < 0.0001) and 5s (p < 0.0001) EEG segments duration in the Left hemisphere.

		SST based GLCM Feature Set						STFT based GLCM Feature Set					
	Metric	LR	SVM	kNN	NB	BT	S-kNN	LR	SVM	kNN	NB	BT	S-kNN
1s	ACC	92.5	92.5	92.6	92.2	92.7	91	90	90.3	90.4	88.7	90.7	89.1
	PRE	95.4	95.7	95.8	95.2	94.6	94.1	91.8	92.5	93.4	92.2	93.1	92.7
	SEN	92.8	92.5	92.7	92.5	94.1	91.8	92.7	92.3	91.5	89.9	92.4	90.2
	F1-S	94.1	94.1	94.2	93.9	94.4	92.9	92.2	92.4	92.4	91.1	92.7	91.4
5s	ACC	94.1	94.4	94.4	94.5	93.6	93.3	94.1	94.4	94.1	94.4	93.9	93.9
	PRE	95.6	96.2	96.8	96.2	95.7	95.6	95.6	96.2	96.6	96.3	95.6	96.2
	SEN	95.2	95.2	94.5	95.3	94.4	93.9	95.2	95.2	94.3	94.9	94.9	94.4
	F1-S	95.4	95.7	95.7	95.8	95.1	94.8	95.4	95.7	95.4	95.6	95.3	95.3

The classification metrics of GLCM feature sets that consist of second-order statistical features for SST and STFT approaches of different EEG segment sizes are demonstrated in Table 4.15 and 4.16. While using the BT classifier for the SST approach with a segment length of 1s in the left hemisphere (shown in Table 4.15), the highest classification performance is achieved with 92.7% ACC, 94.6% PRE, 94.1% SEN and 94.4 % F1-S values; using the same classifier, the highest classification performance is obtained with the scores of 90.7% ACC, 93.1% PRE, 92.4% SEN and

92.7% F1-S for the STFT approach. Additionally, for the 5s segment duration, classification success is increased in both SST (94.5% ACC) and STFT (94.4% ACC) approaches. On the other hand, for the right hemisphere, lower classification successes are achieved for both approaches, both in the 1s EEG segment duration and the 5s EEG segment duration (demonstrated in in Table 4.16).

Table 4.16: Performance Evaluation results of GLCM based feature sets for 1s (p < 0.0001) and 5s (p < 0.0001) EEG segments duration in the Right hemisphere.

	Metric	SST based GLCM Feature Set						STFT based GLCM Feature Set					
		LR	SVM	kNN	NB	BT	S-kNN	LR	SVM	kNN	NB	BT	S-kNN
1s	ACC	**88.8**	88.6	88.4	88.1	88.7	86.1	85.3	85.4	85	83.8	**86.1**	83.4
	PRE	91.3	90.9	91.5	92.1	90.5	90	87.9	88.4	88.6	88.2	89.2	88
	SEN	91.2	91.5	90.6	89.1	92.1	88.2	89.4	88.8	87.8	86.4	89.1	85.8
	F1-S	91.3	91.2	91	90.6	91.3	89.1	88.6	88.6	88.2	87.3	89.2	86.9
5s	ACC	90	90.1	**92.8**	90.1	91.9	91.5	90.1	91	92.7	90.1	91.6	91
	PRE	91.6	92.1	96.8	95.1	94.2	94.5	91.6	92.4	96.5	95.2	93.8	93.7
	SEN	93.2	94.1	92.1	89.4	93.2	92.4	93.4	93.9	92	89.3	93.2	92.2
	F1-S	92.4	93.1	94.4	92.2	93.7	93.4	92.5	93.2	94.2	92.2	93.5	92.9

To observe the advantages of the SST method and the contribution of the segment duration to the classification performance more clearly, the features obtained from the right hemisphere and left hemisphere are combined to create combined feature sets for both 1s, and 5s EEG segments duration. Classification performances of combined HOJ-TF-moment-based, and combined GLCM-based feature sets obtained for different segment sizes, using SST and STFT approaches are shown in Figure 4.13. For the combined HOJ-TF-moment-based feature set, the classification metrics of all classifiers for both SST and STFT approaches are increased in the 5s segment duration. For the same feature set, the SST approach in both segment lengths provided higher performance metrics than the STFT approach (shown in Figure 4.13a). For the combined GLCMbased feature set, classification with 5s segment duration signals is also better in both methods (shown in Figure 4.13b). Examples of misclassified and correctly classified seizure segments are given in Figure 4.14.
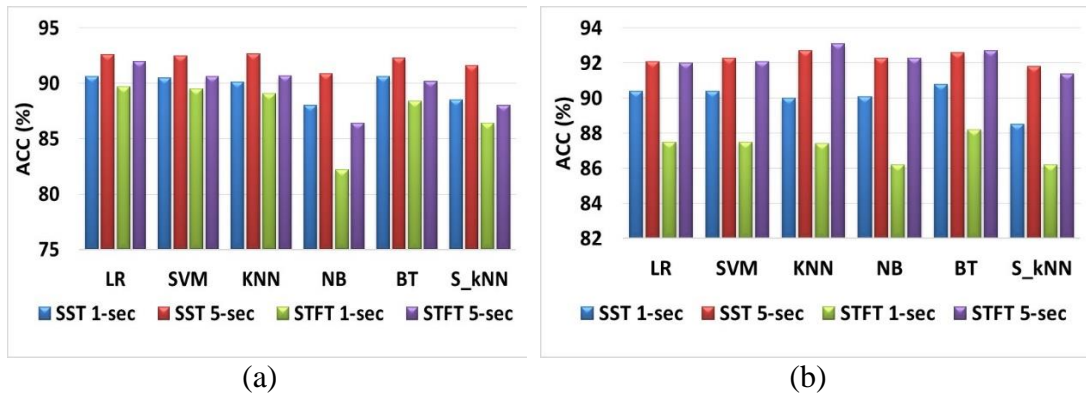
Figure 4.13: Classification accuracy (% ACC) of (a) HOJ-TF-moment based combined feature sets, (b) GLCM based combined feature sets obtained using SST and STFT approaches for 1s and 5s EEG segments durations.
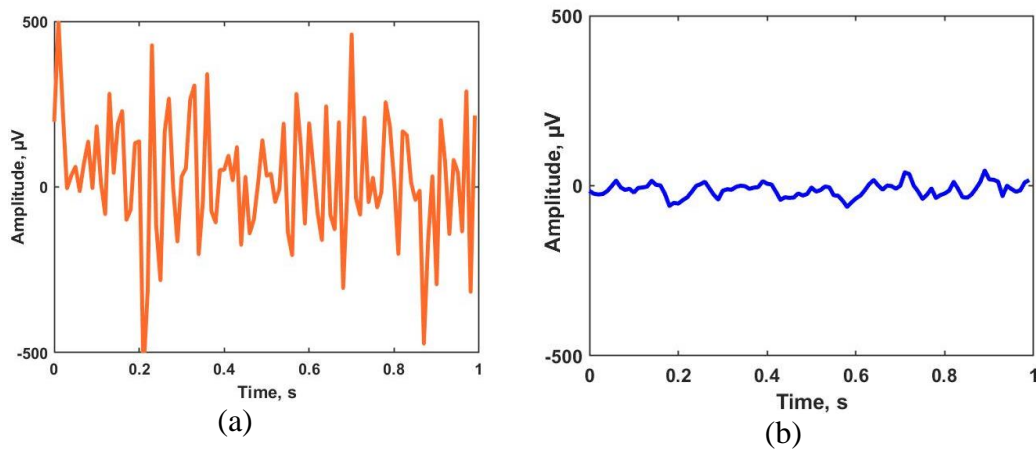
Figure 4.14: Examples of (a) misclassified and (b) correctly classified seizure segments.

Since the difference between methods is more pronounced in the 1s segment size, the precision and sensitivity values of the classifiers and the patient-based performance of the SST approach are given for 1s segment duration, and shown in Figures 4.15 and 4.16, respectively. Precision values for the classifiers, which show the ratio of seizure data correctly classified to the data assigned to the seizure class by classifiers, for 1s segment duration (the difference between methods is more pronounced) in both approaches are given in Figure 4.15a,c. Similarly, sensitivity values for the classifiers, which indicates the ratio of accurately detected seizure data to the total seizure data, for 1s segments duration in both approaches are given in Figure 4.15b,d. Higher Precision values are obtained in all classifiers for the SST approach than the STFT approach using both combined HOJ-TF-moment-based feature set, and the combined

GLCM-based feature set. Similarly, higher sensitivity values are obtained in the SST approach for all classifiers and both feature sets.

(a)   (b)

(c)   (d)
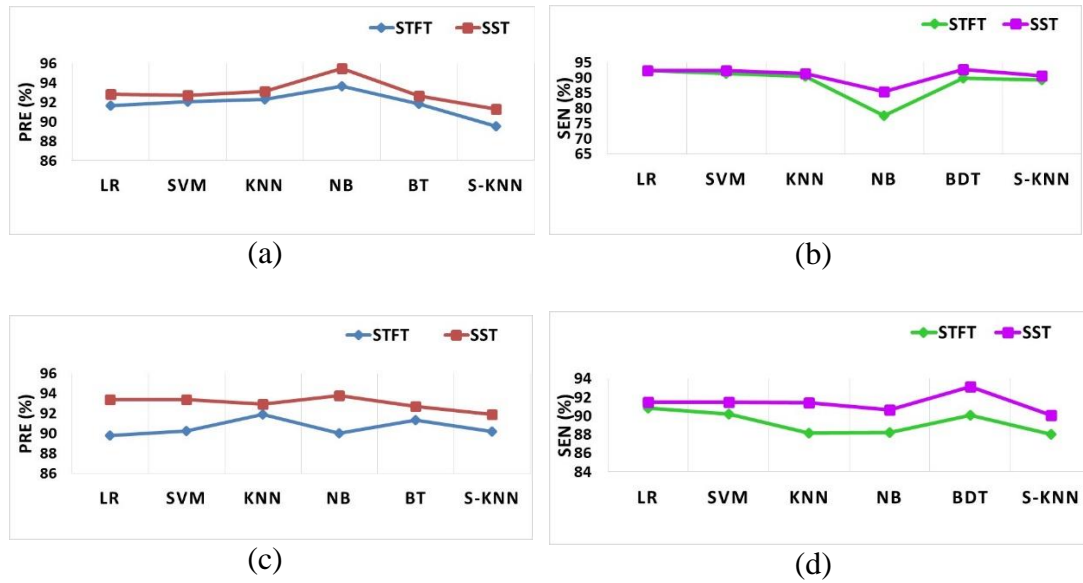
Figure 4.15: Changes in Precision and Sensitivity values on a classifier basis in 1s EEG segments in both methods: (a) Precision values and (b) Sensitivity values obtained from combined HOJ-TF-moment based feature set; (c) Precision values and (d) Sensitivity values obtained from combined GLCM based feature set.

(a)   (b)

Figure 4.16: Patient based average (a) SEN and (b) FPR values obtained using the HOJ-TF-moment based feature set and GLCM based set of SST approach for 1s EEG segment duration.

In the study conducted with the IKCU data set, the classification process is carried out by combining the features obtained from all patient data due to the low number of patients and the short total duration of pre-seizure and seizure EEG signals (inter-patient classification process). In order to reveal the success of the SST approach to

classify pre-seizure and seizure EEG segments based on intra-patient, the performance of patient-based classification is also evaluated for 1s segment duration. The averages of the SEN and FPR values obtained from all classifiers are calculated and shown in Figure 4.16. It is remarkable that the patient-based SEN values are high. However, in 5 patients (Patient-3, Patient-4, Patient-5, Patient-12, and Patient-13) with lower SEN performance, the FPR is also high (average FPR values for all patient; for HOJ-TF moment based feature set: 11.6%, for GLCM based feature set: 13.9%). The fact that the number of pre-seizure segments in these 5 patients is much less than the number of seizure segments is thought to cause this situation. The low success of pre-seizure and seizure classification in these patient data causes a decrease in classification performances performed by combining all patient data.

Using the CHB-MIT public epileptic EEG data set, SST based seizure detection approach is performed. HOJ-TF moments based and GLCM based feature sets are created using TFRs that obtained utilizing the SST approach for seizure and inter-seizure EEG segments. Similar to the IKCU data set, log-normalization is used to obtain the HOJ-TF moment-based feature set, and the 1×16 feature vector is obtained for each EEG segment. Again, 2nd order statistical GLCM-based features such as contrast, correlation, energy, and homogeneity are calculated, thus 1×4 GLCM feature vector is obtained for each seizure and inter-seizure EEG segment.

The statistical significance of the difference between the inter-seizure and seizure groups in the obtained feature sets is determined for each patient by applying the ANOVA test $\alpha = 0.05$. Using various classifiers and statistical metrics such as ACC, PRE, and SEN, the success of a patient-based seizure detection approach is demonstrated.

The results of the classification performances of the patient-based seizure detection approach and the p values obtained as a result of the ANOVA test are summarized in Tables 4.17-4.18. The HOJ-TF moment based feature set of the SST approach provided successful patient-based seizure detection with high SEN, PRE, and ACC values except for patient chb13 ($p < 0.001$) and chb21 ($p < 0.01$) (given in Table 4.17). Lower SEN values (higher than 80%) are obtained for patients chb06 (SVM:83.6%, kNN:82.8%, LR:84.9%), chb14 (SVM:84%, kNN:78%, LR:89.2%), chb16 (SVM:81.7%, kNN:85.8%, LR:81.9%),and chb18 (SVM:80.6%, kNN:80.8%,

LR:81%), while high ACC and PRE values (with p < 0.005) are achieved. The kNN classifier achieved the highest average seizure detection success with 89.1% SEN, 92.6% PRE, and 94.5% ACC values for all patients. On the other hand, high patient-based performance evaluation results (p < 0.001) are obtained using GLCM based feature set of the SST approach except for patients chb13 (p = 0.07), chb21 (p = 0.3) (less than 80%, given in Table 4.18). Additionally, higher average seizure detection performance with 90.3% SEN, 93.4% PRE, and 95.1% ACC values are achieved using the kNN classifier.

Table 4.17: Performance Evaluation results of HOJ-TF moment based feature sets of CHBMIT data set (p < 0.01, 600 inter-seizure segments are investigated for each patient.)

Patient	Segment	SVM			kNN			LR		
		SEN	PRE	ACC	SEN	PRE	ACC	SEN	PRE	ACC
chb01	481 seizure	88.1	98.3	94.2	94.4	96.9	96.2	96.3	97.5	97.3
chb02	172 seizure	86.3	85.7	93.8	88.1	84	93.6	87	88.5	94.6
chb03	402 Seizure	98.3	99	99.1	99	99	99.3	97.7	98.3	98.5
chb04	262 Seizure	92	94.4	95.9	94.9	93.3	96.5	93.2	93.8	96.1
chb05	558 Seizure	97.7	97	97.4	97.8	96.8	97.5	97.7	97.3	97.6
chb06	137 Seizure	83.6	88.6	94.9	82.8	89.9	95.1	84.9	87.9	95.1
chb07	325 Seizure	98.2	98.5	98.9	98.5	98.5	99.1	98.6	98.2	98.9
chb08	919 Seizure	93.9	97	94.6	95	97.2	95.3	95.1	96.8	95.2
chb09	276 Seizure	96	99.7	98.7	98.2	99.5	99.3	95.9	98.4	98.3
chb10	447 Seizure	92.9	97.7	96.2	94.8	97.4	96.7	92.8	96.5	95.5
chb11	806 Seizure	94.8	98.5	96.4	96.3	98	96.9	97.2	98.6	97.8
chb12	641 Seizure	83.8	91.3	87.7	87.8	91.2	89.3	85.7	89.7	87.7
chb13	253 Seizure	45.7	77	81.5	56.6	76	81.9	52.8	78.2	81.8
chb14	169 Seizure	84	94.3	95.4	78	94	94.2	89.2	92.4	96.1
chb15	1396 Seizure	94.8	79.9	77.8	89.8	89.2	85.3	91.8	85.7	82.7
chb16	69 Seizure	81.7	85.9	96.7	85.8	86.4	97.2	81.9	82.6	96.4
chb17	293 Seizure	93.4	94	95.9	95.1	93.2	95.9	92.6	93.9	95.7
chb18	317 Seizure	80.6	85.9	88.7	80.8	87.4	89.4	81	87	89.2
chb19	236 Seizure	92.3	100	97.8	94.9	99.4	98.5	96.3	98.1	98.5
chb20	294 Seizure	93.6	99.4	97.7	94.8	98.5	97.7	98	98.3	98.8
chb21	199 Seizure	38.8	63.4	81.1	48.2	68.9	81.7	46.3	66.3	81.3
chb22	204 Seizure	98.2	98.4	99.1	99.3	98.5	99.4	98.2	97	98.8
chb23	424 Seizure	97.9	95.6	97.3	97.7	95.1	97.1	97.4	95.7	97.1
	Average	87.2	92.2	93.8	89.1	92.6	94.5	89.1	92.1	94.3

Table 4.18: Performance Evaluation results of GLCM based feature sets of CHB-MIT data set (p < 0.07 except patient chb21, 600 inter-seizure segments are investigated for each patient.)

Patient	Segment	SVM			kNN			LR		
		SEN	PRE	ACC	SEN	PRE	ACC	SEN	PRE	ACC
chb01	481 seizure	100	100	100	100	99.6	99.9	100	100	100
chb02	172 seizure	99.9	100	99.9	99.9	100	99.9	99.9	100	99.9
chb03	402 Seizure	99	99.7	99.7	99	99.7	99.6	99	99.8	99.7
chb04	262 Seizure	91.1	97	96.5	93.9	94.9	96.6	91.6	96	96.3
chb05	558 Seizure	98.6	96.4	97.7	98.5	96.8	97.8	98.3	96.8	97.7
chb06	137 Seizure	85.3	91	95.7	84.6	91.1	95.6	83.8	91.9	95.6
chb07	325 Seizure	99.2	98.9	99.6	99.1	99.1	99.6	99.1	99.2	99.6
chb08	919 Seizure	94.3	96.8	94.7	94.9	97.2	95.3	94.5	96.5	94.8
chb09	276 Seizure	97.2	99.7	99.1	98.4	99.6	99.4	97	99.2	98.9
chb10	447 Seizure	94.1	98.6	97.1	97.5	98.7	98.5	94.9	98.1	97.2
chb11	806 Seizure	95.9	99.3	97.4	96.9	98.4	97.6	97.2	98.6	97.9
chb12	641 Seizure	79	87.3	83.2	86.1	89.8	87.9	80.3	84.4	82.2
chb13	253 Seizure	43.1	89.6	81.6	54.9	74.2	80.9	46.2	86.2	81.9
chb14	169 Seizure	93	98.4	98.2	93.8	98.1	98.2	94.4	97.5	98.2
chb15	1396 Seizure	86.9	93.3	86.4	88.9	90.7	85.9	88.4	91.4	86
chb16	69 Seizure	90.3	90.8	98	89.5	91.1	98	90.2	91.4	98.1
chb17	293 Seizure	94.8	92.2	95.8	95.9	93	96.3	94.1	93	95.7
chb18	317 Seizure	78.7	85.1	87.2	82.5	89.1	90.5	78	84.9	87.2
chb19	236 Seizure	89	100	96. 9	93.2	99.5	98.1	95.8	99.1	98.6
chb20	294 Seizure	95.4	100	98.5	96.7	99.6	98.9	98.7	99.2	99.4
chb21	199 Seizure	6.9	25.2	75.4	34.2	53.2	76.2	17.5	51	75.6
chb22	204 Seizure	98.8	98.8	99.4	99.6	98.7	99.6	99	99	99.4
chb23	424 Seizure	98.9	95.4	97.6	98.8	95.5	97.6	98.2	95.9	97.6
	Average	87.4	92.8	94.6	90.3	93.4	95.1	88.5	93.4	94.7

In order to compare the seizure detection success of the GLCM and HOJ-TF moment-based feature sets of SST approach, patient-based SEN and FPR values are obtained by averaging SEN and FPR values of three classifiers. The obtained patient-based SEN and FPR values are graphically given in Figure 4.17. Higher average SEN values are obtained using GLCM based feature set of SST approach except for patients chb08, chb12, chb13, chb19, and chb21 than that of HOJ-TF moment based feature set of SST. In addition, average SEN values that are greater than 80% are achieved using both the HOJ-TF moment-based feature set and the GLCM-based feature set, except for chb13 and chb21 patients, for seizure detection approach. On the other hand, it is remarkable that low FPR values are achieved in all patients except patient chb15 (average FPR values for all patient; for HOJ-TF moment based feature set: 4.71%, for GLCM based feature set: 3.58%). The fact that the number of seizure segments examined is more than the number of inter-seizure segments may have led to these results for this patient.
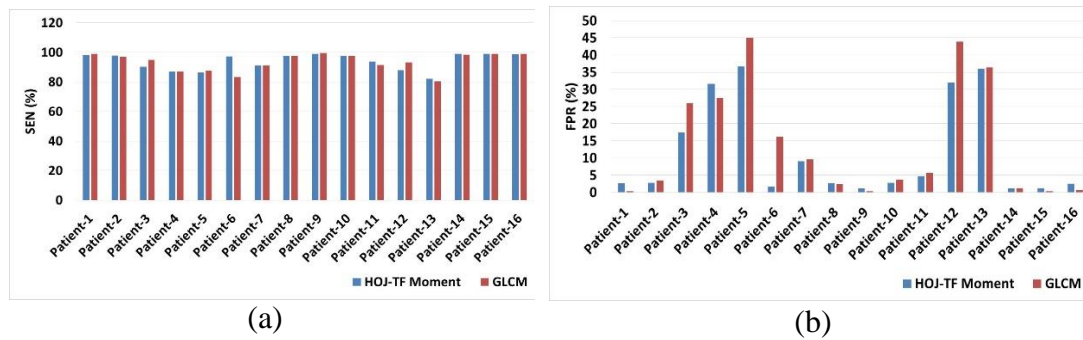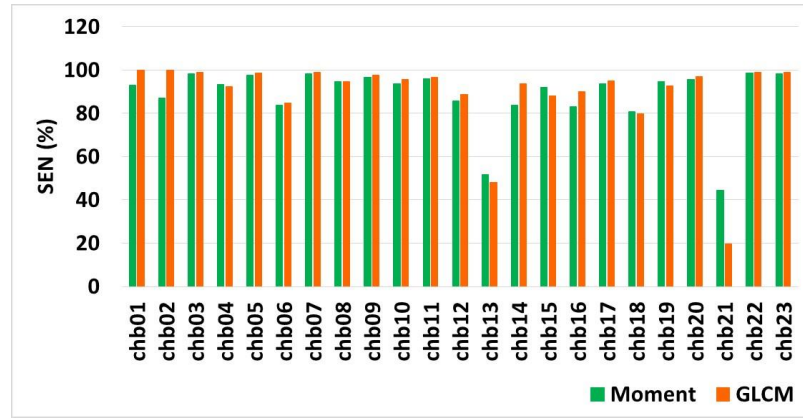
(a)
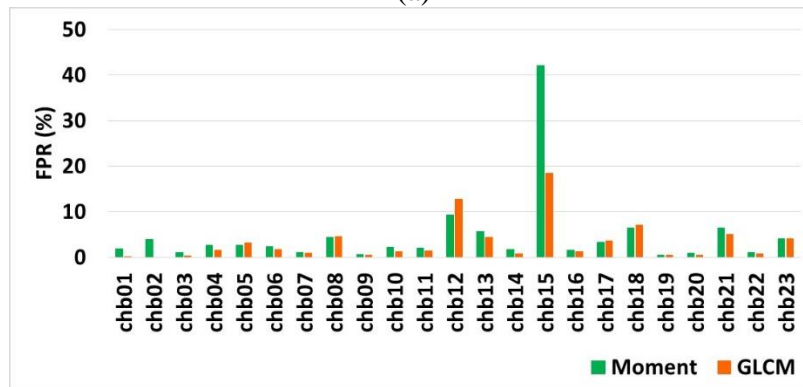
(b)

Figure 4.17: Patient based average (a) SEN and (b) FPR values obtained using the HOJ-TF-moment based feature set and GLCM based set of SST approach for 1s EEG segment duration.

In order to test the proposed method on a real-life scenario, we trained the proposed model using one data set, and tested using another data set. The sensitivity and accuracy of classification obtained by using the models trained by CHB-MIT data, and tested by unlabeled features of IKCU data set are demonstrated in Figure 4.18. Data from subject chb03 is used to create models by SVM, kNN, and LR classifiers, and then those models are used to classify the seizures of subject-14 in the IKCU data set. Sensitivity and accuracy values of subject-14 for HOJ-TF moment based feature set of SST approach are 97.8%, 98.5%, 99.3%, and 98.2%, 98.7%, 97.9%, for SVM, kNN, and LR, respectively (shown in Figure 4.18a). However, sensitivity and accuracy values of the created models of subject chb03 are 99%, 98.3%, 97.7% and 99.3%, 99.1%, 98.5%, respectively. Although the models obtained using the GLCM-based features of the chb03 subject are successful in detecting the seizure of the subject-14 in the IKCU data set except for SVM, it failed to detect the pre-seizure data. While

88

high SEN values are obtained, lower ACC values are resulted (illustrated in Figure 4.18b).

(a)   (b)
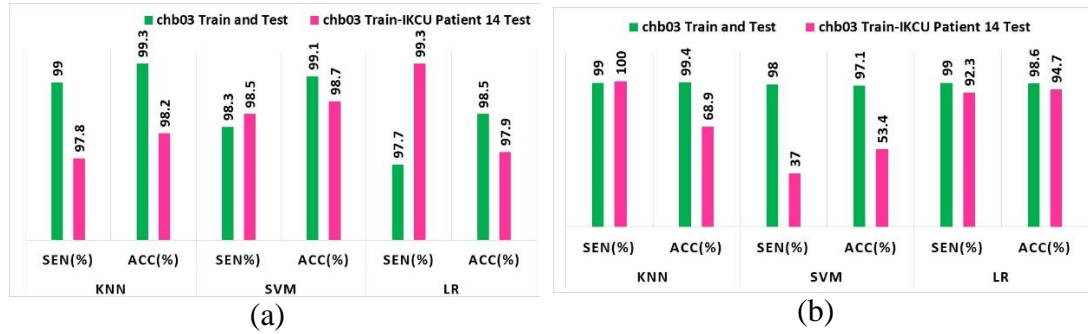
Figure 4.18: Classification of epileptic seizures of subject-14 in IKCU data set using the classifier based models of subject chb03 in CHB-MIT data set for (a) HOJ-TF moment based feature set and (b) GLCM based feature set.

Table 4.19: Comparison of classification performances of various seizure detection studies that used the CHB-MIT data set.

Author	Patient	Approaches	Classifiers	Performance Metrics
Samiee et al. [49]	23 Patients	GLCM	SVM	SEN: 70.19%, SPE: 97.74%
Thodoroff et al. [67]	23 Patients	Recurrent CNN		SEN: 85%
Ayodele et al. [65]	23 Patients	CNN		SEN: 71.45%
Jana et al. [129]	23 Patients	DWT	ANN, LDA, SVM, ELM	SEN: 71.42%, PRE: 73.88% ACC: 99.14%, F1 score: 71.53%
Zhou et al. [66]	23 patient	CNN		SEN: 96.9%, SPE: 98.1%, ACC: 97.5%
Xiang et al. [29]	18 patient	Fuzzy Entropy Sample Entropy	SVM	SEN: 98.27%, ACC: 98.31% SEN: 97.01%, ACC: 97.16%
Alickovica et al. [38]	Not given	EMD, DWT, WPD	RF, SVM, MLP, kNN	DWT, WPD: 100% ACC EMD: 95.35% ACC
Dash et al. [130]	23 patient	IFDT	HMM	SEN: 96.64%, PRE: 98.73%, ACC: 99.60%
Proposed Approach	23 patient	SST	SVM, kNN, LR	SEN: 90.3%, PRE: 93.4% ACC: 95.1%

Some studies in which seizure detection was performed using the CHB-MIT data set are summarized in Table 4.19. This table contains the utilized methods, classifiers, number of patient, and performance metrics. According to studies using 23 patient data [49, 65, 67, 129] except study [66, 130], the performance evaluation results of our proposed SST-based approach are higher. In addition, with our proposed approach, higher SEN values are obtained than two studies using CNN [65, 67]. In another CNN study [66] better performance for seizure detection was achieved. However, although

it was stated that 23 patient data were used in this study, it was not stated how many EEG segments were evaluated for each patient. In the study [130] in which higher performance evaluation results were obtained, many features such as 2-D power spectral density, time-domain features, dynamic mode decomposition power, variance, and Katz fractal dimension were used in addition to the Iterative Filtering Decomposition Technique. Computing a large number of features causes computational complexity. In study [29] in which 18 patients data were used and in study [38], it was not specified which patient data were used. If patients with low seizure detection performance results and high p-values (chb13 and chb21) are excluded from the study, higher average performance values may be obtained for our proposed study.

There are studies in the literature applying deep learning techniques to the detection of seizures on the CHB-MIT data set, providing higher accuracies than the proposed SST approach [66]. However, in the present study, a successful seizure detection method is presented using machine learning approaches and a new TF method, SST with improved localization properties. Additionally, for the IKCU data set, higher seizure classification performances are achieved using the proposed SST approach than the classical TF analysis method, STFT.

4.4.2   Deep Learning Based Approach

In this section, we propose an image-based utilization of TFRs obtained by the high-resolution SST of EEG signals. SST approach provides a close to ideal TF energy distribution by assigning the TF components of the signal into the instantaneous frequency (IF) trajectory resulting in very high TF localization of the signal components. Epileptic seizures cause abrupt changes on the statistics of EEG signals which are non-stationary in nature. Hence, the aim of this study is to apply a high-resolution TF analysis method such as SST into the representation of epileptic EEG signals to be able to capture the fast spectral variations of EEG signals during seizures. We train a CNN architecture with these TF images to achieve high segment-based seizure detection and prediction performances. The performance evaluation of both

seizure detection and prediction is based on a segment-based method which consists of 1 s and 5 s long EEG segments instead of the whole seizure event. The proposed approach is tested on two datasets; IKCU dataset we collected and the CHB-MIT dataset to detect and predict epileptic seizures with outstanding validation accuracies.

4.4.2.1 Deep CNN Architecture

In the proposed study, a novel network architecture is adapted from the 50-layer Residual Neural Network (ResNet-50) model, which is an advanced CNN architecture. ResNet-based approaches have been developed to prevent degradation and vanishing gradients problems as the network's depth increases in CNN architectures [131]. ResNet architecture adds shortcuts between layers to overcome this problem. In our proposed method, TFR images are used as input to train the network. Using TFR images, the energy density of the signals may be expressed as color pixels. In order to achieve high classification performance, all information in TF pixels must be processed with minimum loss. The information in TF energy density of nonstationary signals is critical when analyzing these signals [132]. In recent years, TFR images have been used frequently for training deep learning-based architectures [133, 134]. Hence, in this study, a new CNN architecture is designed inspired by ResNet-50 architecture to classify the calculated TF images. The original ResNet-50 architecture has widely been used in many studies with successful results [134]. Nevertheless, it may be further optimized for binary classification problems with less training set. Hence, in this study, we use an optimized version of the ResNet-50. The proposed architecture includes fewer filters than the ResNet-50 and aims to increase the accuracy of the binary classification problem compared to the ResNet-50 while reducing the training cost.

First, the TF-images recorded at 500 DPI resolution are resized to 128x128x3 dimensions to reduce the training cost and are given as input to the deep network. Then, zero-padding is performed to balance the kernel sizes. Proposed architecture was implemented in 5 stages. In the first stage, one convolutional layer (including; convolution (Conv) (7x7), strides of 2, batch normalization (BN), and rectified linear unit (ReLU) function as the activation function), and one pooling layer (maximum) (3x3) strides of 2 have been used, respectively. The second stage consists of two blocks called convolutional block and identity block, both consist of 3 repetitive

convolutional layers and a step called shortcut that adds the incoming unaltered input array to the output of the convolutional layers. In the convolutional block, unlike in the identity block, the input array participates in the adding step after passing through Conv and BN layers on the shortcut phase. In the convolutional and identity blocks, the convolutional layers have 1x1, 3x3, and 1x1 kernel sizes, respectively. In the shortcut phase of the convolutional block, the convolutional layer has a 1x1 kernel size. Shortcuts have been used for preventing the deep network from overfitting, and also used to reduce and optimize computational complexity. After the second stage, the identity block is used by repeating 2, 3, 4, and 5 times, respectively. The proposed architecture includes 50-layer similar to the ResNet-50 architecture. The proposed architecture was not added more layers in order not to increase the training cost. It is modified for the binary classification problem by reducing the number of filters in the convolutional and identity blocks. The filter numbers in repetitive convolutional and identity blocks are as follows: while Stage-1 is preserved exactly as in ResNet-50, in Stage-2, convolutional block and all identity blocks have 16, 32, and 64 filters, respectively. The number of filters is increased in sub-stages so as to extract deeper features. Stage-3 has 32, 64, and 128 filters. In all sub-stages of Stage-4, similar to the ResNet-50 architecture the number of filters kept fixed but reduced to 128. Similarly, the number of filters is reduced, chosen as 256, and fixed in all substages of Stage-5. Deep residual features are extracted from the last stage. An average pooling (2x2) process was performed before the fully connected layer with 8192 neurons to reduce the large deep residual features array. Finally, the SoftMax function [135] has been used as a binary classifier to classify deep residual features. The deep network has over 23.5 million trainable parameters.

During the training phase of the network, Adam Optimizer was used, due to the effective choice of hyperparameters. Furthermore, different batch sizes have been tested in the training phase to obtain the best training result, and the batch size has been optimized to 64 as parameter tuning. Epochs have been selected as 50 in order to specify standards in all training phases, not to increase the training cost, and to observe the robustness of the model. The learning rate was chosen as 0.1, 0.01, 0.001, and 0.0001, to observe its effect.

Two different cross-validation methods are adopted to evaluate the robustness of the proposed models. The k-fold CV [136] method is utilized based on a patient-correlated detection (PCD) approach where the trained model contains a mixed amount of data from all patients. Hence, the trained model preserves some of the characteristics of all patients used for training. Although this method does not evaluate well the accuracy in testing new patients, it is more successful in testing the data unused for training the model. The other method used for testing our results is the leave-one-out cross-validation (LOOCV) [137]. In the LOOCV method, the subjects-folds used for testing are not considered for training. Therefore, it can be used for patient-independent detection (PID) validation. In the PID method, since the patient data used as test data are not included in any training phase, the trained model does not have any characteristic features of these patient data. Therefore, compared to the PCD method, this method better evaluates accuracy in testing new patients. Moreover, the LOOCV method is advantageous in choosing a more robust model compared to other CV methods [138]. In this study, since patients are selected and excluded, the LOOCV method works as a leave-subject-out CV approach.

Additionally, SEN, PRE, ACC, F1-S, area under the receiver operating characteristic curve (ROC-AUC) [29, 125, 139], and mean squared error (MSE) [137] values are calculated during the segment-based evaluation phase [140] of the proposed models, in order to investigate the imbalanced dataset effects further. Moreover, imbalance ratio (IR) [141] values are calculated for all training sets.

4.4.2.2   Experimental Results and Discussion

Using the IKCU dataset which includes 10-channel EEG signals of 16 epilepsy patients, segment-based seizure detection approach is performed. All pre-seizure and seizure EEG segments are divided into non-overlapping 1 s- and 5 s-long segments. The high-resolution TFR of each EEG segment is calculated using the SST method. The magnitude square of SST matrices are considered as images and used as input for the proposed CNN architecture. PID and PCD validation methods are used to test the performance of the proposed image-based CNN approach. Two different segment durations are tested in order to reveal the contribution of the duration– TF resolution

to the performance of the proposed approach. The number of segments used to training and test phases of the proposed approach for all cases are given in Table 4.20.

Table 4.20: The number of segments reserved for training and testing for IKCU dataset (Note: Tr-S=Training, Te-S=Testing, and Tot-S=Total Size).

CV Type	1s Duration		5s Duration	
	5-fold CV	LOOCV	5-fold CV	LOOCV
Tr-S	7856	9206	1520	1781
Te-S	1964	614	380	119
Tot-S	9820	9820	1900	1900

In the PCD approach, IR is 1 for both 1 s and 5 s long segments. In the PID approach, IR is calculated as 1.004 and 1.011 for 1 s and 5 s segments, respectively. Hence, no imbalanced dataset effect was encountered during the training of the IKCU dataset. Initially, we compared the proposed ResNet-50-based architecture to the traditional ResNet-50 architecture. The comparison was conducted with the 5 s long SST segments obtained from the IKCU data set. Traditional ResNet-50 is tested using PCD and PID validation methods, and average ACC of 94.78% and 90.97% were obtained respectively. The proposed architecture is achieved an average ACC of 99.06% and 97.22% and revealed an average of 5.27% significant difference compared to the traditional ResNet-50 architecture. Further, it takes 519 s to train the traditional ResNet-50 architecture and 428 s to train the proposed modified ResNet-50 architecture using 5 s long SST images. Thus, the proposed architecture provides a 17.53% gain of training time. Therefore, all subsequent experiments are conducted on the proposed architecture. Additionally, we compare our results by the SST approach with spectrograms obtained by the traditional TFR approach, STFT. In our experiments, a Hamming window and overlap of 50% are utilized for STFT calculation for both 1 s and 5 s long EEG segments. The seizure detection performance for all cases in terms of SEN, PRE, ACC, cross-entropy (CE)-Loss, and F1-S for the segment-based analysis are presented in Tables 4.21-4.22.

Table 4.21: The segment-based seizure detection performance obtained using the
PID validation model for 1 s long EEG segments of the IKCU dataset.

Patient	SST 1s (%)				STFT 1s (%)			
	ACC	PRE	SEN	F1-S	ACC	PRE	SEN	F1-S
Patient 1	96.58	98.72	94.77	96.70	86.97	89.74	85.37	87.50
Patient 2	96.09	98.40	94.17	96.24	86.16	88.78	84.71	86.70
Patient 3	93.65	97.12	90.99	93.96	82.74	85.26	81.60	83.39
Patient 4	91.37	96.47	87.76	91.91	82.74	84.94	81.79	83.34
Patient 5	91.21	96.79	87.28	91.79	83.39	85.90	82.21	84.01
Patient 6	95.77	98.08	93.87	95.93	85.69	88.18	84.40	86.25
Patient 7	95.77	98.40	93.60	95.94	85.18	87.82	83.79	85.76
Patient 8	96.74	99.04	94.79	96.87	87.79	90.38	86.24	88.26
Patient 9	95.90	98.40	93.88	96.09	87.79	90.71	86.02	88.30
Patient 10	95.28	97.76	93.27	95.46	85.18	87.50	84.00	85,71
Patient 11	94.95	97.44	92.97	95.15	85.50	88.14	84.10	86.07
Patient 12	91.69	96.79	88.05	92.21	83.50	85.90	82.46	84.14
Patient 13	92.02	97.12	88.34	92.52	82.90	85.26	81.85	83.52
Patient 14	97.39	99.68	95.40	97.49	88.27	91.03	86.59	88.75
Patient 15	97.72	100.0	95.36	97.62	88.76	91.67	86.93	89.24
Patient 16	97.07	99.36	95.09	97.18	89.57	91.03	87.41	89.18
Average	**94.95**	**98.10**	**92.47**	**95.19**	**85.76**	**88.27**	**84.34**	**86.26**

Table 4.22: The segment-based seizure detection performance obtained using the
PID validation model for 5 s long EEG segments of the IKCU dataset.

Patient	SST 5s (%)				STFT 5s (%)			
	ACC	PRE	SEN	F1-S	ACC	PRE	SEN	F1-S
Patient 1	99.16	100.0	98.39	99.19	96.64	96.72	96.72	96.72
Patient 2	98.32	100.0	96.83	98.39	94.96	95.08	95.08	95.08
Patient 3	96.64	96.72	96.72	96.72	90.76	93.44	89.06	91.20
Patient 4	94.96	95.08	95.08	95.08	89.92	91.80	88.89	90.32
Patient 5	94.12	95.08	93.55	94.31	89.92	90.16	90.16	90.16
Patient 6	97.48	96.72	98.33	97.52	93.28	93.44	93.44	93.44
Patient 7	97.48	98.36	96.77	97.56	95.80	96.72	95.16	95.93
Patient 8	99.16	100.0	98.39	99.19	97.48	98.36	96.77	97.56
Patient 9	99.16	98.36	100.0	99.17	**99.16**	100.0	98.27	99.13
Patient 10	98.32	98.36	98.36	98.36	95.80	95.80	96.67	96.23
Patient 11	98.32	98.36	98.36	98.36	94.12	95.08	93.55	94.31
Patient 12	92.44	93.44	91.94	92.68	90.76	95.08	87.88	91.34
Patient 13	91.60	93.44	90.48	91.94	89.92	95.08	86.57	90.63
Patient 14	**100.0**	100.0	100.0	100.0	98.32	98.36	98.36	98.36
Patient 15	99.16	100.0	98.39	99.19	97.48	98.36	96.77	97.56
Patient 16	99.16	98.36	100.0	99.17	96.64	96.72	96.72	96.72
Average	**97.22**	**97.64**	**96.97**	**97.30**	**94.44**	**95.64**	**93.75**	**94.67**

Segment-based seizure detection performance for the 1 s segment duration using PID
method is presented in Table 4.21. For 1 s segment duration, while by using the SST-
based CNN approach, the highest patient-independent seizure detection performance

(97.72% ACC, 100% PRE, 95.40% SEN, and 97.62% F1-S) is achieved for "Patient-15", the maximum seizure detection performance (89.57% ACC, 91.03% PRE, 87.41% SEN, and 89.18% F1-S) is obtained utilizing the STFT-based CNN approach for "Patient-16". For the same validation model of 5 s segment duration, similarly, maximum seizure detection performance (100% ACC, PRE, SEN, and F1-S) is achieved using the SST-based CNN approach for "Patient-14". However, lower seizure detection performances have been achieved using STFT based CNN approach (shown in Table 4.22). In addition to the performance evaluation values given in Tables 4.21 and 4.22, the average ROC-AUC values are also calculated. In the PID approach, the ROC-AUC values obtained using SST 1 s, STFT 1 s, SST 5 s, and STFT 5 s are 0.963, 0.912, 0.987, and 0.944, respectively.

Table 4.23: The segment-based seizure detection performance obtained using the PCD validation model for both 1 s and 5 s long EEG segments of the IKCU dataset

	Folds	SST					STFT				
		ACC	Loss	PRE	SEN	F1-S	ACC	Loss	PRE	SEN	F1-S
1s	Fold-1	95.42	0.256	97.03	94.23	95.61	**88.34**	0.387	88.77	87.00	87.88
	Fold-2	**96.54**	0.242	98.68	94.13	96.35	85.92	0.450	87.75	85.30	86.51
	Fold-3	93.78	0.289	96.26	91.96	94.06	86.83	0.423	87.75	86.80	87.27
	Fold-4	96.08	0.243	96.94	95.53	96.23	88.03	0.396	89.31	87.65	88.47
	Fold-5	93.71	0.289	96.14	91.95	94.00	87.79	0.398	89.22	87.66	88.43
	Avr.	**95.11**	**0.264**	**97.01**	**93.56**	**95.25**	**87.38**	**0.411**	**88.56**	**86.88**	**87.71**
5s	Fold-1	99.25	0.017	98.51	100.0	99.25	94.21	0.121	96.52	92.82	94.63
	Fold-2	98.95	0.018	99.00	99.00	99.00	**98.68**	0.075	100.0	97.57	98.77
	Fold-3	99.21	0.018	99.44	99.01	99.22	96.32	0.086	98.01	95.17	96.57
	Fold-4	**99.47**	0.017	100.0	98.88	99.44	95.53	0.098	97.51	94.23	95.84
	Fold-5	98.42	0.019	98.01	98.99	98.50	97.37	0.079	98.01	97.04	97.52
	Avr.	99.06	0.018	98.99	99.18	99.08	96.42	0.092	98.01	95.37	96.67

We also tested the performance of SST and STFT based CNN approaches for segment-based epileptic seizures detection using PCD validation method (Table 4.23). For 1 s segment duration, the best seizure detection accuracy calculated using the "Fold-2" PCD model of SST based CNN approach is 96.54%, which is significantly higher than the best accuracy calculated using the "Fold-1" PCD model of STFT based CNN approach (88.34%). Similarly, for the 5 s segment duration, the highest seizure detection accuracy (99.47%) for the SST based CNN approach is achieved using

"Fold-4" PCD model, but the maximum seizure detection accuracy (98.68%) is obtained using the "Fold-2" PCD model for the STFT based CNN approach. Additionally, for both 1 s and 5 s long segment durations, all average recall, precision, and F1-score values calculated using the SST based CNN approach (for 1 s: 93.56% SEN, 97.01% PRE, and 95.25% F1-S; and for 5 s: 99.18% SEN, 98.99% PRE, and 99.08% F1-S) are significantly higher than those calculated for the STFT based CNN approach (for 1 s: 86.88% REC, 88.56% PRE, and 87.71% F1-S; for 5 s: 95.37% SEN, 98.01% PRE, and 96.67% F1-S). It is also observed that the average CE-Loss calculated using the SST-based CNN approach is lower than that of the STFT-based CNN approach for all cases. In the PCD approach, the average ROC-AUC values obtained using SST 1 s, STFT 1 s, SST 5 s, and STFT 5 s are 0.970, 0.942, 0.996, and 0.973, respectively.

Table 4.24: Average accuracy and training duration comparison versus learning rate hyperparameters in PCD based approach for each fold in the IKCU dataset.

Learning Rate	SST 1s		SST 5s		STFT 1s		STFT 5s	
	ACC (%)	TT(s)	ACC (%)	TT(s)	ACC (%)	TT(s)	ACC (%)	TT(s)
0.1	92.45	578	96.95	111	83.69	613	94.68	98
0.01	93.55	1093	98.41	234	84.96	1058	95.89	189
0.001	**95.11**	**2168**	**99.06**	**428**	**87.38**	**2000**	**96.42**	**346**
0.0001	94.67	4076	97.43	973	86.98	4004	95.76	798

In addition, to further explore the advantages of the proposed SST-based CNN approach, all steps of the classification algorithm are repeated utilizing a CWT on 5 s long segments. In our experiments, Morlet wavelet is employed, a frequently utilized mother wavelet, to calculate the scalogram of EEG segments [142], which are used to train the network. The average accuracy and MSE values are demonstrated for tested TFR methods, and validation models in Figures 4.19a and 4.19b. It is noteworthy that, while the CWT-based approach yields higher average ACC and lower average MSE values compared to the STFT method, the proposed SST approach provided the highest average ACC and lowest average MSE values for both validation models. Additionally, each approach provides higher average performance metrics using PCD based validation model.
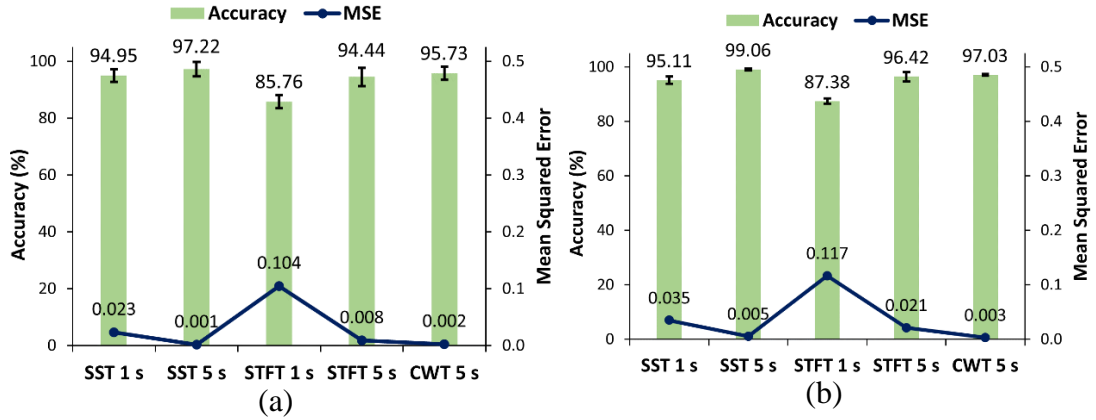
Figure 4.19: Comparison of average accuracy and MSE obtained using (a) PID (standard deviations for accuracy values: ±2.24% (SST 1s), ±2.58% (SST 5s), ±2.27% (STFT 1s), ±3.26% (STFT 5s), and ±2.31% (CWT 5 s)) and (b) PCD (standard deviations for accuracy values: ±1:30% (SST 1s), ±0.40% (SST 5s), ±0.99% (STFT 1s), ±1.71% (STFT 5s), and ±0.35% (CWT 5s)) based validation models for IKCU dataset.

As shown in Table 4.24, resulting ACC and calculated training durations are given for various learning rate hyperparameters in the PCD method. The best scenario in all segments occurred at a 0.001 learning rate. Although the models provide lower training time at higher learning rates, they reached local minima points. Using a lower learning rate of 0.001, we reach the global minimum. The best training and validation ACC, and CE-Loss values, and the best confusion matrix in the test phase of the PCD method with 5s SST segments are given in Figure 4.20. Note that, ACC values converge to the upper, and CE-Loss values converge to the lower limits. Therefore, overfitting or underfitting are not observed in any of the trained models. Notice also that SST 5s models converged before 50 epochs, hence it is fixed to 50 to compare all models on equal conditions. Moreover, SST 5s model is almost fully capable of distinguishing seizure from pre-seizure.
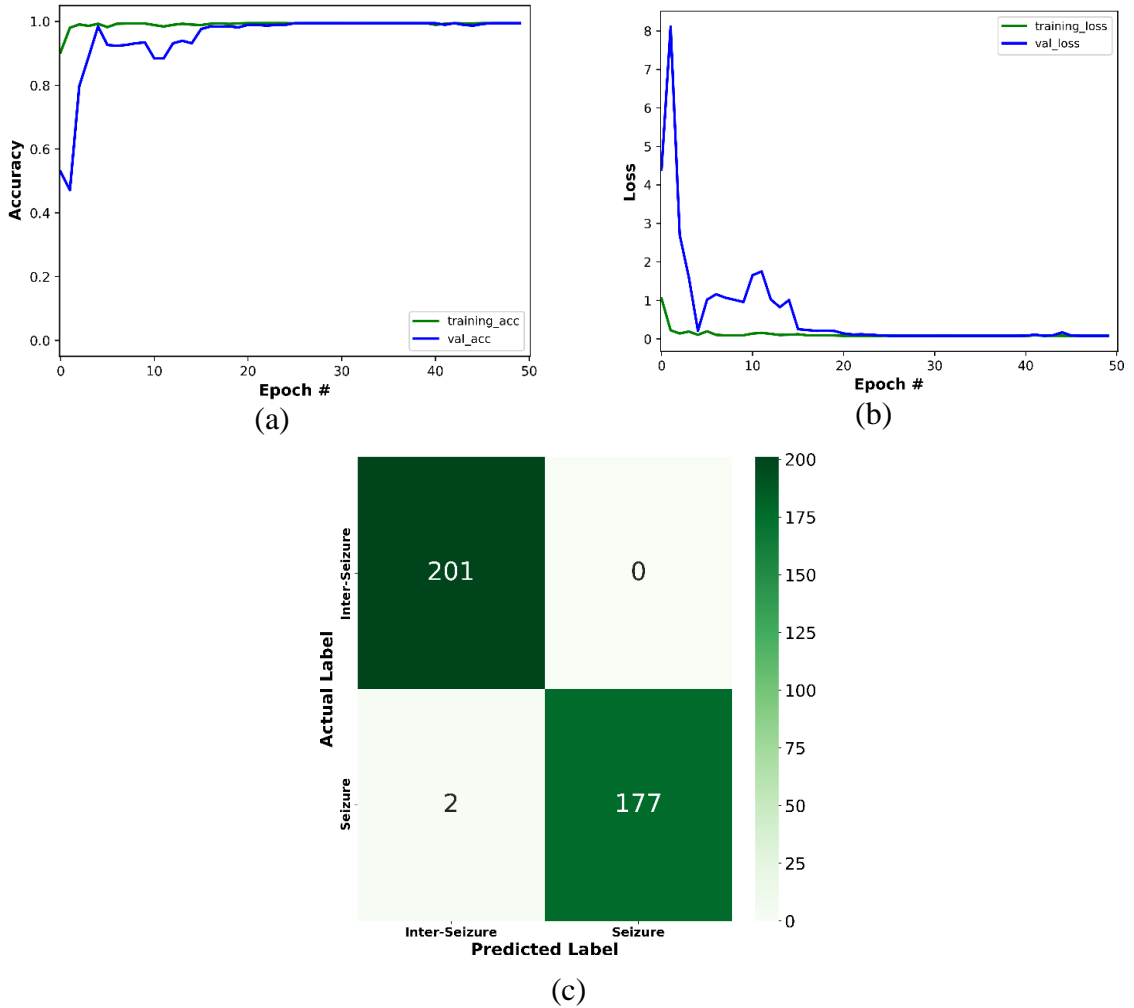
Figure 4.20: Example performance graphs obtained in the 4th-fold of PCD method with 5s long SST segments; the best (a) training and validation accuracies, (b) CE-Losses, and (c) the confusion matrix in the IKCU dataset.

Based on the conducted experiments, the highest performing 5 s long SST images are selected and used to train several well-known architectures. Testing phase performance comparisons with that of the proposed network are shown in Figure 4.21. Results emphasize the superiority of the proposed architecture in classifying SST images. Notice that, AlexNet yields the lowest classification performance. The proposed ResNet-based architecture provides a significant improvement of 5.27% compared to traditional ResNet-50 [131, 134], 24.33% compared to AlexNet [133, 143], 12.86% compared to VGG16 [134], and 15.59% compared to SqueezeNet [133].
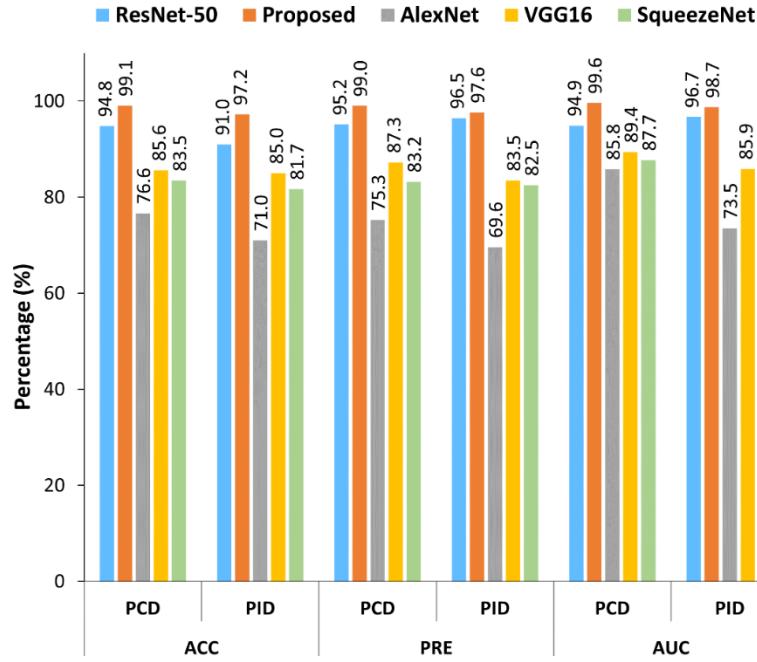
Figure 4.21: Comparison of proposed architecture with well-known CNN
architectures using 5 s long SST segment in IKCU dataset.

We applied the proposed SST-based CNN approach to CHB-MIT Epileptic EEG
dataset which was previously employed in other deep learning studies, and compared
our performance with existing literature. Two different classification problems are
addressed using this dataset. Segment-based seizure detection: the SST-based CNN
model is trained to differentiate between inter-seizure and seizure EEG segments,
Segment-based seizure prediction: the model is trained to distinguish inter-seizure and
pre-seizure EEG segments. Signals in this dataset are sampled with 256 Hz providing
a sufficient TF resolution. Hence, the proposed approach is only conducted using 1 s
long segment duration. Using LOOCV- and CV-based validation models for segment
based seizure detection and prediction, we evaluate the performance of our proposed
approach.

In addition, the patient-independent prediction (PIP) approach similar to the PID
method, and the patient-correlated prediction (PCP) approach similar to the PCD
method utilized above were used to validate the success of segment-based seizure
prediction models on the CHB-MIT dataset. For this experiment, variable numbers of
training and testing sets are formed because the number of seizure segments of each
patient is different. Using the CHB-MIT dataset, in the PCD-based method, a total of
23080 SST segments are used, with 18464 for training and the rest of 4616 for testing

in each fold. This data includes a total of 9280 seizure segments and a total of 13800 inter-seizure segments (600 segments for each subject). Seizure segments are variable in each patient and contain an average of 403 (min 66 and max 1396) SST 1 s segments. In this method, the IR was calculated as 1.49. In the PCP-based method, a total of 20700 SST segments are used, where 16560 segments used for training and 4140 for testing at each fold.

These segments include a total of 6900 pre-seizure segments (300 segments for each subject) and a total of 13800 inter-seizure segments (600 segments for each subject). Furthermore, in the PIP based method, 19800 segments are used for training and 900 segments for testing at each fold. In both PCP and PIP methods, the IR value was calculated as 2. As the PID method contains a variable number of seizure segments like the PCD method, an average of 22077 segments for training and 1003 segments for testing are used in each fold. In this method, the IR value was calculated as 2.25. The reason for the data imbalance is the variation in the number of seizure segments in CHB-MIT database. Although IR affects our models, its level is negligible. Performance evaluation results of the experiments carried out with the proposed approach are demonstrated in Tables 4.25 and 4.26 for the segment-based seizure detection and prediction tasks, respectively.

Table 4.25: The segment-based seizure detection (inter-seizure vs seizure) and segment-based seizure prediction (inter-seizure vs pre-seizure) performances of the proposed SST-based CNN approach obtained using the CV-based validation model for 1 s EEG segments of the CHB-MIT dataset

Folds	Seizure Detection					Seizure Prediction				
	ACC	Loss	PRE	SEN	F1-S	ACC	Loss	PRE	SEN	F1-S
Fold-1	99.76	0.011	99.86	99.75	99.80	96.81	0.143	99.13	96.20	97.64
Fold-2	99.46	0.015	99.64	99.46	99.55	97.10	0.115	99.28	96.48	97.86
Fold-3	99.61	0.013	99.71	99.64	99.67	97.71	0.087	99.46	97.17	98.30
Fold-4	99.35	0.017	99.82	99.10	99.46	96.33	0.194	98.88	95.75	97.29
Fold-5	99.98	0.009	100.0	99.66	99.83	96.62	0.169	98.99	96.06	97.50
Avr.	99.63	0.013	99.81	99.52	99.66	96.91	0.142	99.15	96.33	97.72

It can be observed from Table 4.25 that generally high segment-based seizure detection performances in terms of accuracy ($\geq$99.35%), precision ($\geq$99.64%), sensitivity ($\geq$99.10%), and F1-score ($\geq$99.46%) are achieved using the PCD validation model. The proposed SST based CNN approach provides equally high performance for the

more challenging segment based seizure prediction problem with accuracy ($\geq$96.33%), precision ($\geq$98.88%), sensitivity ($\geq$95.75%), and F1-score ($\geq$97.29%) for the PCP validation model. On the other hand, by using the PID validation model (given in Table 4.26), while maximum segment-based seizure detection performances (100% ACC, PRE, SEN, and F1-S) are obtained for patients chb07 and chb23, the highest segment-based seizure prediction performances are achieved (100% ACC, PRE, SEN, and F1-S) for patients chb09 and chb20 using PIP approach. Additionally, the average accuracy and MSE vales given in terms of conducted task and validation models, in Figure 4.22. Note that the PCD validation model shows higher average segment-based seizure detection ACC (99.63%) and lower average MSE values (0.003), PIP validation model provides better performance (97.92% ACC, and 0.02 MSE) for segment-based seizure prediction task.

Table 4.26: The segment-based seizure detection (inter-seizure vs seizure) and segmentbased seizure prediction (inter-seizure vs pre-seizure) performances of the proposed SST-based CNN approach obtained using the LOOCV-based validation model for 1 s EEG segments of the CHB-MIT dataset

Patient	Seizure Detection (%)				Seizure Prediction (%)			
	ACC	PRE	SEN	F1-S	ACC	PRE	SEN	F1-S
chb01	99.17	99.33	99.17	99.25	99.44	99.67	99.50	99.58
chb02	99.09	99.16	99.66	99.41	98.88	99.17	99.17	99.17
chb03	98.60	99.67	99.00	99.33	98.65	99.00	99.00	99.00
chb04	98.96	98.83	99.66	99.24	99.22	99.50	99.33	99.41
chb05	99.22	99.67	98.84	99.25	98.31	98.67	98.83	98.75
chb06	99.59	100.0	99.50	99.75	97.75	98.33	98.33	98.33
chb07	100.0	100.0	100.0	100.0	99.78	99.83	99.83	99.83
chb08	99.34	99.83	98.52	99.17	96.63	97.33	97.66	97.49
chb09	99.89	99.83	100.0	99.91	100.0	100.0	100.0	100.0
chb10	99.14	99.67	98.84	99.25	96.18	97.00	97.32	97.16
chb11	99.50	99.17	99.66	99.41	98.78	99.17	99.00	99.08
chb12	99.68	99.33	100.0	99.66	95.96	96.83	97.16	96.99
chb13	99.30	99.50	99.50	99.50	94.44	96.67	95.08	95.87
chb14	99.48	99.50	99.83	99.66	99.11	99.50	99.17	99.33
chb15	99.60	99.67	99.01	99.34	96.18	97.00	97.32	97.16
chb16	98.06	99.17	98.67	98.92	95.73	96.67	96.99	96.83
chb17	98.66	99.33	98.68	99.00	95.56	97.50	95.90	96.69
chb18	98.26	98.50	98.83	98.66	99.00	99.33	99.17	99.25
chb19	99.16	99.50	99.33	99.41	99.33	99.67	99.34	99.50
chb20	99.66	99.83	99.67	99.75	100.0	100.0	100.0	100.0
chb21	97.00	98.67	97.37	98.02	93.89	96.33	94.60	95.46
chb22	99.50	100.0	99.34	99.67	99.67	99.83	99.67	99.75
chb23	100.0	100.0	100.0	100.0	99.56	99.50	99.83	99.66
Average	99.17	99.49	99.26	99.37	97.92	98.54	98.36	98.45
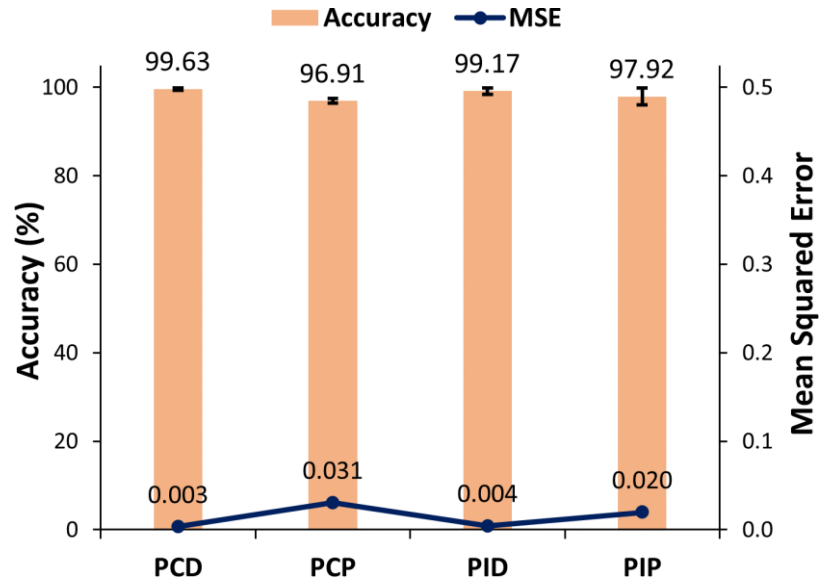
Figure 4.22: Comparison of average accuracy and MSE values obtained using segment-based PCD, PCP, PID, and PIP models (standard deviations for accuracy values: ±0.25%, ±0.53%, ±0.69%, and ±1.90%, respectively) in the CHB-MIT dataset.

Table 4.27: Comparison of recent segment-based seizure detection and prediction studies conducted using CHB-MIT dataset with proposed work.

Problem	Author	No. of Patient	Feature	Classifier	No. of Seizure	ACC (%)	SEN (%)
Seizure Detection	Ayodele et al. [65]	23	Features maps	RCNN	198	-	71.45
	Li et al. [136]	24	EEG time-series	NLSTM	127	95.29	95.42
	Liang et al. [143]	23	EEG waveforms	LRCN	198	99	84
	Hossain et al. [144]	23	EEG time-series	CNN	198	98.05	90.00
	Thodorof et al. [67]	23	Image based	LSTM	198	-	85.00
	Wei et al. [145]	24	EEG time-series	CNN	151	81.49	70.68
	Zhang et al. [134]	9	STFT	CNN	-	98.26	98.01
	Zhou et al. [66]	24	EEG time series	CNN	-	62.3	61.2
	Zhou et al. [66]	24	EEG frequency-series	CNN	-	97.5	96.9
	This Worka	23	SST	CNN	144	99.17	99.26
	This Workb	23	SST	CNN	144	99.63	99.52
Seizure Prediction	Liu et al. [146]	2	EEG features	CNN	36	-	91.5
	Shahbazi et al. [147]	14	STFT	LSTM	49	-	98.21
	Tsiouris et al. [140]	24	EEG features	LSTM	185	-	99.84
	Zhou et al. [66]	24	EEG time series	CNN	-	59.5	61.8
	Zhou et al. [66]	24	EEG frequency-series	CNN	-	95.6	94.2
	This Worka	23	SST	CNN	144	97.92	98.36
	This Workb	23	SST	CNN	144	99.91	96.33

Performance comparison of recent segment-based seizure detection and prediction studies conducted on the CHB-MIT dataset with the proposed approach is demonstrated in Table 4.27. The best performance evaluation results are highlighted

in boldface numbers. Hossain et al. [144] introduced a segment-based seizure detection approach in which the multi-channel raw EEG data were used as input to the CNN model. Using the cross patient validation model, the proposed approach provides the average 90.00% SEN, 91.65% SPE, 98.05% ACC for all patients. In another study [143], four-class segment-based seizure detection approach was proposed. EEG waveform images of normal, pre-seizure, seizure and post-seizure EEG data were used as input to an 18-layer Long-Term recurrent convolutional network (LRCN). By using cross patient seizure detection model, 84% sensitivity, 99% specificity, and 99% accuracy were achieved. The segment-based seizure detection approach was proposed by using the multichannel time-series EEG signals based 12-layer CNN model in another study. The merger of the increasing and decreasing sequences (MIDS) and data augmentation method was utilized, separately, and achieved cross patient performance evaluation results. Using multi-channel EEG, 70.68% sensitivity, 81.49% ACC, and 92.30% specificity values were achieved [145]. In a study conducted by Zhang et al. [134], three different CNN models (VGG16, VGG19, and ResNet-50) based segment-based seizure detection approaches were performed using STFT based preprocessing step. Maximum 98.26% seizure detection accuracy was achieved using 9 patients EEG recordings. It is noteworthy that among all seizure detection methods compared, both PID and PCD validation results of our SST-based CNN methods are significantly higher.

Further, the segment-based seizure prediction performance of the proposed SST-based CNN approach is tested and compared with similar studies in the literature (given in Table 4.27). The 3-layer CNN-based seizure detection and prediction method using the CHB-MIT data set has been presented using both time domain and frequency domain signals as inputs for classification [66]. In the segment-based seizure detection, while this approach presented an average of 62.3% ACC, and 61.2% REC values for the time domain inputs, for the frequency domain inputs average 97.5% ACC and 96.9% REC values were presented. Additionally, in the segment-based seizure prediction, average 95.6% ACC, and 94.2% REC values were achieved for the frequency domain inputs. LSTM based CNN method is utilized in another segment-based seizure prediction study. Spectrograms of corresponding signals were used as input. For 14 patients, an average of 98.21 SEN was obtained [147]. The performance of segment-based seizure prediction obtained in that study is higher than that of our

study. While EEG data of 14 patients, and 49 seizure segments are examined in that study, EEG data of 23 patients and 144 seizure segments are evaluated in our study. In another segment-based seizure prediction study [140], statistical moments, zero crossings, WT coefficients, PSDs of EEG subbands, and cross-correlation were calculated as features and utilized as input for LSTM. For the pre-seizure window of 120 min, an average of 99.84% SEN, and 99.86% SPE were achieved for 24 patients. In that study, higher segment-based seizure prediction sensitivity was obtained compared to the proposed approach at the expense of comprehensive and computationally expensive feature extraction step.

Seizure events cause changes in time and frequency characteristics of EEG signals. Thus, the correct distribution of epileptic EEG signals' energy into the joint time-frequency plane is very effective in the classification process. SST is a recently developed TF reassignment method that provides a close to an ideal representation of non-stationary signals in the TF plane. In our recent work [148], TF representations obtained by SST are used as input for both machine and deep learning methods using only IKCU Epilepsy dataset. Higher-order TF moments are manually extracted and classified using three classifiers. Higher classification performance is achieved by using a standard CNN architecture trained by SST images. The present study presents utilization of the high-resolution TF representations obtained by SST in the segment-based classification of epileptic EEG signals. We propose treating those SST energy distributions as images and utilize them in the training of a deep network. Among other network architectures, the proposed modified ResNet-50 architecture yielded better classification performance. The layer-filters of the proposed architecture are optimized according to our classification problem. Further, the hyperparameters used in the training of the network are fine-tuned by making performance comparisons. While constructing the deep network, it was aimed to extract all valuable information of the energy distribution in TFR images with residual features. Experimental results have emphasized the advantages of the proposed architecture in the segment-based classification problem.

4.5 Comparison of the proposed epileptic EEG detection and classification approaches

In our study, epileptic seizure detection is performed using EMD and derivative approaches, the DMD approach, which is a matrix decomposition method, and the SST approach, a new TF method. Pre-seizure and seizure EEG segments are decomposed into IMFs using the EMD and EEMD method, and time, spectral and non-linear features are calculated using the first 3 IMFs (IMF1, IMF3, IMF2) after the IMF selection process. In order to compare the success of EMD and EEMD methods, the same features are obtained using the approximation and detail coefficient of the DWT approach and directly from the EEG signal itself. While the EEMD method gives more successful results than the EMD approach for all conditions and classifiers, the most unsuccessful classification results are obtained by using features calculated from the EEG signal itself. DMD spectra are obtained for pre-seizure and seizure EEG segments using the DMD approach, which is a simple matrix decomposition method. Although the DMD spectrum has been defined in the literature [58, 98], different features other than DMD powers have not been calculated using this spectrum. In our study, it is proposed to calculate DMD subband powers and DMD-HOS moments as features. In addition, although the multi-channel DMD approach has been used in the literature, the single-channel DMD approach has been proposed in our study. The success of the DMD approach is compared with the classical PSD obtained using the Welch method. The classification performance of both MC-DMD and SC-DMD approaches is higher than that of the PSD approach. In addition, the proposed SC-DMD based approach has been at least as successful as the MC-DMD based approach. Another seizure detection study is carried out using the high TF resolution SST approach which is proposed to overcome the disadvantages of classical TF approaches. In the machine learning based SST approach, HOJ-TF moment-based and GLCM-based features are calculated as features using the magnitude square of SST. The same features are computed using the STFT method that is the classical TF analysis method to compare the success of SST. The SST approach provided higher classification accuracy than STFT for each condition and classifier. In the deep learning based SST approach, SST image are used as an input for CNN.

(a)

(b)

(c)

(d)

(e)
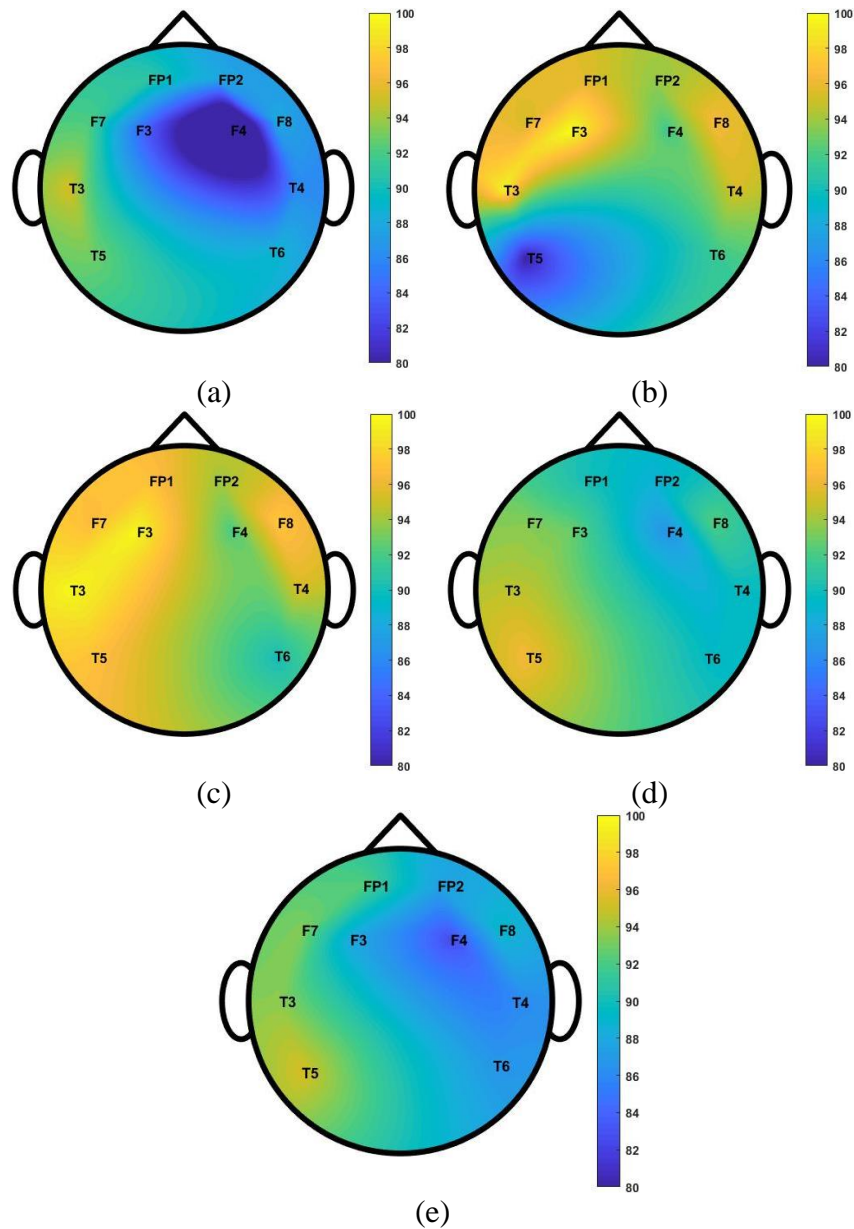
Figure 4.23: Topographic map of channel based classification accuracies of (a) EEG based (b) EMD based (c) EEMD based (d) SC-DMD based, and (e) SST based approaches.

For the comparison of machine learning-based approaches, Channel-based classification performances of the proposed SC-DMD, SST, EMD, and EEMD approaches are given with a topographic map in Figure 4.23. The topographic map is created by averaging the ACC values obtained with all classifiers for each method. It was stated by the expert neurologists that epileptic attacks in the used data set are left hemisphere-focused. It is noteworthy that the channel-based classification success of the EEG-based seizure detection approach (shown in Figure 4.23a) is very low, while

is very high for the EEMD-based seizure detection approach (given in Figure 4.23c). It is also remarkable that in all proposed methods, the channels in the left hemisphere yielded successful results of seizure detection (given in Figures 4.23b-4.23e).
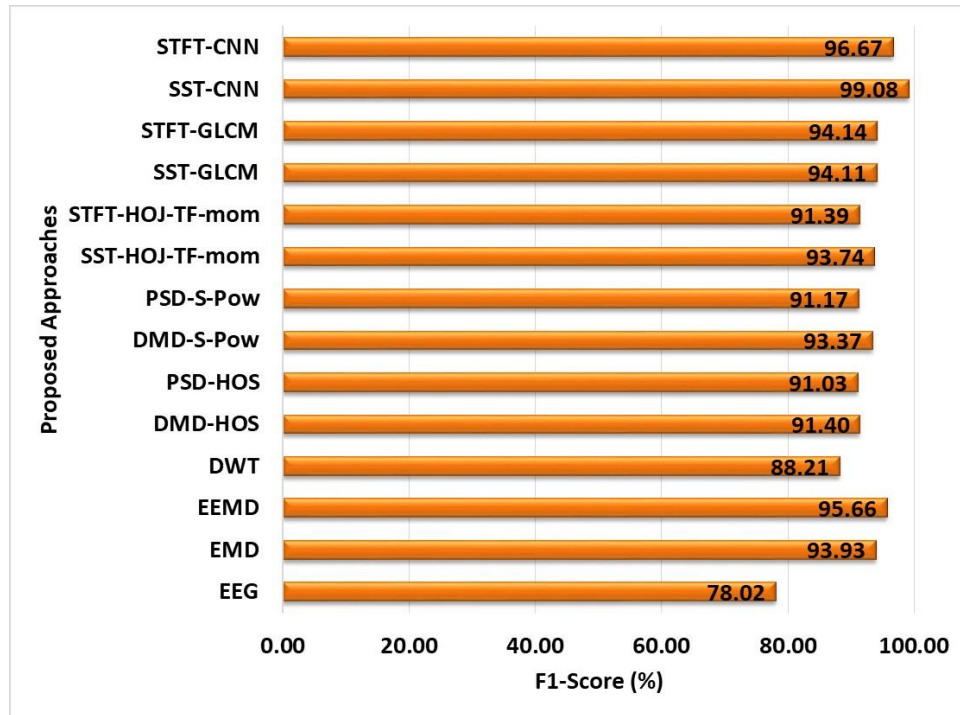
Figure 4.24: Comparing of F1-S values of proposed epileptic seizure detection approaches.

Average F1-S obtained by the proposed methods, and by the classical approaches are calculated for comparison and given in Figure 4.24. Average F1-S values are achieved by averaging the F1-S values obtained with all classifiers for each method. The F1-S of the proposed EMD and EEMD-based approaches, are higher than those of DWT and EEG-based approaches. In the DMD-based seizure detection approach, higher F1-S values are obtained than that of the traditional PSD approach for the subband power-based feature set (S-Pow), and moment-based feature set (HOS). Finally, in the SST-based epileptic seizure detection approach, higher F1-S values are obtained for each feature set compared to the STFT approach. In addition, both ML-based and DL-based proposed SST methods, demonstrate a high performance rates in classifying our pre-seizure and seizure segments of IKCU data set. However, the DL based SST approach (SST-DL) provided better F1-S than the ML-based approaches.

5. Classification of Alzheimers' Dementia by Using EEG Signals and Advanced Signal Decomposition Methods

In this part of the thesis, two different approaches named EMD and derivatives, and SST are performed to distinguish EEG segments of control and AD patients.

5.1 Alzheimer's Dementia EEG data set (IKCU AD data set)

EEG data were recorded from patients who were evaluated in İzmir Katip Çelebi University Faculty of Medicine, Department of Neurology dementia polyclinic and diagnosed with early-stage Alzheimer's disease by laboratory tests and neuroimaging. EEG signals (30 min for each patient) of 15 AD patients (8 Females; 7 Males, the average age is 64.53±8.47, average Mini-mental test score (MMT) is 22/30), were recorded using Philips Alice-6 device, from 19 different channels and at a sampling frequency of 200 Hz. These signals were collected using surface electrodes from electrode positions of Fp1, F7, T3, T5, O1, O2, T6, T4, F8, Fp2, F3, Fz, F4, C3, Cz, C4, P3, Pz, P4 using an International 10-20 electrode system. In order to compare the EEG data of AD patients, EEG recordings were collected from the age-matched control subjects (CS) (5 Females; 6 Males, the average age is 57.09±5.28) using the same recording system and electrode placement. EEG records of CS were collected from healthy volunteers meeting the following criteria;

1. Without any neurological or psychiatric disease,

2. Those who did not drink caffeine-containing beverages on the day of EEG recording,

3. No history of alcohol and substance abuse,

4. Not using any medication that affects cognitive processes,

In order to collect these EEG signals for our study, ethical approval numbered 83 and dated 22.10.2020 is obtained from the Clinical Research Ethics Committee of Izmir Katip Celebi University.

In previous studies [74] since it is important to examine different cortical regions in AD, it has been proposed to divide the brain into 5 clusters named Anterior (Fp1, F3, Fz, Fp2, F4), Posterior (P3, O1, Pz, P4, O2), Central (C3, Cz, C4), Temporal/left (T3, T5, F7) and Temporal/right (T4, T6, F8) to capture the differences in different regions of the brain. In our study, all the results are given by considering these 5 different brain clusters. In order to achieve related classification performances of brain clusters, average classification performances are calculated considering corresponding EEG channels. These 5 brain clusters are demonstrated with different colors in Figure 5.1.
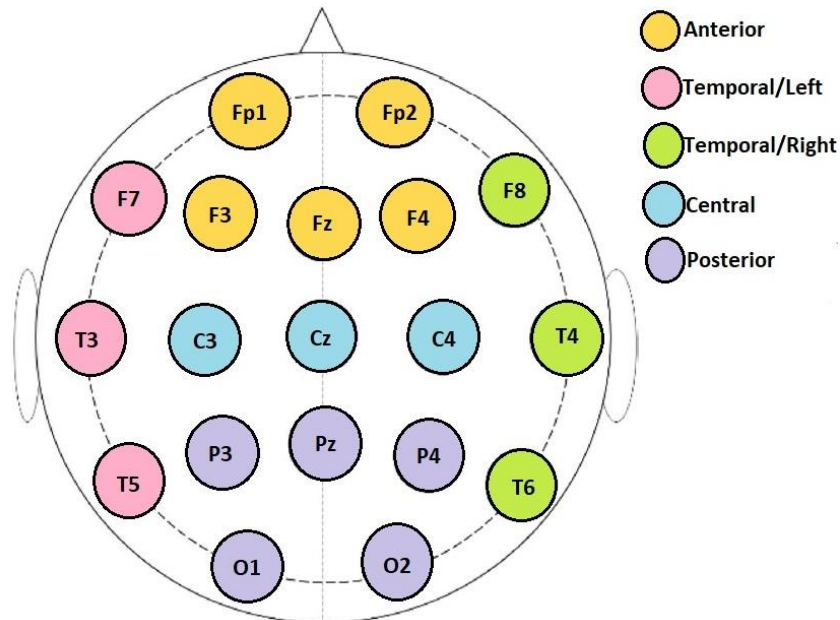
Figure 5.1: Brain clusters with regard to the electrode sites. The anterior cluster is demonstrated with yellow, the temporal right and left clusters are demonstrated with green and pink respectively, the posterior cluster is demonstrated with light purple, and the central cluster is demonstrated with blue color.

110

5.2 Preprocessing

At this stage, to remove power line interference and various noises, a Butterworth type II band-pass filter with 0.5-40 Hz cutoff frequencies, is applied to each EEG segment. All EEG signals are analyzed using two different segment durations as 1 min and 5s. EEG signals divided into non-overlapping 1min and 5s segment durations separately. Two different approaches called EMD and derivative and SST are used to achieve efficient classification performance for AD and control EEG signals.

5.3 Results and Discussions of EMD and its Derivative

IKCU AD data set containing 19-channels EEG signals of 11 CS and 15 AD patients was investigated utilizing EMD, and EEMD methods, and it is aimed to distinguish EEG segments of control and AD patients with high performance.

First, in order to identify the most distinctive IMFs of EMD and EEMD methods, the hybrid IMF selection procedure including energy-based, correlation coefficients-based, PSD distance-based, and T-test-based IMF selection methods detailed in Section 4.2.1 was applied to the achieved IMFs. The example of achieved IMFs using EMD and EEMD methods are presented in Figure 5.2. The energy, correlation coefficients, PSD distance, and p-value [14, 111-114], of each IMF, were calculated and ranking matrices were achieved for each EEG segment of control subjects and AD patients. By combining the ranking matrices obtained for each segment, a separate ranking matrix was obtained for the control subjects and AD patients. The first column of these ranking matrices shows the IMFs with the highest priority. High priority IMFs are identified by plotting the histogram of the 1st column of the ranking matrices (given in Figure 5.3). When this histogram is evaluated, it is seen that the first 7 IMFs (IMF1, IMF2, IMF3, IMF4, IMF5, IMF6, and IMF7) are distinctive for both control subjects and AD patients.
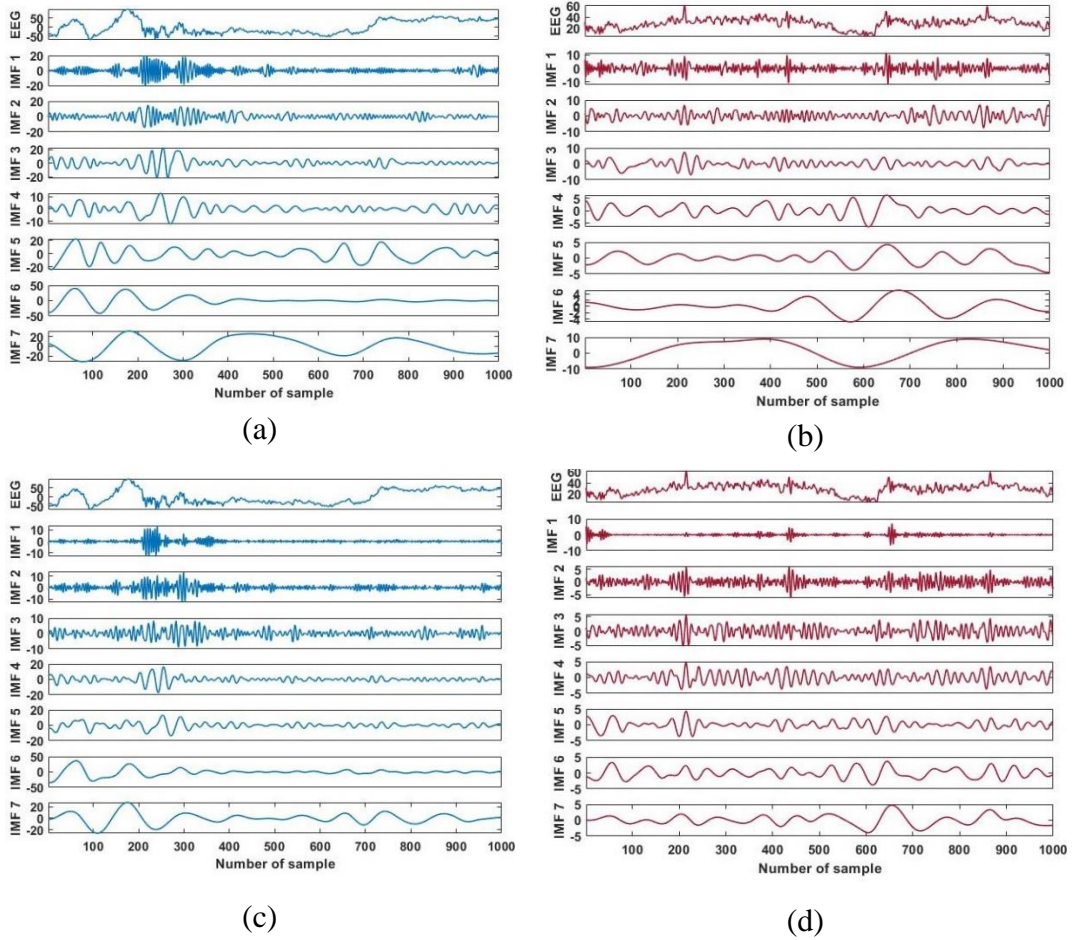
Figure 5.2: (a) Surface EEG signal control subject and its first seven IMFs obtained using EMD, (b) Surface EEG signal of AD patient and its first seven IMFs obtained using EMD, (c) Surface EEG signal control subject and its first seven IMFs obtained using EEMD, (d) Surface EEG signal of AD patient and its first seven IMFs obtained using EEMD.
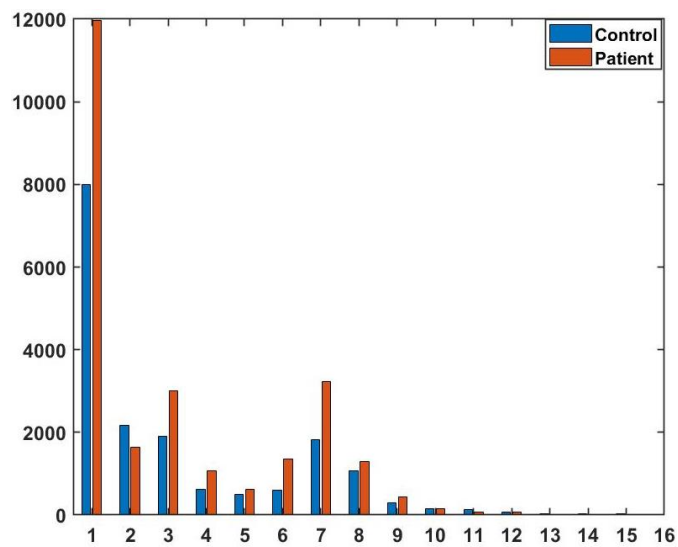
Figure 5.3: Histogram of first priority selected IMFs of EEMD method

5.3.1 Feature Extraction

7 time domain and 5 spectral features are computed for each EEG segment of control subjects and AD patients using the selected IMFs. To compare the performance of EMD and EEMD based classification approaches, DWT based classification approach, which is frequently used for the analysis of non-stationary signals, was also conducted [38, 92]. The discrete wavelet transform decomposes the input signal $X[n]$ into sub-frequency components by preserving the time-frequency resolution. Here, at each decomposition level, the input signal is passed through both high-pass and low-pass filters. The output of these high-pass and low-pass filters are named the detail (DC) and approximation (AC) signals, respectively, and the approximation signal is re-decomposed until the decomposition level is satisfied [92]. Daubechies4 (db4) mother wavelet and 5 level decomposition are used for the proposed study.

5.3.1.1 Time Domain Feature Set

After the IMF election process, using selected IMFs, each subband of DWT, 5 EEG subbands, and EEG segments itself, conventional features, including energy, mean, skewness, and kurtosis values (these formulations are given in Section 4.2.2.1 as equation (4.4)) and Hjorth parameters (activity, mobility, complexity) are extracted. [24, 38, 92].

$$\mu = \frac{1}{N} \sum_{n=0}^{N-1} X[n]$$

$$Activity = var\ (X[n]) = \sigma^2 = \frac{1}{N} \sum_{n=0}^{N-1} (X[n] - \mu)^2$$

$$Mobility = \sqrt{\frac{var(\frac{dX[n]}{dn})}{var(X[n])}}$$

$$Complexity = \frac{Mobility(\frac{dX[n]}{dn})}{Mobility(X[n])}$$

(5.1)

In the above Equations, $X[n]$ indicates the analized signal, N is the size of the signal. μ is the mean value.

5.3.1.2 Spectral Domain Feature Set

Total power, spectral Entropy, 1st, 2nd, and 3rd moments are computed utilizing the spectrum of signals or selected IMFs calculated by the periodogram method [26, 62] to achieve the spectral feature dataset. These formulations are given in Section 4.2.2.2 as Equation (4.5).

5.3.2 Experimental Results

After performing pre-processing stage and removing various noises, by using EMD, and EEMD approaches and multiple classifiers 19-channel EEG signals of 16 AD patients and 11 CS were analyzed. All EEG segments were decomposed into IMFs using EMD and EEMD methods and the hybrid IMF selection process including energy, correlation, power spectral distance, and statistical significance measures was conducted for EMD and EEMD approaches in order to identify the IMFs that satisfied the highest classification performance. Following the IMF selection process, time-domain (Energy, Mean value, Skewness, and Kurtosis, and Hjorth parameters) and spectral-domain (Total power, Spectral Entropy, 1st, 2nd, and 3rd moments) feature sets were generated using the selected seven IMFs (IMF1-7) of EMD and EEMD approaches, approximation and 5 detail coefficients of DWT and itself of the EEG signal. Finally, two classes of CS and early-stage AD were distinguished using four types of classifiers DT, SVM, kNN, and RF.

Tables 5.1 and 5.2 indicate the results of the evaluation of three decomposition methods, the case of no decomposition, and four types of classifiers for time domain and spectral domain feature sets, respectively, for 1min segment duration. Here, while the classification results of the combined feature set of corresponding IMFs (in EMD and EEMD approaches) are indicated with the component of IMFa-IMFb (or IMFa-b), classification results of the combined feature set of approximation and 5 detail

coefficients of DWT are demonstrated with the component of AC+DC1-5. Additionally, results of the case of no decomposition are shown with component of EEG.

From Tables 5.1 and 5.2, it is noticed that for both time-domain and spectral-domain feature sets, the DWT yield the highest performances to distinguish two classes, and the lowest classification performances are achieved using the EMD approach. While the highest classification performance with 84.60% ACC, 87.25% F1-S is obtained from IMF 1-2-3 component of EMD by using DT classifier, the highest classification performance with 92.09% ACC, 93.49% F1-S is obtained from IMF 1-5 component of EEMD by using RF classifier for the time domain feature set (Shown in Table 5.1). In addition, for the spectral domain feature set, IMF 1-7 components of both EMD-based (88.36% ACC, 90.52% F1-S) and EEMD-based (90.31% ACC, 92.06% F1-S) approaches are reached the highest classification performances using the RF classifier (demonstrated in Table 5.2). The fact that the IMF1-7 component of the EMD and EEMD approaches yield better performances in most cases, especially for the spectral feature set, or that the performance does not change much compared to other cases, supports the success of the IMF selection process. Hence, for the rest of the thesis, we used the IMF1 to 7 component of both approaches for the analyses.

Table 5.1: Performance evaluation results (%) of time-domain feature-set for CS and AD EEG classification for 1 min segment duration.

| Method	Component	DT		SVM		kNN		RF	
		ACC	F1-S	ACC	F1-S	ACC	F1-S	ACC	F1-S
EMD	**IMF 1-2-3**	**84.60**	**87.25**	72.64	78.34	**83.90**	**87.04**	**90.12**	**91.95**
	IMF 1-3-7	80.38	83.81	71.19	77.81	73.04	78.40	87.05	89.43
	IMF 1-2-3-7	82.86	85.76	72.32	78.36	76.25	80.91	89.80	91.70
	IMF 1 to 5	82.92	85.77	73.86	79.28	80.76	84.51	89.26	91.24
	IMF 1 to 7	82.54	85.58	**73.20**	**78.97**	75.92	80.84	88.71	90.80
EEMD	**IMF 1-2-3**	84.05	86.72	**88.64**	**91.26**	90.22	92.02	92.08	**93.60**
	IMF 1-3-7	81.79	84.93	81.44	86.22	85.14	87.74	89.15	91.15
	IMF 1-2-3-7	83.63	86.44	83.89	88.07	88.22	90.39	91.55	93.16
	IMF 1 to 5	84.86	87.47	87.53	90.51	**90.60**	**92.30**	**92.09**	93.49
	IMF 1 to 7	**84.33**	**87.01**	83.01	87.54	89.35	91.32	91.24	92.86
DWT	**AC+DC1-5**	93.71	94.92	84.13	87.59	91.09	92.82	**96.51**	**97.14**
EEG	**All EEG**	90.81	91.73	75.37	83.26	85.36	88.35	**91.16**	**92.71**

Table 5.2: Performance evaluation results (%) of spectral-domain feature-set for CS and AD EEG classification for 1 min segment duration.

Method	Component	DT		SVM		kNN		RF	
		ACC	F1-S	ACC	F1-S	ACC	F1-S	ACC	F1-S
EMD	IMF 1-2-3	82.51	85.50	77.48	82.54	78.95	83.01	86.98	89.34
	IMF 1-3-7	80.17	83.64	72.42	79.31	72.25	77.86	84.74	87.54
	IMF 1-2-3-7	**83.08**	**85.97**	77.39	82.63	77.32	81.89	87.97	90.15
	IMF 1 to 5	82.51	85.42	**80.11**	**84.61**	**81.12**	**84.93**	88.12	90.28
	IMF 1 to 7	82.51	85.42	79.53	84.63	78.80	83.28	**88.36**	**90.52**
EEMD	IMF 1-2-3	82.93	85.89	88.43	90.82	88.48	90.66	88.24	90.44
	IMF 1-3-7	80.70	84.01	82.59	86.44	82.15	85.57	86.07	88.64
	IMF 1-2-3-7	82.03	85.01	87.94	90.55	87.02	89.54	88.73	90.63
	IMF 1 to 5	83.83	86.59	**89.23**	**91.53**	**89.38**	**91.37**	89.96	91.80
	IMF 1 to 7	**83.90**	**86.66**	88.90	91.30	88.99	91.08	**90.31**	**92.06**
DWT	AC+DC1-5	91.24	92.77	77.15	82.80	91.91	93.47	**93.35**	**95.66**
EEG	All EEG	88.52	90.25	72.00	80.71	85.77	88.20	**90.09**	**91.72**

For 1 min segment duration, the CS/AD classification accuracy obtained using three different approaches according to different brain clusters for both time domain and spectral domain feature sets are given in Figure 5.4. Here, the classification accuracy obtained using the IMF 1 to 7 component for the EMD and EEMD approaches is evaluated. According to this figure, when all brain clusters and classifiers are considered, both time domain and spectral domain feature sets of the DWT method provided more successful results in distinguishing control subjects and AD patients compared to other methods. In addition, the EMD method is also the most unsuccessful approach in distinguishing between control subjects and AD patients when both feature sets and all brain clusters are considered. For the time-domain feature set, while the highest classification accuracies are obtained using RF classifier for EMD (91.53%) and EEMD (93.90%) approaches from the temporal/right brain cluster, the highest classification accuracy for the DWT (97.40%) approach is obtained from the temporal/left brain cluster using the RF classifier (shown in Figure 5.4a). For the spectral domain feature set, it is also noticed that the best classification performances are obtained by DWT and RF classifier with an ACC of 95.23% from the temporal/right brain cluster. This is followed by EEMD and EMD approaches, using the same classifier with classification accuracies of 93.20 and 91.40, respectively from the same brain cluster (shown in Figure 5.4b).
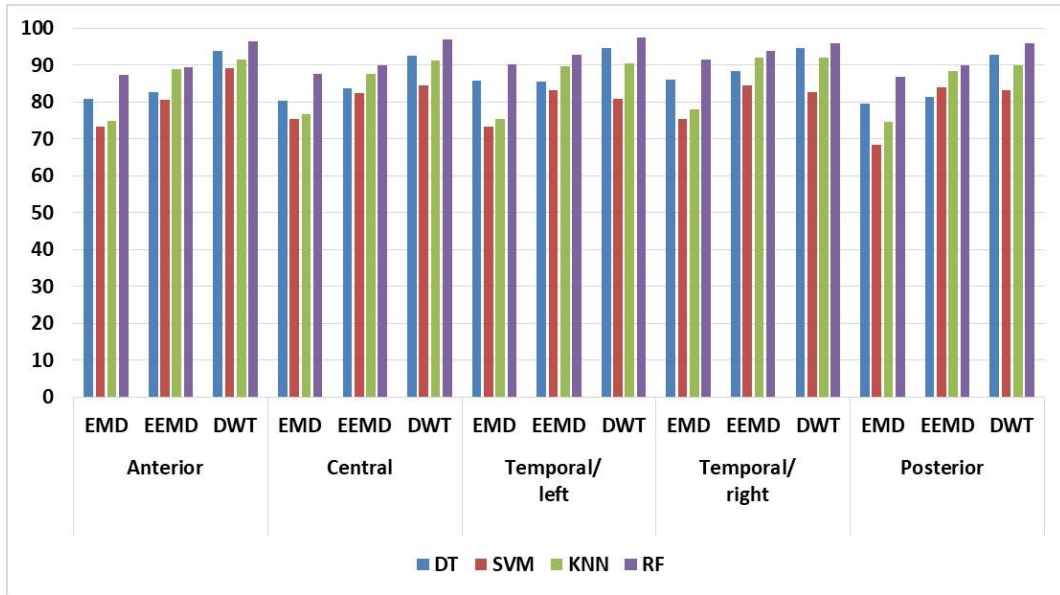
(a)
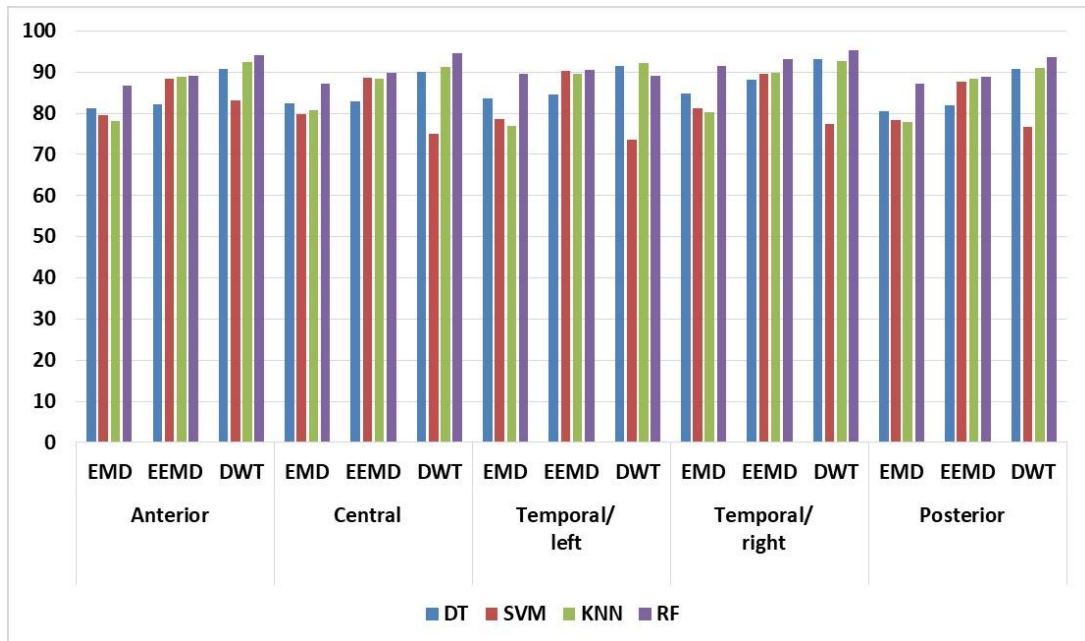
(b)

Figure 5.4: The CS/AD classification accuracy for different classifiers and different brain clusters obtained using (a) time-domain feature set, and (b) spectral-domain feature set.

In order to reveal the effect of the segment duration on the classification performance, the same processes are carried out for the 5s segment duration. Tables 5.3 and 5.4 present the performance evaluation results of the various classifiers based on different brain clusters and approaches for 5s segment duration. Accuracy and F1-score values

are presented in these tables as performance metrics. While Table 5.3 shows the performance evaluation results achieved using time-domain feature sets of proposed approaches, Table 5.4 exposes the performance evaluation results obtained utilizing the spectral-domain feature set of those approaches. It is noteworthy in both tables that the decrease in segment duration reduces the success of distinguishing EEG segments of AD patients and control subjects. In addition, the highest classification performances are obtained from the temporal/right brain cluster with the RF classifier for both feature sets. The highest classification performance for the time-domain feature set with 93.33% ACC, and 94.63% F1-S, is obtained by the DWT approach using the RF classifier (given in Table 5.3). In addition, the highest classification performance with 92.10% ACC and 93.61% F1-S for the spectral domain feature set is obtained by the DWT method (given in Table 5.4). After the DWT approach, the second most successful performance is obtained using the EEMD method with 91.40% ACC for the time-domain feature set and 89.20% ACC for the spectral domain feature set.

Table 5.3: Performance evaluation results (%) of time-domain feature-set for CS and AD EEG classification for 5s segment duration

| Brain Cluster	Method	DT		SVM		kNN		RF	
		ACC	F1-S	ACC	F1-S	ACC	F1-S	ACC	F1-S
Anterior	EEG	85.06	87.38	80.02	84.85	84.14	86.90	**86.58**	**87.55**
	EMD	75.32	78.86	64.92	72.61	62.92	67.36	**81.76**	**84.41**
	EEMD	80.18	82.92	72.82	76.55	76.76	79.25	**87.08**	**88.71**
	DWT	88.42	89.86	82.32	85.54	80.08	82.90	**93.04**	**93.96**
Central	EEG	83.67	87.43	72.83	81.73	81.07	85.80	**86.50**	**89.58**
	EMD	75.93	81.32	68.80	78.15	67.07	75.16	**81.93**	**86.09**
	EEMD	81.00	85.14	72.53	79.89	76.63	81.84	**87.23**	**89.98**
	DWT	85.70	88.89	75.20	82.64	78.87	84.15	**91.10**	**93.10**
Temporal/ Left	EEG	87.57	89.45	64.23	75.93	85.20	87.85	**88.17**	**89.68**
	EMD	78.13	82.14	67.90	75.65	66.97	73.74	**85.83**	**88.59**
	EEMD	82.40	85.08	76.17	80.23	79.63	82.46	**89.00**	**90.71**
	DWT	89.00	90.60	73.60	78.90	80.27	83.73	**93.33**	**94.31**
Temporal/ Right	EEG	85.80	88.58	71.53	80.38	80.53	84.27	**88.60**	**90.91**
	EMD	80.00	83.84	69.57	76.73	69.40	75.09	**86.33**	**88.98**
	EEMD	84.97	87.45	78.63	81.88	82.37	84.83	**91.40**	**92.82**
	DWT	88.80	90.88	78.23	82.70	82.13	85.23	**93.33**	**94.63**
Posterior	EEG	85.58	88.09	72.80	80.30	81.94	85.14	**86.36**	**88.28**
	EMD	75.94	80.04	64.72	73.32	68.66	73.51	**82.42**	**85.61**
	EEMD	81.02	83.96	73.30	77.55	77.36	80.24	**87.94**	**89.80**
	DWT	86.48	88.67	75.54	80.49	78.96	82.34	**91.96**	**93.33**

Table 5.4: Performance evaluation results (%) of spectral-domain feature-set for CS and AD EEG classification for 5s segment duration

Brain Cluster	Method	DT		SVM		kNN		RF	
		ACC	F1-S	ACC	F1-S	ACC	F1-S	ACC	F1-S
Anterior	**EEG**	82.96	85.94	71.30	78.14	78.16	83.53	**83.72**	**86.34**
	EMD	73.46	76.91	63.84	73.77	64.62	70.74	**79.44**	**82.24**
	EEMD	78.84	81.79	70.42	75.95	80.92	83.41	**85.36**	**87.23**
	DWT	87.52	89.19	75.68	80.39	79.40	82.71	**91.50**	**92.67**
Central	**EEG**	81.90	84.76	64.63	76.11	81.03	84.05	**83.10**	**85.57**
	EMD	74.23	80.15	66.17	78.26	68.27	76.64	**79.93**	**84.43**
	EEMD	80.47	84.79	70.93	79.66	78.80	83.81	**85.87**	**88.95**
	DWT	85.60	88.77	69.83	79.50	77.57	83.34	**89.93**	**92.21**
Temporal/ Left	**EEG**	85.40	87.19	66.30	76.09	85.67	87.87	**86.77**	**88.34**
	EMD	77.67	81.76	62.80	75.66	66.97	74.11	**84.03**	**86.92**
	EEMD	82.83	85.65	72.33	77.79	80.37	83.70	**87.90**	**89.71**
	DWT	89.53	91.13	64.67	75.35	76.63	81.17	**92.60**	**93.76**
Temporal/ Right	**EEG**	86.17	88.14	70.90	76.32	84.23	86.49	**87.90**	**89.61**
	EMD	78.90	82.75	65.57	76.84	66.50	73.29	**84.00**	**86.90**
	EEMD	84.27	86.90	72.93	77.55	85.40	87.71	**89.20**	**90.98**
	DWT	88.30	90.55	73.57	79.74	82.00	84.95	**92.10**	**93.61**
Posterior	**EEG**	84.08	86.44	63.78	72.82	83.00	85.59	**85.38**	**87.52**
	EMD	75.30	79.36	61.72	74.14	65.56	71.91	**80.82**	**82.80**
	EEMD	80.34	83.33	71.78	77.47	80.26	83.36	**86.38**	**88.45**
	DWT	86.50	88.62	67.30	76.50	77.06	81.08	**90.56**	**92.13**

For 1 min segments duration, the variation of the average sensitivity and false discovery rate obtained by calculating the average of the SEN and FDR values obtained from the classifiers according to the approaches and brain clusters is given in Figure 5.5 (5.5 (a) for the time-domain feature set and (b) for the spectral-domain feature set.). Here, while sensitivity indicates the ratio of accurately detected AD segment to the total AD segment, the false discovery rate denotes the ratio of CS segments mistakenly classified as AD to the number of all segments classified in AD class. Obtaining low FDR values along with high SEN values reveals the success of the classification. It is noteworthy that high SEN and low FDR values are obtained by DWT and EEMD methods for each brain cluster. Additionally, the DWT method yields the highest SEN and lowest FDR values for both time domain and spectral domain feature sets. However, the EMD method has been more unsuccessful when compared to the method in which the EEG signals themselves are used without applying any decompositions. Moreover, when the classification successes in all brain clusters are considered, the classification successes performed with time-domain feature sets are higher (given in Figure 5.5(a)).
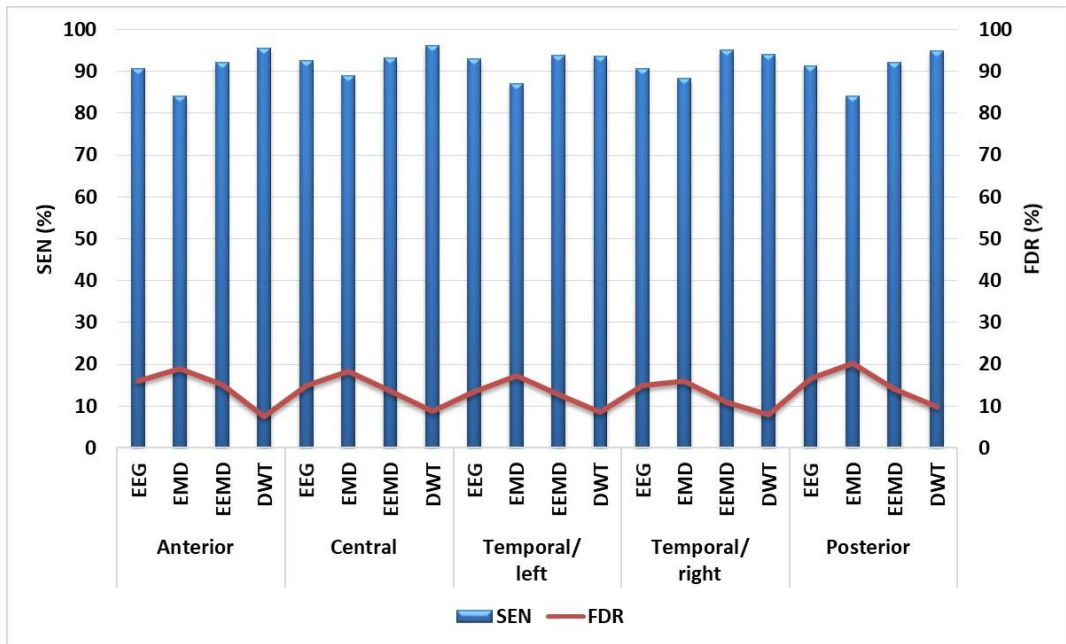
(a)
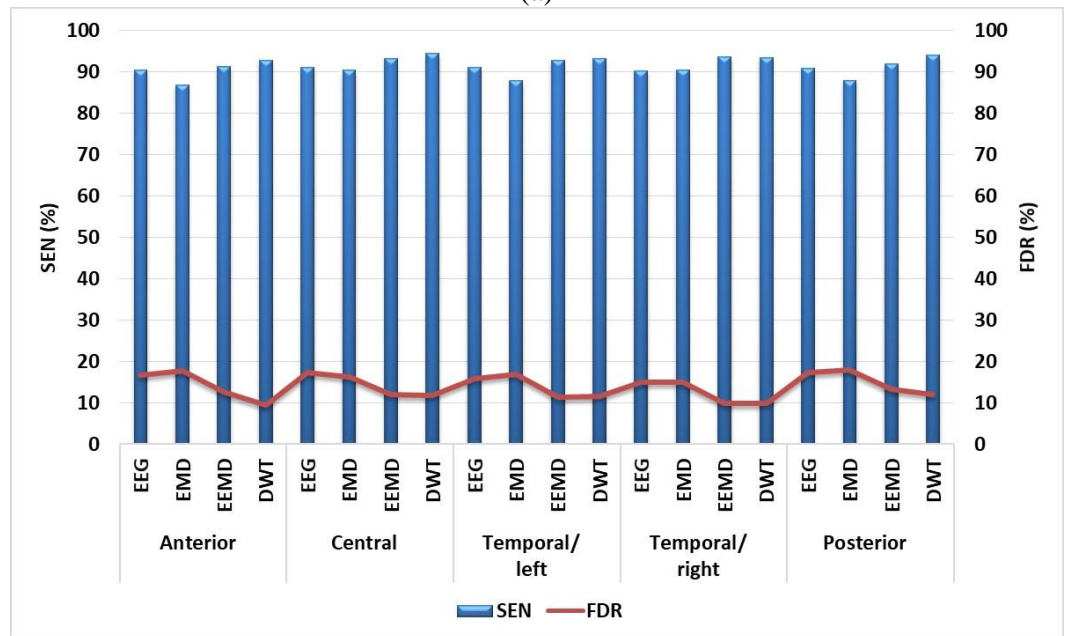
(b)

Figure 5.5: Comparison of average sensitivity and false discovery rate values obtained using different approaches and brain clusters; for (a) time-domain feature set and (b) spectral-domain feature set.

5.4 Results and Discussions of SST Methods

In this section, the time-frequency representation-based feature extraction and classification model to distinguish EEG segments of control subjects and AD patients is introduced. TF representations of EEG segments are achieved using nowel SST and conventional STFT methods. The magnitudes of SST and STFT are used for feature extraction, and 18 different joint TF features are calculated to obtain feature sets. Various classifiers are performed to classify the features extracted utilizing SST and STFT to distinguish the EEG segments of control subjects and AD patients.

Two approaches are proposed for feature extraction using TF representations. (i) TF representations of all EEG subbands are used for feature calculation separately, as previous studies have shown that there are distinctive differences in the EEG signals of control subjects and AD patients in the low-frequency EEG subbands. (ii) Secondly, TF representations containing all EEG subbands are used for feature extraction.

Examples of TF representations obtained for the 5s EEG segment duration of a control subject and AD patient using the SST and STFT methods described in detail in Section 3.1.3 are given in Figure 5.6. The TF representations of the EEG subbands are given in Figures 5.7 and 5.8 as an example for 5s segment duration of AD patients.
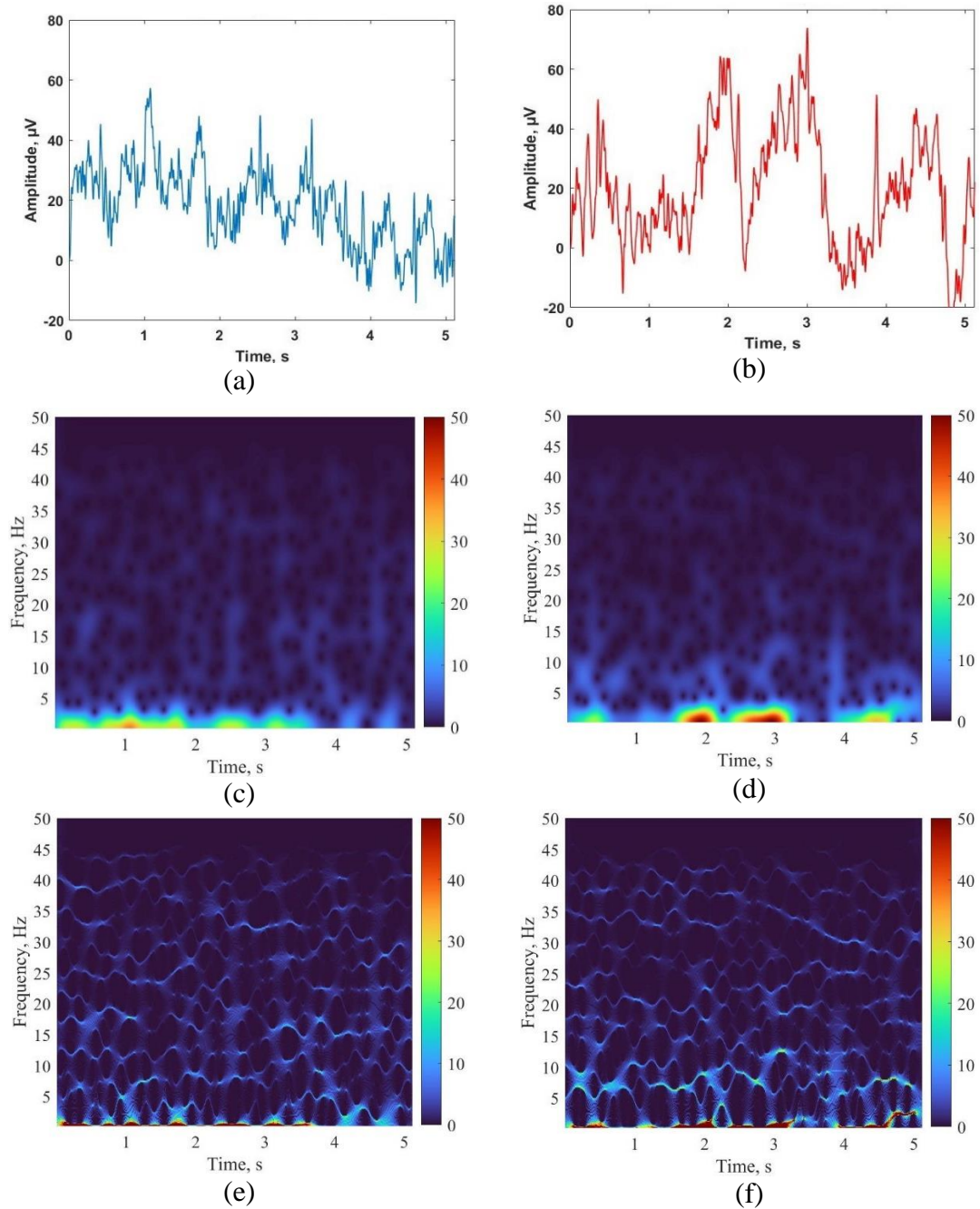
Figure 5.6: 5s duration EEG segments, (a) control subject, (b) AD patient; magnitude STFT of (c) control subject EEG segment, (d) AD patient EEG segment; magnitude SST of (e) control subject EEG segment, (f) AD patient EEG segment.
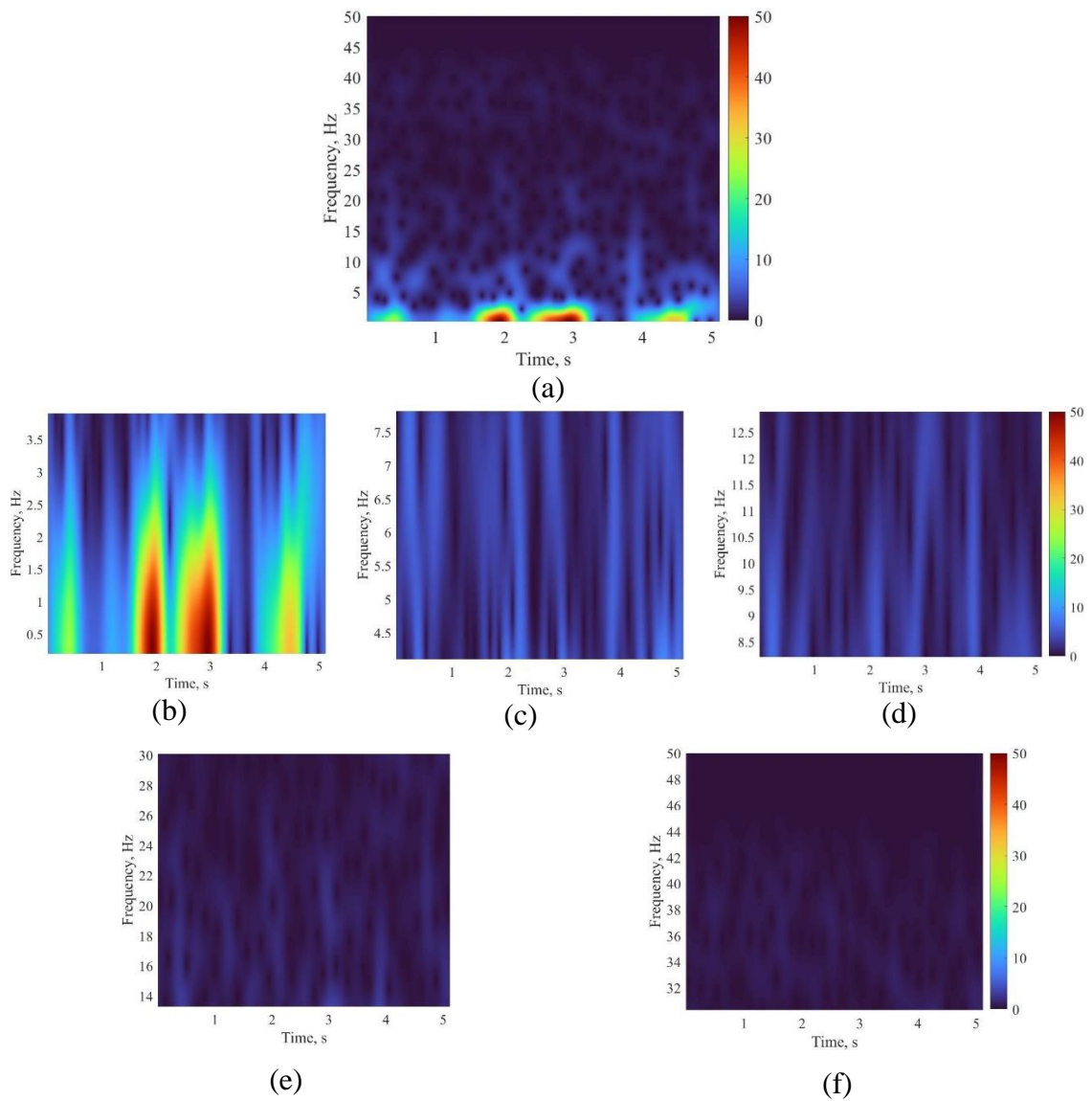
Figure 5.7: For 5s. Segment duration of AD patient EEG, magnitude STFT of (a) all EEG, (b) Delta EEG subband, (c) Theta EEG subband, (d) Alpha EEG subband, (e) Beta EEG subband, and (f) Gamma EEG subband.
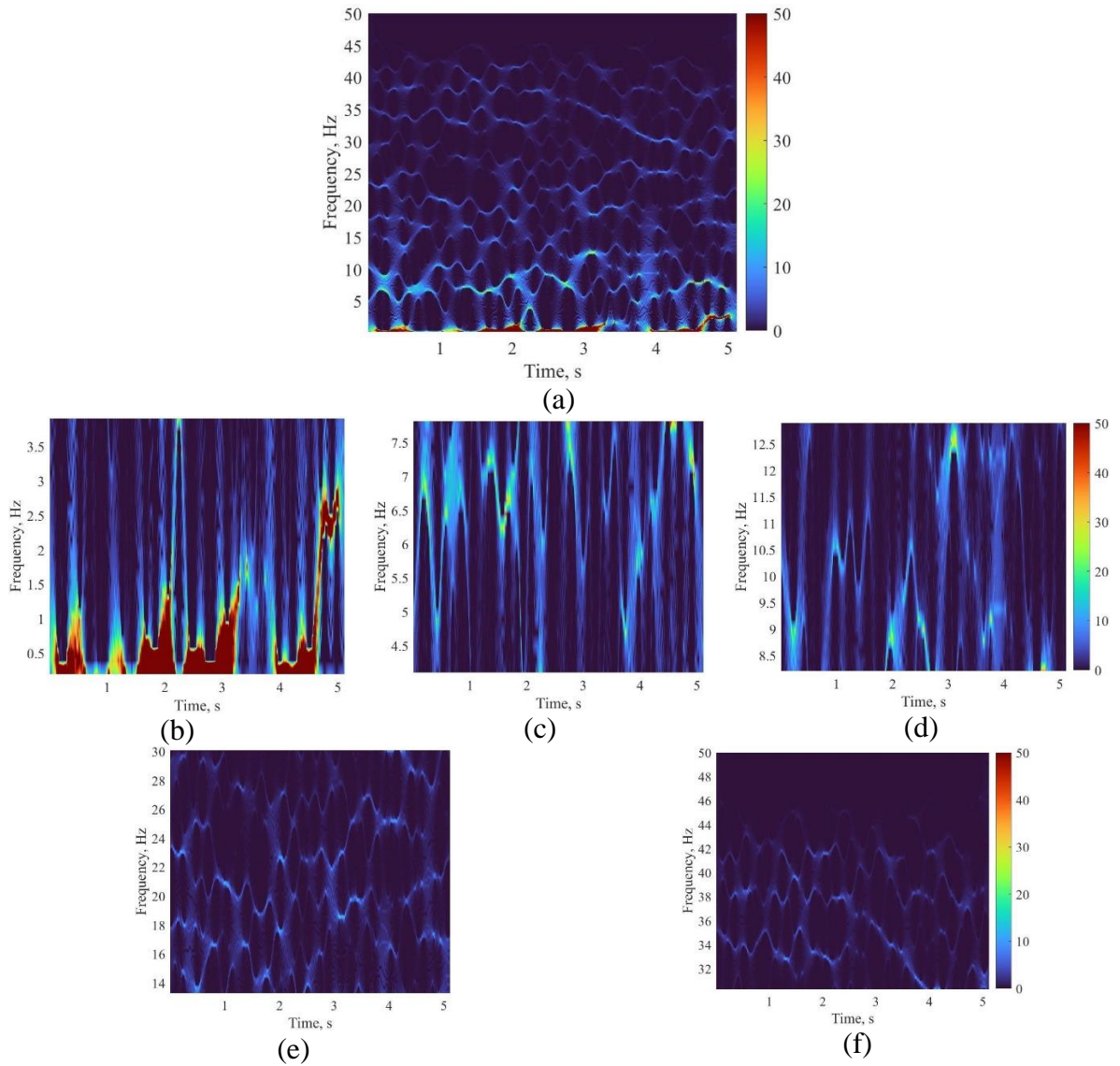
Figure 5.8: For 5s. Segment duration of AD patient EEG, magnitude SST of (a) all EEG, (b) Delta EEG subband, (c) Theta EEG subband, (d) Alpha EEG subband, (e) Beta EEG subband, and (f) Gamma EEG subband.

5.4.1   Feature Extraction

In this study, joint TF features-based feature sets are generated from joint TF density estimates obtained by STFT and SST methods. In the STFT calculations, a Gaussian window is used with a 50% overlap.

Only time or only frequency domain features or their combination have limited performance, because of non-stationary properties of EEG signals. Therefore, TF based features that is the extending versions of time-only or frequency-only features [23], are extracted using obtained TFRs. In our proposed study, we calculated 18 different TF-based features.

1. Time-frequency flux:

$$TF_{flux} = \sum_{n=1}^{N-l} \sum_{m}^{M-k} |S(n+l, m+k) - S(n,m)| \qquad (5.2)$$

Here, $S(n,m)$ is the density obtained by the magnitude square of the SST and STFT, l and m determine the direction of signal energy in the TF domain. In this study, the three TF flux directions considered are the t axis using ($l = 0; m = 1$) called F1, the f axis using ($l = 1; m = 0$) called F2, and the diagonal axis ($l = 1; m = 1$) called F3.

2. Time-frequency flatness

$$F_4 = NM \frac{\prod_{n=1}^{N} \prod_{m=1}^{M} |S(n,m)|^{\frac{1}{NM}}}{\sum_{n=1}^{N} \sum_{m=1}^{M} S(n,m)} \qquad (5.3)$$

Here, if there is a single zero value in TF distribution TF flatness is calculate as zero. So, in practical implementations, all zeros of a TFD are replaced by very small values (for this study we replaced zeros with epsilon).

3. Time-frequency energy concentration measure

$$F_5 = (\sum_{n=1}^{N-l} \sum_{m}^{M-k} |S(n,m)|^{1/2})^2 \qquad (5.4)$$

4. Time-frequency entropy

- Normalized Renyi entropy

$$F_6 = -\frac{1}{2}\log_2\left(\sum_{n=1}^{N}\sum_{m=1}^{M}\left(\frac{S(n,m)}{\sum_{n=1}^{N}\sum_{m=1}^{M}S(n,m)}\right)^3\right) \qquad (5.5)$$

- Shannon entropy

$$F_7 = -\sum_{n=1}^{N}\sum_{m=1}^{M}\frac{S(n,m)}{\sum_{n=1}^{N}\sum_{m=1}^{M}S(n,m)}\log_2\left(\frac{S(n,m)}{\sum_{n=1}^{N}\sum_{m=1}^{M}S(n,m)}\right) \qquad (5.6)$$

5. The statistical features

$$Mean = F_8 = \mu = \frac{1}{NM}\sum_{n=1}^{N}\sum_{m=1}^{M}S(n,m)$$

$$Standard\ deviation = F_9 = \sigma^2 = \sqrt{\frac{1}{NM}\sum_{n=1}^{N}\sum_{m=1}^{M}(S(n,m)-\mu)^2}$$

$$Skewness = F_{10} = \frac{1}{NM\sigma^3}\sum_{n=1}^{N}\sum_{m=1}^{M}(S(n,m)-\mu)^3$$

$$(5.7)$$

$$Kurtosis = F_{11} = \frac{1}{NM\sigma^4}\sum_{n=1}^{N}\sum_{m=1}^{M}(S(n,m)-\mu)^4$$

$$Coefficient\ of\ variation = F_{12} = \frac{\sigma}{\mu}$$

$$Median\ absolute\ deviation = F_{13} = \frac{1}{NM}\sum_{n=1}^{N}\sum_{m=1}^{M}|S(n,m)-\mu|$$

6. TF subband energies

$$F_{14} = TF_\delta = \sum_{n=1}^{N} \sum_{m=1}^{M_\delta} S(n,m)$$

$$F_{15} = TF_\theta = \sum_{n=1}^{N} \sum_{m=M_\delta+1}^{M_\theta} S(n,m)$$

$$F_{16} = TF_\alpha = \sum_{n=1}^{N} \sum_{m=M_\theta+1}^{M_\alpha} S(n,m) \tag{5.8}$$

$$F_{17} = TF_\beta = \sum_{n=1}^{N} \sum_{m=M_\alpha+1}^{M_\beta} S(n,m)$$

$$F_{18} = TF_\gamma = \sum_{n=1}^{N} \sum_{m=M_\beta+1}^{M} S(n,m)$$

Here, frequency subset TF_δ contains frequency values corresponding to δ sub-band frequencies $(f_k \in [0-4]\text{ Hz})$ of the EEG, TF_θ contains frequency samples corresponding to θ sub-band frequencies $(f_k \in [4-8]\text{ Hz})$ of the EEG, etc. Hence 5 subband power features for $\delta\text{: }[0-4]$ Hz, $\theta\text{: }[4-8]$ Hz, $\alpha\text{: }[8-13]$ Hz, $\beta\text{: }[13-30]$ Hz, and $\gamma\text{: }[30-50]$ Hz bands are obtained considering the sampling frequency of 200 Hz

5.4.2 Experimental Results

In this section, SST and STFT based TFR approaches are proposed to obtain distinctive information between control subject and AD patient EEG segments. EEG data recorded from 19 different channels from 15 AD patient and 11 control subjects, are examined. 5s duration EEG segments are obtained from these EEG signals separately, and time-frequency representations are obtained for each EEG segment using both STFT and SST approaches. Using the TF representations joint TF features are

computed. In our simulations, 18 different Joint TF features are calculated using estimated TFR and 1×18 joint TF feature vector is obtained for each EEG segment.
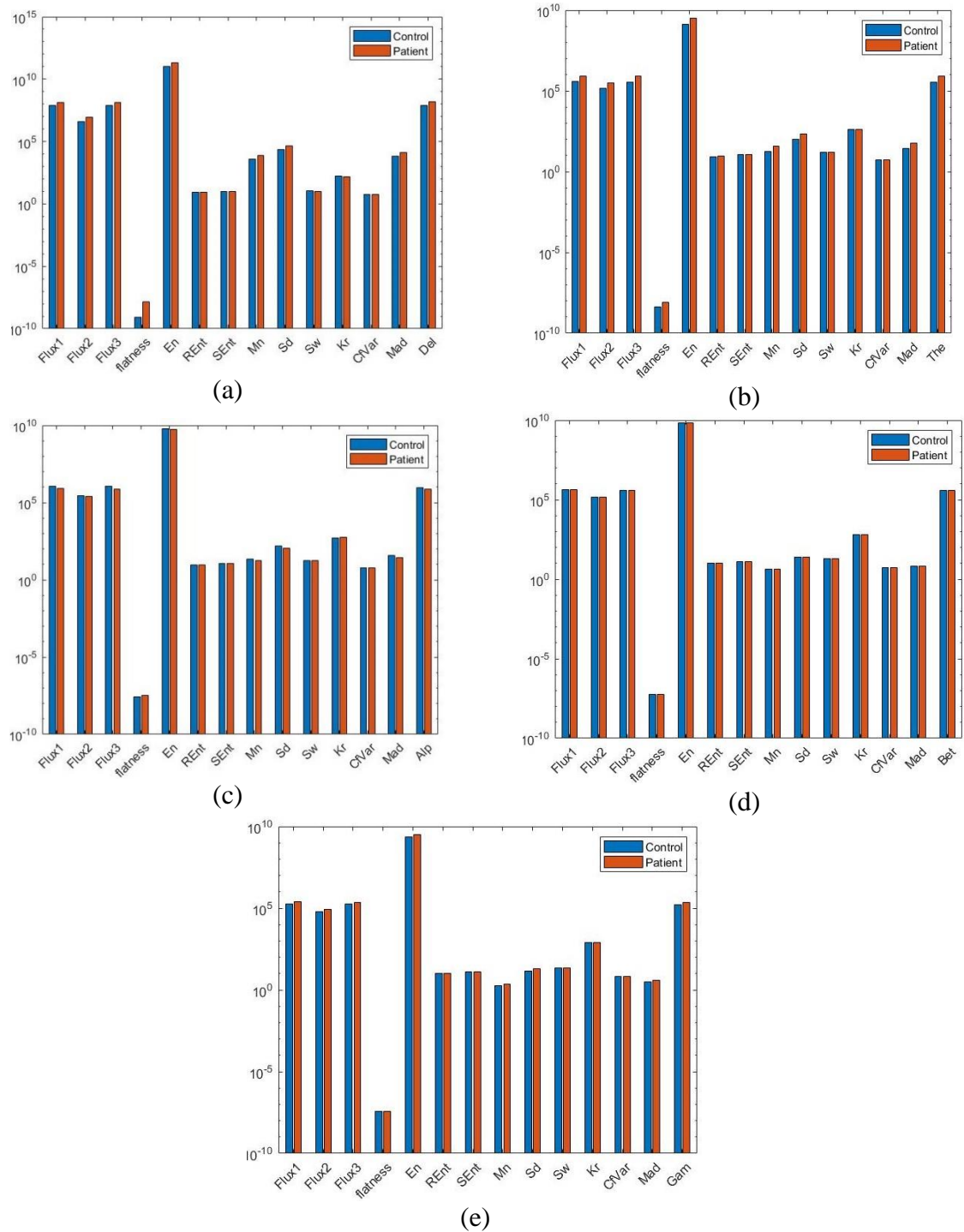
Figure 5.9: Variation of joint TF features in EEG subbands for control subjects and AD patients; for (a) Delta subband, (b) Theta subband, (c) Alpha subband, (d) Beta subband, and (e) Gamma subband.

First, joint TF features are calculated by using TF representations obtained from EEG subbands separately, and classification performances are evaluated using 4 different classifiers and 10-fold cross-validation. The variation of the obtained features in each EEG subband according to the control subjects and AD patients is shown in Figure 5.9 by calculating the average of the calculated features of SST based approach. Here, it is noteworthy that there is a more distinct difference between the features obtained from the EEG segments of control subjects and AD patients in the low-frequency delta and theta EEG subbands compared to the other subbands.

(a)

(b)

(c)

(d)

(e)
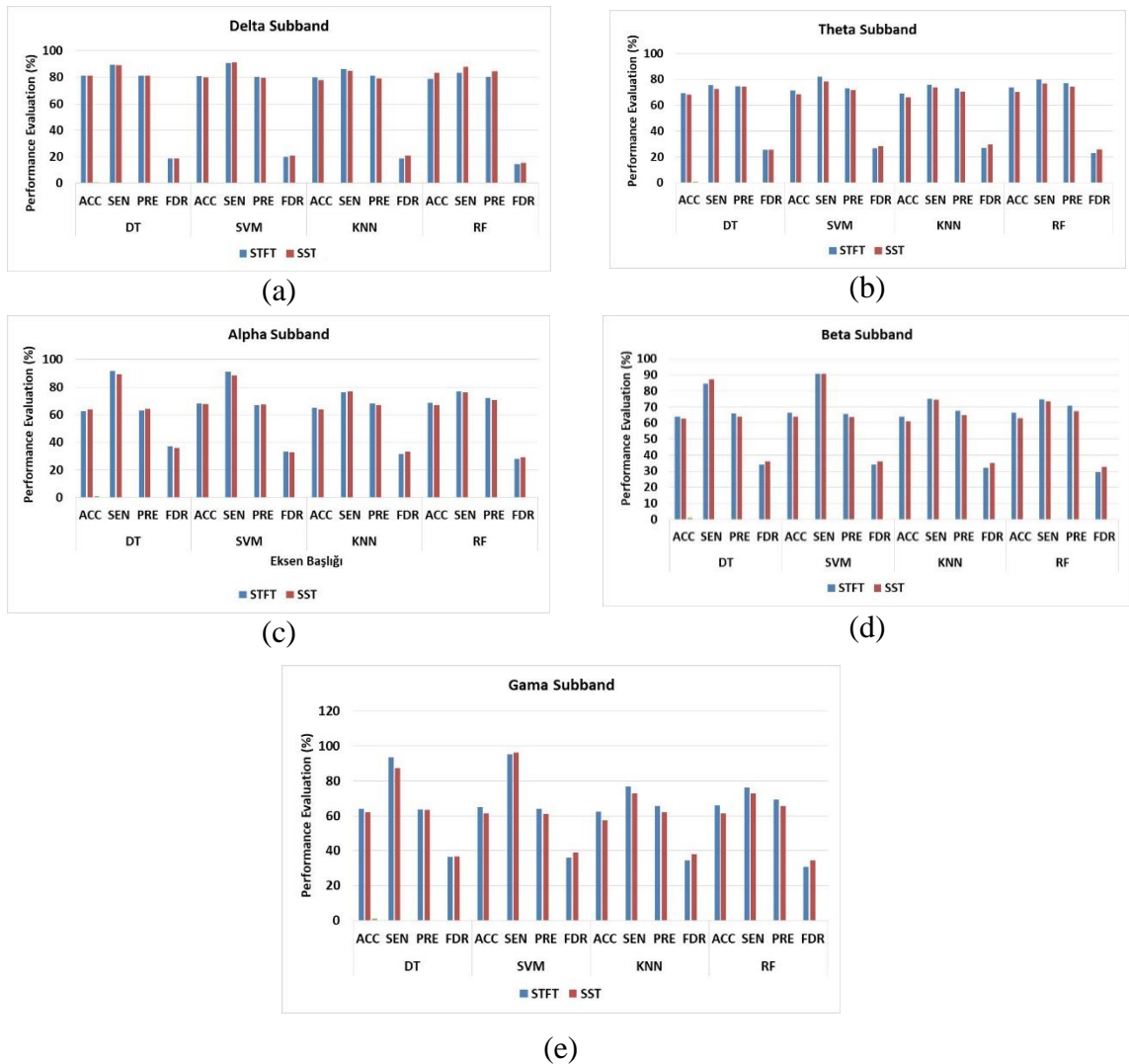
Figure 5.10: Performance evaluation results of SST and STFT based control subject and AD patients' EEG segment distinguish for different EEG subband; (a) Delta subband, (b) Theta subband, (c) Alpha subband, (d) Beta subband, and (e) Gamma subband

129

Performance evaluation for SST and STFT based approaches using ACC, SEN, PRE, and FDR performance matrices are performed utilizing the features calculated for each EEG subband and the results are given in Figure 5.10. In Figure 5.10, no significant difference is observed between the classification accuracies obtained with the SST and STFT approaches. Also, when all classifiers are considered, the highest classification performances are obtained for the delta subband. In this subband, the ACC is greater than 80% and SEN is greater than 85% for both approaches and all classifiers. Classification performance decreased for both approaches in Alpha, Beta and Gamma subbands containing high frequency information.

Table 5.5: Brain cluster based classification results of SST and STFT based approaches for the delta subband

| Brain Cluster	Method	DT		SVM		kNN		RF	
		ACC	F1-S	ACC	F1-S	ACC	F1-S	ACC	F1-S
Anterior	STFT	81.96	85.96	81.70	86.02	78.84	82.61	**83.12**	**86.15**
	SST	82.40	86.31	80.74	85.29	77.04	81.19	**83.08**	**86.11**
Central	STFT	78.67	83.24	76.77	83.13	76.07	81.53	**79.60**	**83.70**
	SST	77.90	82.61	75.97	82.82	74.43	80.49	**79.83**	**83.94**
Temporal/ Left	STFT	83.20	86.61	83.60	86.63	81.80	85.35	**86.60**	**88.81**
	SST	84.00	87.30	81.87	85.58	80.03	84.02	**86.37**	**88.64**
Temporal/ Right	STFT	81.87	85.37	82.60	85.63	81.40	84.21	**85.07**	**87.45**
	SST	79.67	83.25	83.03	85.88	81.23	84.03	**85.20**	**87.55**
Posterior	STFT	81.30	85.09	81.10	85.35	79.46	83.59	**82.88**	**85.93**
	SST	80.80	84.88	79.54	84.58	77.04	81.72	**82.60**	**85.73**

Also, since the highest classification performance is obtained from the delta subband, the brain cluster-based classification results are given in Table 5.5 for this EEG subband and both approaches. The highest classification performances for both approaches are obtained using RF classifier from temporal/left brain clusters (STFT: 86.60% ACC, 88.81% F1-S; SST: 86.37% ACC, 88.64% F1-S). In addition, no significant performance difference is observed between the methods when all brain clusters are taken into account.

In the second part of the study, TF representations obtained using SST and STFT approaches, containing all EEG subbands are used for feature extraction. The classification results of the joint TF features calculated from the obtained TF

representations are shown in Table 5.6. The highest performance to distinguish the EEG segments of control subjects and AD patients was obtained with 94.07% ACC and 95.04 F1-S from Temporal/Left brain cluster using the STFT method and RF classifier.

Table 5. 6: Brain cluster based classification results of SST and STFT based approaches for all

| Brain Cluster	Method	DT		SVM		kNN		RF	
		ACC	F1-S	ACC	F1-S	ACC	F1-S	ACC	F1-S
Anterior	STFT	89.80	91.31	80.02	83.57	81.18	84.56	**93.00**	**94.03**
	SST	88.46	90.40	78.28	82.90	74.46	79.34	**91.42**	**92.83**
Central	STFT	88.57	91.23	79.63	85.34	81.77	86.68	**92.40**	**94.12**
	SST	86.93	89.94	74.77	82.72	74.07	81.38	**90.37**	**92.58**
Temporal/ Left	STFT	91.17	92.67	77.50	82.42	81.83	85.44	**94.07**	**95.04**
	SST	89.90	91.63	74.10	80.03	75.37	80.89	**92.67**	**93.89**
Temporal/ Right	STFT	89.57	91.63	83.73	87.11	84.70	87.95	**93.43**	**94.72**
	SST	88.80	90.16	79.53	83.36	78.97	82.08	**92.23**	**93.23**
Posterior	STFT	88.54	90.63	79.00	83.37	80.34	84.25	**92.26**	**93.58**
	SST	86.94	89.28	75.12	80.81	72.74	78.37	**90.94**	**92.53**
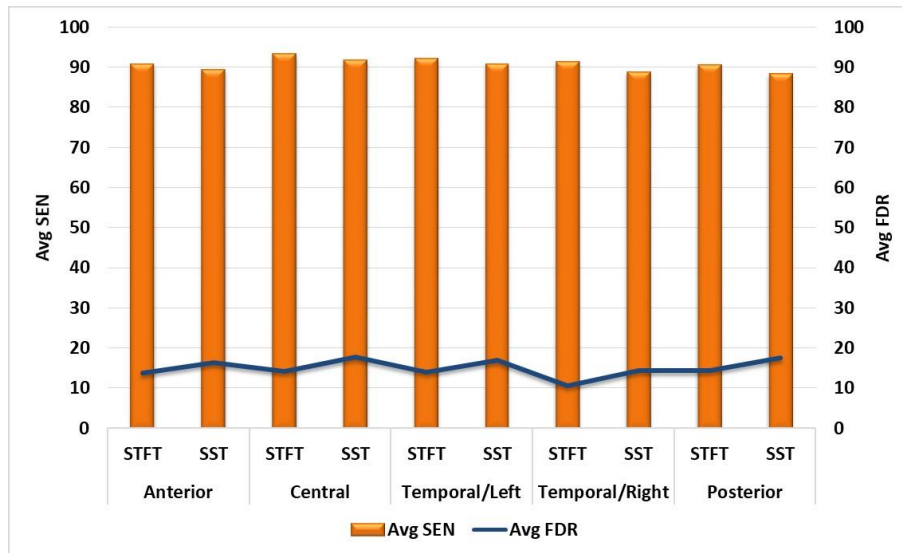
Figure 5.11: Comparison of average sensitivity and false discovery rate values obtained using STFT and SST approaches according to different brain clusters.

Moreover, the variation of the average sensitivity and false discovery rate obtained by calculating the average of the SEN and FDR values obtained from the classifiers according to the approaches and brain clusters is given in Figure 5.11. The highest average SEN and lowest average FDR values (STFT: 93.25% SEN, 14.13% FDR; SST: 91.79% SEN, 17.67% FDR) are obtained from the central brain cluster for both STFT and SST approaches. However, lower FDR values are obtained for the Temporal/Left and Temporal/Right brain clusters. For all brain clusters, the STFT approach provided slightly higher classification performances than the SST approach.

5.5 Comparison of the proposed CS/AD EEG classification approaches

In this part of the thesis, we introduced different approaches and features to obtain discriminative information between EEG segments of AD patients and control subjects. Firstly, performance evaluation is conducted using DWT, which is a classical decomposition method, and EMD and EEMD, which are relatively new decomposition methods, and different feature sets, and the performances of the methods are compared. In order to demonstrate the success of the decomposition methods, the same analyses are carried out using the EEG signal itself without any decomposition. While 5-level decomposition and Daubechies4 (db4) mother wavelet are used for DWT, the IMF selection process is performed for EMD and EEMD methods. Hybrid IMF selection method including energy, correlation coefficient, PSD distance, and t-test-based IMF selection methods suggested for EMD and EEMD methods in our previous studies is also applied for this EEG data set. Time-domain based (energy, mean, skewness, kurtosis, activity, mobility, and complexity) and spectral-domain based features (total power, spectral entropy, 1st, 2nd, and 3rd moments) are computed by using the selected 7 IMFs (IMF1, IMF2, IMF3, IMF4, IMF5, IMF6, and IMF7) of EMD and EEMD methods, and detail and approximation coefficients of DWT method. It was noted that DWT, which is the classical decomposition method, yield more successful results in the problem of distinguishing EEG segments of AD patients and control subjects.

Secondly, the TF representation-based approach has been proposed for distinguishing EEG segments of AD patients and control subjects. Here, the classical TF method STFT and the recently proposed SST method, which provides high-resolution TF representation, are used to obtain the TF representation. It has been observed that time-only and frequency-only features are frequently used with different approaches to distinguish EEG segments of AD patients and control subjects. However, the TF approach and joint TF features have not been found to be used for this problem. In our study, 18 different joint TF features (three TF flux, TF-Flatness, TF energy concentration measure, two TF entropy, six different statistical features, and five TF subband energies) are calculated by using TF representations obtained using SST and STFT methods. STFT, which is the classical TF approach, among the proposed TF representation-based approaches to distinguish EEG segments of AD patients and control subjects, yields relatively more successful results.

All proposed methods for the problem of distinguishing EEG segments of AD patients and control subjects are compared and the results of the comparison are presented in Figures 5.12 and 5.13. Since the highest classifications performances are obtained by using the RF classifier in all proposed methods, the variation of ACC, SEN and FDR values obtained using this classifier according to the methods and different brain clusters are shown in Figure 5.12. Because of the most successful classification performance for DWT, EMD, and EEMD methods are obtained using time-domain features of 5s segment duration, the classification results of this feature set are used for comparison. Using time-domain feature sets of DWT and EEMD approaches, the highest classification performances of 93.33% ACC, 95.40% SEN, 6.13% FDR and 91.40% ACC, 93.75% SEN, 8.07% FDR are obtained from temporal/right brain cluster, respectively. For the EMD and SST approach, the most significant classification performances are obtained from the temporal/left brain cluster with 85.83% ACC, 91.23% SEN, 13.90% FDR, and 92.67% ACC, 95.03% SEN, 7.23% FDR, respectively. However, the most pronounced performance considering all approaches is observed for the STFT approach with 94.07% ACC, 95.90% SEN, 5.80% FDR.
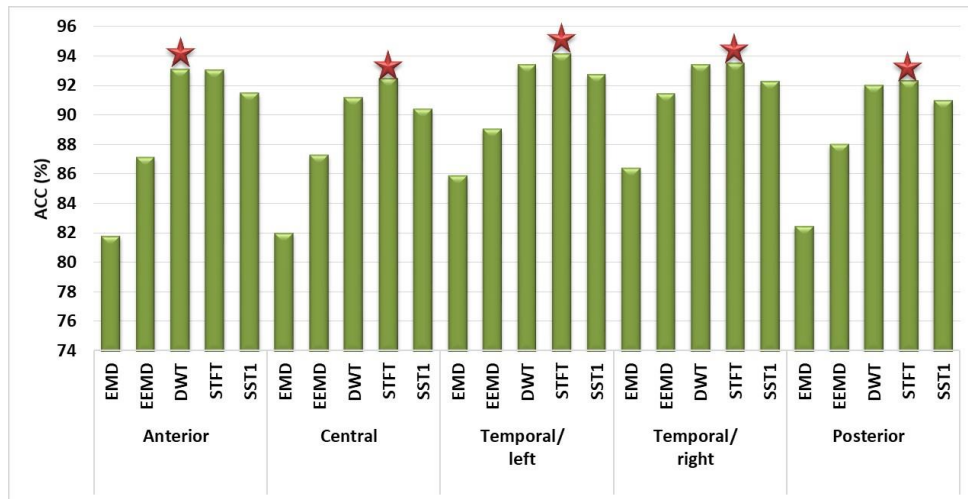
(a)
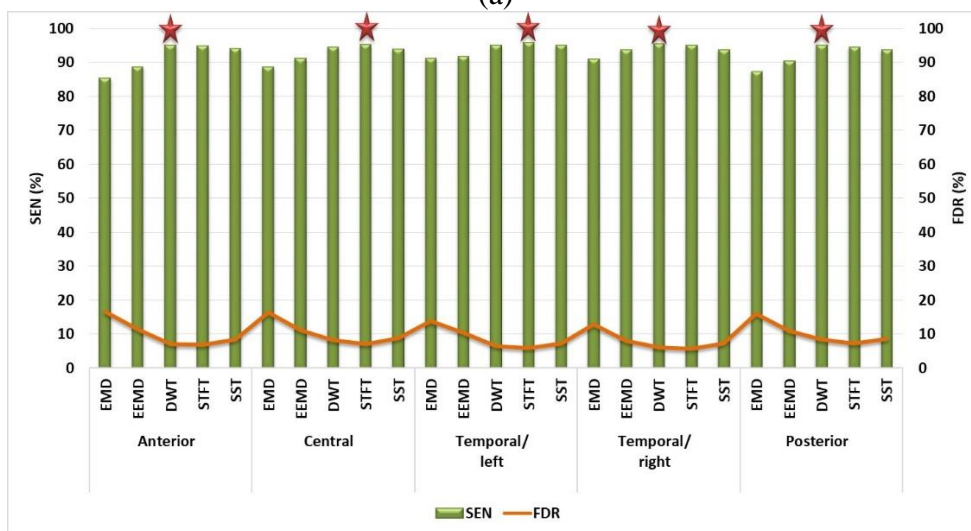
(b)

Figure 5.12: Comparison of sensitivity and false discovery rate values obtained using RF classifier according to all proposed methods and different brain clusters.

In addition, channel-based F1-S values are given on the topography map (shown in Figure 5.13) in order to determine the most successful channel in distinguishing the EEG segments of control subjects and AD patients by conducting channel-based comparisons rather than brain cluster-based comparisons. A single F1-S value is obtained for each channel by calculating the average of the F1-S values obtained from all classifiers for all approaches. Here, in order to create the color ranges, the maximum and minimum F1-S values are obtained by considering the F1-S values obtained from all methods. This maximum and minimum value range is divided into 5 equal parts and one color is assigned for each part.

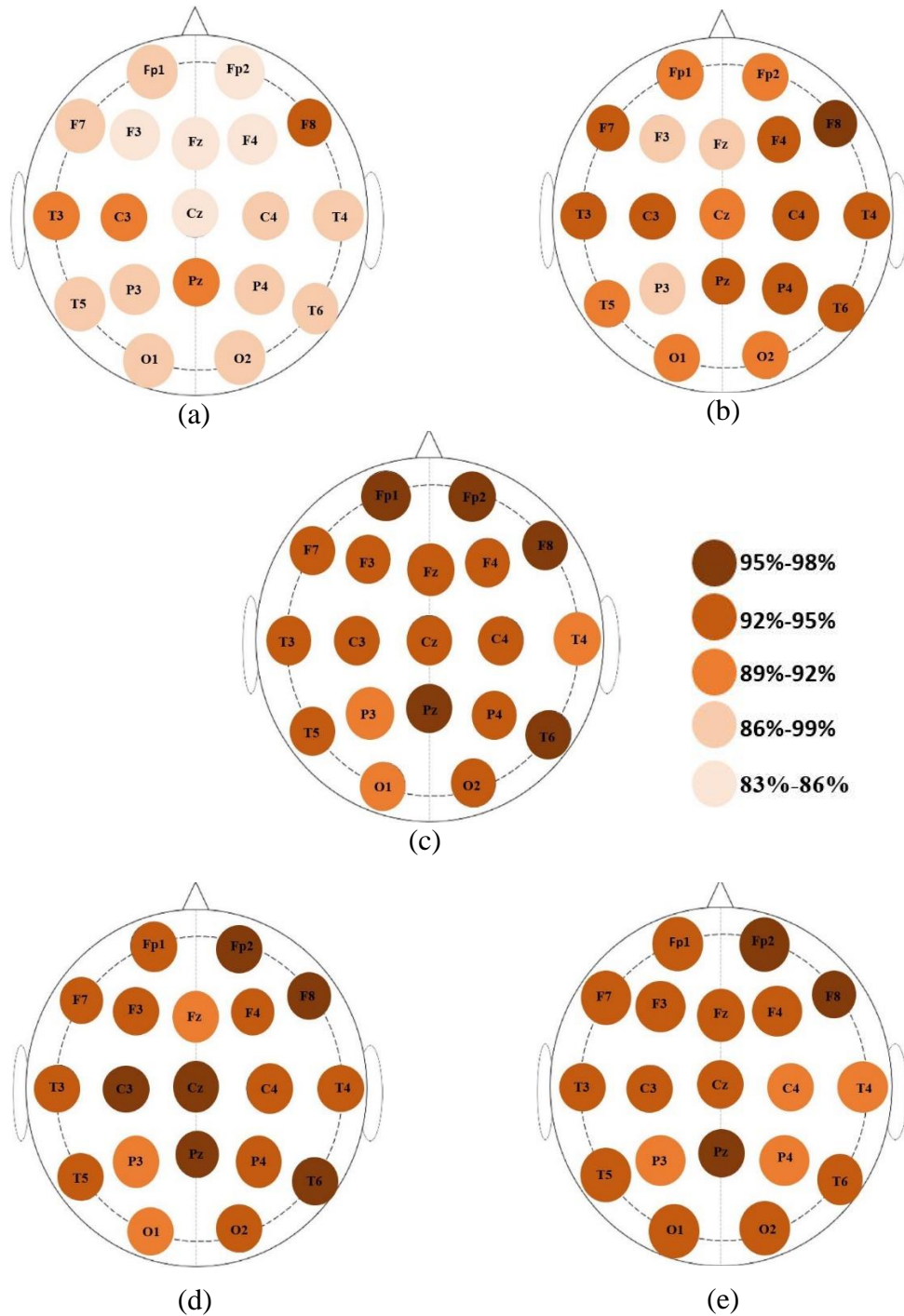Figure 5.13: Topographic map of channel based average F1-S of (a) EMD based (b) EEMD based (c) DWT based (d) STFT based, and (e) SST based approaches.

If this topography map is evaluated (in Figure 5.13), the most successful control subject and AD patient EEG segment classification performances for all methods are obtained from the F8 channel. In addition, the DWT method provided higher channel-

based F1-S values compared to the EMD and EEMD methods. The STFT method, on the other hand, provided higher F1-S values, especially for the channels in the central and temporal/right brain cluster, compared to the SST-based control subject AD patient EEG segment classification approach. Compared to DWT, there is an increase in F1-S values obtained from channels in the central and temporal/right brain clusters using the STFT approach. Therefore, the most successful approach among the proposed control subject AD patient EEG segment discrimination approaches is STFT, which is one of the approaches based on TF representation.

Table 5.7: Performance comparison of control subjects AD patient EEG signal distinguish studies.

Ref.	Classes type	Subjects number	Feature	Performance (%)
[74]	AD/CS	14 AD/ 10 CS	Statistical and Spectral	91.77% ACC
[77]	AD/CS	10 AD/ 8 CS	Approximate Entropy	70%-80% SEN, 75%100%SPE
[79]	Mild AD/ Moderate AD/ CS	20 Mild AD 15 Moderate AD 24 CS	Spectral Power Cherance Phase Synchrony	88.6% ACC, 90.% SEN
[80]	Mild AD/ Moderate AD/ CS	11 Mild AD 10 Moderate AD 11 CS	Amplitude modulation rate of change	90.6 ACC%, 90.5% SEN
[81]	AD/CS	50 AD 50 CS	Wavelet feature Spectral complexity	88%-96% ACC
[83]	CS/AD	79 AD 82 CS	Higuchi fractal dimantion Spectral entropy	66%-77% ACC
[89]	CS/AD	11 AD 11 CS	Lempel-Ziv complexity Central tendency metric	90.9% SEN, 72.7% SPE
[90]	CS/AD	11 AD 11 CS	Lempel-Ziv	77.27%-78.25% ACC
[92]	Mild AD/ Moderate AD/ CS	31 Mild AD 20 Moderate AD 35 CS	DWT and EMD Based features	EMD: 91.35% ACC DWT: 97.64% ACC
[93]	CS/AD	50 AD 50 CS	Spectral feature DWT feature	94% ACC
Proposed Study	**CS/AD**	**15 AD 11 CS**	**EMD** **EEMD** **DWT** **STFT** **SST**	**90.12% ACC** **92.09% ACC** **93.35% ACC** **94.07% ACC** **92.67% ACC**

In addition to comparing the performances of the proposed methods, a comparison is conducted with the success of the studies in the literature to classify the EEG segments of control subjects and AD patients (given in Table 5.7). In Table 5.7, in some studies

[79, 80, 92], both the problem of distinguishing the EEG signals of two-class control subjects and AD patients and the problem of distinguishing EEG signals of three-class control subjects, mild AD and moderate AD patients are evaluated. In other studies [74, 77, 81, 89, 90, 93], only the problem of distinguishing the EEG signals of control subjects and AD patients are studied. When the studies of distinguishing the EEG signals of control subjects and AD patients are evaluated [74, 77, 81, 89, 90, 93], the classification performances obtained within the scope of our study are more prominent. Again, according to the studies of distinguishing three-class control subjects, mild AD and moderate AD EEG signals, the classification performances obtained within the scope of our study are more pronounced [79, 80]. Only in the study [92], higher performance values are presented than our proposed study. However, AD detection performances are given in that study. The problem of separating the EEG signals of moderate AD patients from other groups can provide higher success than other problems. In our study, the problem of distinguishing the EEG signals of mild AD and control subjects is evaluated. The distinction between these data sets is more difficult. Nevertheless, significant classification performances are obtained in our proposed study (STFT: 94.07% ACC, 95.90% SEN, 5.80% FDR).

6. Conclusion

Within the scope of the thesis, various methods have been proposed for disease detection and follow-up with advanced signal processing methods by using EEG signals of two different neurologic disorders, Epilepsy and Alzheimer's dementia, which have a high incidence in the world and seriously affect the quality of life. Due to the ease of recording and low cost, long-term EEG signals can effectively be used to detect neurological disorders. However, monitoring and analysis of long-term EEG recordings by neurologists is very time consuming and exhausting. Therefore, to help neurologists in the high-quality analysis of EEG signals, various signal processing and analysis approaches such as time domain, frequency domain, time-frequency domain, and other advanced methods have been developed [18, 21, 22, 44, 62-65, 120].

Firstly, EMD and derivative, DMD, and SST-based epileptic seizure detection, prediction, and classification approaches are introduced. Two different EEG datasets, IKCU and CHB-MIT, are examined for epilepsy detection, prediction, and classification. There are many studies in the literature for the detection and classification of epileptic seizures. Many studies have been performed in this field by using EMD and derivative approaches used in our study [14, 38, 42, 61-63, 95, 96]. EMD and its extensions (ensemble, multivariate and other) are suitable for the analysis of nonlinear and non-stationary signals such as EEG. In these methods, EEG signals are decomposed into IMFs which are zero–mean oscillations. Determining which of these IMFs contain useful information is vital for the success of the analysis. In most of the previous studies, the first 5 IMFs [95] or first 4 IMFs [32, 61, and 63] have been selected, because they contain high-frequency information. In other words, no IMF selection process was performed in the initial stage of these studies. On the other hand, there are several IMF selection procedures presented in the literature based on energy, correlation coefficient, power spectrum, and statistical significance [14, 111–114]. If the signal to be analyzed contains noise, the energy and correlation coefficient of the

IMFs where the noise component is dominant, will be high and misleading [111]. Therefore, the use of these IMF selection methods alone is not sufficient to determine the appropriate IMFs. In our study, we propose a hybrid IMF selection approach considering energy, correlation, power spectral distance, and statistical significance measures. We explore the advantages of the proposed IMF selection in either EMD or EEMD approaches as opposed to using randomly selected IMFs. In our epileptic EEG classification experiments, the proposed EMD- and EEMD-based approaches outperformed the EEG-based and DWT-based approaches for all classifiers and feature sets we used. The selection algorithm for both EMD and EEMD suggests IMF1, IMF3 and IMF2 in this order. We use these IMFs separately and their combinations for feature extraction and evaluate the classification performance. The classification performance of selected IMFs and their combinations were generally higher than the classification success of randomly selected IMF1–4. It is obvious that in another signal processing problem, the selection algorithm may yield a completely different set of IMFs. Hence the use of first k IMFs in the classification process, as generally done in previous studies, is not the best approach. In our simulations, highest classification accuracies were obtained by using the EEMD approach where the discriminative information about epileptic seizures in the channels may be revealed more clearly (shown in Figure 4.4). Note that, working with 3 or more IMFs increases both the computational load and processing time. It may be concluded that performing an IMF selection procedure before obtaining the features directly affects the success and computational load of the study.

The DMD method presented as a solution to problems encountered in fluid flow studies has recently been applied to neurological signals and successful results have been obtained [58, 97-100]. In this study, we explore the application of DMD method to single-, as well as multi-channel epileptic EEG signals. A new DMD-spectral based approach is presented to distinguish pre-seizure and seizure EEG signals. In the literature, multi-channel EEG data are used for DMD analysis. While simultaneous analysis of multi-channel EEG signals with DMD algorithm provides an advantage in terms of computation time, the effect of EEG channels on classification performance cannot be evaluated. In our study, a single-channel-EEG based DMD approach is presented. We observe that single-channel-based classification performance is higher than multi-channel based classification performances. Hence, it was shown that the

DMD algorithm can successfully be used for data recorded from a single channel as well. On the other hand, the DMD Spectrum and Power Spectral Density are similar. However, while different EEG segments may be analyzed and simultaneously characterized using the DMD algorithm by creating high-dimensional EEG data matrices, these EEG segments must be separately analyzed using the Fourier transform or similar approaches. In our experiment, the Welch Periodogram method using the FT is utilized to estimate the power spectral density for comparative analysis. Additionally, FT calculates the power spectrum at each uniformly placed frequency samples $f_k = \frac{F_s}{N}; k = 0, 1, ..., N - 1,$ N is the number of samples, while DMD spectrum is calculated only for frequency values of the extracted modes of the signal. As such, the DMD spectrum may display more than one power component, or no power at some frequencies. The higher-order DMD spectral moments, and DMD sub-band powers are introduced as novel features of DMD spectrum in this study, and successfully applied for the classification of pre-seizure and seizure EEG signals. On the other hand, in our previous study conducted using the same IKCU data set, and applying EMD, EEMD and DWT methods, we achieved 97.14%, 98.13%, and 94.56% accuracy values respectively. However, as discussed in that study, EMD and EEMD approaches have the disadvantage of computational complexity over DWT method. The computational complexity of EMD is $O(N_s L N_x)$ where N_s is the number of shifting iterations to extract each intrinsic mode function (IMF), L denotes the number of IMFs, N_x is the length of the signal, and $O(.)$ shows the order of computation. This complexity is multiplied by the number of ensembles N_e in EEMD [115, 125] making EMD and its variants computationally expensive iterative methods. The single channel based DMD proposed by us, which clearly has the computational advantages, resulted 96.7% classification accuracy. The computational complexity of the DMD algorithm is reported as $O(KNM)$, where K is the number of modes, N and M are the dimensions of the data matrix [126]. Thus, the above encouraging classification results together with the computational advantages, indicate that the proposed DMD method may be applied to the analysis of univariate signals such as single EEG channels and other non-stationary signals.

In the literature, quite large amount of studies have been presented for epileptic seizure detection and classification using TF analysis methods. The proposed method

provides an alternative to those methods with successful results obtained on two different data sets. A high-resolution TF method called SST is utilized to define a classification scheme for epileptic EEG signals. For the proposed machine learning based SST approach, novel features, i.e., HOJ-TF moments and GLCM based features are extracted using the SST representation. The proposed method is applied to classify pre-seizure and seizure EEG segments in the IKCU data set, and to detect seizures in the CHB-MIT data set. Classification performances of the proposed approach using various classifiers are evaluated by means of statistical metrics. Same experiments are performed using the STFT of EEG segments to compare the performance of our proposed method. For the IKCU data set, using the HOJ-TF-moment based feature set, higher classification performance is achieved in the SST approach than that of the STFT for both left and right hemispheres. In addition, the classification accuracies in both hemispheres are increased at 5s segment duration over 1s for both approaches (shown in Tables 4.13, 4.14). While the SST approach reaches higher classification performance in both hemispheres for the GLCM feature set with 1s segment duration; for the same feature set with 5s segment duration, the classification accuracies of both approaches are very close (Shown in Tables 4.15 and 4.16). Moreover, using both HOJ-TF-moment-based and GLCM based feature sets, higher precision and recall values for each classifier are achieved in the SST approach of the 1s segment duration (given in Figure 4.15). As for the patient-based tests, seizure detection performances of over 95% are obtained for most patients in both HOJ-TF moment and GLCM-based feature sets (shown in Figure 4.16). This shows that the proposed method actually captures the differences in EEG signals just before the seizure onset and right after the onset. A seizure detection experiment is performed on CHB-MIT data set using the proposed SST-based method with successful results using both HOJ-TF moment-based (94.5% ACC) and GLCM based (95.1% ACC) feature sets. For the deep learning based SST approach, TF spectra of EEG segments are obtained by SST transform, which is a recent and popular high-resolution TF analysis approach. These TF images are used to train a ResNet-based CNN architecture. The proposed method was tested on two different datasets (IKCU and CHB-MIT) in order to validate its robustness and compare its success with existing studies. Moreover, two different CV methods have been used to prove the transparency of the obtained results. Especially, SST was used the for the first time to

analyze epileptic EEG signals in conjunction with DL, as well as TF-images obtained from SST were used to train a CNN architecture for the first time, to the best of our knowledge. Results demonstrated that outstanding performance is achieved in predicting and detecting seizures from EEG signals. Particularly, the validation of the proposed models with the PIP-based method indicates that it works well in testing new patients. In our previous study [125], EMD and EEMD based Epileptic seizure classification approach is introduced using the IKCU data set. Classification accuracies of 94.56 %, 97.14 % and 98.13%, were obtained, respectively, for DWT, EMD and EEMD approaches that have greater computational cost $O(41N_s NlogN)$ in EMD and multiplied by the number of ensembles N_e in EEMD approach [115, 125]. Upon these evaluations, it may be concluded that the proposed SST based methods having lower computational cost $O(N_v Nlog2N)$ [57] and above performance evaluation results, may be applied to epileptic seizure classification and detection with satisfactory results.

In the second part of the thesis, various methods have been proposed to distinguish the EEG signals of control subjects and AD patients. In the literature, many methods have been proposed to obtain distinctive information between the EEG signals of AD patients and control subjects [74-94]. In many studies, it was reported that low-frequency delta subband power of EEG signals of AD patients increased compared to control subjects [74, 76-78]. It is also emphasized that the complexity and synchronization measurements calculated from the EEG signals of AD patients are lower than those of the control subjects [74-90]. In the proposed study, various signal decomposition methods such as EMD, EEMD, and DWT and TF representation-based approaches such as STFT and SST are presented to classify EEG segments of control subjects and AD patients. First, IMFs are obtained from the signals using the EMD and EEMD methods, and then the IMFs that showed the most significant differences between the two groups are selected by applying the previously suggested IMF selection procedures. 7-time domain and 5-spectral domain features are calculated using selected 7 IMFs and 5 detail and approximation coefficients of DWT. Signal decomposition processes are conducted for both 1min and 5s EEG segment durations. For the 1min segment duration, all the proposed approaches yield prominent classification performances. While the highest classification accuracies are obtained using EMD (91.53%) and EEMD (93.90%) approaches from the temporal/right brain

142

cluster, the highest classification accuracy for the DWT (97.40%) approach is obtained from the temporal/left brain cluster for 1 min segment duration. In the proposed TF representation-based approach to distinguish EEG segments of AD patients and control subjects, TF representations obtained using both STFT and SST approaches for 5s segment duration are used to calculate features. 18 different TF features are calculated using the TF density functions obtained utilizing the SST and STFT approaches. For the SST approach, the most significant classification performance is obtained from the temporal/left brain cluster with 92.67% ACC, 95.03% SEN, 7.23% FDR. However, the most pronounced performance is observed for the STFT approach with 94.07% ACC, 95.90% SEN, 5.80% FDR. When the performances of all proposed methods are compared for 5s segment duration, the classification performance of the STFT-based approach was higher than the other approaches. Although decomposition-based approaches have been used frequently in the literature for the classification of EEG signals of control subjects and AD patients, TF representation-based approaches have been used less frequently. The performance results, which are presented in detail, show that the traditional decomposition method DWT and the conventional TF representation method STFT-based approaches can be used successfully in distinguishing the EEG signals of AD patients and control subjects.

With the following items summarized the objectives are achieved in this thesis;

1. The hybrid IMF selection method that includes different approaches such as energy, correlation, power spectral distance, and statistical significance test are performed and the advantages of this IMF selection process are presented in detail for EMD and EEMD methods.
2. It has been shown that the EEMD method can be used successfully in the classification of both Alzheimer's Dementia and epileptic EEG signals.
3. In addition to the literature, a single-channel DMD approach has been proposed for epileptic seizure detection and it has been shown that successful results can be obtained by using this approach in channel-based seizure detection.
4. Higher-order DMD moments and DMD sub-band powers-based novel features are introduced using the DMD spectrum, using these features prominent performance evaluation results are achieved.

5. SST-based seizure detection study is performed and different features are calculated using TF representations.

6. Again, the SST-based CNN approach is used for the first time in the literature for the detection of epileptic seizures and successful results are obtained.

7. TF representation-based AD patient and control subjects EEG classification study is performed by calculating joint TF features and promising performance results are obtained.

References

[1] M. Sertbas¸ K. Ülgen, and T. Çakır. Investigation of the effects of neurological diseases on human brain metabolism by a computational systems biology approach. New Biotechnolog 2012; 29: 150.

[2] W. H. Organization, Neurological disorders: public health challenges. World Health Organization, 2006.

[3] Feigin VL, Abajobir AA, Abate KH, Abd-Allah F, Abdulle AM, et al. Global, regional, and national burden of neurological disorders during 1990–2015: a systematic analysis for the global burden of disease study 2015. The Lancet Neurology 2017; 16(11):877–897.

[4] Adoukonou T, Adogble L, Agbetou M, Donne Gnonlonfoun D, Houinato D, et al. Prevalence of the major neurological disorders in a semi-urban community in northern benin. Eneurologicalsci 2020; 19: 100242.

[5] W. Atlas, Country resources for neurological disorders 2004," Geneva: World Health Organization 2004; 232–239.

[6] Sridhar C, Bhat S, Acharya UR, Adeli H, Bairy GM. Diagnosis of attention deficit hyperactivity disorder using imaging and signal processing techniques. Computers in biology and medicine 2017; 88: 93–99.

[7] Lee PF, Kan DPX, Croarkin P, Phang CK, and Doruk D. Neurophysiological correlates of depressive symptoms in young adults: a quantitative EEG study. Journal of Clinical Neuroscience 2018; 47: 315–322.

[8] Zhang H, Su J, Wang Q, Liu Y, Good L, Pascual JM. Predicting seizure by modeling synaptic plasticity based on EEG signals-a case study of inherited

epilepsy. Communications in Nonlinear Science and Numerical Simulation 2018; 56: 330–343.

[9] Janvale G, Kendre, Mehrotra S. Mental and behavioural disorders related to alcohol and their effects on EEG signals–an overview. Procedia-Social and Behavioral Sciences 2014; 133:116–121.

[10] Noback CR, Ruggiero DA, Strominger NL, Demarest RJ. The human nervous system: structure and function. Springer Science & Business Media 2005; 744.

[11] Mai JK, Paxinos G. The human nervous system. Academic press 2011.

[12] Young PA, Young PH, Tolbert DL. Basic clinical neuroscience, Lippincott Williams & Wilkins 2008.

[13] Mtui E, Gruener G, Dockery P. Fitzgerald's Clinical Neuroanatomy and Neuroscience E-Book. Elsevier 2020.

[14] Zahra A, Kanwal N, ur Rehman N, Ehsan S, McDonald-Maier KD. Seizure detection from EEG signals using multivariate empirical mode decomposition. Computers in Biology and Medicine 2017; 88: 132 – 141.

[15] Bajaj V, Pachori RB. Classification of seizure and nonseizure EEG signals using empirical mode decomposition. IEEE Transactions on Information Technology in Biomedicine 2011; 16(6): 1135–1142.

[16] Fisher RS, Cross JH, French JA, Higurashi N, Hirsch E, Jansen FE, et al. Operational classification of seizure types by the international league against epilepsy: Position paper of the ilae commission for classification and terminology. Epilepsia 2017; 58(4): 522–530.

[17]   Scheffer IE, Berkovic S, Capovilla G, Connolly MB, French J, Guilhoto L, et al. Ilae classification of the epilepsies: position paper of the ilae commission for classification and terminology. Epilepsia 2017; 58(4): 512–521.

[18] Raghu S, Sriraam N, Hegde AS, Kubben PL. A novel approach for classification of epileptic seizures using matrix determinant. Expert Systems with Applications 2019; 127: 323–341.

[19] Faust O, Acharya UR, Adeli H, Adeli A. Wavelet-based EEG processing for computer-aided seizure detection and epilepsy diagnosis. Seizure 2015; 26: 56–64.

[20] Fürbass F, Kampusch S, Kaniusas E, Koren J, Pirker S, Hopfengartner R, et al. Automatic multimodal detection for long-term seizure documentation in epilepsy. Clinical Neurophysiology 2017; 128 (8): 1466–1472.

[21] Mahmoodian N, Boese A, Friebe M, Haddadnia J. Epileptic seizure detection using cross-bispectrum of electroencephalogram signal. Seizure 2019; 66: 4–11.

[22] Yuan Q, Zhou W, Zhang L, Zhang F, Xu F, Leng Y, et al. Epileptic seizure detection based on imbalanced classification and wavelet packet transform. Seizure 2017; 50: 99–108.

[23] Khan NA, Ali S. A new feature for the classification of non-stationary signals based on the direction of signal energy in the time–frequency domain. Computers in biology and medicine 2018; 100: 10–16.

[24] Fasil O, Rajesh R. Time-domain exponential energy for epileptic EEG signal classification. Neuroscience Letters 2019; 694: 1–8.

[25] Kang JH, Chung YG, Kim SP. An efficient detection of epileptic seizure by differentiation and spectral analysis of electroencephalograms. Computers in biology and medicine 2015; 66: 352–356.

[26] Iscan Z, Dokur Z, Demiralp T. Classification of electroencephalogram signals with combined time and frequency features. Expert Systems with Applications 2011; 38(8):10 499–10 505.

[27] Bandarabadi M, Teixeira CA, Rasekhi J, Dourado A. Epileptic seizure prediction using relative spectral power features. Clinical Neurophysiology 2015; 126(2): 237–248.

[28] Tawfik NS, Youssef SM, Kholief M. A hybrid automated detection of epileptic seizures in EEG records. Computers & Electrical Engineering 2016; 53: 177–190.

[29] Xiang J, Li C, Li H, Cao R, Wang B, Han X, et al. The detection of epileptic seizure signals based on fuzzy entropy. Journal of neuroscience methods 2015; 243: 18–25.

[30] Raghu S, Sriraam N, Temel Y, Rao SV, Hegde AS, Kubben PL. Performance evaluation of DWT based sigmoid entropy in time and frequency domains for automated detection of epileptic seizures using svm classifier. Computers in biology and medicine 2019; 110: 127–143.

[31] Yuan Q, Zhou W, Li S, Cai D. Epileptic EEG classification based on extreme learning machine and nonlinear features. Epilepsy research 2011; 96(1-2): 29–38.

[32] Sharma M, Pachori RB, Acharya UR. A new approach to characterize epileptic seizures using analytic time frequency flexible wavelet transform and fractal dimension. Pattern Recognition Letters 2017; 94: 172–179.

[33] Oppenheim AV. Discrete-time signal processing. Pearson Education India; 1999.

[34] Kıymık MK, Güler I, Dizibüyük A, Akın M. Comparison of STFT and wavelet transform methods in determining epileptic seizure activity in EEG signals for real-time application. Computers in biology and medicine 2005; 35(7): 603–616.

[35] Adeli H, Zhou Z, Dadmehr N. Analysis of EEG records in an epileptic patient using wavelet transform. Journal of neuroscience methods 2003; 123(1): 69–87.

[36] Riaz F, Hassan A, Rehman S, Niazi IK, Dremstrup K. EMD-based temporal and spectral features for the classification of EEG signals using supervised learning. IEEE Transactions on Neural Systems and Rehabilitation Engineering 2015; 24(1): 28–35.

[37] Adeli H, Ghosh-Dastidar S, Dadmehr N. Wavelet-chaos methodology for analysis of EEGs and EEG subbands to detect seizure and epilepsy. IEEE Transactions on Biomedical Engineering 2007; 54(2): 205–211.

[38] Alickovic E, Kevric J, Subasi A. Performance evaluation of empirical mode decomposition, discrete wavelet transform, and wavelet packed decomposition for automated epileptic seizure detection and prediction. Biomedical signal processing and control 2018; 39: 94–102.

[39] Moctezuma LA, Molinas M. Classification of low-density EEG for epileptic seizures by energy and fractal features based on EMD. The Journal of Biomedical Research 2020; 34(3): 178–188.

[40] Wu J, Zhou T, Li T. Detecting epileptic seizures in EEG signals with complementary ensemble empirical mode decomposition and extreme gradient boosting. Entropy 2020; 22(2): 140.

[41] Kumar MR, Rao YS. Epileptic seizures classification in EEG signal based on semantic features and variational mode decomposition. Cluster Computing 2019; 22(6): 13 521–13 531.

[42] Pachori RB, Sharma R, Patidar S. Classification of normal and epileptic seizure EEG signals based on empirical mode decomposition in Complex system modelling and control through intelligent soft computations. Springer, 2015; 367–388.

[43] Hassan AR, Subasi A, Zhang Y. Epilepsy seizure detection using complete ensemble empirical mode decomposition with adaptive noise. Knowledge-Based Systems 2020; 191: 105333.

[44] Correa AG, Orosco L, Diez P, Laciar E. Automatic detection of epileptic seizures in long-term EEG records. Computers in biology and medicine 2015; 57: 66–73.

[45] Zhang T, Chen W, Li M. Generalized stockwell transform and SVD-based epileptic seizure detection in EEG using random forest. Biocybernetics and Biomedical Engineering 2018; 38(3): 519 – 534.

[46] Quintero-Rincon A, Pereyra M, Giano C, Risk M, Batatia H. Fast statistical model-based classification of epileptic EEG signals. Biocybernetics and Biomedical Engineering 2018; 38(4):877–889.

[47] Ibrahim S, Djemal R, Alsuwailem A. Electroencephalography (EEG) signal processing for epilepsy and autism spectrum disorder diagnosis. Biocybernetics and Biomedical Engineering 2018; 38(1): 16–26.

[48] Tzallas AT, Tsipouras MG, Fotiadis DI. Epileptic seizure detection in EEGs using time–frequency analysis. IEEE transactions on information technology in biomedicine 2009; 13(5): 703–710.

[49] Samiee K, Kiranyaz S, Gabbouj M, Saramaki T. Long-term epileptic EEG classification via 2D mapping and textural features. Expert Systems with Applications 2015; 42(20): 7175 – 7185.

[50] Li Y, Cui W, Luo M, Li K, Wang L. Epileptic seizure detection based on time-frequency images of EEG signals using gaussian mixture model and gray level co-occurrence matrix features. International journal of neural systems 2018; 28(07): 1850003.

[51] Lian J, Shi Y, Zhang Y, Jia W, Fan X, Zheng Y. Revealing false positive features in epileptic EEG identification. International Journal of Neural Systems 2020; 2 050 017–2 050 017.

[52] Daubechies I. A nonlinear squeezing of the continuous wavelet transform based on auditory nerve models. Wavelets in medicine and biology 1996; 527–546.

[53] Thakur G, Wu HT. Synchrosqueezing-based recovery of instantaneous frequency from nonuniform samples. SIAM Journal on Mathematical Analysis 2011; 43(5): 2078–2095.

[54] Oberlin T, Meignen S, Perrier V. Second-order synchrosqueezing transform or invertible reassignment? Towards ideal time-frequency representations. IEEE Transactions on Signal Processing 2015; 63(5): 1335–1344.

[55] Ali S, Ferdous MJ, Hamid E, Molla K. Time-frequency coherence of multichannel EEG signals: Synchrosqueezing transform based analysis. International Journal of Computer Science Trends and Technology 2016; 4(3): 40–48.

150

[56] Ahrabian A, Looney D, Stankovic L, Mandic DP. Synchrosqueezing-based time-frequency analysis of multivariate data. Signal Processing 2015; 106: 331–341.

[57] Mamli S, Kalbkhani H. Gray-level co-occurrence matrix of Fourier synchro-squeezed transform for epileptic seizure detection. Biocybernetics and Biomedical Engineering 2019; 39(1): 87–99.

[58] Solaija MSJ, Saleem S, Khurshid K, Hassan SA, Kamboh AM. Dynamic mode decomposition based epileptic seizure detection from scalp EEG. IEEE Access 2018; 6: 38 683–38 692.

[59] Bilal M, Rizwan M, Saleem S, Khan MM, Alkatheir MS, Alqarni M. Automatic seizure detection using multi-resolution dynamic mode decomposition. IEEE Access 2019; 7: 61 180–61 194.

[60] Bandil MK, Wadhwani A. Multi-resolution EEG and EEG sub-band features optimization for epileptic classification using hybrid evolutionary computing technique. Procedia Computer Science 2019; 152: 243–251.

[61] Pachori RB, Patidar S. Epileptic seizure classification in EEG signals using second-order difference plot of intrinsic mode functions. Computer methods and programs in biomedicine 2014; 113(2): 494–502.

[62] Das AB, Bhuiyan MIH. Discrimination and classification of focal and non-focal EEG signals using entropy-based features in the EMD-DWT domain. Biomedical Signal Processing and Control 2016; 29: 11 – 21.

[63] Djemili R, Bourouba H, Korba MA. Application of empirical mode decomposition and artificial neural network for the classification of normal and epileptic EEG signals. Biocybernetics and Biomedical Engineering 2016; 36(1): 285 – 291.

[64] Acharya UR, Oh SL, Hagiwara Y, Tan JH, Adeli H. Deep convolutional neural network for the automated detection and diagnosis of seizure using EEG signals. Computers in biology and medicine 2018; 100: 270–278.

[65] Ayodele K, Ikezogwo W, Komolafe M, Ogunbona P. Supervised domain generalization for integration of disparate scalp EEG datasets for automatic epileptic seizure detection. Computers in Biology and Medicine 2020; 103757.

[66] Zhou M, Tian C, Cao R, Wang B, Niu Y, Hu T, *et al*. Epileptic seizure detection based on EEG signals and CNN. Frontiers in neuroinformatics 2018; 12: 95.

[67] P. Thodoroff, J. Pineau, and A. Lim, "Learning robust features using deep learning for automatic seizure detection," in Machine learning for healthcare conference, 2016, pp. 178–190.

[68] Dening T, Sandilyan MB. Dementia: definitions and types. Nursing Standard (2014+) 2015; 29(37): 37.

[69] Savva GM, Zaccai J, Matthews FE, Davidson JE, McKeith I, Brayne C. Prevalence, correlates and course of behavioural and psychological symptoms of dementia in the population. The British Journal of Psychiatry 2009; 194(3): 212–219.

[70] Association A, et *al*. 2018 Alzheimer's disease facts and figures. Alzheimer's & Dementia 2018; 14(3): 367–429.

[71] Association A. 2019 Alzheimer's disease facts and figures. Alzheimer's & dementia 2019; 15(3): 321–387.

[72] Cantone M, Di Pino G, Capone F, Piombo M, Chiarello D, Cheeran B, *et al*. The contribution of transcranial magnetic stimulation in the diagnosis and in the management of dementia. Clinical Neurophysiology 2014; 125(8): 1509–1532.

[73] Prince M, Bryce R, Albanese E, Wimo A, Ribeiro W, Ferri CP. The global prevalence of dementia: a systematic review and metaanalysis. Alzheimer's & dementia 2013; 9(1): 63–75.

[74] Tzimourta KD, Giannakeas N, Tzallas AT, Astrakas LG, Afrantou T, Ioannidis P, *et al*. EEG window length evaluation for the detection of alzheimer's disease over different brain regions. Brain sciences 2019; 9(4): 81.

[75] Yu H, Lei X, Song Z, Wang J, Wei X, Yu B. Functional brain connectivity in alzheimer's disease: An EEG study based on permutation disalignment index. Physica A: Statistical Mechanics and its Applications 2018; 506: 1093–1103.

[76] Garn H, Waser M, Deistler M, Benke T, Dal-Bianco P, Ransmayr G, *et al*. Quantitative EEG markers relate to alzheimer's disease severity in the prospective dementia registry austria (prodem). Clinical Neurophysiology 2015; 126(3): 505–513.

[77] Abasolo D, Hornero R, Espino P, Poza J, Sanchez CI, Rosa R. Analysis of regularity in the EEG background activity of alzheimer's disease patients with approximate entropy. Clinical neurophysiology 2005; 116(8): 1826–1834.

[78] Waser M, Garn H, Schmidt R, Benke T, Dal-Bianco P, Ransmayr G, *et al*. Quantifying synchrony patterns in the EEG of alzheimer's patients with linear and non-linear connectivity markers. Journal of Neural Transmission 2016; 123(3): 297–316.

[79] Cassani R, Falk TH, Fraga FJ, Kanda PA, Anghinah R. The effects of automated artifact removal algorithms on electroencephalography-based Alzheimer's disease diagnosis. Frontiers in aging neuroscience 2014; 6: 55.

[80] Falk TH, Fraga FJ, Trambaiolli L, Anghinah R. EEG amplitude modulation analysis for semi-automated diagnosis of alzheimer's disease. EURASIP Journal on Advances in Signal Processing 2012; 2012(1): 1–9.

[81] Kulkarni N, Bairagi V. Extracting salient features for EEG-based diagnosis of Alzheimer's disease using support vector machine classifier. IETE Journal of Research 2017; 63(1): 11–22.

[82] Tylova L, Kukal J, Hubata-Vacek V, and Vysata O. Unbiased estimation of permutation entropy in EEG analysis for alzheimer's disease classification. Biomedical Signal Processing and Control 2018; 39: 424–430.

[83] Staudinger T, Polikar R. Analysis of complexity based EEG features for the diagnosis of Alzheimer's disease. Annual International Conference of the IEEE Engineering in Medicine and Biology Society; 2011. IEEE; 2011. 2033–2036.

[84] Yang AC, Wang SJ, Lai KL, Tsai CF, Yang CH, Hwang JP, *et al*. Cognitive and neuropsychiatric correlates of EEG dynamic complexity in patients with alzheimer's disease. Progress in Neuro-Psychopharmacology and Biological Psychiatry 2013; 47: 52–61.

[85] Deng B, Cai L, Li S, Wang R, Yu H, Chen Y, *et al*. Multivariate multi-scale weighted permutation entropy analysis of EEG complexity for alzheimer's disease. Cognitive neurodynamics 2017; 11(3): 217–231.

[86] Jeong J, Kim SY, Han SH. Non-linear dynamical analysis of the EEG in Alzheimer's disease with optimal embedding dimension. Electroencephalography and clinical Neurophysiology 1998; 106(3): 220–228.

[87] Ahmadlou M, Adeli H, Adeli A. Fractality and a wavelet-chaos-methodology for EEG-based diagnosis of Alzheimer disease. Alzheimer Disease & Associated Disorders 2011; 25(1): 85–92.

[88] Gomez C, Mediavilla A, Hornero R, Abasolo D, Fernandez A. Use of the higuchi's fractal dimension for the analysis of MEG recordings from alzheimer's disease patients. Medical engineering & physics 2009; 31(3): 306–313.

[89] Abasolo D, Hornero R, Gomez C, Garcıa M, Lopez M. Analysis of EEG background activity in Alzheimer's disease patients with Lempel–Ziv complexity and central tendency measure. Medical Engineering & Physics 2006; 28(4): 315-322.

[90] Simons S, Abasolo D. Distance-based lempel–ziv complexity for the analysis of electroencephalograms in patients with Alzheimer's disease. Entropy 2017; 19(3): 129.

[91] Dauwels J, Vialatte F, Musha T, Cichocki A. A comparative study of synchrony measures for the early diagnosis of Alzheimer's disease based on EEG. NeuroImage 2010; 49(1): 668–693.

[92] Safi MS, Safi SMM. Early detection of Alzheimer's disease from EEG signals using hjorth parameters. Biomedical Signal Processing and Control 2021; 65: 102338.

[93] Bairagi V. EEG signal analysis for early diagnosis of alzheimer disease using spectral and wavelet based features. International Journal of Information Technology 2018; 10(3): 403–412.

[94] Berte F, Lamponi G, Calabro RS, Bramanti P. Elman neural network for the early identification of cognitive impairment in alzheimer's disease. Functional neurology 2014; 29(1): 57.

[95] Li S, Zhou W, Yuan Q, Geng S, Cai D. Feature extraction and recognition of ictal EEG using EMD and SVM. Computers in biology and medicine 2013; 43(7): 807–816.

[96] Bizopoulos PA, Tsalikakis DG, Tzallas AT, Koutsouris DD, Fotiadis DI. EEG epileptic seizure detection using k-means clustering and marginal spectrum based on ensemble empirical mode decomposition. ın 13th IEEE International Conference on BioInformatics and BioEngineering. IEEE; 2013. 1–4.

[97] Kutz JN, Brunton SL, Brunton BW, Proctor JL. Dynamic mode decomposition: data-driven modeling of complex systems. SIAM, 2016.

[98] Brunton BW, Johnson LA, Ojemann JG, Kutz JN. Extracting spatial–temporal coherent patterns in large-scale neural recordings using dynamic mode decomposition. Journal of neuroscience methods 2016; 258: 1–15.

[99] Seo JH, Tsuda I, Lee YJ, Ikeda A, Matsuhashi M, Matsumoto R, *et al*. Pattern recognition in epileptic EEG signals via dynamic mode decomposition. Mathematics 2020; 8(4): 481.

[100] Karabiber Cura O, Akan A. Analysis of epileptic EEG signals by using dynamic mode decomposition and spectrum. Biocybernetics and Biomedical Engineering 2021; 41(1): 28–44.

[101] Rout SK, Biswal PK. An efficient error-minimized random vector functional link network for epileptic seizure classification using VMD. Biomedical Signal Processing and Control 2020; 57: 101787.

[102] Tirunagari S. Dynamic mode decomposition for computer vision and signal processing (Ph.D. dissertation) United Kingdom: University of Surrey; 2016.

[103] Ramos-Aguilar R, Olvera-Lopez JA, Olmos-Pineda I, Sanchez-Urrieta S. Feature extraction from EEG spectrograms for epileptic seizure detection. Pattern Recognition Letters 2020; 133: 202 – 209.

[104] Daubechies I, Lu J, Wu HT. Synchrosqueezed wavelet transforms: An empirical mode decomposition-like tool. Applied and computational harmonic analysis 2011; 30(2): 243–261.

[105] Li C, Liang M. A generalized synchrosqueezing transform for enhancing signal time–frequency representation. Signal Processing 2012; 92(9): 2264–2274.

[106] Yu G, Yu M, Xu C. Synchroextracting transform. IEEE Transactions on Industrial Electronics 2017; 64(10): 8042–8054.

[107] Adem K. Diagnosis of breast cancer with stacked autoencoder and subspace KNN. Physica A: Statistical Mechanics and its Applications 2020; 551: 124591.

[108] Liu M. Fingerprint classification based on adaboost learning from singularity features. Pattern Recognition 2010; 43(3): 1062 – 1070.

[109] Grewal S, Gotman J. An automatic warning system for epileptic seizures recorded on intracerebral EEGs. Clinical neurophysiology 2005; 116(10): 2460–2472.

[110] Public Data set: CHB-MIT EEG dataset. 2020 [accessed 16.05.2020]. https://physionet.org/content/chbmit/1.0.0/.

[111] Junsheng C, Dejie Y, Yu Y. Research on the intrinsic mode function (IMF) criterion in EMD method. Mechanical systems and signal processing 2006; 20(4): 817–824.

[112] Peng Z, Peter WT, Chu F. A comparison study of improved hilbert–huang transform and wavelet transform: application to fault diagnosis for rolling bearing. Mechanical systems and signal processing 2005; 19(5): 974–988.

[113] Lozano M, Fiz JA, Jane R. Performance evaluation of the hilbert–huang transform for respiratory sound analysis and its application to continuous adventitious sound characterization. Signal Processing 2016; 120: 99–116.

[114] Komaty A, Boudraa AO, Augier B, Dare-Emzivat D. EMD-based filtering using similarity measure between probability density functions of IMFs. IEEE Transactions on Instrumentation and Measurement 2013; 63(1): 27–34.

[115] Wang YH, Yeh CH, Young HWV, Hu K, Lo MT. On the computational complexity of the empirical mode decomposition algorithm. Physica A: Statistical Mechanics and its Applications 2014; 400: 159 – 167.

[116] Colak OH. Preprocessing effects in time–frequency distributions and spectral analysis of heart rate variability. Digital Signal Processing 2009; 19(4): 731–739.

[117] Acharya UR, Sree SV, Swapna G, Martis RJ, Suri JS. Automated EEG analysis of epilepsy: a review. Knowledge-Based Systems 2013; 45: 147–165.

[118] Gajic D, Djurovic Z, Gligorijevic J, Di Gennaro S, Savic-Gajic I. Detection of epileptiform activity in EEG signals based on time-frequency and non-linear analysis. Frontiers in Computational Neuroscience 2015; 9: 38.

[119] Gajic D, Djurovic Z, Di Gennaro S, Gustafsson F. Classification of EEG signals for detection of epileptic seizures based on wavelets and statistical pattern recognition. Biomedical Engineering: Applications, Basis and Communications 2014; 26(02): 1450021.

[120] Alotaiby TN, Alshebeili SA, Alotaibi FM, Alrshoud SR. Epileptic seizure prediction using CSP and LDA for scalp EEG signals. Computational intelligence and neuroscience 2017; 2017.

[121] Cui S, Duan L, Qiao Y, Xiao Y. Learning EEG synchronization patterns for epileptic seizure prediction using bag-of-wave features. Journal of Ambient Intelligence and Humanized Computing 2018; 1–16.

[122] Moctezuma LA, Molinas M. EEG channel-selection method for epileptic-seizure classification based on multiobjective optimization. Frontiers in Neuroscience2020; 14: 593.

[123] Bhattacharyya A, Pachori RB. A multivariate approach for patient-specific EEG seizure detection using empirical wavelet transform. IEEE Transactions on Biomedical Engineering 2017; 64(9): 2003–2015.

[124] Fu R, Tian Y, Shi P, Bao T. Automatic detection of epileptic seizures in EEG using sparse CSP and fisher linear discrimination analysis algorithm. Journal of Medical Systems 2020; 44(2): 1–13.

[125] Karabiber Cura O, Kocaaslan Atli S, Ture H.S, Akan A. Epileptic seizure classifications using empirical mode decomposition and its derivative. BioMedical Engineering OnLine 2020; 19(1): 1–22.

[126] Erichson NB, Brunton SL, Kutz JN. Compressed dynamic mode decomposition for background modeling. Journal of Real-Time Image Processing 2019; 16(5): 1479–1492.

[127] Akan A, Unsal RB. Time–frequency analysis and classification of temporomandibular joint sounds. Journal of the Franklin Institute 2000; 337(4): 437 – 451.

[128] Chen Y, Li H, Hou L, Bu X. Feature extraction using dominant frequency bands and time-frequency image analysis for chatter detection in milling. Precision Engineering 2019; 56: 235–245.

[129] Jana GC, Sabath A, Agrawal A. Performance analysis of supervised machine learning algorithms for epileptic seizure detection with high variability EEG datasets: A comparative study. In 2019 International Conference on Electrical, Electronics and Computer Engineering (UPCON). IEEE; 2019. 1–6.

[130] Dash DP, Kolekar MH, Jha K. Multi-channel EEG based automatic epileptic seizure detection using iterative filtering decomposition and hidden markov model. Computers in Biology and Medicine 2020; 116: 103571.

[131] He K, Zhang X, Ren S, Sun J. Deep residual learning for image recognition. In 2016 IEEE Conference on Computer Vision and Pattern Recognition (CVPR); 2016. 770–778.

[132] Hammond J, White P. The analysis of non-stationary signals using time-frequency methods. Journal of Sound and vibration 1996; 190(3): 419–447.

[133] Jadhav P, Rajguru G, Datta D, Mukhopadhyay S. Automatic sleep stage classification using time–frequency images of cwt and transfer learning using convolution neural network. Biocybernetics and Biomedical Engineering 2020; 40(1): 494–504.

[134] Zhang B, Wang W, Xiao Y, Xiao S, Chen S, Chen S, *et al*. Cross-subject seizure detection in EEGs using deep transfer learning. Computational and Mathematical Methods in Medicine 2020; 2020.

[135] Cui Y, Wu D. EEG-based driver drowsiness estimation using convolutional neural networks. Neural Information Processing 2017; 822–832.

[136] Li Y, Yu Z, Chen Y, Yang C, Li B, *et al*. Automatic seizure detection using fully convolutional nested LSTM. International Journal of Neural Systems 2020; 30(4): 2 050 019–2 050 019.

[137] Ozdemir MA, Degirmenci M, Izci E, Akan A. EEG-based emotion recognition with deep convolutional neural networks. Biomedical Engineering / Biomedizinische Technik 2021; 66(1): 43–57.

[138] Gholamiangonabadi D, Kiselov N, Grolinger K. Deep neural networks for human activity recognition with wearable sensors: Leave-one-subject-out cross-validation for model selection. IEEE Access 2020; 8: 133 982–133 994.

[139] Karabiber Cura O, Akan A. Classification of epileptic EEG signals using synchrosqueezing transform and machine learning. International Journal of Neural Systems 2021; 31(5): 2150005. DOI: 10.1142/s0129065721500052

[140] Tsiouris KM, Pezoulas VC, Zervakis M, Konitsiotis S, Koutsouris DD, Fotiadis DI. A long short-term memory deep learning network for the prediction of

epileptic seizures using EEG signals. Computers in biology and medicine2018; 99: 24–37.

[141] Zhu R, Guo Y, Xue JH. Adjusting the imbalance ratio by the dimensionality of imbalanced data. Pattern Recognition Letters 2020; 133: 217-223.

[142] Yuan Y, Xun G, Jia K, Zhang A. A multi-context learning approach for EEG epileptic seizure detection. BMC systems biology 2018; 12(6): 47–57.

[143] Liang W, Pei H, Cai Q, Wang Y. Scalp EEG epileptogenic zone recognition and localization based on long-term recurrent convolutional network. Neurocomputing 2020; 396: 569–576.

[144] Hossain MS, Amin SU, Alsulaiman M, Muhammad G. Applying deep learning for epilepsy seizure detection and brain mapping visualization. ACM Transactions on Multimedia Computing, Communications, and Applications (TOMM) 2019; 15(1): 1–17.

[145] Wei Z, Zou J, Zhang J, Xu J. Automatic epileptic EEG detection using convolutional neural network with improvements in time-domain. Biomedical Signal Processing and Control 2019; 53: 101551.

[146] Liu CL, Xiao B, Hsaio WH, Tseng VS. Epileptic seizure prediction with multi-view convolutional neural networks. IEEE Access 2019;7: 170 352–170 361.

[147] Shahbazi M, Aghajan H. A generalizable model for seizure prediction based on deep learning using cnn-lstm architecture. In 2018 IEEE Global Conference on Signal and Information Processing (GlobalSIP); 2018. 469–473.

[148] Karabiber Cura O, Ozdemir MA, Akan A. Epileptic EEG classification using synchrosqueezing transform with machine and deep learning techniques. In 28th European Signal Processing Conference (EUSIPCO). IEEE; 2021. 1210–1214.

Appendices

Appendix A

Publications from the Thesis

Conference Papers

1. Karabiber Cura O, Özdemir MA, Pehlivan S, Akan A. A Dynamic Mode Decomposition Based Approach for Epileptic EEG Classification. 2020 28th European Signal Processing Conference (EUSIPCO 2020), 1-5. Doi: 10.23919/eusipco47968.2020.9287719 (TamMetin Bildiri/Sözlü Sunum) (Yayın No: 6363536)

2. Karabiber Cura O, Özdemir MA, Akan A (2021). Epileptic EEG Classification Using Synchrosqueezing Transform with Machine and Deep Learning Techniques. 2020 28th European Signal Processing Conference (EUSIPCO 2020), 1-5., Doi: 10.23919/eusipco47968.2020.9287347 (Tam Metin Bildiri/Sözlü Sunum) (Yayın No: 6363543)

3. Karabiber Cura O, Akan A (2020). Epileptic EEG Classification Using Synchrosqueezing Transform and Machine Learning. 2020 Medical Technologies Congress (TIPTEKNO), Doi: 10.1109/TIPTEKNO50054.2020.9299317 (Tam Metin Bildiri/Sözlü Sunum) (Yayın No: 6855074)

4. Karabiber Cura O, Pehlivan S, Akan A. (2020). Classification of Epileptic EEG Signals Using Dynamic Mode Decomposition. 2020 28th Signal Processing and Communications Applications Conference (SIU), Doi: 10.1109/SIU49456.2020.9302302 (Tam Metin Bildiri/Sözlü Sunum) (Yayın No: 6855054)

5. Karabiber Cura O, Akan A, Kocaaslan Atli S (2019). Selection of Intrinsic Mode Functions for Epileptic EEG Classification Using Ensemble Empirical Mode Decomposition. 2019 Medical Technologies Congress (TIPTEKNO), 335-338., Doi: 10.1109/TIPTEKNO.2019.8895000 (Tam Metin Bildiri/Sözlü Sunum) (Yayın No: 5614555)

6. Karabiber Cura O, Kocaaslan Atli S, Sadighzadeh R, Akan A (2018). Classification of Epileptic EEG Data by Using Ensemble Empirical Mode Decomposition. 2018 26th Signal Processing and Communications Applications Conference (SIU), 2018(1), 1-4., Doi: 10.1109/SIU.2018.8404453 (Tam Metin Bildiri/Sözlü Sunum) (Yayın No: 4275318)

7. Karabiber Cura O, Sadighzadeh R, Akan A (2017). Seizure Detection from Pre-Attack EEG Signals Using Ensemble EmpiricalMode Decomposition. 9th International Symposium on Image Processing, Wavelet and Applications (Özet Bildiri/Sözlü Sunum) (Yayın No: 4152793)

8. Karabiber Cura O, Akan A (2017). Investigation of epileptic EEG data using ensemble empirical mode decomposition. 2017 Medical Technologies National Congress (TIPTEKNO), 343, Doi: 10.1109/TIPTEKNO.2017.8238086 (Tam Metin Bildiri/Sözlü Sunum) (Yayın No: 3823522)

Journal Articles

1. Karabiber Cura O, Akan A. Classification of Epileptic EEG Signals Using Synchrosqueezing Transform and Machine Learning. International Journal of Neural Systems 2021; 31(5): 2150005. Doi: 10.1142/S0129065721500052.

2. Karabiber Cura O, Akan A. Analysis of epileptic EEG signals by using dynamic mode decomposition and spectrum. Biocybernetics and Biomedical Engineering 2021; 41(1): 28-44.

3. Karabiber Cura O, Kocaaslan Atli S, Ture H.S, Akan A. Epileptic seizure classifications using empirical mode decomposition and its derivative. BioMedical Engineering OnLine 2020; 19(1): 1–22.

4. Ozdemir MA, **Karabiber Cura O**, Akan A. Epileptic EEG Classification by Using Time-Frequency Images for Deep Learning. International Journal of Neural System 2021. Doi: https://doi.org/10.1142/S012906572150026X

5. Karabiber Cura O, Akan A. Future of Time-Frequency Signal Processing. Digital Signal Processing 30th Anniversary Special Issue: Future Signal Processing. **Accepted**.

6. The article about Alzheimer's Dementia Classification is under preparation.

Curriculum Vitae

Name Surname: Ozlem Karabiber Cura

Education:

2016–2021   İzmir Kâtip Çelebi University
             PhD in Biomedical Technologies

2012–2014   Erciyes University,
             B.Sc (Double major) in Electrical Electronics Engineering

2010–2014   Erciyes University,
             B.Sc in Biomedical Engineering

Work Experience:

2015-   Research Assistant, İzmir Kâtip Çelebi University, Department of Biomedical Eng.

Conference Papers

1. Karabiber Cura O, Özdemir MA, Pehlivan S, Akan A. A Dynamic Mode Decomposition Based Approach for Epileptic EEG Classification. 2020 28th European Signal Processing Conference (EUSIPCO 2020), 1-5. Doi: 10.23919/eusipco47968.2020.9287719 (TamMetin Bildiri/Sözlü Sunum) (Yayın No: 6363536)

2. Karabiber Cura O, Özdemir MA, Akan A (2021). Epileptic EEG Classification Using Synchrosqueezing Transform with Machine and Deep Learning Techniques. 2020 28th European Signal Processing Conference (EUSIPCO 2020), 1-5., Doi: 10.23919/eusipco47968.2020.9287347 (Tam Metin Bildiri/Sözlü Sunum) (Yayın No: 6363543)

3. Karabiber Cura O, Akan A (2020). Epileptic EEG Classification Using Synchrosqueezing Transform and Machine Learning. 2020 Medical Technologies Congress (TIPTEKNO), Doi: 10.1109/TIPTEKNO50054.2020.9299317 (Tam Metin Bildiri/Sözlü Sunum) (Yayın No: 6855074)

4. Karabiber Cura O, Pehlivan S, Akan A. (2020). Classification of Epileptic EEG Signals Using Dynamic Mode Decomposition. 2020 28th Signal Processing and Communications Applications Conference (SIU), Doi: 10.1109/SIU49456.2020.9302302 (Tam Metin Bildiri/Sözlü Sunum) (Yayın No: 6855054)

5. Karakus D, **Karabiber Cura O**, Yesilkaya B, Akan A (2019). Desıgn of Brain-Computer Interface for Controlling a Virtual Keyboard. 2019 Medical Technologies Congress (TIPTEKNO), 343-345., Doi: 10.1109/TIPTEKNO.2019.8895133 (Tam Metin Bildiri/Sözlü Sunum) (Yayın No: 5614657)

6. Karabiber Cura O, Akan A, Kocaaslan Atli S (2019). Selection of Intrinsic Mode Functions for Epileptic EEG Classification Using Ensemble Empirical Mode Decomposition. 2019 Medical Technologies Congress (TIPTEKNO), 335-338., Doi: 10.1109/TIPTEKNO.2019.8895000 (Tam Metin Bildiri/Sözlü Sunum) (Yayın No: 5614555)

7. Ata A, Yesilkaya B, **Karabiber Cura O**, Akan A (2019). Control of SeriousGames Designed for Alzheimer'xxs and Dementia Patients by EEG Signals. 2019 Medical Technologies Congress (TIPTEKNO), 339-342., Doi: 10.1109/TIPTEKNO.2019.8895043 (Tam Metin Bildiri/Sözlü Sunum) (Yayın No: 5614625)

8. Kovan I, Unay M, **Karabiber Cura O**, Akan A (2018). Analysis of EEG Signals to Extract the Effects of Transcranial Magnetic Stimulation on Depression. 2018 Tıp Teknolojileri Kongresi (Tam Metin Bildiri/Sözlü Sunum) (Yayın No: 4726274)

9. Yasar B, Yesilkaya B, **Karabiber Cura O**, Akan A (2018). A New Method to Detect Diabetic Retinopathy. 2018 Tıp Teknolojileri Kongresi (Tam Metin Bildiri/Sözlü Sunum) (Yayın No: 4726376)

10. Karabiber Cura O, Kocaaslan Atli S, Sadighzadeh R, Akan A (2018). Classification of Epileptic EEG Data by Using Ensemble Empirical Mode Decomposition. 2018 26th Signal Processing and Communications Applications Conference (SIU), 2018(1), 1-4., Doi: 10.1109/SIU.2018.8404453 (Tam Metin Bildiri/Sözlü Sunum) (Yayın No: 4275318)

11. Çiklaçandir S, **Karabiber Cura O**, Kalafat Y, Can Fc (2017). Design a Robot Insect Inspired by theCamouflage Characteristics of the Leaf Insect. International Conference on Engineering Technologies (ICENTE'xx17), 668-671. (Tam Metin Bildiri/Sözlü Sunum)(Yayın No: 3823421)

12. Karabiber Cura O, Sadighzadeh R, Akan A (2017). Seizure Detection from Pre-Attack EEG Signals Using Ensemble EmpiricalMode Decomposition. 9th International Symposium on Image Processing, Wavelet and Applications (Özet Bildiri/Sözlü Sunum) (Yayın No: 4152793)

13. Karabiber Cura O, Sahin S, Akan A (2017). Görsel Gelistirme Modülü Kullanılarak Mamografi Görüntüsünden Lezyon Tespiti. Tıp Teknolojileri Kongresi, TIPTEKNO 2017, 100-103., Doi: 978-1-5386-0633-9/17 (Tam Metin Bildiri/Sözlü Sunum) (Yayın No: 3789661)

14. Karabiber Cura O, Akan A (2017). Investigation of epileptic EEG data using ensemble empirical mode decomposition. 2017 Medical Technologies National Congress (TIPTEKNO), 343, Doi: 10.1109/TIPTEKNO.2017.8238086 (Tam Metin Bildiri/Sözlü Sunum) (Yayın No: 3823522)

15. Sayilgan E, **Karabiber Cura O**, Isler Y (2017). Use of clustering algorithms and extreme learning machine in determining arrhythmia types. 2017 25th Signal Processing and Communications Applications Conference (SIU), Doi: 10.1109/SIU.2017.7960236 (Tam Metin Bildiri/Sözlü Sunum) (Yayın No: 3820879)

16. Karabiber Cura O, Sayilgan E, Isler Y (2017). Arrhythmia Classification Using Fuzzy C-Means Clustering. International Conference of Applied Sciences, Engineering and Mathematics (IBU-ICASEM 2017), 98 (Özet Bildiri/Sözlü Sunum) (Yayın No: 3535788)

17. Karabiber Cura O, Isler Y (2016). Lineer Regresyon Yöntemi Ile Hormon Degerlerine Göre Menstrual Döngü Gününün Tespiti. TIPTEKNO 2016 (Tam Metin Bildiri/Sözlü Sunum) (Yayın No: 3506620)

18. Karabiber Cura O, Isler Y (2016). Lineer Regresyon Yöntemi Kullanılarak Insüline Bagımlı Diyabetik Çocuklarda C-Peptit Konsantrasyonunun Asit seviyesi ve Yasa Baglı Tespiti. BIYOMUT 2016 (Tam Metin Bildiri/Sözlü Sunum) (Yayın No: 3506655)

19. Karabiber Cura O, Isler Y (2016). Arduino Lilypad Kullanılarak Elektrodermal Aktivite Kayıt Sisteminin Tasarlanması. BIYOMUT 2016 (Tam Metin Bildiri/Sözlü Sunum) (Yayın No: 3506641)

20. Karabiber Cura O, Isler Y (2016). Kas Hareketlerinin ve Cinsiyetin Elektodermal Aktivite Üzerine Etkileri. TIPTEKNO 2016 (Tam Metin Bildiri/Sözlü Sunum) (Yayın No: 3506613)

21. Karabiber Cura O, Dolu N, Güven A (2014). Uyku Süresi Ve Dikkat Arasindaki Iliskinin P100 Dalgasiyla Degerlendirilmesi. TIPTEKNO 2014 (Tam Metin Bildiri/Sözlü Sunum) (Yayın No: 3506667)

Journal Articles

1. Karabiber Cura O, Akan A. Classification of Epileptic EEG Signals Using Synchrosqueezing Transform and Machine Learning. International Journal of Neural Systems 2021; 31(5): 2150005. Doi: 10.1142/S0129065721500052.

2. Karabiber Cura O, Akan A. Analysis of epileptic EEG signals by using dynamic mode decomposition and spectrum. Biocybernetics and Biomedical Engineering 2021; 41(1): 28-44.

3. Karabiber Cura O, Kocaaslan Atli S, Ture H.S, Akan A. Epileptic seizure classifications using empirical mode decomposition and its derivative. BioMedical Engineering OnLine 2020; 19(1): 1–22.

4. Ozdemir MA, **Karabiber Cura O**, Akan A. Epileptic EEG Classification by Using Time-Frequency Images for Deep Learning. International Journal of Neural System 2021. Doi: https://doi.org/10.1142/S012906572150026X

5. Karabiber Cura O, Akan A. Future of Time-Frequency Signal Processing. Digital Signal Processing 30th Anniversary Special Issue: Future Signal Processing. **Accepted.**

Chapter in an edited book

1. Biyomedikal Mühendisligi ve Uygulamaları, Bölüm adı: (Biyomedikal Sinyal Isleme ve Uygulamaları) (2019), Akan Aydin, **Karabiber Cura Ozlem**, Elektrik Mühendisleri Odası Bilimsel Yayınları, Editör: Koçak Onur, Erogul Osman, Basım sayısı: 1, ISBN: 978-605-01-1242-9, Türkçe (Bilimsel Kitap), (Yayın No: 5451074)

2. Biyomedikal Mühendisligi ve Uygulamaları, Bölüm adı: (Biyomedikal Görüntü Isleme ve Uygulamaları) (2019), Akan Aydin, **Karabiber Cura Ozlem**, Elektrik Mühendisleri Odası Bilimsel Yayınları, Editör: Koçak Onur, Erogul Osman, Basım sayısı: 1, ISBN: 978-605-01-1242-9, Türkçe (Bilimsel Kitap), (Yayın No: 5451082)

3. Epilepsy, Chapter Name: Epileptic EEG Classification by Using Advanced Signal Decomposition Methods (2021), Akan Aydin, **Karabiber Cura Ozlem**, Edited by Sandro Misciagna: Published: April 28th 2021, DOI: 10.5772/intechopen.87314, ISBN: 978-1-83962-289-2